Sulfate reduction and iron-manganese cycling in intertidal surface sediments of the southern North Sea

Dissertation
zur Erlangung des Grades eines Doktors der Naturwissenschaften
– Dr. rer. nat. –
angenommen bei der Fakultät für Mathematik und Naturwissenschaften
der Carl von Ossietzky Universität Oldenburg

von
Katja Bosselmann
geboren am 31.07.1972 in Bremen

Gutachter:

Prof. Dr. H.-J. Brumsack

Prof. Dr. M.E. Böttcher

Prüfer:

Prof. Dr. G. Liebezeit

Eingereicht am: 12.11.2007

Disputation am: 17.12.2007

So eine Arbeit wird eigentlich nie fertig.

Man muss sie für fertig erklären, wenn man nach Zeit und Umständen

das Mögliche getan hat.

Johann Wolfgang von Goethe (1787)

Table of contents

Abstract

The main focus of this thesis was the investigation of factors controlling the cycle of manganese, iron and sulfur in different types of intertidal sediments. Measurements were carried out to investigate the seasonal dynamics of the biogeochemical reactions in the sedimentary sulfur cycle and the closely connected element cycles of iron and manganese. The interactions of geochemical and microbial processes with the decomposition of organic matter were compared between sand, mixed and mud flats. Concurrent measurements of microbial sulfate reduction, dissolved and reactive iron and manganese pools, organic stock and temperature dynamics in different sediments demonstrate the strong effect of the activity of sulfate-reducing bacteria on metal cycling.

The main interest of the **first chapter** was the regulation of the overall sulfate reduction activity in different sediment types and the formation and accumulation of reduced sulfur compounds compared to the sulfur geochemistry. Special focus was the application of a model to estimate the response of microbial sulfate reduction during the daily temperature variations under the influence of the tidal dynamics. Seasonal investigations were performed to verify the influence of different factors as temperature, availability of organic matter and metal oxides in surface sediments. Maximum activities of sulfate reducing bacteria were detected at the sediment surface of the upper 10 cm depth at all sites. The vertical distribution of microbial activity showed decreasing sulfate reduction rates (SRR) accompanied by only small decline of organic carbon with depth, even at the finer grained stations (N, D). Thus, lower SRR with depth may have been caused by the shift of the reactive to the more refractory organic matter at depth. This indicates that besides temperature, the availability of reactive organic matter as the main SRR-controlling factors in the investigated intertidal flats. Moreover, the organic poor permeable sediments showed considerably high mineralization rates and point out the important role of marine sands for carbon and sulfur cycling. The mixed and muddy stations represent highly productive sediments where intensive sulfate reduction leads to high accumulation of reduced sulfur. The pool size of the total reduced sulfur compounds (TRIS) and especially acid volatile sulfur (AVS) showed a dynamic seasonal response at all investigated stations and was not permanently trapped in the sediment. The results demonstrated that especially at the sediment surface, where the highest activity of sulfate reducing bacteria occurred, abiotic re-oxidizing processes superimposed the bacterial sulfide production and led to a rapid turnover of reduced sulfur compounds. The oxidative sulfur cycling in the advection-driven sandy sediments was more dynamic compared to the diffusive dominated mixed sediments. Furthermore, the limited availability of reactive iron phases or intermediate sulfur species at the sandy sediments became a process limiting factor for further sulfide fixation and prevented a permanent fixation of sulfide into the thermodynamically more stable pyrite.

The surface of intertidal sediments is characterized by the development of steep temperature gradients. In order to examine the influence of highly dynamic temperature conditions on sulfate reducing activity a model was applied to simulate the development of temperature-induced changes. The model relates the measured SRR to in situ conditions under the influence of the tidal dynamics.

In the **second study** the cycles of manganese and fluxes across the sediment-water interface were investigated in a quantitative manner in order to understand the role of the benthic biogeochemistry on element cycling and interactions between manganese (Mn), iron (Fe), and sulfur (S) in surface sediments (Böttcher et al., 2004; Bosselmann et al., 2003, in prep.). Water column concentrations of dissolved manganese are elevated in the Wadden Sea compared to the open North Sea and showed seasonality with highest Mn concentrations during summer time and low tide (Dellwig et al., 2007). This suggests that tidal flat sediments may form a very important source for dissolved Mn. To quantify the exchange of Mn across the sediment-water interface a combination of pore water, solid phase data and benthic chamber incubations were arranged in different sediments types. From the pore water profiles it becomes evident that the top 15 cm of the surface sediments are most important for Mn cycling and are controlling the metal flux across the sediment-water interface. Gradients and concentrations in pore water responded to the seasonal variation of microbial sulfate reduction and the reservoir of reactive metal oxides. This considers the importance of chemical reduction of MnO_2 by biogenic sulfide in near-surface sediments. Highest Mn release rates (up to 57-90 µmol m^{-2} h^{-1}) were found at the mixed and muddy sediments. The relatively low rates of Mn^{2+} reduction and release (0-55 µmol m^{-2} h^{-1}) at the sandy Station S III reflects high sediment oxidation and low microbial activity (Billerbeck et al., 2006; Walpersdorf et al., in prep). The local seepage of sulfidic pore water at station S I revealed high concentrations of Mn^{2+} probably due to the lateral draining of anoxic pore water downward the sand flat which was postulated by Billerbeck et al., 2006. Furthermore, imbedded fine grained layers may function as sources for locally enhanced Mn^{2+} concentrations at the low water line of the station S I.

The sedimentary Mn and Fe hydr(oxid)e inventory reflected the different reaction kinetics of Fe and Mn. Decline of the Mn_{HCl} and Fe_{HCl} inventory indicated that, especially during the warmer months manganese escaped from the sediment by diffusion, advection and biological activity into the water column whereas the reactive Fe_{HCl} pool was re-precipitated or fixed in the sediment as sulfide. Furthermore, Mn-oxides are reduced by the reaction with Fe^{2+}. Therefore, the oxidation of Fe^{2+} by Mn-oxides acts as a barrier to the upward diffusion of dissolved iron on the way to the sediment-water interface. The Fe_{HCl} inventory showed lower seasonal variations compared to the Mn_{HCl} content which reflected that the most important part of the Fe is restricted to the sediment. The rate of daily Mn_{HCl} depletion from march to august amounted of 82-1320 µmol m^{-2} d^{-1} at station S III and 408-2232 µmol m^{-2} d^{-1} at station N I, which means a pool size reduction of 56 % at station N I and up to 42 % at the sandy stations S I, S III. But the net loss of the sedimentary Mn_{HCl} (which was detected with benthic chambers), amount of 5-43 µmol m^{-2} d^{-1} at station N II and 1-3 µmol m^{-2} d^{-1} at station S III. This indicated that more than 90 % of released Mn^{2+} was recycled back in the water column and re-precipitated to the sediment. The domination of Mn release during spring and summer leads to a depletion of the sedimentary Mn_{HCl} inventory. Therefore, the flux of dissolved Mn^{2+} out of the sediment was larger than the external supply from the overlying water and was not balanced by re-sedimentation as observed during the colder month. Decreasing reductive conditions within the sediment during autumn and winter leads to lower release rates and major part of the Mn-cycling was

restricted to the sediment. The external input of Mn oxide enriched particles from of the water column generated during this month a replenishment of the sedimentary Mn_{HCl} pool.

Chapter three describes an in situ monitoring technique to visualize the spatial distribution of dissolved sulfide and/or activity of sulfate reducing bacteria in a 2-dimensional manner. The procedure has been laboratory tested and applied to intertidal surface sediments under in-situ conditions. The technique is based on the fixation of dissolved hydrogen sulfide as black silver-sulfide (Ag_2S) on photographic paper, modified after Lehmann & Bachofen, 1999. The accumulation of Ag_2S can be measured densitometrically by using a conventional flat bed scanner and imaging software. The colour change is quantitatively related to the amount of Ag_2S. Here, we present the further development and evaluation of the technique by performance of calibration experiments and comparative measurements of sulfate reduction rates using the whole-core $^{35}SO_4^{2-}$ tracer incubation technique (Kallmeyer et al., 2004). The 2D Photopaper technique was deployed within the top 15 cm in different types of intertidal sediments, where high activities of sulfate reducing bacteria have been found (Bosselmann et al., in prep.).

Comparative measurements of sulfate reduction rates using the whole-core $^{35}SO_4^{2-}$ tracer incubation technique (Kallmeyer et al., 2004) reflected that the zones of sulfide production and depletion are readily apparent in the sulfur prints of the sediment profiles and also illustrate the influence of different hydrodynamic conditions for the sulfur cycling. As an effect of tidal flushing, permeable surface sediments are flushed with oxygen rich water which leads to a stimulation of subsurface S-cycling in intertidal sediments. But even at the mixed station anaerobic re-oxidation by oxidized iron and/or manganese phases may become competing processes (Aller & Rude, 1988; Fossing & Jørgensen 1990; Afonso & Stumm, 1992). Therefore, the 2D Photopaper technique provides information about the supply and the retention time of hydrogen sulfide at a high spatial resolution, which was rapidly re-oxidized especially at the sand flat surface. Variances between calculated sulfide concentrations and pore water measurements point out that the sulfur fixation on the photopaper is superimposed by rapid sulfide oxidation or precipitation processes. During the deployment time only free sulfide reacts with the active photographic layer and indicated the net sulfide production. Therefore the 2D Photopaper technique is a monitoring for the mean retention time of free sulfide and allows a semi-quantitative impression of sulfide production and consumption zones. In addition to the expected 2-dimensional impression of sulfide distribution, the detailed resolution of the photo paper images permits information of textural changes visualizing details of internal sediment structures as grain sizes and particles as mussels. Measured sulfide concentrations in the pore water showed good agreements with with sulfide concentrations determined by densitometric photo paper images. Calibration experiments showed that the mean intensities of darkening were quantitatively related to the amount of Ag_2S. The sensitivity of this method denotes detection limits from 50 µM for 24 hour incubation to more than 1000 µM with appropriate shorter deployment times. Duplicate measurements offered reliable and reproducible results with a maximum standard deviation of ± 2 pixel cm^{-2} equal to the concentration of ± 2.7 µm cm^{-2} sulfide. A saturation of the grey scale intensity for the densitometric measurement was reached after 8 hours of deployment in 1000 µM sulfide solution.

Kurzfassung

Zielsetzung der vorliegenden Dissertation ist die Erfassung der saisonalen Dynamik der gekoppelten Mangan-, Eisen- und Schwefel-Kreisläufe in unterschiedlichen intertidalen Sedimenten. Hierzu wurden saisonale Untersuchungen in Sand-, Misch-, und Schlick-Sedimenten durchgeführt, um Aufschluss über die Wechselwirkung von geochemischen und mikrobiellen Prozessen beim Abbau von organischem Material zu erhalten. Vergleichende Messungen der mikrobiellen Sulfatreduktion, des Gehaltes an gelöstem und reaktivem Eisen und Mangan, des organischen Kohenlstoffs sowie die Temperaturdynamik in den verschiedenen Sedimenten verdeutlichen den Effekt der bakteriellen Sulfatreduktion auf den Metallkreislauf.

Im Anschluss an die Einführung im ersten Kapitel befasst sich das **zweite Kapitel** mit der Charakterisierung von Steuermechanismen der mikrobiellen Sulfatreduktion in verschiedenen Sedimenttypen sowie mit der Formation und Akkumulation von reduzierten Schwefelverbindungen. Charakteristisch für die Oberflächensedimente in intertidalen Systemen ist die Ausbildung von steilen Temperaturgradienten. Daher wurde ein wesentlicher Schwerpunkt auf die Anwendung eines Modells zur Simulation der temperaturinduzierten Ratenänderungen der Sulfatreduktion gelegt, und zwar unter besonderer Berücksichtigung des Einflusses der dynamischen Temperaturänderung infolge des Wechsels zwischen Ebbe und Flut.

Zur Erfassung von verschiedenen saisonal geprägten Einflüssen, wie der Verfügbarkeit von organischem Material und Metalloxiden, Temperatur etc. auf die mikrobiellen Umsatzraten, wurden saisonale Untersuchungen im Oberflächensediment durchgeführt. Maximale Sulfatreduktion wurde an allen untersuchten Stationen innerhalb der oberen 10 cm des Sedimentes gemessen. Darüber hinaus wurde auch an den kohlenstoffreichen Standorten (N, D) ein Rückgang der mikrobiellen Sulfatreduktion mit zunehmender Tiefe verzeichnet, was auf den Übergang von reaktivem zu refraktärem organischen Material mit zunehmender Tiefe zurückzuführen ist. Dies verdeutlicht, dass neben der Temperatur die Verfügbarkeit von organischem Material einen der Hauptfaktoren für die Regulation mikrobieller Umsatzraten in intertidalen Sedimenten darstellt. Darüber hinaus zeigten die permeablen Sedimente bei geringem Kohlenstoffgehalt hohe Mineralisationsraten, was die Bedeutung von marinen Sanden für den Kohlenstoff- und Schwefelkreislauf unterstreicht. Misch- und Schlick-sedimente repräsentieren hochproduktive Sedimente, in denen intensive Sulfatreduktion, im Gegensatz zu den sandigen Standorten, zu hoher Akkumulation von reduzierten Schwefel-verbindungen führt. Das Reservoir an reduzierten Schwefelverbindungen zeigte an allen Standorten eine ausgeprägte Saisonalität und wurde nicht langfristig im Sediment fixiert. Diese Ergebnisse demonstrieren, dass insbesondere an der Sedimentoberfläche, wo hohe Raten von Sulfatreduktion gemessen wurden, abiotische Reoxidations Prozesse die bakterielle Sulfidproduktion überlagern und einen schnellen Umsatz von reduzierten Schwefelverbindungen zur Folge haben. Die begrenzte Verfügbarkeit an reaktiven Eisenoxiden in den permeablen Sedimenten limitierte während der warmen Sommermonate eine Fixierung von reduziertem Sulfid im Sediment.

Zur Erfassung der saisonalen Dynamik des Eisen-, Mangan- und Schwefelkreislaufes, wurde im **dritten Kapitel** der Austausch von gelöstem Eisen und Mangan über die Sediment-Wassergrenze ermittelt. Der Wasserkörper des Rückseitenwattes weist, im Vergleich zur Nordsee, eine deutliche erhöhte Konzentration an gelöstem Mn^{2+} auf. Höchstwerte, die während der Sommermonate und bei Niedrigwasser erreicht werden, deuten darauf hin, dass intertidale Sedimente eine bedeutende Quelle für Mn sind (Dellwig et al., 2007). Zur Erfassung der Mn^{2+}-Flussraten wurden Analysen des Porenwassers und der sedimentären Festphase durchgeführt, sowie benthische Kammern in verschiedenen Sedimenten eingesetzt. Diese Untersuchungen verdeutlichten, dass innerhalb der oberen 15 cm in intertidalen Sedimenten eine intensive Rezyklierung von Fe und Mn stattfindet und somit entscheidend den Austausch von gelöstem Fe und Mn aus dem Sediment in die Wassersäule bestimmt. Die Abhängigkeit der Mn Flüsse von der Aktivität Sulfat reduzierender Bakterien und der Verfügbarkeit von reaktivem Mn verdeutlicht den Einfluss der abiotischen Mn-Reduktion durch biogenes Sulfid an der Sedimentoberfläche. Höchste Mn-Flüsse wurden im Misch- und Schlickwatt gemessen und (57-90 µmol m^{-2} h^{-1}), während niedrige Sulfatreduktionsraten und höhere Sauerstoffversorgung in permeablen Sedimenten nur geringe Mn-Flüsse zuließen (0-55 µmol m^{-2} h^{-1}). An der Wasserlinie (S I) wurden lokal hohe Mn -Flüsse gemessen und das Austreten von sulfidischem Porenwasser beobachtet, was entweder einem lateralen Transport hangabwärts der Sandbank zuzuschreiben ist (Billerbeck et al., 2006a) oder auf eingebettete Mn -reiche Schlickschichten zurückzuführen ist.

Der sedimentäre Fe -und Mn -Pool spiegelt die unterschiedliche Reaktionskinetik von Fe und Mn wider. Die Abnahme des Mn_{HCl} Reservoirs durch Diffusion von Mn^{2+} aus dem Sediment in die Wassersäule war während der warmen Monate besonders ausgeprägt. Der Fe_{HCl} -Pool hingegegen zeigt deutlich geringere saisonale Schwankungen, was auf eine intensive Rezyklierung an der Sedimentoberfläche und/oder die Ausfällung als Sulfid im Sediment zurückzuführen ist. Zusätzlich unterliegt das reduzierte Fe^{2+} einer Reoxidation durch Mn-Oxid und stellt eine weitere Barriere für den aufwärts gerichteten Transport über die Sediment-Wassergrenze dar. Die Abnahme des reaktiven Mn $_{HCl}$ betrug von März bis August 82-1320 µmol m^{-2} d^{-1} an der Station S III und 408-2232 µmol m^{-2} d^{-1} an Station N I. Das bedeutet einen Rückgang des Mn_{HCl} Reservoirs um 56 % an Station N I und bis zu 42 % an den sandigen Stationen SI, III. Der deutlich höhere Netto -Fluss (von 5-43 µmol m^{-2} d^{-1} an Station N II und 1-3 µmol m^{-2} d^{-1} an Station S III) verdeutlicht, dass mehr als 90 % des ausgetretenen Mn^{2+} in der Wassersäule rezykliert und wieder ausgefällt wurde. Der Rückgang des Mn_{HCl} Reservoirs im Frühjahr und Sommer verdeutlicht, dass der Austritt von Mn^{2+} aus dem Sediment überwiegt und nicht durch einen Eintrag von partikulärem Material ausgeglichen wird. Geringere Mn -Flüsse im Herbst und Winter sind auf einen Rückgang der reduktiven Bedingungen im Sediment zurückzuführen und der Mn Kreislauf vollzieht sich stärker innerhalb des Sedimentes. Der Eintrag von partikulärem Mn aus der Wassersäule bewirkt die Regenerierung des sedimentären Mn -Pools.

Die im **Kapitel vier** präsentierte in situ Technik ermöglicht die Abbildung der räumlichen Verteilung von gelöstem Sulfid und somit der Aktivität von Sulfat reduzierenden Bakterien im Sediment. Das Verfahren wurde unter Labor- und Feldbedingungen in intertidalen Sedimenten getestet. Diese

Methode basiert auf einer modifizierten Technik der Fixierung von gelöstem Sulfid als schwarzes Silbersulfid (Ag_2S) in Fotopapier, nach Lehmann & Bachofen (1999). Die Akkumulation von Ag_2S kann mit Hilfe eines Scanners und bildverarbeitender Software als Schwärzung densitometrisch gemessen werden. Der Farbumschlag erfolgt quantitativ zu der Menge des gebildeten Ag_2S. Zur Bewertung und Weiterentwicklung dieser Technik wurden Kalibrationsversuche und vergleichende Messungen der Sulfatreduktion mittels Radiotracer (Kallmeyer et al., 2004) durchgeführt. Die 2D Fotopapier Technik wurde in unterschiedlichen Sedimenten innerhalb der oberen 15 cm eingesetzt, wo die höchste Aktivität an Sulfat reduzierenden Bakterien gefunden wurde (Bosselmann et al., in prep.). Die gemessenen SRR belegen, dass die Zonen der Sulfidentstehung und -abnahme mit den Schwefeldrucken übereinstimmen und veranschaulichen den Einfluss verschiedener hydrodynamischer Bedingungen auf den Schwefelkreislauf. Das tiefere Eindringen von sauerstoffreichem Wasser und gelöster und partikulärer organischer Substanz in permeablen Sanden führt zu einer Stimulation und Intensivierung des Schwefelkreislaufs. Die 2D Fotopapier Technik stellt Informationen über die Aufenthaltszeit von gelöstem Sulfid speziell an der schnell oxidierten Sedimentoberfläche mit einer hohen Auflösung dar. Abweichungen zwischen der somit abgeleiteten und der gemessenen Konzentration im Porenwasser verdeutlichen, dass die Fixierung des Sulfids im Fotopapier durch schnelle Ausfällungs- und Oxidationsprozesse beeinträchtigt wird. Während der Inkubationszeit im Sediment reagiert nur freies gelöstes Sulfid mit der fotoaktiven Schicht und repräsentiert somit die Netto-Sulfidproduktion. Die 2D Fotopapier-Technik ermöglicht eine Bestimmung der mittleren Verweildauer von gelöstem Sulfid und eignet sich somit als halbquantitative Messung der Sulfidproduktions- und -verbrauchszonen im Sediment. Darüber hinaus ermöglichen die Fotopapiere eine sehr hochauflösende Abbildung der Strukturen im Sediment (wie Korngrößen, Wurmbauten, Muschelschalen etc.). Im Porenwasser gemessene Sulfidkonzentrationen zeigen eine Übereinstimmung der ermittelten Größenordungen der Sulfidgehalte. Darüber hinaus bestätigten Kalibrationsversuche, dass es einen quantitativen Zusammenhang zwischen dem Schwärzungsgrad und der Sulfidkonzentration gibt. Nachweisgrenzen der Methode liegen bei 50 µM für eine 24 Stunden-Inkubation und reichen bis 1000 µM bei entsprechend verringerter Verweildauer im Sediment. Eine Übersättigung der Schwarzfärbung trat bei einer Konzentration von 1000 µM nach 8 Stunden Inkubation auf. Parallelmessungen wiesen mit einer Standard -Abweichung von ± 2 pixel cm^{-2} entsprechend einer Sulfidkonzentration von ± 2.7 µmol cm^{-2} glaubwürdige und reproduzierbare Ergebnisse auf.

Introduction

Introduction

The continental shelf

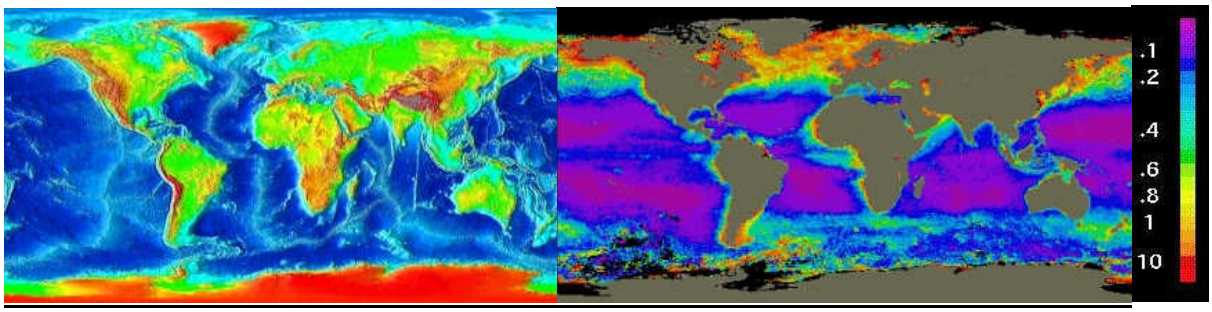

Figure 1: Sea floor (left: depth; light blue represents the shelf area) and marine primary production (right: mg m^{-3}; purple represents low and red high pigment concentrations), NASA SeaWIFS satellite image.

The continental shelf represents the seaward extension of the continental mainland and is limited by the shelf break with the adjacent continental slope. Mean water depth is 130 m, maximum depths of 350 m are reached in the polar region (Wollast, 2002). Continental margin sediments consist of shelf (mainly sands) and intertidal sediments. The total shelf area comprises only about 7.5 % of the world oceans surface and 0.5 % of the global water volume (Jørgensen, 1983b) but is a region of a particularly high primary productivity, where up to one third of the pelagic primary production is thought to take place (Jørgensen, 1996) and additional organic matter (OM) is supplied through benthic primary production (Cahoon, 1999). This high productivity is caused by riverine input of nutrients and organic matter, the aeolian input of trace metals from the mainland and the upwelling of nutrient-rich water from deep sea regions (Wollast, 1991; Gattuso et al., 1998; Berner, 1989). Shallow water depths of near shore waters allow a sufficient light supply supporting benthic primary production (Jahnke et al., 2000) 90 % of the OM material produced is remineralized in the sediments of shallow coastal areas (Wollast, 1991), which therefore play an important role in global carbon cycling.

Southern North Sea and Wadden Sea

The North Sea covers an area of 530 000 km^2 on the continental shelf with an average depth of 94 m and a water volume of 43 000 km^3 (Buchwald, 1990). In the transition zone between land and open sea, the largest interconnected tidal area worldwide developed. The European Wadden Sea stretches along a 450 km coast line from Den Helder in the Netherlands to Esbjerg in the north of Denmark with a total size of approximately 10 000 km^2. The area consists of barrier islands, back-barrier tidal areas with sheltered and open tidal flats, lagoons and estuaries (Streif, 1990). The tide is semi-diurnal with a tidal range of 1.2-2 m in the Danish and Dutch Wadden Sea region increasing to maximum heights of 3 to 3.5 m in the vicinity of the Elbe and Weser estuaries (van Beusekom, 2005). The intertidal areas in the Southern North Sea are characterised by a shallow water depth of 2-3 m in average and

salinities are lower than the in open North Sea. Salinity gradients gradually develop from below 26 to 34 from land to sea and are presumably controlled by weather conditions, in particular influenced by rainfall and freshwater input in the catchment area (Dellwig et al., 2007). Furthermore, larger seasonal temperature amplitudes (19 °C) occur in the Wadden Sea as compared to the adjacent German Bight, where water depths reach 20m near Helgoland and salinity and temperature conditions are controlled by the open sea (Ehlers et al., 1994; Buchwald, 1990).

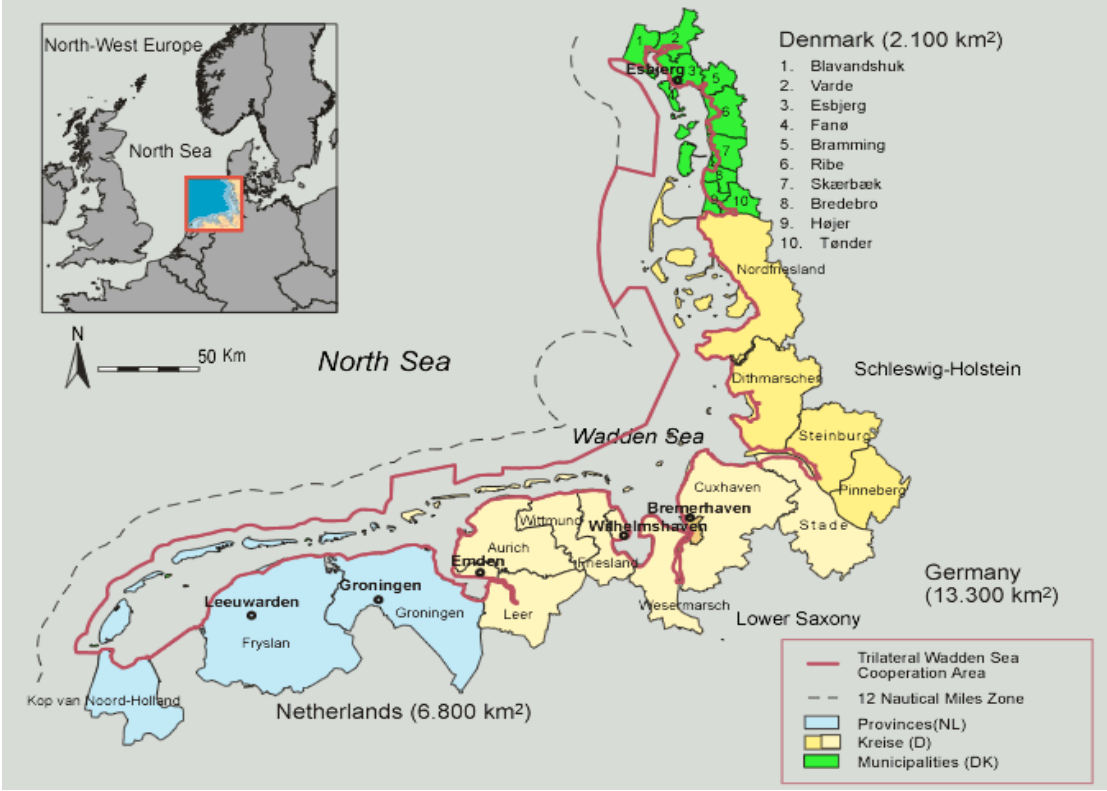

Figure 2: The Trilateral Cooperation Area (Source/derived: The Common Wadden Sea Secretariat (CWSS).

The (East Frisian) Wadden Sea developed 7 500 years BP as a result of Holocene sea-level rise. Sediments consist of various lithofacies, e.g. tidal flat, brackish and lagoon sediments, and peat layers (Streif, 1990; Dellwig et al., 1999, 2002). The sequence of different lithofacies reflects the response of the depositional area to sea level fluctuations and palaeoenvironmental changes (Dellwig et al., 1999, 2002). But coastal morphology is subject to continuous change influenced by natural forces and anthropogenic impact. Approximately one third of the former tidal area has been embanked since the 15th century (Gätje & Reise, 1998). Diverse terrestrial marshland, brackish and marine habitats disappeared over the last 1,000 years due to large-scale habitat transformation (Lotze et al., 2005). The diking interrupted large-scale inundations and resulted in a reduction of the Wadden Sea area to nearly half of its former size, and large areas of salt marshes, mud flats and brackish lagoons were

transformed into farmland (Reise, 2005). This areal loss has diminished the capacity of the Wadden Sea to dissipate wave and tidal energy. Enhanced hydrodynamics led to a decrease in the deposition of fine grained sediment which, as a consequence, was lost from the Wadden Sea (Figure 3; Lotze et al., 2005). Today, sediments of the Wadden Sea are dominated by medium to fine sands, becoming progressively finer toward the mainland coasts (Flemming & Ziegler, 1995; Zeiler et al., 2000; Chang et al., 2006). A coastal ecosystem once rich in marsh plants, sea grass and diatoms on mud flats shifted to one dominated by sandy tidal flats with less autochthonous phototrophic production and dependent primarily on allochthonous plankton supply.

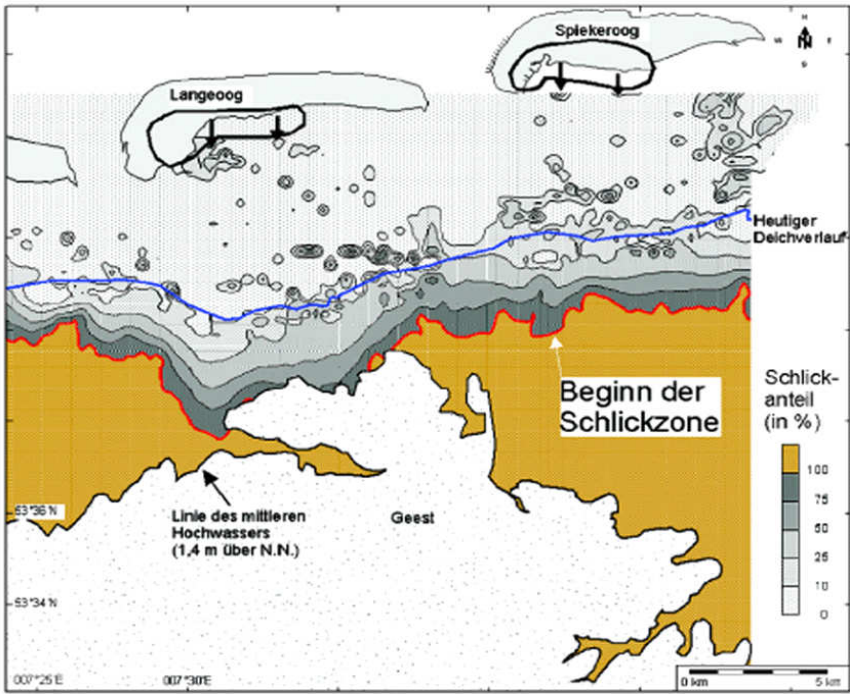

Figure 3: Reconstructed distribution of fine grained sediments after diking in the East Frisian Wadden Sea. The mud and most of the mixed flats were lost after diking the back-barrier region of Spiekeroog (Flemming, 2002).

Intertidal sediments

Tidal areas, e.g. the back-barrier tidal flats of the German Wadden Sea, represent a very dynamic and highly biological productive ecosystem in the transition zone between the terrestrial and marine environment but the processes controlling their unique geochemical environment are still poorly understood. Coastal marine sediments are influenced by riverine input of dissolved and particulate organic matter (Berner, 1989). In near shore waters, high nutrient concentrations lead to increased phytoplankton growth which generates up to 30 % of the total oceanic primary production (Walsh, 1991; Wollast, 1991). Furthermore, the Wadden Sea system is subject to solute and particle exchange between the coastal environment and the adjacent open North Sea mainly driven by the tidal water movement and to a much smaller extent by submarine groundwater discharge (Shaw et al., 1998;

Moore et al., 2002; Burnett et al., 2003). The Wadden Sea acts as import zone for particulate material and exports dissolved mineralisation products into the open North Sea (Postma, 1984).

The intertidal area is strongly affected by a semi-diurnal change between inundation and air-exposure, which causes the sediment chemistry and microbial activity to respond dramatically to seasonal and meteorological changes such as variations in organic matter and oxygen supply, light and temperature as well as current- and wave-induced erosion and advective transport processes. As a result, intertidal sediments are characterized by tidal and seasonal changes of their biological, chemical and physical properties, and transformation processes at the sediment-water interface. A variety of processes occurs particularly in the sediment surface layer driving the biogeochemical cycling of organic matter (OM) and redox sensitive metals.

Tidally induced hydrodynamic forcing results in a highly variable oxygen penetration with the deepest penetration during inundation. Typically, oxygen O_2 is rapidly consumed within the upper few millimetres in marine sediments. The tidally induced deeper O_2 penetration increases the availability and participation of O_2 in element cycling and results in higher O_2 consumption rates (OCR) while sulfate reduction rates (SRR) are lowered during submergence (Forster et al., 1996; Dauwe et al., 2001; Werner et al., 2006; Billerbeck et al., 2006b). In permeable sediments O_2 penetration reached its maximum in winter, whereas during summer the penetration depth was reduced due to a higher sedimentary O_2 demand (4.2-2.4 cm, see Billerbeck et al., 2006b).

Furthermore, enhanced pore water circulation was observed on different temporal and spatial scales. These tidal induced pore water movements may have implications for sedimentary mineralization and recycling of metabolic products (Billerbeck et al., 2006a).

Additionally, under the influence of tides, steep vertical temperature gradients can develop in intertidal sediments. Typical diurnal temperature fluctuations occur rapidly during the change between tidal inundation and exposure further intensified by temperature variations between day and night. Vertical temperature profiles reflect that the steepest semidiurnal fluctuations level off in a constant average temperature in about 20 cm depth. In areas dominated by mesophilic microorganisms, decreasing temperatures slow down biological activity and associated chemical processes. Therefore, sulfate reducing activity, for instance, is strongly dependent on temperature, except for psychrophilic populations.

Transport processes in marine sediments

Biogeochemical processes in sediment and overlying water column of marine environments are influenced by transport and exchange of solutes and particles between both compartments. The dominant transport process is dependent on sediment properties such as permeability, faunal activity, sediment depth and tidal dynamics.

Diffusive transport processes are important in fine grained, cohesive sediments (grain size ≤ 63 µm). Molecular diffusion is driven by concentration gradients of solutes and influenced by molecule size, temperature and salinity (Berner, 1971). Diffusive transport is only effective over small distances (micrometre to millimetre) and is an important solute transport mechanism mainly from the deep into the upper sediment layers where bioturbation or advective pore water flow enhance the transport velocity. In intertidal sediments, diffusional transport also gains increasingly in importance during low tide exposure, when advective pore water transport and bioirrigation are low (Huettel et al., 1996; Webster et al., 1996).

In contrast, advective pore water flow is the most important transport process in permeable sediments. The permeability of sediments depends on grain size, sediment sorting and porosity, and can be altered by biological activity. Burrowing and tube dwelling faunal activity can both, increase or decrease permeability (Meadows & Tait, 1989; D`Andrea et al., 2002). Permeability can also be reduced by diatoms producing adhesive extracellular polymeric substances (EPS) and by bacterial growth within the sediment pore space (Smith & Underwood, 1998; Thullner et al., 2002). Pore water advection is driven by pressure gradients along the sediment surface which can be induced by density differences, at topographical structures (e.g. wave ripples and mounds) or pressure gradients between pore water and sea level (Webster et al., 1996; Huettel & Gust, 1992; Huettel & Rusch, 2000). Advective pore water transport can exceed diffusive solute transport by orders of magnitude and leads to an enhanced flux and penetration depth of particles, e.g. algae and bacteria, up to several centimetres deep into the sand flats (Huettel & Rusch, 2000; Huettel et al., 2003). Therefore, intertidal sandy flats have shown to function as efficient biocatalytic filters for particulate organic matter (Huettel & Rusch, 2000; Rusch & Huettel, 2000; Rusch et al., 2000, 2001).

Tidally driven discharge of pore water and associated nutrient export has been observed for beaches and salt marshes (Agosta, 1985; Campbell & Bate, 1998; Ullman et al., 2003). This is explained by `subtidal pumping` a wave-induced hydrostatic pressure gradient (Riedl et al., 1972; van der Loeff, 1981; Shum & Sundby, 1996). Tidally induced pore water movements in permeable sediments were also observed by Billerbeck et al., (2006a) in the form of a draining mechanism working at different temporal and spatial scales with 1) a rapid ‘skin circulation’ during inundation within the top sediment layer and 2) a slower ‘body circulation’ during exposure of the tidal flat through the surface and deeper layers of the sediment with long flow paths and long pore water residence times. This fast exchange of substances between the water column and sandy surface sediments therefore leads to a rapid and effective degradation of organic substances. High aerobic mineralization in the upper sediment layers due to enhanced O_2 supply and anaerobic degradation processes deeper in the sediment are fuelled by the filtration of suspended particles and dissolved organic matter from the water column into the permeable sea bed (Huettel et al., 1996; Rusch et al., 2001).

Burrowing and tube dwelling benthic macrofaunal activity enhances solute transport through passive or active flushing of tube networks that penetrate deeply into the anoxic zone of the sediment (Anderson & Meadows, 1978). The process of burrow flushing and its geochemical consequences is defined as bioirrigation and is an important control mechanism for sediment biogeochemistry (Aller,

2001; Davis, 1974; Aller & Aller, 1998; Wenzhöfer & Glud, 2004). Flushing of burrow networks removes metabolites and reduced species from bulk pore waters and simultaneously promotes the exchange with the oxygenated overlying water which leads to re-oxidation reactions near burrow walls (Aller & Aller, 1998). In fine grained sediments, bioirrigation is driven by diffusional transfer across the burrow walls, whereas in sands, ventilation flow can penetrate the surrounding sediment by advection (Meysman et al., 2006). Physical reworking of sediments due to bioturbation results in mass transport of solutes and particles (Aller, 1994b; Graf & Rosenberg, 1997). In heavily bioturbated sediments the enhanced transport leads to an increased return of nutrients and other solutes to the overlying water and fosters benthic-pelagic coupling and primary productivity of near shore marine environments (Rowe et al., 1975).

Degradation of organic matter

Microbial degradation of organic matter as an early diagenetic process includes a variety of aerobic, anaerobic and fermentative mineralization processes. The oxidation of organic carbon is performed by microorganisms that apply an array of electron acceptors yielding different amounts of free energy (Table 1). Prokaryotes are of particular importance and possess versatile aerobic and anaerobic metabolic pathways. In muddy sediments of the German Wadden Sea, prokaryotes were found in high abundances of up to 4-10^9 bacteria cm^{-3} (Llobet-Brossa et al., 1998, 2002). Bacterial communities of the Wadden Sea and the open North Sea showed nearly similar composition of bacterial populations (Rink et al., 2003).

In general, carbon mineralization in sediments is mediated by a consecutive depth sequence of respiratory processes, including different inorganic electron acceptors (O_2 > NO_3^- > Mn (IV) > Fe (III) > SO_4^{2-} > CO_2). This sequence of electron acceptors shows that oxidants are consumed in a predictable order (Table 1) with preferential use of electron acceptors yielding higher free energy ($\Delta G°$) available for respiration (Froelich et al., 1979).

Table 1: Free energy yield, $\Delta G°$, per mol organic C for carbon oxidation reaction in marine sediments (after Jørgensen, 2000).

	Process	Reaction	$\Delta G°$ (kJ mol^{-1})
1	Aerobic respiration	$CH_2O + O_2 \rightarrow CO_2 + H_2O$	-479
2	Denitrification	$5CH_2O + 4NO_3^- \rightarrow CO_2 + 2N2 + 4HCO_3^- + 3H_2O$	-453
3	Mn (IV) reduction	$CH_2O + 3CO_2 + H_2O + 2MnO_2 \rightarrow 2Mn^{2+} + 4HCO_3$	-349
4	Fe (III) reduction	$CH_2O + 7CO_2 + 4Fe(OH)_3 \rightarrow 4Fe^{2+} + 8HCO_3^- + 3H_2O$	-114
5	Sulfate reduction	$2CH_2O + SO_4^{2-} \rightarrow H_2S + 2HCO_3^-$	-77
6	Methanogenesis	$CH_3COO^- + H^+ \rightarrow CH_4 + CO_2$	-28

Under steady state conditions a vertical zonation of the mineralization pathways establishes where the different processes can spatially overlap with each other (Canfield et al., 1993a; Kostka et al., 1999; Thamdrup, 2000). Aerobic respiration produces the largest $\Delta G°$ and mainly occurs in the surface

sediment layer (Table 1). In intertidal sediments, the O_2 penetration depth varied diurnal and seasonally, induced by alternating tidal exposure and inundation (Polerecky et al., 2005; Werner et al., 2006). Thermodynamically, O_2 is the most favourable electron acceptor but the re-supply of O_2 from the overlying water into the sediment is limited. In coastal marine sediments and other areas of high productivity the high input of organic matter leads to a rapid depletion of O_2 in the sediment (Jørgensen, 2000). Under anoxic conditions, facultative anaerobic denitrifying bacteria reduce nitrate by using and transforming nitrite, nitrous oxide and di-nitrogen oxide progressively to nitrogen. If O_2 is present, denitrifying bacteria also perform aerobic mineralization (Herbert, 1999).

The sedimentary Fe and Mn cycles involve two main redox transformations of reduced dissolved Fe^{2+} and Mn^{2+} and particulate oxidized Fe (III) and Mn (III), (IV) which are coupled to the biogeochemical cycles of other elements such as C, N, S and P (Chapter 2, 3).

While most bacteria use O_2 or nitrate as electron acceptor for the oxidation of carbon to CO_2 most SO_4, Fe and Mn reducing bacteria are dependent on the activity of fermenting bacteria. They use the products of fermentation (e.g. formate, acetate, lactate, propionate, butyrate and H_2) as electron donors for the reduction of Fe (III), Mn (IV) or SO_4. Iron reducers out-compete sulfate reducers for the same electron donors and therefore sulfate reduction takes place below the zone of Fe reduction but abiotic redox processes (such as reduction of Mn oxides by Fe^{2+}, Equ. 5, Table 2) lead to an overlap of these processes within the sediment. Because of high dissolved sulfate concentrations in marine environments sulfate reduction is an important metabolic pathway which typically accounts for 25-50 % of the total carbon oxidation in coastal sediments (Jørgensen, 1982). The significance of sulfate reduction decreases with declining carbon input and increasing water depth. In most marine sediments nitrate oxidation accounts for less than 4 % of total carbon oxidation and is of minor importance (Jørgensen, 1982; Canfield et al., 1993b). Fe reducers contribute up to 6 % of all detected bacteria in muddy sediments of the German Wadden Sea (Mussmann et al., 2005). Fe (III) reduction contributes in average 17 % to the total carbon mineralization in continental margin sediments. Mn (IV) reduction is of less significance due to the usually lower Mn oxide content in marine sediments (Thamdrup, 2000).

Methane is generated below the sulfate reduction zone as the end product of anaerobic organic matter degradation. Whereas highest sulfate reducing activity typically occurs in the surface layer of the sediment depending on quantity and quality of organic matter sedimentation, methane oxidation takes place down to several meters below the sediment surface. Methanogenic organisms use acetate, C1 compounds, CO_2 or H_2 to gain only small amounts of energy (Jørgensen, 2000; Table 1).

Iron and manganese in aquatic systems

Surface rocks on earth contain Mn and Fe in average quantities of 0.072 % and 3.6 % by mass (Martin & Meybeck, 1979). Fe and Mn function as electron-transfer system which shapes chemical gradients in the O_2 deficient zones because of their ability to change rapidly between multiple

oxidation states. Their oxidized forms are relatively immobile due to a low solubility. Mn (III) and (VI) are practically insoluble in water at neutral pH. The Fe and Mn content in a given sediment depends on the composition of the source rocks and the weathering conditions, furthermore the mixture with biogenic materials and sand, silt and clay fractions (Thamdrup, 2000 and cited references therein). Additionally groundwater seepage and hydrothermal inputs may lead to local enhancement of Fe and Mn concentrations. Post-depositional redistribution through reductive mobilization leads to a depletion of redox sensitive metals from anoxic horizons and an enrichment above them. Within the sediment, Mn and iron (Fe) act as important terminal electron acceptors for the oxidation of organic matter.

Sedimentary manganese cycle

Mn represents the second most abundant transition metal in the earth crust (Morgan & Stumm, 1964). Mn oxides function as reactive oxidizing agent and mainly occur with other sediment particles as aggregates or coatings (Burns & Burns, 1979). They can adsorb a variety of cations and incorporate other metals in their surface (Cu, Co, Cd, Zn, Ni, Pb and certain radio nuclides; Bacon et al., 1980; Todd et al., 1988; Wei & Murray, 1991).

Reduced Mn^{2+} may precipitate as an authigenic mineral (mainly carbonates, but mixed Mn (II)/Fe (II) phosphates have also been identified (Friedl et al., 1997) or adsorb to clay minerals and, after upward transport, re-precipitate as an oxide in the surface sediment or escape to the overlying water due to slow oxidation rates (Middelburg et al., 1987; Aller, 1994a). Mn (II) also exists in a variety of minerals such as e.g. Ca-rhodochrosite ($(MnCa)CO_3$) (Suess, 1979; Böttcher, 1998), alabandite (MnS) (Böttcher & Huckriede, 1997), reddingite ($Mn_3(PO_4)_2*3H_2O$) (Tebo et al., 1997). For Mn, recent studies elucidate vernadite (γ-MnO_2; Wehrli, 1990; Friedl et al., 1997) to be the main product in marine environments but various other oxidation products are possible which contain different contents of Mn (III) and Mn (VI) (Burdige, 1993; De Vitre & Davison, 1993). Mn (III) and (VI) are practically insoluble in water at neutral pH (Thamdrup, 2000). Mn oxides can be chemically reduced by humic substances, phenols and microbial metabolites such as oxalate and pyruvat (Stone & Morgan, 1984; Stone, 1987; Sunda & Kieber, 1994). Furthermore, Mn oxides can be reduced with sulfide and FeS, SO_4 and S_0 and microbially by acid volatile sulfides (Aller & Rude, 1988). Possible interactions were found with ammonia and/or organic nitrogen, and anoxic nitrification of NH^{4+} to NO^{3-} during Mn-reduction (Luther et al., 1997; Hulth et al., 1999). The redox reactions of Mn are directly or indirectly mediated by chemoautothrophic and heterotrophic biological activity and play an intermediate role between the O_2 and C cycling (Lovley, 1991; Nealson & Myers, 1992).

A horizontal redistribution occurs with Mn (II) being released out of the sediment and subsequent re-oxidation in the water column. That way, a net removal of Mn from reduced sediments and anoxic basins leads to an enrichment of Mn in oxidized adjacent sediments (Sundby & Silberberg, 1981, 1985; Canfield et al., 1993a, b; Thamdrup et al., 1994).

Table 2: Mn-redox reactions in marine sediments (modified after Aller, 1994a)

	Reaction	Equation
1	Mn oxidation	$2Mn^{2+} + O_2 + 2\,H_2O \rightarrow 2MnO_2 + 4\,H^+$
2	Dissimilatory Mn red.	$CH_2O + 2MnO_2 + 3CO_2 + H_2O \rightarrow 2Mn^{2+} + 4HCO_3^-$
3	Anoxic nitrification	$4MnO_2 + NH_4^+ + 6H^+ \rightarrow 4Mn^{2+} + NO_3^- + 5\,H_2O$
4	N_2 generation	$3MnO_2 + 2NH_4^+ + 4H^+ \rightarrow 3Mn^{2+} + N_2 + 6H_2O$
5	Fe oxidation	$MnO_2 + 2Fe^{2+} + 2H_2O \rightarrow Mn^{2+} + 2FeOOH + 2H^+$
6	Sulphide oxidation I	$4MnO_2 + FeS + 8H^+ \rightarrow 4Mn^{2+} + SO_4^{2-} + Fe^{2+} + 4\,H_2O$
7	Sulphide oxidation II	$MnO_2 + SH^- + 3H^+ \rightarrow Mn^{2+} + S_0 + 2H_2O$
8	Anoxic precipitation	$x\,Mn2+ + (1\text{-}x)\,Ca^{2+} + 2HCO_3^- \rightarrow Mn_xCa_{(1-x)}CO_3 + CO_2 + H_2O$

Sedimentary iron cycle

In contrast, differences in reaction kinetics and thermodynamics i.e. faster oxidation rates of Fe^{2+} and oxidation of Fe^{2+} by oxidized Mn, O_2 and nitrate impede the diffusion of dissolved Fe into the overlying water (Stumm & Morgan, 1981; Lovley & Phillips, 1988). The rapid oxidation with O_2 strongly depends on pH and increases in rate with increasing pH (Millero et al., 1987). Microbial Fe^{2+} oxidation in the absence of O_2 is possible when coupled to dissimilatory nitrate reduction (Straub et al., 1996, then a catalyst like Cu^{2+} is needed). Therefore only small variations of 0.5-6 % in total Fe contents were found in sediments from shelf to deep sea which were mainly attributed to pre-depositional factors (Raiswell & Canfield, 1998). In marine sediments Fe oxides account for about 28 % of the total Fe as most of the Fe is bound in aluminium-silicates (Raiswell & Canfield, 1998). The main oxidation product for Fe, is ferrihydrite which structural formula is uncertain (also known as: amorphous ferric(hydr)oxides, hydrous ferric oxide, or $Fe(OH)_3$; Thamdrup, 2000 and cited references therein). Fe oxides are divided into crystalline and amorphous, poorly crystalline Fe of which the latter is most important for microbial Fe reduction (Thamdrup, 2000). Additionally, in some clays lattice bound Fe (III) (26 %) have shown to be bacterially reducible (Stucki et al., 1987; Kostka et al., 1996, 1999). A larger number of precipitates were identified for Fe^{2+}, including pure or mixed carbonates, vivianite ($Fe_3(PO_4)_2$+$8H_2O$) and iron sulfides (Berner, 1989). Large amounts of non-sulfide-bound Fe^{2+} are presumed to be not identified yet. Fe^{2+} containing sheet silicates have been shown to be of importance in special environments as deep sea and the tropics (e.g. Amazon sediments; Haese et al., 1997; Michalopoulos & Aller, 1995).

Table 3: Fe-redox reactions in marine sediments (modified after Aller, 1994a)

	Reaction	Equation
1	Fe oxidation	$2Fe^{2+} + O_2 + 2 H_2O \rightarrow 2FeOOH + 2 H^+$
2	Oxidation denitrification	$10 FeCO_3 + 2NO_3^- + 24H_2O \rightarrow 10Fe(OH)_3 + N_2 + 10HCO_3^- + 8H^+$
3	Oxidation - Mn red.	$2Fe^{2+} + MnO_2 + 2H_2O \rightarrow 2FeOOH + Mn^{2+} + 2 H^+$
4	Dissimilatory Fe red.	$CH_2O + 4FeOOH + 7CO_2 + H_2O \rightarrow 2Fe^{2+} + 8HCO_3^-$
5	Chemical Fe red.	$FeOOH + SH^- + 2H^+ \rightarrow Fe^{2+} + S_0 + 2H_2O$
6	Precipitation	$Fe^{2+} + SH^- \rightarrow FeS + H^+$
7	Pyrite formation I	$FeS + S_0 \rightarrow FeS_2$
8	Pyrite formation II	$FeS + S_x^{2-} \rightarrow FeS_2 + S_{(x-1)}^{2-}$

Terrestrial weathering of rocks and sheet silicates (as e.g. biotite, pyroxene, amphibole, olivine) releases Fe to a major fraction as Fe oxides (most abundant as goethite (α-FeOOH) and hematite (α-Fe_2O_3) and less abundant as lepidocrocite (g-FeOOH), maghemite (γ-Fe_2O_3) and magnetite ($Fe^{2+}Fe_2^{3+}O_4$) and a minor amount is incorporated into clay minerals (Haese, 2000). Depositional Fe and Mn forms can be divided into free oxides, with metals as major cations and minor constituents in silicates. In marine sediments 28 % of the total Fe consists of Fe oxides, the rest being classified as non- or poorly reactive silicate-bound iron (Raiswell & Canfield, 1998; Canfield, 1989; Wallmann et al., 1993; Kostka & Luther, 1994; Thamdrup et al., 1994; Haese et al., 1997). Higher contents were found in soils, especially in a heavily weathered environment as the tropics (Cornell & Schwertmann, 1996; Canfield, 1997). Fe (III) is also a significant electron acceptor for carbon oxidation in freshwater sediments (Flies et al., 2005; Kappler et al., 2004), rice fields (Achtnich et al., 1995a, b) and aquifers (Jakobsen & Postma, 1999).

Iron and manganese reduction

In the sequence of redox processes, Mn and Fe reduction begins after depletion of O_2 and nitrate but before net sulfate reduction and can be mediated chemically or microbially (Thamdrup, 2000). Phylogenetic diverse bacteria and *Archea* are known as dissimilatory reducers for Fe (III) and Mn (IV). More bacteria have been isolated capable for Fe reduction probably indicating the higher importance of Fe reduction compared to Mn reduction (Thamdrup, 2000). Besides Fe reducing prokaryotes where the reduction process mainly supports growth, also fermenters, methanogens and sulfate reducing bacteria were proven to reduce Fe (Lovley, 1991; Bond & Lovley, 2002; Lovley et al., 1993a). Most Fe reducing bacteria in cultures are able to reduce O_2, NO_3, S_o and Mn as alternative electron acceptors (Thamdrup, 2000; Lovley et al., 1996, 1998). Presumably, complex organic matter is oxidized by a consortium of Mn/Fe reducers and fermentative bacteria (Lovley, 1991).

Bacteria can reduce Fe oxides as well as Fe (III) bound to clay minerals indicated by a green colour transition in pelagic sediments (Lyle, 1983; König et al., 1997). Some *Geobacter* species are

chemotactic to Fe^{2+} and Mn^{2+} and require direct contact with Fe (III) oxides in order to reduce them. In contrast, *Shewanella* and *Geothrix* species produce chelators that solubilise Fe (III) and release electron shuttling compounds that transfer electrons from the cell surface to the surface of Fe (III) oxides not in direct contact with the cells (Lovley et al., 2004). Magnetotactic microorganisms contain single domain magnetic particles which permit them to orient themselves in the earth's geomagnetic field and chemotactic gradients (Lovley, 1995; Bazylinski et al., 1988; Balkwill et al., 1980).

Fe reducers contribute up to 6 % of detected bacteria in muddy sediments of the German Wadden Sea (Mussmann et al., 2005). Sulfate reducing bacteria may also reduce Fe (III) (Lovley, 1991) leading to the formation of siderite ($FeCO_3$) which is unstable under the presence of H_2S (Coleman et al., 1993) or indirectly reduce Fe (III) as they produce sulfide (see chapter sulfur cycling; Pyzik & Sommer, 1981).

The oxidation and reduction of Mn (III), (IV) occurs typically by direct chemical reaction with e.g. reduced iron and sulfide or indirectly mediated by chemoautotrophic and heterotrophic biological activity (Lovley, 1991; Nealson & Myers, 1992; Thamdrup et al., 1994). Therefore, sulfate reduction is likely involved in Mn mobilization via chemical reduction of Mn oxides by sulfide (Burdige, 1993) resulting in a short scale metal cycling at the sediment surface with enrichment of oxidized Mn and Fe precipitates and indicates the close coupling between the biogeochemical processes of metal and sulfur cycle (Burdige & Nealson, 1986). The biogeochemical cycling of Mn is controlled by redox transformations involving dissolved Mn^{2+} and insoluble oxides and oxy(hydroxid)es of Mn (III) (IV) (Stumm & Morgan, 1981). Oxidized Fe is readily reduced by H_2S (Pyzik & Sommer, 1981) and H_2S and ferrous iron become electron donors for Mn oxides and thus function as control for the accumulation of dissolved sulfide in the sediments (Table 2, Fe Equ. 5; Goldhaber & Kaplan, 1974; Canfield, 1989; Canfield et al., 1992). The oxidation of Mn^{2+} by NO^{3-} plays a minor role in the investigated sediments (Luther et al., 1997; Table 3, Mn Equ. 5+7). The inhibition of methanogenesis and sulfate reduction by Fe reduction results in the competition for common substrates (e.g. acetate, hydrogen; Lovley & Phillips, 1988). But sulfate reduction is not completely inhibited but takes places simultaneously with Fe reduction. During incubation experiments processes occurred simultaneously when acetate or hydrogen was added in high concentrations and sulfate reduction was not completely inhibited (Lovley & Phillips, 1988). Additionally, incubation experiments showed that Fe concentrations ≥ 50 µmol cm^{-3} inhibit 90 % of sulfate reducing activity presumed that the population of Fe reducing bacteria were high enough (Lovley & Phillips, 1987; Aller & Rude, 1988; King, 1990).

Furthermore, the redox potential of Fe oxides varied inversely to their grain size most pronounced at crystal size <1µm (Langmuir, 1971; Murray, 1979; Cornell & Schwertmann, 1996). Typical grain sizes are 10-100 nm for crystalline Fe oxides and 1-10 nm for ferrihydrite in soils and sediments (Schwertmann, 1988; Drodt et al., 1997). The reduction potentials of the Fe (III) oxides are much stronger pH dependent than other redox couples and increase by a 59 mV per unit decrease in pH. Therefore, at lower pH the reduction of hematite and goethite is energetically more favourable than sulfate reduction (Kostka & Nealson, 1995; Postma & Jacobsen, 1996). Abiotic Fe and Mn reduction are chemically favourable processes with a wide spectrum of organic and inorganic reductants.

Hydrogen sulfide and, for Mn, ferrous iron appear to be the most important agents for abiotic reduction of Fe and Mn oxides. Mn and Fe oxides are also reduced by a range of organic compounds as catechol, ascorbate (Stone & Morgan, 1984). Slower reactions were found for Fe oxides at circumneutral pH but humic substances were found to stimulate Fe reduction (LaKind & Stone, 1989; Lovely et al., 1991). Rapid Fe cycling helps to maintain the oxides in a poorly crystalline state and exerts a positive influence on microbial Fe reduction (Thamdrup, 2000). Importance of Fe reduction increases in sediments with low sulfate reducing activity as in the deep seas or on continental slopes (e.g. Canfield, 1993a). Mn oxide concentrations are generally low compared to other electron acceptors such as Fe oxides and sulfate, therefore the contribution of Mn reduction to carbon mineralization in most marine sediments was estimated to be globally insignificant (Thamdrup, 2000). However, the redox cycle of Mn may contribute significantly to the re-oxidation of reduced Fe and sulfur species (Canfield et al., 1993a, b; Aller, 1994a, b; Thamdrup et al., 1994). Microbial Mn reduction becomes an important mineralization process in sediments where Mn oxide concentrations reached at least 20 µmol cm^{-3} (Thamdrup, 2000).

Sedimentary sulfur-cycling

The largest of all sulfur pools is represented by the oceans sea water which contains concentrations of 28.7 mM of dissolved sulfate or a total of about 1.3* 10^9 teragrams (Schidlowski, 1989). An important and major quantitative part of the global sulfur cycles is related to the sedimentary sulfur transformation where it is tightly connected to the carbon mineralization (Berner, 1989). Sulfur is involved in several biological processes which are facilitated by its ability to undergo changes in oxidation states over an eight electron shift, between -2 and +6 (Table 4). Furthermore, sulfur is essential to living organisms, being a component of amino acids, coenzymes and vitamins, but some compounds can also have toxic effects (such as H_2S; Vairavamurthy et al., 1995a, b).

Major pathways for the removal of sulfate from the oceans to the sediments are:

- precipitation of sulfate minerals as evaporates e.g. gypsum ($CaSO_4 \cdot 2H_2O$), calcium sulfate ($CaSO_4$), anhydrite by rapid evaporation and as a minor sink with carbonate minerals e.g. calcite, aragonite ($CaCO_3$),

- formation of sulfide minerals (FeS), particularly pyrite (FeS_2), and

- formation of organic sulfur.

The importance of each pathway depends on local depositional conditions (Berner, 1989). The major removal process for sulfur is the burial of iron sulfides, pyrite and organic sulfur (Vairavamurthy et al., 1995a, and cited references therein).

Table 4: Important sulfur compounds and their oxidation states (modified after Ehrlich, 1996).

Sulfur Compound	Formula	Oxidation state of S
Sulfide	S^{2-}	- 2
Polysulfide	S_n^{2-}	-2, 0
Elemental Sulfur -ring form	S_8	0
Hyposulfite (dithionite)	$S_2O_4^{2-}$	+ 3
Sulfite	SO_3^{2-}	+ 4
Thiosulfate *	$S_2O_3^{2-}$	-1, + 5
Dithionate	$S_2O_6^{2-}$	+ 5
Trithionate	$S_3O_6^{2-}$	-2, + 6
Tetrathionate	$S_4O_6^{2-}$	-2, + 6
Pentathionate	$S_5O_6^{2-}$	-2, + 6
Sulfate	SO_4^{2-}	+ 6

* outer S -1 inner S +5

The initial step in the biological transformation is the assimilatory or dissimilatory sulfate reduction. Assimilatory sulfate reduction is performed by autotrophic organisms for biosynthetic production of organic sulfur compounds, whereas dissimilatory sulfate reduction proceeds via anaerobic pathways for bacterial energy yield. Assimilatory sulfate reduction is the less significant process and contributes to only 3 % of the total sulfide production (Jørgensen, 1983a). Most of the known dissimilatory sulfate reducers are bacteria but also some thermophilic archaea are known (Stetter et al., 1996). The extracellular product of microbial sulfate reduction, H_2S, is toxic to aerobic and in higher concentrations also to anaerobic organisms. *Desulfovibrio* has a high tolerance to its metabolic product (up to 50 mM H_2S; Miller, 1950). The rate of dissimilatory sulfate reduction (SRR) in intertidal sediments may vary considerably between 0.2–104 mmol $m^{-2}day^{-1}$ (Skyring, 1987; Trudinger, 1992). In relation to other competing reactions, the regulation and seasonal variation of sulfate reduction showed the highest dynamics within a short distance of the sediment-water interface. Most of the reduction (up to 99 %) takes place in the upper 10 cm of the sediment and only 1-2 % below 1 m depth (Jørgensen, 1983a). In the surface sediment, biogeochemical processes are influenced by sudden changes of temperature, re-suspension and organic matter sedimentation. In intertidal surface sediments where sulfate is abundant, the rate of microbial sulfate reduction is controlled primarily by temperature and the availability of degradable organic matter (e.g. Westrich & Berner, 1988; Böttcher et al., 1997; Rusch et al., 1998). Sedimentation of fresh organic matter leads to increased surficial sulfate reduction rates which often decrease with depth in response to increasing amounts of refractory organic matter (Berner, 1978). Furthermore, the activity of sulfate reducing bacteria is closely coupled to the burial and cycling of sedimentary sulfur, iron and manganese compounds. Only about 10 % of the sulfide produced by microbial sulfate reduction is permanently buried in the sediment, while about 90 % of the reduced sulfide is re-oxidized to sulfate (Jørgensen, 1977, 1982; Berner & Westrich, 1985). Most sulfides precipitate more or less permanently as iron sulfides FeS and

FeS_2 in the sediment if reactive iron phases are available. Reactive iron phases represent the pools readily available for reduction by H_2S or microbes (Canfield, 1989; Thamdrup et al., 1994; Kostka & Luther, 1994).

Figure 4 gives an overview about the cycling and transformation of sulfur and the close coupling to the iron and manganese cycles. Oxidation of reduced sulfur compounds occurs via chemical and biological pathways and is predominant at oxic-anoxic interfaces where oxidants such as O_2 and metal oxides are abundant (e.g. Thamdrup et al., 1994). Many processes take place simultaneously, depending on the overall redox chemistry and the availability of electron donors and acceptors in different sediment types and are therefore difficult to quantify. In organic rich sediments typically 25-50 % of the sediment O_2 consumption is used either directly or indirectly for the re-oxidation of sulfide (Jørgensen, 1982). Products of the sulfide oxidation may be sulfate or reduced sulfur compounds, e.g. elemental sulfur, sulfides, polysulfides and thiosulfate, polythionate or sulfite, which are water soluble and may be exchanged via the pore water. Some oxidation products are highly reactive sulfur nucleophiles (e.g. polysulfides, sulfite, thiosulfate) and react further with organic molecules.

Organic sulfur functions as important sink in organic rich and iron limited sediments such as carbonate systems (e.g. coral reef systems). Intermediate compounds may be transformed by further processes, such as respiratory bacterial reduction to H_2S, bacterial or chemical oxidation, chemical precipitation or bacterial disproportionation to H_2S and SO_4^{-2} (Thamdrup et al., 1994). In the presence of sulfide-scavenging agents such as iron and manganese compounds the microbial disproportionation of S_0 to sulfate and sulfide was observed as follows:

Equ. 1: $$\mathbf{4S_0 + 4H_2O \rightarrow SO_4^{2-} + 3H_2S + 2H^+}$$

The importance of this process in producing large isotopic fractionations has been described by e.g. Thamdrup et al., 1993; Böttcher, 2001, 2005; Böttcher et al., 2001; Lovley & Phillips, 1994.

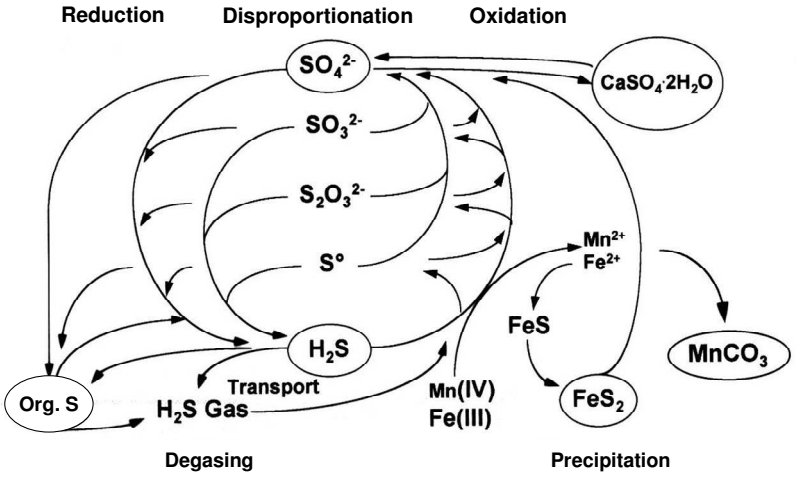

Figure 4: Sulfur undergoes cyclic transformations (modified from Böttcher, 1999).

Due to the high recycling efficiencies of reactive manganese- and iron(oxyhydr)oxides, these metals serve as electron shuttles in a short-scale metal cycling at the sediment-water interface**.** Reduced Fe^{2+} and Mn^{2+} diffuse to the sediment surface where they are re-oxidized and precipitated again. Only about 10 % of the produced sulfide is precipitated by iron as sulfide and is ultimately converted to pyrite. In contrast to a continuous cycling of sulfur between the H_2S and sulfate pools, pyrite provides a continuous sink in the sulfur cycle. The remaining 90 % are re-oxidized abiotically or by bacterial processes. Iron monosulfide is formed in solution in two competing mechanisms (Jørgensen, 1983a): the hydrogen sulfide pathway,

Equ. 2: Fe^{2+} H_2S -> FeS + $2H^+$

and the bisulfide way, which involves the formation of complexes of $FeSH^+$ and the solid $Fe(SH)_2$

Equ. 3: Fe^{2+} 2 HS^- -> $Fe(HS)_2$

The second stage of the reaction involves the condensation of $Fe(SH)_2$ to FeS with the release of dissolved sulfide (Rickard et al., 1995 and references therein).

Equ. 4: $Fe(SH)_2$ -> FeS + H_2S

The hydrogen sulfide pathway dominates in acid pH and at sulfide concentrations below 10^{-3} M whereas the bisulfide pathway is faster at neutral to alkaline pH and sulfide concentrations above 10^{-3} M and temperatures below 25 °C (Rickard & Luther, 1997). Most pyrite reactions suggested a two step process. First H_2S reacts with dissolved Fe^{2+} or reactive Fe (III) to form meta stabile iron sulfide compounds which subsequently react with elemental sulfur or polysulfides to form pyrite (FeS_2) (Berner, 1970; Pyzik & Sommer, 1981).

Equ. 5: FeS + S_0 -> FeS_2

A more rapid process is also possible with H_2S acting as oxidant in the absence of S_0 (Rickard & Luther, 1997).

Equ. 6: $FeS + H_2S \rightarrow FeS_2 + H_2$

A third way is the progressive solid state oxidation of precursor iron sulfides (Schoonen & Barns, 1991). Microbial sulfate reduction is mainly limited by the availability of reactive organic matter whereas the pyritization rate is additionally controlled by supply of reactive iron and dissolved sulfate from the overlying water (Berner, 1989). Therefore, pyrite formation is of minor importance in deep sea- and carbonate sediments (Morse & Berner, 1995).

The effect of temperature and organic matter content on microbial activity and corresponding iron cycling in the investigated intertidal surface sediments has been demonstrated by studies of microbial sulfate reduction (Böttcher et al., 1998, 2000; 2004; Bosselmann et al., 2003, in prep.). Abiotic reduction with inorganic compounds are competing processes for microbial mediated reduction and difficult to distinguish. Bacterial Mn and Fe reduction inhibits and therefore competes with sulfate reduction when a sufficient amount of reactive metal oxides is available (Lovley & Phillips, 1987; King, 1990) as well as Mn reduction can partially inhibit Fe reduction (Lovley & Phillips, 1987; Myers & Nealson, 1988; Thamdrup et al., 1994). Therefore, anaerobic sulfate reduction is an important pathway of organic matter decomposition (Jørgensen, 1977, Canfield et al., 1993a,b).

References

Achtnich, C., F. Bak and R. Conrad, 1995a, Competition for electron donors among nitrate reducers, ferric iron reducers, sulfate reducers, and methanogens in anoxic paddy soil: Biology and Fertility of Soils, 19: 65-72.

Achtnich, C., A. Schuhmann, T. Wind, and R. Conrad, 1995b, Role of Interspecies H_2 Transfer to Sulfate and Ferric Iron-Reducing Bacteria in Acetate Consumption in Anoxic Paddy Soil: FEMS Microbiology Ecology, 16: 61-69.

Agosta, K., 1985, The effect of tidally induced changes in the creekbank water table on pore water chemistry: Estuarine, Coastal and Shelf Science, 21: 389-400.

Aller, R. C., 1994a, The Sedimentary Mn Cycle in Long-Island Sound - Its Role as Intermediate Oxidant and the Influence of Bioturbation, O_2, and $C_{(Org)}$ Flux on Diagenetic Reaction Balances: Journal of Marine Research, 52: 259-295.

Aller, R. C., 1994b, Bioturbation and Remineralization of Sedimentary Organic-Matter - Effects of Redox Oscillation: Chemical Geology, 114: 331-345.

Aller, R. C., 2001, Transport and reactions in the bioirrigation zone. In: Boudreau B.P., Jørgensen, B. B. (eds), The Benthic Boundary Layer: Oxford, Oxford University Press: 269-301.

Aller, R. C., and J. Y. Aller, 1998, The effect of biogenic irrigation intensity and solute exchange on diagenetic reaction rates in marine sediments: Journal of Marine Research, 56: 905-936.

Aller, R. C., and P. D. Rude, 1988, Complete oxidation of solid phase sulfides by manganese and bacteria in anoxic marine sediments: Geochimica et Cosmochimica Acta, 52: 751-765.

Anderson, J. G., and P. S. Meadows, 1978, Microenvironments in marine sediments: Proc. R.Soc. Edinburgh Sect. B, 76: 1-16.

Bacon, M. P., P. G. Brewer, D. W. Spencer, J. W. Murray, and J. Goddard, 1980, Lead-210, polonium-210, manganese and iron in the Cariaco Trench: Deep Sea Research Part A. Oceanographic Research Papers, 27: 119-135.

Balkwill, D. L., D. Maratea, and R. P. Blakemore, 1980, Ultrastructure of a magnetotactic spirillum: Journal of Bacteriology, 141: 1399-1408.

Bazylinski, D. A., R. B. Frankel, and H. W. Jannasch, 1988, Anaerobic magnetite production by a marine, magnetotactic bacterium: Nature, 334: 518-519.

Berner, R. A., 1970, Sedimentary pyrite formation: American Journal of Science, 268: 1-23.

Berner, R. A., 1971, Principles of Chemical Sedimentology, McGraw-Hill.

Berner, R. A., 1978, Sulfate reduction and the rate of depostition of marine sediments: Earth Planet.Sci.Lett., 37: 492-498.

Berner, R. A., 1982, Burial of organic carbon and pyrite sulfur in the modern ocean: its geochemical and environmental significance: American Journal of Science, 282: 451-473.

Berner, R. A., 1989, Biogeochemical cycles of carbon and sulfur and their effect on atmospheric oxygen over phanerozoic time: Paleogeogr. Paleoclimatol. Palaeoecol., 75: 97-122.

Berner, R. A., and J. T. Westrich, 1985, Bioturbation and the early diagenesis of carbon and sulfur: American Journal of Science, 285: 193-206.

Billerbeck, M., U. Werner, K. Bosselmann, E. Walpersdorf, and M. Huettel, 2006a, Nutrient release from an exposed intertidal sand flat: Marine Ecology Progress Series, 316: 35-51.

Billerbeck, M., U. Werner, L. Polerecky, E. Walpersdorf, D. de Beer, and M. Huettel, 2006b, Surficial and deep pore water circulation governs spatial and temporal scales of nutrient recycling in intertidal sand flat sediment: Marine Ecology Progress Series, 326: 61-76.

Böttcher, M. E., 1998, Manganese (II) partitioning during experimental precipitation of rhodochrosite-calcite solid solutions from aqueous solutions: Marine Chemistry, 62: 287-297.

Böttcher, M. E., 1999, The stable isotopic geochemistry of the sulfur and carbon cycles in a modern karst environment: Isotopes in Environmental and Health Studies, 35: 39-61.

Böttcher, M. E., 2001, Sulfur isotope fractionation in the biogeochemical sulfur cycle of marine sediments: Isotopes in Environmental and Health Studies, 37: 97-99.

Böttcher, M. E., B. Hespenheide, H. J. Brumsack, and K. Bosselmann, 2004, Stable isotope biogeochemistry of the sulfur cycle in modern marine sediments: I. Seasonal dynamics in a temperate intertidal sandy surface sediment: Isotopes in Environmental and Health Studies, 40: 267-283.

Böttcher, M. E., B. Hespenheide, E. Llobet-Brossa, C. Beardsley, O. Larsen, A. Schramm, A. Wieland, G. Böttcher, U. G. Berninger, and R. Amann, 2000, The biogeochemistry, stable isotope geochemistry, and microbial community structure of a temperate intertidal mudflat: an integrated study: Continental Shelf Research, 20: 1749-1769.

Böttcher, M. E., and H. Huckriede, 1997, First occurrence and stable isotope composition of authigenic gamma-MnS in the central Gotland Deep (Baltic Sea): Marine Geology, 137: 201-205.

Böttcher, M. E., B. Thamdrup, M. Gehre, and A. Theune, 2005, $^{34}S/^{32}S$ and $^{18}O/^{16}O$ fractionation during sulfur disproportionation by Desulfobulbus propionicus: Geomicrobiology Journal, 22: 219-226.

Böttcher, M. E., B. Thamdrup, and T. W. Vennemann, 2001, Oxygen and sulfur isotope fractionation during anaerobic bacterial disproportionation of elemental sulfur: Geochimica et Cosmochimica Acta, 65: 1601-1609.

Bond, D. R., and D. R. Lovley, 2002, Reduction of Fe(III) oxide by methanogens in the presence and absence of extracellular quinones: Environmental Microbiology, 4: 115-124.

Buchwald, K., 1990, Nordsee. Ein Lebensraum ohne Zukunft?: Göttingen, Verlag Die Werkstatt.

Burdige, D. J., 1993, The Biogeochemistry of Manganese and Iron Reduction in Marine-Sediments: Earth-Science Reviews, 35: 249-284.

Burdige, D. J., and K. H. Nealson, 1986, Chemical and microbial studies of sulfide mediated manganese reduction: Geomicrobiology Journal, 4: 361-387.

Burnett, W. C., H. Bokuniewicz, M. Huettel, W. S. Moore, and M. Taniguchi, 2003, Groundwater and pore water inputs to the coastal zone: Biogeochemistry, v. 66, p. 3-33.

Burns, R. J., and V. M. Burns, 1979, Manganese oxides: In: Marine Minerals, in R. G. Burns (eds), Reviews in Minerology, 6: Washington DC, Mineralogy Society of America: 1-46.

Cahoon, L. B., 1999, The role of benthic microalgae in neritic ecosystems: Oceanography and Marine Biology, 37: 47-86.

Campbell, E. E., and G. C. Bate, 1998, Tide-induced pulsing of nutrient discharge from an unconfined aquifer into an *Anaulus australis*-dominated surf-zone: Water SA, 24: 365-370.

Canfield, D. E., 1989, Reactive iron in marine sediments: Geochimica et Cosmochimica Acta, 53: 619-632.

Canfield, D. E., 1997, The geochemistry of river particulates from the continental USA: Major elements: Geochimica et Cosmochimica Acta, 61: 3349-3365.

Canfield, D. E., B. B. Jørgensen, H. Fossing, R. Glud, J. Gundersen, N. B. Ramsing, B. Thamdrup, J. W. Hansen, L. P. Nielsen, and P. O. J. Hall, 1993a, Pathways of Organic-Carbon Oxidation in 3 Continental-Margin Sediments: Marine Geology, 113: 27-40.

Canfield, D. E., R. Raiswell, and S. Bottrell, 1992, The Reactivity of Sedimentary Iron Minerals toward Sulfide: American Journal of Science, 292: 659-683.

Canfield, D. E., B. Thamdrup, and J. W. Hansen, 1993b, The Anaerobic Degradation of Organic-Matter in Danish Coastal Sediments - Iron Reduction, Manganese Reduction, and Sulfate Reduction: Geochimica et Cosmochimica Acta, 57: 3867-3883.

Chang, T. S., B. W. Flemming, E. Tilch, A. Bartholomä, and R. Wöstmann, 2006, Late Holocene stratigraphic evolution of a back-barrier tidal basin in the East Frisian Wadden Sea, southern North Sea: transgressive deposition and its preservation potential: Facies, 52: 329-340.

Cornell, R. M., and U. Schwertmann, 1996, The Iron Oxides: Weinheim, VCH.

D'Andrea, A. F., R. C. Aller, and G. R. Lopez, 2002, Organic matter flux and reactivity on a South Carolina sandflat: The impacts of porewater advection and macrobiological structures: Limnology and Oceanography, 47: 1056-1070.

Dauwe, B., J. J. Middelburg, and P. M. J. Herman, 2001, Effect of oxygen on the degradability of organic matter in subtidal and intertidal sediments of the North Sea area: Marine Ecology Progress Series, 215: 13-22.

Davis, R. B., 1974, Tubificids alter profiles of redox potential and pH in porfundal lake sediments: Limnology and Oceanography, 19: 342-346.

de Beer, D., F. Wenzhofer, T. G. Ferdelman, S. E. Boehme, M. Huettel, J. E. E. van Beusekom, M. E. Bottcher, N. Musat, and N. Dubilier, 2005, Transport and mineralization rates in North Sea sandy intertidal sediments, Sylt-Rømø Basin, Wadden Sea: Limnology and Oceanography, 50: 113-127.

De Vitre, R. R., and W. Davison, 1993, Manganese particles in freshwater: In: H. P. van Leeuwen and J. Buffle (eds), Environmental Particles, 2: Boca Raton, Lewis: 317-352.

Dellwig, O., K. Bosselmann, S. Kölsch, M. Hentscher, J. Hinrichs, M. E. Böttcher, R. Reuter, and H.-J. Brumsack, 2007, Sources and fate of manganese in a tidal basin of the German Wadden Sea: Journal of Sea Research, 57: 1-18.

Dellwig, O., M. E. Böttcher, M. Lipinski, and H. J. Brumsack, 2002, Trace metals in Holocene coastal peats and their relation to pyrite formation (NW Germany): Chemical Geology, 182: 423-442.

Dellwig, O., F. Watermann, H. J. Brumsack, and G. Gerdes, 1999, High-resolution reconstruction of a holocene coastal sequence (NW Germany) using inorganic geochemical data and diatom inventories: Estuarine Coastal and Shelf Science, 48: 617-633.

Drodt, M., A. X. Trautwein, I. König, E. Suess, and C. B. Koch, 1997, Mossbauer spectroscopic studies on the iron forms of deep-sea sediments: Physics and Chemistry of Minerals, 24: 281-293.

Ehlers, J., 1994, Geomorphoplogie und Hydrographie des Wattenmeeres: In: J. L. Lozán, E. Rachor, K. Reise, and H. v. Westernhagen (eds), Warnsignale aus dem Wattenmeer: Berlin, Blackwell Wissenschaftsverlag.

Flemming, B., A. Bartholomä, G. Irion, I. Kröncke, and A. Wehrmann, 2002, Naturraum Wattenmeer: Akademie der Geowissenschaften zu Hannover, 20: 150-159.

Flemming, B., and K. Ziegler, 1995, High-resolution grain size distribution patterns and textural trends in the backbarrier environment of Spiekeroog island (southern North Sea): Senckenbergiana maritima, 26: 1-24.

Flies, C. B., H. M. Jonkers, D. de Beer, K. Bosselmann, M. E. Böttcher, and D. Schüler, 2005, Diversity and vertical distribution of magnetotactic bacteria along chemical gradients in freshwater microcosms: Fems Microbiology Ecology, 52: 185-195.

Forster, S., M. Huettel, and W. Ziebis, 1996, Impact of boundary layer flow velocity on oxygen utilisation in coastal sediments: Marine Ecology Progress Series, 143: 173-185.

Friedl, G., 1997, Solid phases in the cycling of manganese in eutrophic lakes: New insights from EXAFS spectroscopy: Erratum to Friedl, B. Wehrli, and A. Manceau (1997): Geochimica et Cosmochimica Acta, 61: 3277.

Froelich, P. N., G. P. Klinkhammer, M. L. Bender, N. A. Luedtke, G. R. Heath, D. Cullen, P. Dauphin, D. Hammond, B. Hartman, and V. Maynard, 1979, Early oxidation of organic matter in pelagic sediments of the eastern equatorial Atlantic: suboxic diagenesis: Geochimica et Cosmochimica Acta, 43: 1075-1090.

Gätje, C., and K. Reise, 1998, Ökosystem Wattenmeer. Austausch-, Transport- und Stoffwandlungs-prozesse: Berlin, Heidelberg, New York, Springer Verlag.

Gattuso, J. P., M. Frankignoulle, and R. Wollast, 1998, Carbon and carbonate metabolism in coastal aquatic ecosystems: Annual Review of Ecology and Systematics, 29: 405-434.

Goldhaber, M. B., and I. R. Kaplan, 1974, The sulfur cycle: In: E. D. Goldberg (eds), The Sea, Wiley: 569-655.

Graf, G., and R. Rosenberg, 1997, Bioresuspension and biodeposition: A review: Journal of Marine Systems, 11: 269-278.

Haese, R. R., J. Schramm, M. M. R. van der Loeff, and H. D. Schulz, 2000, A comparative study of iron and manganese diagenesis in continental slope and deep sea basin sediments of Uruguay (SW Atlantic): International Journal of Earth Sciences, 88: 619-629.

Haese, R. R., K. Wallmann, A. Dahmke, U. Kretzmann, P. J. Müller, and H. D. Schulz, 1997, Iron species determination to investigate early diagenetic reactivity in marine sediments: Geochimica et Cosmochimica Acta, 61: 63-72.

Herbert, R. A., 1999, Nitrogen cycling in coastal marine ecosystems: Microbiology Reviews, 23: 563-590.

Huettel, M., and G. Gust, 1992, Impact of Bioroughness on Interfacial Solute Exchange in Permeable Sediments: Marine Ecology Progress Series, 89: 253-267.

Huettel, M., H. Røy, E. Precht, and S. Ehrenhauss, 2003, Hydrodynamical impact on biogeochemical processes in aquatic sediments: Hydrobiologia, 494: 231-236.

Huettel, M., and A. Rusch, 2000, Transport and degradation of phytoplankton in permeable sediment: Limnology and Oceanography, 45: 534-549.

Huettel, M., W. Ziebis, and S. Forster, 1996, Flow-induced uptake of particulate matter in permeable sediments: Limnology and Oceanography, 41: 309-322.

Hulth, S., R. C. Aller, and F. Gilbert, 1999, Coupled anoxic nitrification manganese reduction in marine sediments: Geochimica et Cosmochimica Acta, 63: 49-66.

Jahnke, R. A., J. R. Nelson, R. L. Marinelli, and J. E. Eckman, 2000, Benthic flux of biogenic elements on the Southeastern US continental shelf: influence of pore water advective transport and benthic microalgae: Continental Shelf Research, 20: 109-127.

Jakobsen, R., and D. Postma, 1999, Redox zoning, rates of sulfate reduction and interactions with Fe-reduction and methanogenesis in a shallow sandy aquifer, Rømø, Denmark: Geochimica et Cosmochimica Acta, 63: 137-151.

Jørgensen, B. B., 1977, The sulfur cyle of a coastal marine sediment (Limfjorden, Denmark): Limnology and Oceanography, 22: 814-832.

Jørgensen, B. B., 1982, Mineralization of organic matter in the sea bed-the role of sulphate reduction: Nature, 296: 643-645.

Jørgensen, B. B., 1983a, The microbial sulfur cycle. In: W. E. Krumbein (eds), Microbial geochemistry: London, Blackwell: 91-124.

Jørgensen, B. B., 1983b, Processes at the sediment-water interface. In: B. Bolin, and R. C. Cook (eds), The major biogeochemical cycles and their interactions: SCOPE: 477-509.

Jørgensen, B. B., and K. Richardson (eds), 1996, Eutrophication in coastal marine ecosystems: Am. Geophys. Union: 115-135.

Jørgensen, B. B., 2000, Bacteria and marine biogeochemistry: In: H. D. Schulz, and M. Zabel (eds), Marine Geochemistry: Berlin, Springer Verlag: 173-207.

Kallmeyer, J., T. G. Ferdelman, A. Weber, H. Fossing, and B. B. Jørgensen, 2004, A cold chromium distillation procedure for radiolabeled sulfide applied to sulfate reduction measurements: Limnology and Oceanography: Methods, 2: 171-180.

Kappler, A., M. Benz, B. Schink, and A. Brune, 2004, Electron shuttling via humic acids in microbial iron (III) reduction in a freshwater sediment: Microbiology Ecology, 47: 85-92.

King, G. M., 1990, Effects of added manganic and ferric oxides on sulfate reduction and sulfide oxidation in intertidal sediments: FEMS Microbiology Letters, 73: 131-138.

König, I., M. Drodt, E. Suess, and A. X. Trautwein, 1997, Iron reduction through the tan-green color transition in deep-sea sediments: Geochimica et Cosmochimica Acta, 61: 1679-1683.

Kostka, J. E., and G. W. Luther, 1994, Partitioning and Speciation of Solid-Phase Iron in Salt-Marsh Sediments: Geochimica et Cosmochimica Acta, 58: 1701-1710.

Kostka, J. E., and K. H. Nealson, 1995, Dissolution and Reduction of Magnetite by Bacteria: Environmental Science and Technology, 29: 2535-2540.

Kostka, J. E., J. W. Stucki, K. H. Nealson, and J. Wu, 1996, Reduction of structural Fe(III) in smectite by a pure culture of *Shewanella putrefaciens* strain MR-1: Clays and Clay Minerals, 44: 522-529.

Kostka, J. E., J. Wu, K. H. Nealson, and J. W. Stucki, 1999, The impact of structural Fe (III) reduction by bacteria on the surface chemistry of smectite clay minerals: Geochimica et Cosmochimica Acta, 63: 3705-3713.

LaKind, J. S., and A. T. Stone, 1989, Reductive dissolution of goethite by phenolic reductants: Geochimica et Cosmochimica Acta, 53: 961-971.

Langmuir, D., 1971, Particle size effect on the reaction geothite = hematite + water: American Journal of Science, 271: 147-156.

Lehmann, C., and R. Bachofen, 1999, Images of concentrations of dissolved sulfide in the sediment of a lake and implications for internal sulfur cycling: Sedimentology, 46: 537-544.

Llobet-Brossa, E., R. Rabus, M. E. Böttcher, M. Könneke, N. Finke, A. Schramm, R. L. Meyer, S. Grötzschel, R. Rosselló-Mora, and R. Amann, 2002, Community structure and activity of sulfate-reducing bacteria in an intertidal surface sediment: a multi-method approach: Aquatic Microbial Ecology, 29: 211-226.

Llobet-Brossa, E., R. Rosselló-Mora, and R. Amann, 1998, Microbial community composition of Wadden Sea sediments as revealed by fluorescence in situ hybridization: Applied and Environmental Microbiology, 64: 2691-2696.

Lotze, H. K., K. Reise, B. Worm, J. van Beusekom, M. Busch, A. Ehlers, D. Heinrich, R. C. Hoffmann, P. Holm, C. Jensen, O. S. Knottnerus, N. Langhanki, W. Prummel, M. Vollmer, and W. J. Wolff, 2005, Human transformations of the Wadden Sea ecosystem through time: a synthesis: Helgoland Marine Research, 59: 84-95.

Lovley, D. R., 1991, Dissimilatory Fe(III) and Mn(IV) Reduction: Microbiological Reviews, 55: 259-287.

Lovley, D. R., 1995, Microbial Reduction of Iron, Manganese, and other Metals: Advances in Agronomy, 54: 175-231.

Lovley, D. R., 1997, Microbial Fe(III) reduction in subsurface environments: Microbiology Reviews, 20: 305-313.

Lovley, D. R., J. D. Coates, E. L. Blunt-Harris, E. J. P. Phillips, and J. C. Woodward, 1996, Humic substances as electron acceptors for microbial respiration: Nature, 382: 445-448.

Lovley, D. R., J. L. Fraga, E. L. Blunt-Harris, L. A. Hayes, E. J. P. Phillips, and J. D. Coates, 1998, Humic substances as a mediator for microbially catalyzed metal reduction: Acta Hydrochimica et Hydrobiologica, 26: 152-157.

Lovley, D. R., D. E. Holmes, and K. P. Nevin, 2004, Dissimilatory Fe(III) and Mn(IV) reduction: Advances in Microbial Physiology, 49: 219-286.

Lovley, D. R., and E. J. P. Phillips, 1987, Competitive mechanisms for inhibition of sulfate reduction and methane production in the zone of ferric iron reduction in sediments: Applied and Environmental Microbiology, 53: 2636-2641.

Lovley, D. R., and E. J. P. Phillips, 1988, Manganese inhibition of microbial iron reduction in anaerobic sediments: Applied and Environmental Microbiology, 53: 145-155.

Lovley, D. R., and E. J. P. Phillips, 1994, Novel Processes for Anaerobic Sulfate Production from Elemental Sulfur by Sulfate-Reducing Bacteria: Applied and Environmental Microbiology, 60: 2394-2399.

Lovley, D. R., E. J. P. Phillips, and D. J. Lonergan, 1989, Microbially Catalyzed Reduction of Iron in Aquatic Sediments and Groundwater: Abstracts of Papers of the American Chemical Society, 198: 82-GEOC.

Lovley, D. R., E. E. Roden, E. J. P. Phillips, and J. C. Woodward, 1993, Enzymatic Iron and Uranium Reduction by Sulfate Reducing Bacteria: Marine Geology, 113: 41-53.

Luther, G. W., B. Sundby, B. L. Lewis, P. J. Brendel, and N. Silverberg, 1997, Interactions of manganese with the nitrogen cycle: Alternative pathways to dinitrogen: Geochimica et Cosmochimica Acta, 61: 4043-4052.

Lyle, M., 1983, The green-brown color transition in marine sediments: A marker of the Fe(III)-Fe(II) redox boundary: Limnology and Oceanography, 28: 1026-1033.

Martin, J.-M., and M. Meybeck, 1979, Elemental mass-balance of material carried by major world rivers: Marine Chemistry, 7: 173-206.

Meadows, P. S., and J. Tait, 1989, Modification of sediment permeability and shear strength by two burrowing invertebrates: Marine Biology, 101: 75-82.

Meysman, F. J. R., O. S. Galaktionov, B. Gribsholt, and J. J. Middelburg, 2006, Bio-irrigation in permeable sediments: An assessment of model complexity: Journal of Marine Research, 64: 589-627.

Michalopoulos, P., and R. C. Aller, 1995, Rapid Clay Mineral Formation in Amazon Delta Sediments: Reverse Weathering and Oceanic Elemental Cycles: Science, 270: 614-617.

Middelburg, J. J., G. J. De Lange, and C. H. van Der Weijden, 1987, Manganese solubility control in marine pore waters: Geochimica et Cosmochimica Acta, 51: 759-763.

Millero, F. J., S. Sotolongo, and M. Izaguirre, 1987, The oxidation kinetics of Fe (II) in seawater: Geochimica et Cosmochimica Acta, 51: 793-801.

Moore, W. S., J. Krest, G. Taylor, E. Roggenstein, S. Joye, and R. Lee, 2002, Thermal evidence of water exchange through a coastal aquifer: Implications for nutrient fluxes: Geophysical Research Letters, 29(14), 1704.

Morgan, J. J., and W. Stumm, 1964, Colloid-chemical properties of manganese dioxide: J.Colloid Sci., 19: 347-359.

Murray, J. W., 1979, Iron oxides: In: R. G. Burns (eds), Marine Minerals, Reviews in Mineralogy, 6: Washington DC, Mineralogical Society of America: 47-97.

Mussmann, M., K. Ishii, R. Rabus, and R. Amann, 2005, Diversity and vertical distribution of cultured and uncultured Deltaproteobacteria in an intertidal mud flat of the Wadden Sea: Environmental Microbiology, 7: 405-418.

Myers, C. R., and K. H. Nealson, 1988, Microbial reduction of manganese oxides: Interactions with iron and sulfur: Geochimica et Cosmochimica Acta, 52: 2727-2732.

Nealson, K. H., and C. R. Myers, 1992, Microbial Reduction of Manganese and Iron - New Approaches to Carbon Cycling: Applied and Environmental Microbiology, 58: 439-443.

Polerecky, L., U. Franke, U. Werner, B. Grunwald, and D. de Beer, 2005, High spatial resolution measurement of oxygen consumption rates in permeable sediments: Limnology and Oceanography: Methods, 3: 75-85.

Postma, D., and R. Jakobsen, 1996, Redox zonation: Equilibrium constraints on the Fe(III)/SO^{4-} reduction interface: Geochimica et Cosmochimica Acta, 60: 3169-3175.

Postma, H., 1984, Introduction to the symposium of organic matter in the Wadden Sea: Neth.Inst.Publ.Ser, 10: 15-22.

Pyzik, A. J., and S. E. Sommer, 1981, Sedimentary iron monosulfides: Kinetics and mechanism of formation: Geochimica et Cosmochimica Acta, 45: 687-698.

Raiswell, R., and D. E. Canfield, 1998, Sources of iron for pyrite formation in marine sediments: American Journal of Science, 298: 219-245.

Reise, K., 2005, Coast of change: habitat loss and transformations in the Wadden Sea: Helgoland Marine Research, 59: 9-21.

Rickard, D., M. A. A. Schoonen, and G. W. Luther, 1995, Chemistry of Iron Sulfides in Sedimentary Environments: In: M. A. Vairavamurthy and M. A. A. Schoonen (eds), Geochemical Transformations of Sedimentary Sulfur, 612: Washington, DC, American Chemical Society: 168-193.

Rickard, D. T., and G. W. Luther, 1997, The formation of pyrite: Abstracts of Papers of the American Chemical Society, 214: 1-GEOC.

Riedl, R. J., N. Huang, and R. Machan, 1972, The subtidal pump: Mechanism of interstitial water exchange by wave action: Marine Biology, 13: 210-221.

Rink, B., M. Lunau, S. Seeberger, H. Stevens, T. Brinkhoff, H. P. Grossart, and M. Simon, 2003, Diversity patterns of aggregate-associated and free-living bacterial communities in the German Wadden Sea., Wilhelmshaven, Forschungszentrum Terramare: 96-98.

Rowe, G. T., C. H. Clifford, K. L. J. Smith, and P. L. Hamilton, 1975, Benthic nutrient regeneration and its coupling to primary production in coastal waters: Nature, 255: 215-217.

Rusch, A., S. Forster, and M. Huettel, 2001, Bacteria, diatoms and detritus in an intertidal sandflat subject to advective transport across the water-sediment interface: Biogeochemistry, 55: 1-27.

Rusch, A., and M. Huettel, 2000, Advective particle transport into permeable sediments - evidence from experiments in an intertidal sandflat: Limnology and Oceanography, 45: 525-533.

Rusch, A., M. Huettel, and S. Forster, 2000, Particulate organic matter in permeable marine sands - Dynamics in time and depth: Estuarine Coastal and Shelf Science, 51: 399-414.

Rusch, A., H. Topken, M. E. Böttcher, and T. Höpner, 1998, Recovery from black spots: results of a loading experiment in the Wadden Sea: Journal of Sea Research, 40: 205-219.

Schidlowski, M., 1989, Organic-Carbon Cycling through Time - a 4 Billion-Year Perspective: Abstracts of Papers of the American Chemical Society, 198: 12-GEOC.

Schoonen, M. A. A., and H. L. Barnes, 1991, Mechanisms of Pyrite and Marcasite Formation from Solution. Hydrothermal Processes: Geochimica et Cosmochimica Acta, 55: 3491-3504.

Schwertmann, U., 1988, Some properties of soil and synthetic iron oxides: In: J. W. Stucki, B. A. Goodman and U. Schwertmann (eds), Iron in Soils and Clay Minerals: Dordrecht, Reidel, D: 203-250.

Shaw, T. J., W. S. Moore, J. Kloepfer, and M. A. Sochaski, 1998, The flux of barium to the coastal waters of the southeastern USA: the importance of submarine groundwater discharge: Geochimica et Cosmochimica Acta, 62: 3047-3054.

Shum, K. T., and B. Sundby, 1996, Organic matter processing in continental shelf sediments-the subtidal pump revisited: Marine Chemistry, 13th International Symposium Chemistry of the Mediterranean, 53: 81-87.

Skyring, G. W., 1987, Sulfate reduction in coastal ecosystems: Geomicrobiology Journal, 5: 295-374.

Smith, D. J., and G. J. C. Underwood, 1998, Exopolymer production by intertidal epipelic diatoms: Limnology and Oceanography, 43: 1578-1591.

Stetter, K. O., 1996, Hyperthermophilic procaryotes: FEMS Microbiology Reviews, 18: 149-158.

Stone, A. T., 1987, Microbial metabolites and the reductive dissolution of manganese oxides: Oxalate and pyruvate: Geochimica et Cosmochimica Acta, 51: 919-925.

Stone, A. T., and J. J. Morgan, 1984, Reduction and dissolution of manganese (III) and manganese (IV) oxides by organics: 2. Survey of the reactivity of organics: Environmental Science and Technology, 18: 617-624.

Straub, K. L., M. Benz, B. Schink, and F. Widdel, 1996, Anaerobic, nitrate-dependent microbial oxidation of ferrous iron: Applied and Environmental Microbiology, 62: 1458-1460.

Streif, H., 1990, Das ostfriesische Küstengebiet. Nordsee, Inseln, Watten und Marschen., 2, Gebrüder Bornträger.

Stucki, J. W., 1987, Microbial reduction of structural iron(III) in smectite: Soil Science Society of America Journal, 51: 1663-1665.

Stumm, W., and J. J. Morgan, 1981, Aquatic Chemistry: New York, Wiley & Sons.

Suess, E., 1979, Mineral phases formed in anoxic sediments by microbial decomposition of organic matter: Geochimica et Cosmochimica Acta, 43: 339-341.

Sunda, W. G., and D. J. Kieber, 1994, Oxidation of Humic Substances by Manganese Oxides Yields Low-Molecular-Weight Organic Substrates: Nature, 367, p. 62-64.

Sundby, B., and N. Silverberg, 1985, Manganese flux in the benthic boundary layer: Limnology and Oceanography, 30: 374-382.

Tebo, B. M., D. B. Edwards, D. J. Kieber, and W. G. Sunda, 1995, Bacterial Mn Oxidation Can Leads to the Degradation and Utilization of Natural Organic Matter: Abstracts of papers of the American chemical society, 209:77-GEOC.

Thamdrup, B., 2000, Bacterial manganese and iron reduction in aquatic sediments, Advances in Microbial Ecology, 16: 41-84.

Thamdrup, B., K. Finster, J. W. Hansen, and F. Bak, 1993, Bacterial Disproportionation of Elemental Sulfur Coupled to Chemical-Reduction of Iron or Manganese: Applied and Environmental Microbiology, 59: 101-108.

Thamdrup, B., H. Fossing, and B. B. Jørgensen, 1994, Manganese, Iron, and Sulfur Cycling in a Coastal Marine Sediment, Aarhus Bay, Denmark: Geochimica et Cosmochimica Acta, 58: 5115-5129.

Thullner, M., J. Zeyer, and W. Kinzelbach, 2002, Influence of microbial growth on hydraulic properties of pore networks: Transport in Porous Media, 49: 99-122.

Todd, J. F., R. J. Elsinger, and W. S. Moore, 1988, The distributions of uranium, radium and thorium isotopes in two anoxic fjords: Framvaren Fjord (Norway) and Saanich Inlet (British Columbia): Marine Chemistry, 23: 393-415.

Trudinger, P. A., 1992, Bacterial sulfate reduction: current status and possible origin., in M. Schidlowiski, S. Golubic, M. M. Kimberley, D. M. McKirdy, and P. A. Trudinger, eds., Early organic evolution: Berlin, Springer: 367-377.

Ullman, W. J., B. Chang, D. C. Miller, and J. A. Madsen, 2003, Groundwater mixing, nutrient diagenesis, and discharges across a sandy beachface, Cape Henlopen, Delaware (USA): Estuarine Coastal and Shelf Science, 57: 539-552.

Vairavamurthy, M. A., and M. A. A. Schoonen, 1995a, Geochemical transformation of sedimentary sulfur: 612: Washington, DC, ACS Symposium Series, 612: 16-37.

Vairavamurthy, M. A., S. K. Wang, B. Khandelwal, B. Manowitz, T. Ferdelman, and H. Fossing, 1995b, Sulfur transformations in early diagenetic sediments from the Bay of Concepcion, of Chile, Geochemical Transformations of Sedimentary Sulfur: ACS Symposium Series, 612: 38-58.

van Beusekom, J. E. E., 2005, A historic perspective on Wadden Sea eutrophication: Helgoland Marine Research, 59: 45-54.

van der Loeff, M. M. R., 1981, Wave effects on sediment water exchange in a submerged sand bed: Netherlands Journal of Sea Research, 15: 100-112.

Wallmann, K., K. Hennies, I. König, W. Petersen, and H. D. Knauth, 1993, New Procedure for Determining Reactive Fe(III) and Fe(II) Minerals in Sediments: Limnology and Oceanography, 38: 1803-1812.

Walsh, J. J., 1991, Importance of Continental Margins in the Marine Biogeochemical Cycling of Carbon and Nitrogen: Nature, 350: 53-55.

Webster, I. T., S. J. Norquay, F. C. Ross, and R. A. Wooding, 1996, Solute exchange by convection within estuarine sediments: Estuarine Coastal and Shelf Science, 42: 171-183.

Wehrli, B., 1990, Redox reactions of metal ions at mineral surfaces: In: W. Stumm (eds), Aquatic Chemical Kinetics: New York, John Wiley & Sons: 311-336.

Wei, C. L., and J. W. Murray, 1991, Th-234/U-238 Disequilibria in the Black-Sea: Deep-Sea Research Part A, Oceanographic Research Papers, 38: S855-S873.

Wenzhöfer, F., and R. N. Glud, 2004, Small-scale spatial and temporal variability in coastal benthic O_2 dynamics: Effects of fauna activity: Limnology and Oceanography, 49: 1471-1481.

Werner, U., M. Billerbeck, L. Polerecky, U. Franke, M. Huettel, J. E. E. van Beusekom, and D. de Beer, 2006, Spatial and temporal patterns of mineralization rates and oxygen distribution in a permeable intertidal sand flat (Sylt, Germany): Limnology and Oceanography, 51: 2549-2563.

Westrich, J. T., and R. A. Berner, 1988, The effect of temperature on rates of sulfate reduction in marine sediments: Geomicrobiology Journal, 6: 99-117.

Wollast, R., 1991, The coastal organic carbon cycle: fluxes, sources, and sinks: In: R. F. C. Mantoura, J. M. Martin and R. Wollast (eds), Ocean margin processes in global change: London, John Wiley & Sons: 365-382.

Wollast, R., 2002, Contiental margins - review of geochemical settings: In: G. Wefer, D. Billet, D. Hebbeln, B. B. Jørgensen, M. Schlüter and T. C. E. van Weering (eds), Ocean margin systems., Springer.

Zeiler, M., J. Schulz-Ohlberg, and K. Figge, 2000, Mobile sand deposits and shoreface sediment dynamics in the inner German Bight (North Sea): Marine Geology, 170: 363-380.

The main objectives of this thesis

This thesis focuses on is the investigation of factors controlling the cycle of manganese, iron and sulfur in different types of intertidal sediments. Field studies and laboratory incubations were carried out to investigate the seasonal dynamics of the biogeochemical reactions in the sedimentary sulfur cycle and the closely connected element cycles of iron and manganese. The interactions of geochemical and microbial processes with the decomposition of organic matter were compared between sand, mixed and mud flats. Concurrent measurements of microbial sulfate reduction, dissolved and reactive iron and manganese pools, organic stock and temperature dynamics in different sediments demonstrate the strong effect of the activity of sulfate reducing bacteria on metal cycling.

The main interest presented in the **2nd chapter** is the regulation of the overall sulfate reduction activity in different sediment types and the formation and accumulation of reduced sulfur compounds in relation to the Fe and Mn cycles. In order to examine the influence of highly dynamic temperature conditions on sulfate reducing activity a model was applied to simulate the development of temperature-induced changes. The Arrhenius equation relates the effect of changing temperature to the rate of biogeochemical processes. Meteorological and tidal conditions regulate the soil heat of intertidal sediments. Under the influence of the tidal changes steep vertical temperature gradients can develop in intertidal sediments. The magnitude of theses gradients is related to the timing of exposure to the atmosphere and meteorological conditions e.g. net radiation, wind speed before tidal inundation etc. The tidal flooding of intertidal sediments induces a rapid exchange of heat across the sediment-water interface and the temperature profiles tend to become equal to the temperature of the overlying water column. The model allows to relate the laboratory determined SRR to in situ conditions under the influence of the tidal dynamics.

In **chapter 3,** the cycles of Mn and its fluxes across the sediment-water interface were investigated in a quantitative manner in order to understand the role of the benthic biogeochemistry on element cycling and interactions between Mn, Fe, and sulfur (S) in surface sediments (Böttcher et al., 2004; Bosselmann et al., 2003, in prep.). A combination of pore water, solid phase analyses and benthic chamber incubations was applied to study Mn cycling in different intertidal sediment types. Intertidal sediments are characterized by tidal and seasonal fluctuations of biological, chemical and physical properties and transformation processes at the sediment-water interface. Therefore, a variety of processes occurs particularly at the sediment-water interface driving the biogeochemical cycling of redox sensitive metals as manganese and iron. Water column concentrations of dissolved manganese (Mn) are elevated in the Wadden Sea compared to the open North Sea and showed seasonality with

highest Mn concentrations during summer time (Dellwig et al., 2007). This indicates that tidal flat sediments may form a very important source for Mn.

Chapter 4 describes an in situ monitoring technique to visualize the spatial distribution of dissolved sulfide in a 2-dimensional manner. The procedure has been laboratory tested and applied to intertidal surface sediments under in-situ conditions. The technique is based on the fixation of dissolved hydrogen sulfide as black silver-sulfide (Ag_2S) on photographic paper, modified after Lehmann & Bachofen (1999). The accumulation of Ag_2S can be measured densitometrically by using a conventional flat bed scanner and imaging software. The colour change is quantitatively related to the amount of Ag_2S. Here, we present the further development and evaluation of the technique by performance of calibration experiments and comparative measurements of sulfate reduction rates using the whole-core $^{35}SO_4^{2-}$ tracer incubation technique (Kallmeyer et al., 2004). The 2D Photopaper technique was deployed within the top 15 cm in different types of intertidal sediments, where high activities of sulfate reducing bacteria have been found (Böttcher et al., 2004, Bosselmann & Böttcher, in prep.).

Overview about enclosed manuscripts

This thesis was carried out within the Research Group `BioGeoChemistry of Tidal Flats` funded by the Deutsche Forschungsgemeinschaft (DFG) as part of the sub-project 7, dealing with `Biogeochemical Processes at the Sediment-Water Interface of Intertidal Sediments` under the leadership of Bo Barker Jørgensen and Michael E. Böttcher.

The thesis comprises seven manuscripts. Chapter 2-4 will be submitted to international scientific journals (therefore, following the review-process, their final published form may differ from the manuscripts presented here as chapters). Four manuscripts (Chapter 5-8) were published with the author´s contribution as co-author.

Chapter 1: provides a general introduction into the subject and gives the scientific context of the manuscripts.

Chapter 2: Microbial sulfate reduction in intertidal sediments surface sediments of the southern North Sea: Seasonal and spatial dynamics, and controlling factors.

by Katja Bosselmann, Michael E. Böttcher

The concept of the study was developed by K. Bosselmann and M.E. Böttcher. Sampling analysis and evaluation of data was carried out by the author who also did the writing, supported by suggestions of the co-author.

Chapter 3: Dynamics of manganese in intertidal surface sediments.

by Katja Bosselmann, Michael E. Böttcher, Hans Jürgen Brumsack and Markus Billerbeck

The study was initiated by K. Bosselmann and M.E. Böttcher. Field experiments were carried out by K. Bosselmann and benthic chamber experiments were performed in common with M. Billerbeck. M. Billerbeck also contributed oxygen data to the manuscript which was written by K. Bosselmann.

Chapter 4: A facile in-situ procedure for dissolved sulfide measurement with a 2D Photopaper Technique in intertidal surface sediments.

by Katja Bosselmann, Michael E. Böttcher, Alexandra Theune and Eva Walpersdorf

The concept of the study was developed by K. Bosselmann, M. E. Böttcher and A. Theune. Sampling analysis and evaluation of data was carried out by K. Bosselmann, who also did the writing. E. Walpersdorf contributed the hydrogensulfide data. The manuscript will be prepared for submission to Limnology & Oceanography: Methods.

Additionally, four manuscripts with my contribution as coauthor are attached in this thesis (Chapter 5-8).

Chapter 5: Sources and fate of manganese in a tidal basin of the German Wadden Sea

by Olaf Dellwig, Katja Bosselmann, Sybille Kölsch, Michael Hentscher , Joachim Hinrichs, Michael E. Böttcher, Rainer Reuter and Hans Jürgen Brumsack, Journal of sea research 57 (1): 1-18 JAN 2007, to which K. Bosselmann contributed a chapter (4.2.2.) about the sedimentary Mn cycling, including sulfate reduction rates and concentrations of dissolved and solid Mn.

Chapter 6: Nutrient release from an exposed intertidal sand flat

By Markus Billerbeck, Ursula Werner, Katja Bosselmann, Eva Walpersdorf, Markus Huettel

Marine ecology progress series 316: 35-51 2006.

This field experiments were carried out by M. Billerbeck, U. Werner., E. Walpersdorf. and benthic chamber experiments with contribution of K. Bosselmann. M. Billerbeck evaluated the manuscript with editorial help from the co-authors.

Chapter 7: Benthic photosynthesis in submerged Wadden Sea intertidal flats

By Markus Billerbeck, Hans Røy, Katja Bosselmann and Markus Huettel

Estuarine coastal and shelf science 71 (3-4): 704-716 FEB 2007

M. Billerbeck., H. Roy., M. Huettel developed the concept for this study. This field experiments were carried out by M. Billerbeck, and benthic chamber experiments with contribution of K. Bosselmann. M. Billerbeck evaluated the manuscript with editorial help from the co-authors.

Chapter 8: Diversity and vertical distribution of magnetotactic bacteria along chemical gradients in freshwater microcosms

Christine B. Flies, Henk M. Jonkers, Dirk de Beer, Katja Bosselmann, Michael E. Böttcher and Dirk Schüler, FEMS Microbiology Ecology 52 (2): 185-195 APR 1 2005.

Experimental lab incubations were performed to correlate the vertical distribution of magnetotactic bacteria to the geochemical zonation in the sediment. In order to retrieve information about biogeochemical stratification, vital for the bacteria, my contributions comprised the measurement of dissolved iron and sulfide in the pore water, the availability of reactive solid iron and the microbial sulfate reduction. In addition, the 2D Photopaper technique was applied to visualize the retention of sulfide within the sediment and to get a 2-dimensional impression of the stratification.

A conclusion at the end of this thesis summarizes the main results and gives an outlook on potential future work.

Further manuscripts not included in this thesis:

Stable isotope biogeochemistry of the sulfur cycle in modern marine sediments: I. Seasonal dynamics in a temperate intertidal sandy surface sediment

Michael E. Böttcher, Britta Hespenheide, Hans Jürgen Brumsack and Katja Bosselmann

Isotopes in environmental and health studies, 40 (4): 267-283 DEC 2004

Anaerobic reactions in a muddy intertidal surface sediments: Results from incubation experiments and pore water modeling

Stephanie Batel, Katja Bosselmann, Hans-Jürgen Brumsack and Michael E. Böttcher (in prep.)

Microbial sulfate reduction in intertidal surface sediments of the southern North Sea:

Seasonal and spatial dynamics and controlling factors.

K. Bosselmann, M. E. Böttcher

In preparation

Abstract

The biogeochemistry of sulfur and the coupled iron-manganese and carbon cycles were studied in temperate intertidal surface sediments of the German Wadden Sea (North Sea). Coastal sampling sites included sand, mixed and mud flats with different organic matter and metal contents and permeability reflecting different hydrodynamic regimes. It was the goal of the present study to verify the influence of temperature, organic matter load and sediment types on the dynamics of biogeochemical reactions in the top of different intertidal surface sediments on a seasonal scale. Rates of microbial sulfatereduction were related to the dynamic of reduced sulfur and iron phases under various sedimentary conditions. Biogeochemical processes in intertidal surface sediments were influenced by diurnal temperature variations. To determine in particular daily sulfate reduction rates (SRR) in intertidal surface sediments, it is essential to consider the temperature shifts during 24 hours confirmed to be an important factor for microbial activity. Here, a model prediction is presented to consider the effect of daily temperature variations on time and depth-integrated sulfate reduction rates.

Introduction

Tidal flats are highly productive marine coastal ecosystems. Coastal marine sediments are influenced by riverine input of dissolved and particulate organic matter and high primary production (Berner, 1989). The back-barrier tidal area of the German Wadden Sea forms a transition zone between the terrestrial and marine environment. In near shore waters, high nutrient concentrations lead to increased phytoplankton growth which generates up to 30 % of the total oceanic primary production (Walsh, 1988; Wollast, 1991). Intertidal sediments are exposed to a number of physical, biological and chemical processes resulting in complex and dynamic biogeochemical cycles. This sedimentary system is adapted to semi-diurnal changes between inundation and air-exposure, which forces the sedimentary microbial and biogeochemical activity to adapt to a highly dynamic environment with additional seasonal and meteorological changes. The intertidal area is strongly affected by variations in oxygen (O_2), light and temperature as well as currents and waves induced enhancement of erosion and advective transport processes. Remineralization of organic matter proceeds to a large part via anaerobic microbial activity. Dissimilation by sulfate reduction may account for more than 50 % of the mineralization (Jørgensen, 1982; Canfield et al., 1993). The rate of dissimilatory sulfate reduction in intertidal sediments may vary considerably between 0.2 and more than at least 104 mmol m^{-2} day^{-1} (Skyring, 1987; Trudinger, 1992). In relation to other competing reactions, the seasonal variations of sulfate reduction are expected to show the highest dynamics close to the surface of the sediment. There, biogeochemical processes may be influenced immediately by changes of, e.g., temperature, biological activity, physical re-suspension and organic matter burial.

The oxidation of organic matter is coupled to reductive processes using O_2, nitrate, manganese (Mn) and iron (Fe) oxy(hydroxi)des and sulfate as the final electron acceptors (e.g. Froelich et al., 1979; Jørgensen, 2005). The activity of sulfate reducing bacteria is closely coupled to the burial and cycling of sedimentary S, Fe and Mn compounds. Only about 10 % of the sulfide produced by microbial sulfate reduction is permanently buried into the sediment, while about 90 % of the reduced sulfide is re-oxidized back to sulfate (Jørgensen, 1977, 1982; Westrich & Berner, 1988). Most of the sulfides precipitate as Fe sulfides FeS and FeS_2 if reactive Fe phases are available and are retained more or less permanently in the sediment. Reactive Fe phases represent the pools readily available for reduction by H_2S or microbes (Canfield, 1989; Thamdrup et al., 1994; Kostka & Luther, 1994). Reduced S compounds may also be re-oxidized in the uppermost sediment layer by the reaction with Mn oxides, O_2 penetrating the upper layer and microbially. Possible products of the sulfide oxidation may be sulfate or intermediate S compounds as thiosulfate, polythionate or sulfite (Pyzik & Sommer, 1981; Afonso & Stumm, 1992). Due to the high recycling efficiencies of reactive Mn (IV) - and Fe (III) oxy(hydroxi)des, these metals may act as electron shuttles on a short scale metal cycling at the sediment-water interface. The reduced Fe^{2+} and Mn^{2+} diffuse to the sediment surface and are re-oxidized and precipitated again (Thamdrup et al., 1994).

Many earlier investigations have shown that the rate of microbial sulfate reduction in surface intertidal sediments where sulfate is abundant is controlled primarily by temperature and the availability of degradable organic matter (e.g. Vosjan, 1974; Westrich & Berner, 1988; Böttcher et al., 1997; Rusch et al., 1998). The quantitative scale of impact of the different factors on microbial sulfate reduction and their spatial and temporal dynamics in intertidal sediments are still not fully understood. Therefore, it was the goal of the present study to assess the regulating factors of microbial sulfate reduction in the top of different intertidal surface sediments on a seasonal base and to develop a new model for the consideration of daily temperature changes. The different study locations represent a range of sediments with different biological activities and hydrodynamic conditions (grain sizes, organic matter and metal content, permeability and porosity). Concurrent measurements of microbial sulfate reduction, reduced S pools, organic stock and temperature dynamics of different sediment types demonstrated the close coupling of the S and metal cycling.

Huettel and Rusch (2000) showed that the advective transport in permeable sediments leads to an enhanced flux and penetration depth of algae into the sand flats which thereby act as an efficient filter for organic matter. The fast exchange of substances between the water column and sandy surface sediments therefore leads to a rapid and effective degradation rate of organic substances. Although, about 70 % of the coastal area of the North Sea consists of sandy sediments only little is known about the biogeochemical processes (Huettel & Rusch, 2000; de Beer et al., 2006). Because of the typically low contents of organic matter and microbial abundance, sandy sediments were considered to be of less importance for benthic mineralization in the coastal areas. Only recently, it became clearer that permeable sediments may act as open-system-type bioreactors acting as filters for the mineralization of organic matter. This type of sediments is characterized by easy transport and fast replacement of educts and metabolic products. In the present study, we compared organic poor permeable sands with muddy and mixed intertidal sediments containing higher amounts of organic matter.

The main aim of this study was to thoroughly understand the regulation of the microbial sulfate reduction and the accumulation of reduced S compounds in different types of intertidal sediments. Meteorological and tidal conditions regulate the heat balance of intertidal sediments. Under the influence of the tides steep but continuously changing vertical temperature gradients can develop in intertidal sediments. The development of theses gradients is related to sedimentology, the timing of exposure to the atmosphere and meteorological conditions e.g. net radiation, wind speed before tidal inundation. The tidal flooding of intertidal sediments promotes a rapid exchange of heat across the sediment-water interface and the temperature profiles tend to become equal to the temperature of the overlying water column over a short time. In order to examine the influence of highly dynamic temperature conditions on sulfate reducing activity a new model has been developed that enables the consideration of fluctuating temperatures due to tidal rhythms on time-integrated sulfate reduction rates based on temperature-dependent sediment incubations.

Material and Methods

Study areas

The study sites are located in the back-barrier area of Spiekeroog Island in the southern North Sea; (Figure 1). The tidal flats of Neuharlingersiel (N I, II) and Janssand (S I, S III) represent intertidal mixed and sandy sediments. As a muddy site, a mud flat in the closed-by Jade Bay (Site Dangast; Figure 1) has been investigated on a seasonal base.

These different sampling sites were chosen to include a range of sediments with different sedimentological and geochemical properties (grain size, organic matter and metal content, permeability and porosity) and biological activities. The tides in this area are semi-diurnal. The Janssand flat is characterized by a slope of on average 1.6 cm m^{-1} toward the low water line and is covered by approximately 1.5 to 2 m of water during high tide. Sampling occurred along a transect which included 4 positions, but the lower sand flat position near the low water line (S I) and an upper sand flat site (S III, approximately 45 m upslope the sand flat) were chosen as the main study areas (Figure 1). The upper parts of this tidal flat become exposed to air for about 6 to 7.5 hours, the lower position falls dry for 3-4 hours during low tide. Hertweck (1995) observed that low macrofaunal abundance at exposed sides at the Janssand is a result of enhanced current velocities. During our investigations only a random occurrence of *Arenicola marina* and *Nereis diversicolor* was found. During summer, we observed a 6-fold decrease in *Arenicola marina* fecal mounds at a station close to the tidal channel compared to the top of the sandflat (Billerbeck, pers. communication). At the position near the water line, layers of finer grained sediment were found in various depths. High current velocities further enhanced by the adjacent fairway channel leads to a permanent reworking of the sediments at the Janssand station. The intertidal flat of Neuharlingersiel represents mixed sediment of various grain size classes (Table 1) and becomes exposed for about 6-7 hours during low tide (Billerbeck et al., 2006). About 10 m away from the sampling location N, two separate sampling events were performed in April and November 2002. This station (N II) is characterized by a slightly higher content of finer grained sediment compared to station N (see Batel, 2003; Peters, 2004). The Dangast station is influenced by the fluvial input of the Weser river and is comparable to an estuarine system (Figure 1). The tidal cycles lead to an inundation time of about 7 hours and an exposure time of circa 5 hours. The surface 10 cm of the sediment was dominated by a mud fraction (Table 1; see Böttcher et al., 2000; Llobet-Brossa et al., 2002).

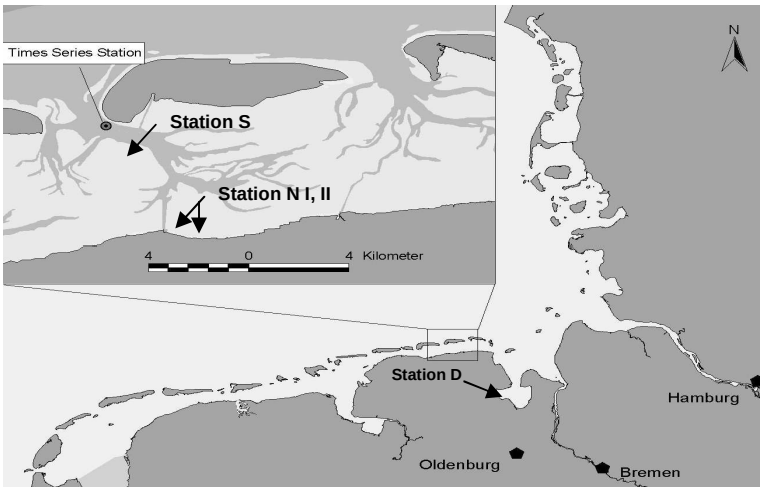

Figure 1: Location of the study areas near the island of Spiekeroog, Wadden Sea, Germany.

Methods

During low tide, several parallel sediment cores (PVC tubes; 3.6 and 2.6 cm width; 20-40 cm length) were sampled in an area of about 1 m^2. The investigations were carried out in the field (in-situ) as well as by incubations and measurements in the laboratory. Sediment cores and interstitial waters were typically analyzed down to about 15 cm depth for a number of parameters: sulfate reduction rates (SRR), total reduced inorganic sulfur (TRIS), acid volatile sulfur (AVS), chromium reducible sulfur (CRS), total organic carbon (TOC), total inorganic carbon (TIC), sulfate (SO_4), dissolved iron (Fe^{2+}), dissolved manganese (Mn^{2+}), reactive Fe and Mn oxides, salinity, water content, grain size.

Two parallel sediment cores were analyzed in 1 cm intervals for porosity by measuring wet density (weight of known volume) and water content (drying at 105 ℃ for 24 h). The pore water temperature was measured in-situ with a digital sensor (GTH 1150 digital thermometer). Total Carbon (TC) was measured from freeze-dried samples using a CNS element analyzer (Fison Instruments, NA 1500, Series 2) and total inorganic carbon (TIC) on a CM 5012 CO_2 coulometer with a CM 5130 acidification module (UIC). Total organic carbon (TOC) content was calculated from the difference of TC and TIC. Freeze-dried sediment samples pre-treated with H_2O_2 (30 %) and washed with distilled water, subsequently dried and were analyzed by laser deflection (Fritsch Analysette 22) to determine grain size distribution. Microbial SRR were measured by the whole-core tracer incubation technique (Fossing & Jørgensen, 1989). For this purpose several parallel sediment cores (2.6 cm wide) were sampled on a seasonal base. Sediment cores were transported to the laboratory and kept under in-situ temperature and dark conditions for further processing. Two parallel cores were stored in darkness at the daily maximum and minimum in-situ temperatures for about 10-12 hours. Carrier-free $^{35}SO_4^{2-}$- radiotracer solution (~200 kBq) was injected in 1 cm intervals down to 15 cm. After 4 hours incubation in the dark, the sediment cores were sliced into 1 cm sections and immediately mixed with

10 ml of a 20 % solution of zinc acetate to interrupt the microbial process and to fix sulfides. Activity of ^{35}S was determined using a Packard Liquid scintillation analyzer (2500IR). The cold two-step distillation procedure was used to recover acid volatile sulfur (AVS = FeS + H_2S + HS^-) and chromium reducible sulfur (CRS = FeS_2 + S^0) from the sediment.

A good agreement of vertical distribution and areal sulfate reduction rates was found by comparing measurements of Billerbeck et al., 2006b and Werner et al., 2003, who used a modified technique for permeable sediments (Figure 2). In this method, oxic seawater tracer solution percolates from the top of the core through the permeable sediment (de Beer et al., 2005). It has the advantage of simulating the natural penetration of O_2 into the surface sediments by pore water advection during incoming tide (de Beer et al., 2005), but has the possible disadvantage of introducing O_2 and probably other than site-specific electron donors into deeper sediment sections that are usually anoxic and limited by reactive organic species.

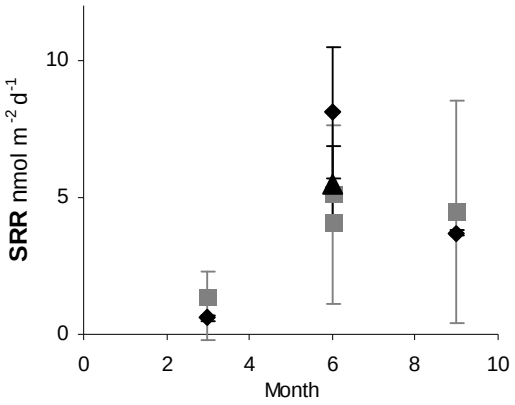

Figure 2: Compared SRR measured by Werner et al., (gray) and data presented in this study (black).

In contrast, the samples from Neuharlingersiel (March 2002) were analysed using the hot one step distillation (Fossing & Jørgensen, 1989; Kallmeyer et al., 2004). The total reduced inorganic S (TRIS) pool was calculated from the individual AVS and CRS measurements by the methylene blue method (Cline, 1969), using a Shimadzu UV-160A spectrophotometer. Extractable Fe was determined from freeze-dried sediment using buffered dithionite-citrate acetic acid solution (Canfield, 1989) and extraction with 0.5 M HCl, respectively (Thamdrup et al., 1994; Kostka & Luther, 1994). Extraction with HCl for 1 hours is selective for the amorphous or poorly crystallized Fe- and Mn oxide and carbonate phases, while citrate-dithionite solution additionally liberates minor amounts of Fe-containing silicates (Canfield, 1989). Both extraction methods showed comparable contents of reactive Fe phases (Figure 3). Therefore, only data of HCl extractable Fe (Fe_{HCl}) are shown.

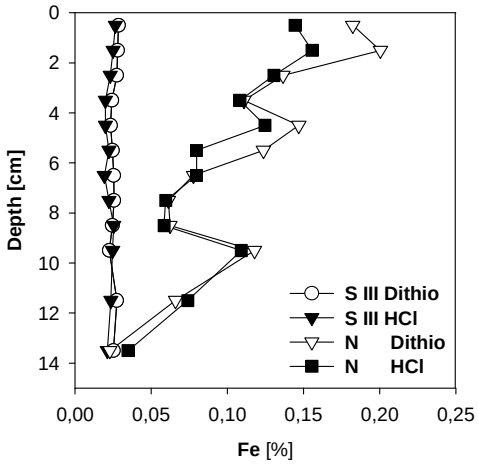

Figure 3: Comparison of dithionite and HCl extracted Fe phases in sediments from station S III and N.

The reactive Fe_{HCl} was calculated from the difference between the HCl leachable Fe and the FeS fraction. Fe was determined spectrophotometrically using reducing Ferrozine (Ferrozine reagent with 1 % hydroxylamine-hydrochloride; Stookey, 1970; Viollier et al., 2000) whereas Mn was quantified by flame atomic absorption spectroscopy (Perkin Elmer AAS).

After sectioning the core in a glove box under inert gas, pore waters were separated from the sediments by centrifugation (centrifuge tube; Saager et al., 1990) through membrane filters (Millipore, Amicon Bioseperations, PVDF-membrane 0.45 µm). An aliquot of the pore water was kept frozen for the determination of sulfate using a Dionex LC30 DX 500, WATERS Ion liquid chromatograph. The concentration of dissolved Fe^{2+} was measured immediately after filtration using Ferrozine reagent with 1 % hydroxylamine-hydrochloride (Stookey, 1970). Another aliquot of pore water was acidified (2 % HNO_3 suprapure) and the concentration of dissolved Fe^{2+} and Mn^{2+} were measured after appropriate dilution by ICP-OES (Perkin Elmer Optima 3000 XL) with Sc as an internal standard or by ICP-MS (Thermo Finnigan MAT ELEMENT). Additional data for dissolved Fe and Mn where obtained using DET techniques and are taken from (Chapter 3 of this thesis). The salinity of the pore water samples was measured with a hand refractometer (Atago, SI Mill-E).

Results

Sediment properties

The stations S I and S III can be characterized as well sorted fine grained sands. The water content ranged from 21-16 % at the upper sand flat station III. Sediments at the lower station I contained finer grained layers in various depths and showed corresponding higher water contents of 27-18 %. The mixed sediments of station N consisted of various grain size classes. The grain sizes at the Dangast station (D) were dominated by the mud fraction (Table 1). The high capacity of clay minerals to adsorb organic matter is typically reflected by a positive correlation to the TOC content (Delafontaine et al.,1996; Böttcher et al., 2000). The pore water salinity varied from 22 to maximum surface values of 35 psu in summer. Salinities below the typically found 33 psu of the German Bight (Dellwig et al. 2007) reflect mixing with freshwater which is contributed to the Wadden Sea by floodgates (e.g. Neuharlingersiel) and rivers (e.g. Weser near Dangast), with highest impact during the rainy seasons in spring and autumn (Table 1).

Table 1: Overview about sediment properties of the different locations

	S I				S III				N I				N II	D						
sampling date	07.06.02	01.10.02	22.07.03	26.03.04	20.03.02	07.06.02	01.10.02	22.07.03	05.04.02	20.06.02	10.10.02	04.08.03	25.11.02	15.04.98	20.05.98	16.06.98	21.07.98	20.08.98	14.10.89	15.01.99
Average 10 cmbsf																				
Temp [°C]	15-25	11-16	20-31	7-10	7-15	15-25	11-16	20-31	7-15	18-31	15-20	22-32	6-11	further information see Böttcher et al., in prep.						
Grain size [%vol]																				
[<2µm]				1.1%				0.6%				6%					15,6%			
[<63µm]				3.1%				1.0%				21.3%					84,1%			
[<580µm]				95.7%				98.3%				72.7%					0,5%			
TOC [%]	0.08-0.2	0.04-0.1	0.06-0.2	0.02-0.3	0.02-0.09	0.003-0.0	0.03-0.1	0.02-0.13	0.4-1.2	0.4-0.6	0.3-0.5	0.4-0.7	0.5-2.6	1-3.3		1,4-3,5		3-3,2		
SO_4 [mM]	23-26	25-26	12-27	21-25	23-30	25-27	22-30	26-29	n.d.	23-26	22-24	22-30	18-24	17-21		17-21	18-26	16-19	22-24	
H_2O [%]	18-20	18-22	18-27	19-28	19-21	17-18	16-21	18-21	22-40	21-30	23-29	21-33	37-84	30-75		55-72		55-63	19-66	
Salinity [psu]	30-31	32-33	30-33	28-31	28-30	32-33	33-35	33-34	n.d.	28-32	28-30	30-32	24-25			26-27		22-23,5		

Total organic carbon

The vertical distribution of organic matter showed seasonally varying contents at all investigated sites. Large TOC variations were found in the upper 5 cm of the sediment decreasing to a relatively constant pool size with depth. The TOC content at station D showed only small seasonal variations. The top 2 cm of the sediment contained about 3 % organic matter which leveled off in 1 % in 15-20 cm depth. At station N, highest surface TOC contents reached about 1.3 % and decreased to a background concentration of 0.5 % in March 2002, while amounts in June, September and July 2003 ranged between 0.4-0.7 %. In contrast, the S stations S I, S III revealed a nearly 10-fold lower content of organic carbon than station N. For instance, surface TOC values at S I ranged from 0.03 to 0.1 %. Higher amounts up to 0.8 % TOC were only found in certain depths with distinct layers of a finer grain size. Station S III showed a low variability of 0.06-0.1 % in organic matter content. The higher TOC contents at S I compared to S III may be a result of the different hydrodynamic conditions. Intensive

wave activity at the low waterline during low tide supported mechanical transport and accumulation of particulate organic matter, including macroalgae, into the porous sandy sediment.

Dissolved sulfate

At station N, the depth distribution of dissolved sulfate followed a decreasing trend during all sampling campaigns in the time series. In July 2003, surface sulfate concentrations decreased from 30 mM to 21 mM within the top 15 cm (Figure 4). This steep sulfate gradient indicated active consumption by microbial sulfate reduction. In contrast, decreasing sulfate concentrations with depth in September and April were closely related to a corresponding decrease in salinity which reflects mixing with freshwater and can not be ascribed to microbial consumption (Figure 4). High variations of sulfate concentrations were observed in the pore water of S I. The vertical distribution of pore water sulfate below oxic surface sediments ranged from 25-22 mM with depth. Spatially restricted spots with anoxic surface conditions exhibited differing vertical pore water profiles (Figure 4). In July 2003 pore water sulfate showed a steep depletion from 25 mM down to 11 mM within the upper 15 cm (Figure 4). In contrast, dissolved sulfate concentrations at S III remained constant with depth during all seasons (Figure 4). This indicates that the high permeability of the sandy sediment leads to a continuous supply of sulfate from the overlying water. Therefore, intense re-oxidation processes of Fe- and/or hydrogen sulfides and re-supply of sulfate from the overlying seawater had the effect that only gross but no net sulfate reduction was reflected in the vertical distribution of sulfate in the pore water profiles.

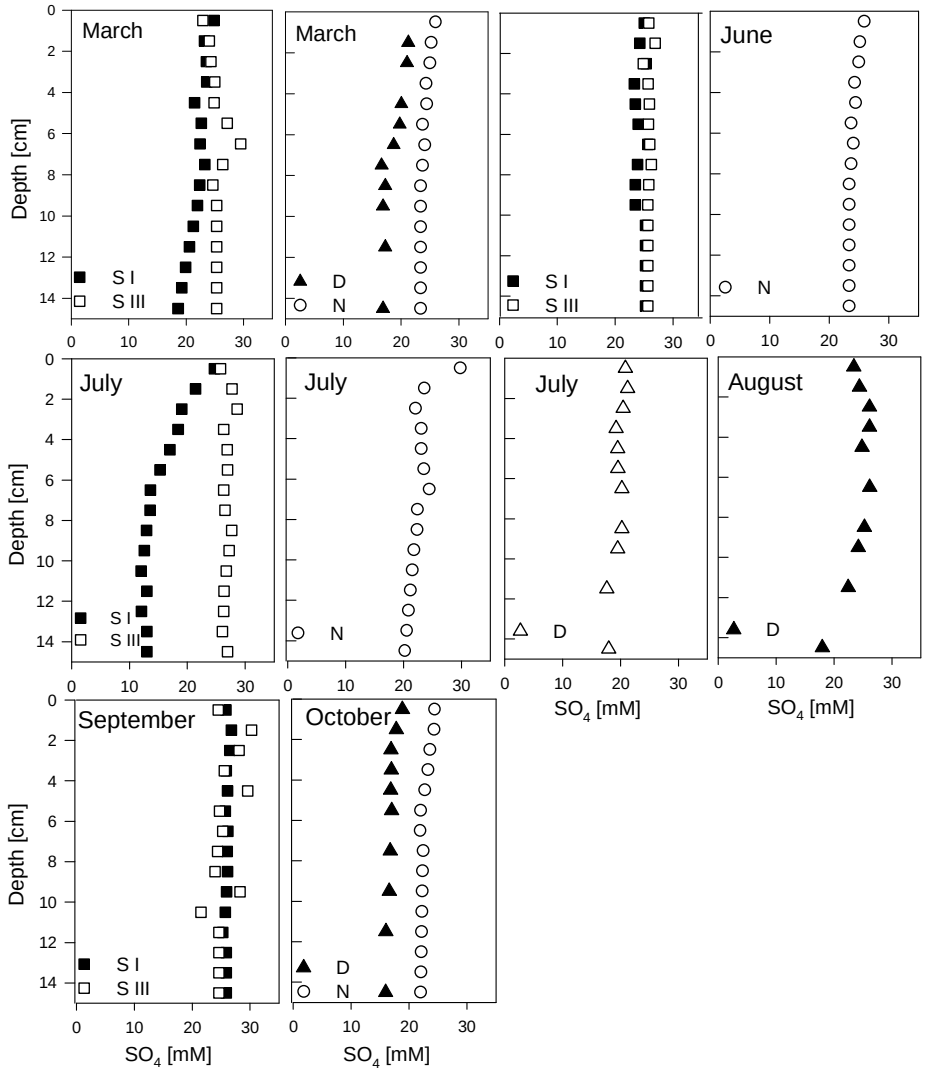

Figure 4: Vertical distribution of pore water sulfate at sandy S I (■), S III (□), the mixed N I (○) and the muddy- station D (▲).

Daily temperature variations

In intertidal sediments, steep vertical temperature gradients can develop under the influence of tides. Typical diurnal temperature fluctuations occur rapidly during the change between tidal inundation and exposure amplified by temperature variations between day and night. Vertical temperature profiles reflect that the steepest semidiurnal fluctuations level off in a constant average temperature in the deeper sediment (15-20 cm: Figure 5). The magnitude of temperature gradients is related to time and duration of air exposure or inundation and the prevailing meteorological conditions, e.g. solar radiation and wind speed. Daily temperature changes in the surface sediments covered a range of 5 - 15 ℃ in March 2002, 15-31 ℃ in June 2002 and July 2003 and 11-20 ℃ in September 2002. Seawater temperatures in the backbarrier area varied during the different seasons from 4℃ in winter and up to 23 ℃ in summer (Figure 9).

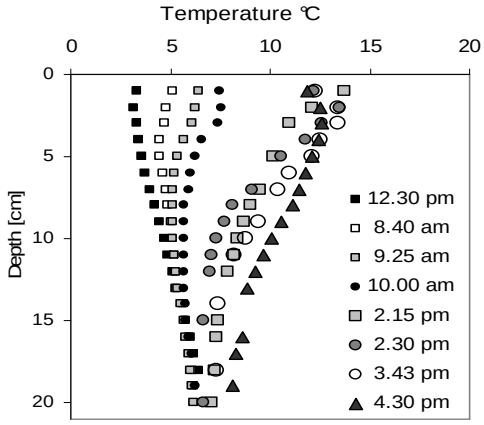

Figure 5: Temperature profiles at the mixed flat N I measured during 24 hours in April 2001.

Sulfate reduction

Site specific depth variation at different temperatures

An important aspect of site specific differences was illustrated by depth profiles of sulfate reduction. Two parallel sediment cores were incubated at the daily maximum- and minimum in-situ temperatures. Generally, rising laboratory incubation temperatures enhanced microbial activity and showed strongest effects in the zone of maximum microbial activity.

Microbial activity at the muddy station D ranged from values of 30-200 nmol cm^{-3} d^{-1} during the colder months in the period from autumn to spring (January data see Böttcher et al., in prep.) to maximum rates of 2800 nmol cm^{-3} d^{-1} in August. Highest sulfate reduction rates were measured mostly in 8 10 cm depth, whereas peak rates in spring were found at the surface.

At station N, maximum SRR varied seasonally from 50 nmol $cm^{-3}d^{-1}$ in March 2002 to 1650 nmol cm^{-3} d^{-1} in July 2003 (Figure 6). Notably high microbial activities were detected within the upper 6 cm of the surface sediment, followed by declining rates below this depth. This is in accordance with the observed maximum SRR at the sediment surface in summer 2003 caused by enhanced deposition of reactive organic matter and elevated sediment temperatures of up to 32 ℃ (Figure 6). Sulfate reduction at the sand flat stations (S I, S III) was about two orders of magnitude lower compared to rates of station N. Maximum SRR at the position S I varied seasonally and ranged from 40 nmol cm^{-3} d^{-1} in spring 2004 to 550 nmol cm^{-3} d^{-1} in summer 2003 (Figure 6). The enhanced input of reactive organic matter in July and September caused peak values at the sediment surface, whereas in March and June maximum rates of microbial activity shifted to greater depths of 5-14 cm (Figure 6).

At station S III, peak rates of sulfate reduction developed within the surficial 4 cm in June 2002 and revealed a second increase deeper in the sediment in summer 2003 (Figure 6). In spring and autumn, the depth of highest activity was found deeper, in 5-15 cm. Lowest rates of 20 nmol cm^{-3} d^{-1} were measured in spring 2002 and maximum rates of 550 nmol cm^{-3} d^{-1} were found in summer 2003 (Figure 6).

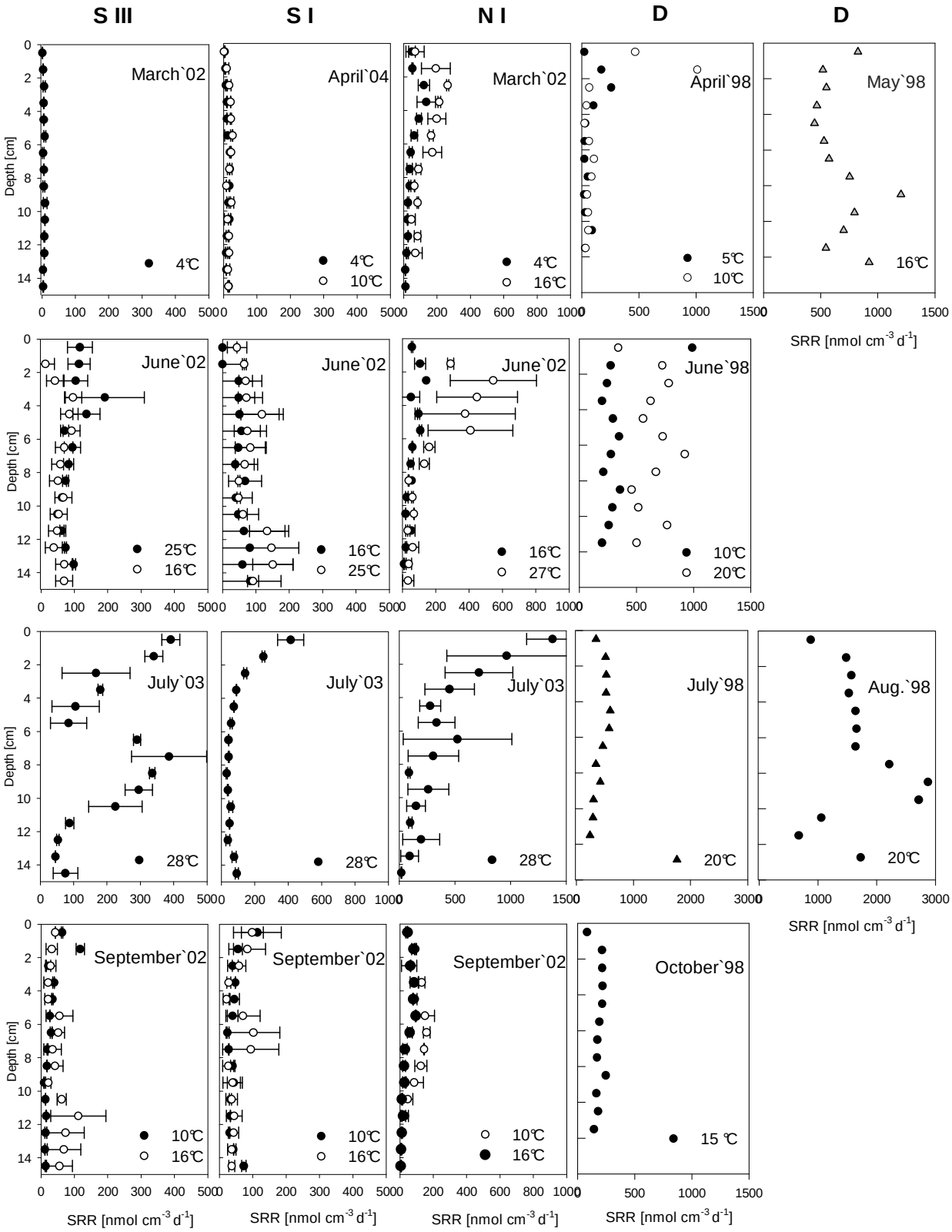

Figure 6: Vertical distribution of average sulfate reduction rates (nmol cm^{-3} d^{-1}, range between two cores given as error bars) at sandy stations S I, S III, the mixed station N I, II and the muddy station D, incubated by daily minimum (dots) and maximum (circles) temperature. Note the different scales.

Model prediction of in-situ sulfate reduction rates with consideration of temperature fluctuations

Microbial sulfate reducing activity has been shown to be strongly influenced by temperature. In order to examine the influence of highly dynamic temperature changes on biogeochemical processes the Arrhenius equation was fitted to simulate the development of temperature dependent reactions. The model prediction is based on measured data sets of temperature and SRR incubated by maximum and minimum daily temperatures. The Arrhenius equation could be defined as apparent activation energy and is simply a prediction of the responding overall rate of sulfate reduction to a change in temperature and does not specifically refer to the complex reaction sequence of sulfate reduction (Benner et al., 2002). The temperature dependence of the reaction was estimated as the `apparent activation energy` (Ea), based on the Arrhenius equation ($R=A*\exp(-Ea/RT)^{-1}$). In order to apply the Arrhenius equation to the kinetic reaction of incubated SRR it can be expressed as:

$$\mathbf{Ea = (R*T1*T2 / (T1-T2)) * \ln (k1 / k2)}$$

where k1 is the rate coefficient at temperature T1 (Kelvin), k2 is the rate coefficient at temperature T2 (Kelvin), R ($8.314*10^{-3}$ kJ $mol^{-1}K^{-1}$) is the gas constant and Ea (kJ mol^{-1}) is the activation energy of the reaction.

Q10 is a quotient of rate increase following a rise of 10 degrees in temperature, expressed by the following equation:

$$\mathbf{Q10:\ \ln K2 / K1 = Ea*1000 / 8{,}314*((T2-T1) / T1*T2)}$$

The actual Q10 describes the temperature regulation of the microbial population at any given time. The activation energy (Ea) of station N ranged from 49 KJ mol^{-1} in March to 75 KJ mol^{-1} in June. The two sandy stations revealed values from 34 KJ mol^{-1} in April 2004 to 43-44 KJ mol^{-1} in June and September (Table 2). Q10 values showed variations of about 1.7-2.8 (Table 2) and is within the range of values generally found for coastal sediments (Kristensen, 2000; Jørgensen, 1977; Skyring, 1987; Westrich & Berner, 1988; Moeslund et al., 1994). Compared to Ea values found in summer and autumn, sulfate reduction in spring required typically lower activation energy in both sediment types. Despite a higher organic matter load at station N, microbial activity in this sediment required higher activation energy than the TOC poor sandy stations S I, S III. Previous workers have determined a range of apparent Ea from 21 to 134 KJ mol^{-1} (Moeslund et al., 1994; Kristensen 2000; Llobet-Brossa et al., 2002; Jørgensen, 1977) and confirmed the data found in these sediments, respectively (Table 2).

Table 2: Activation energy (Ea) and related Q10 values at the mixed station N and sandy stations S I, S III.

		N I	S I	S III
March`02	**Ea**	**49.3**	/	/
	Q10	2.1	/	/
June`02	**Ea**	**74.7**	**43.7**	**40.9**
	Q10	2.8	1.8	1.9
Sept.`02	**Ea**	**68.0**	**41.7**	**42.9**
	Q10	2.7	1.8	1.9
April`04	**Ea**	/	**34.0**	/
	Q10	/	1.7	/

Consequences for integrated sulfate reduction rates

In this study, the model presented above was used to predict in-situ rates of sulfate reduction in intertidal surface sediments based on measured data sets for temperature and SRR in sediments incubated by maximum and minimum daily temperatures. Such a model provides the basis to estimate the response of microbial activity during the daily temperature variations under the influence climate and tidal dynamics.

Table 3: Estimation of the response of sulfate reduction (mmol m^{-2} d^{-1}; integrated over the upper 10 cm) from the temperature model with regard to dynamic daily temperature variations, compared with sulfate reduction rates predicted by the linear average daily temperature.

Station		**N I**		**S I**			**S III**	
Season	Temperature	**Dynamic SRR**	**Linear SRR**	**Dynamic SRR**	**Dynamic SRR**	**Linear SRR**	**Dynamic SRR**	**Linear SRR**
March`02	4 – 16 ℃	**8.5**		4 – 16 ℃		n.d.		
	10 ℃		**11**	**10 ℃**				
June`02	17 – 31 ℃	**17.5**		17 – 31 ℃	**4.1**		**5.6**	
	25 ℃		**22.1**	**25 ℃**		**9.5**		**10.7**
Sept.`02	10 – 20 ℃	**9.8**		10 – 20 ℃	**5.1**			
	15 ℃		**10.7**	**15 ℃**		**8.3**		
April`04	4 – 10 ℃			4 – 10 ℃	**1.4**			
	7 ℃					2.1		

Measured temperature profiles showed that high variations may occur on time scales of hours. At the sediment surface, temperature showed maximum amplitudes of over 15 ℃ during 24 hours in summer. Table 3 shows the effect of temperature variations on microbial activity during 24 hours, predicted for sandy and mixed sediments compared to rates derived from an average daily temperature.

At station N the surface temperature oscillation reached 9 °C in March 2002 and variation damped down below 9 cm depth. The average temperature of 10 °C would amount to 11.1 mmol m^{-2} d^{-1} of sulfate reduction, whereas the model prediction of depth integrated SRR suggests 8.5 mmol m^{-2} d^{-1} within the upper 10 cm. The approximation of SRR by the linear daily average temperature would lead to an overestimation of about 30 %. The temperature modulation predicted in June 2002 that microbial activity extended over a wide range between 8.8-26.3 mmol m^{-2} d^{-1} and reached daily amounts of 17.5 mmol m^{-2} d^{-1}, whereas an average temperature of 21 °C would result in 22.1 mmol m^{-2} d^{-1}, an overestimation of 26 % of the daily SRR. The temperature in autumn ranged from 10-20 °C at station N and modelled data including this daily temperature variation reflected a 9 % lower daily rate than approximated values 10.7 of mmol m^{-2} d^{-1} by using the average daily temperature. At the sandy station S I, the model predicted daily rates of 1.4 mmol m^{-2} d^{-1} in spring 2004. The linear average temperature of 2.1 mmol m^{-2} d^{-1} overestimates the temperature influenced microbial activity up to 50 %. In June, the averaged temperature of 20 °C would overestimate the daily rates up to 130 %. In autumn, the linear average temperature would overestimate the microbial activity by 63 %. At station S III in June the average temperature would imply an overestimation of daily sulfate reduction by 65 %.

Comparison of gross and net SRR

The determination of SRR included a comparison of the reduced ^{35}S, recovered as $AV^{35}S$ and $CR^{35}S$ in the radio-tracer assays. This yields information about the transformation of radio-labeled sulfide on a short-time scale of 4 hours during incubation time. The gross SRR and with this the content of radio-labeled reduced S compounds may have been influenced by biotic or abiotic re-oxidation with O_2 and, even in the reduced sediment, oxidized phases of Fe and/or Mn may become competing electron acceptors (Aller & Rude, 1988; Fossing & Jørgensen, 1990; Afonso & Stumm, 1992). Therefore, $H_2{}^{35}S$ could have been oxidized partly to $^{35}S_0$ and $Fe^{35}S_2$ or completely to $^{35}SO_4^{2-}$ and thus escaped detection. The relative distribution of radio-labeled end products allows approaching the extent to which surface SRR are underestimated as a result of sulfide oxidation and therefore reflects the net rates of sulfate reduction. At the mixed flat station N, the distribution of reduced ^{35}S in March and September showed a constant high $AV^{35}S$ recovery rate of 60-90 % throughout the top 15 cm and indicated low re-oxidation rates. Within the upper 3 cm at station S I, only 0-40 % of the microbial activity was detected in the $AV^{35}S$ fraction. Accordingly, at least 60 % of the $AV^{35}S$ fraction may have been re-oxidized in the surface sediments. Even below the oxygenated zone $AV^{35}S$ recovery was about 20 % and indicated proceeding sulfide oxidation. This supports the assumption that even below the O_2 penetration depth abiotic sulfide oxidation can become a competing process to the biogenic sulfide production in the sediment. Highest $AV^{35}S$ recovery rates up to 80-98 % occurring even in the surface layer of the sediment were found in summer 2003, presumably resulting from enhanced sulfate reduction.

The lowest AVS recovery was observed in the highly oxidized sediments of the upper sand flat position. In spring 2002, the upper 15 cm of the sediment at the S III revealed maximum recovery

rates of 30 % $AV^{35}S$ and total absence of $AV^{35}S$. However, in summer 2003, 60 % of $AV^{35}S$ was recovered in the surface sediments. At both sand flat stations, enhanced SRR in summer 2003 led to a complete transformation of reactive Fe oxy(hydroxi)des to Fe sulfides and to the total exhaustion of the Fe_{HCl} pool (Figure 7). The availability of reactive Fe phases may become a limiting factor for the formation of Fe sulfides (e.g. Morse, 1999).

Distribution of solid S and Fe

The presence of different S and Fe phases in the sediment is visible by distinct color changes representing the zonation of the light-brown colored oxic surface layer, followed by a black zone indicating the accumulation of Fe monosulfide and a subsequent grayish zone which resulted from an increasing content of pyrite. The depth of the brownish surface layer is directly correlated to the O_2 penetration depth and tended to vary spatially at the different locations and showed distinct seasonal changes. The pool of reduced inorganic S compounds buried in the sediment showed a distinct zonation at the sand flat stations (S I, S III). Compared to a clear color sequence at the sandy locations, the sediments of station N exhibited a less sharp zonation of color changes because of the heterogeneous distribution of organic matter and higher bioturbation activity.

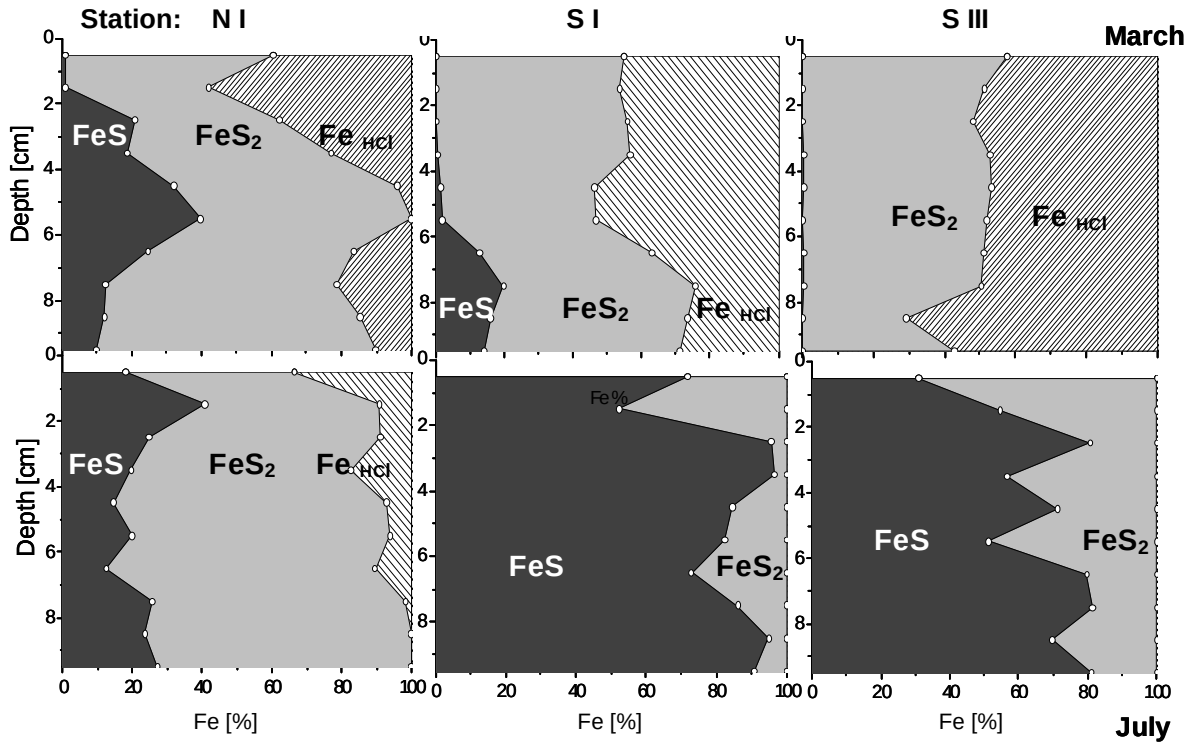

Figure 7: An example of the relative solid phase distribution of Fe sulfide pools of AVS (black, acid volatile sulfide) and CRS (gray, chromium reducible S) and the content of reactive Fe oxides (white striped, Fe_{HCl}) during spring and summer in mixed (N) and sandy sediments (S I, S III).

The data presented in Figure 7 show the relative distribution of different solid Fe sulfide pools. The total reduced inorganic S pools (TRIS) included the AVS and CRS fraction and the content of reactive Fe oxy(hydroxi)des (Fe_{HCl}). The two extreme seasonal conditions during spring and summer presented in Figure 6 demonstrate that the share of the different S species varied considerably between seasons in mixed (N) and sandy sediments (S I, S III). Generally, the inventory of reactive Fe minerals available for microbial and chemical Fe reduction was up to 6-10-fold higher in the mixed (N, 80-2300 ppm from summer to autumn) than in the sandy sediment (S I, S III, 0-310 ppm from summer to winter).

The TRIS inventory at the muddy and mixed stations D,N reflected that intensive microbial sulfate reduction and availability of Fe_{HCl} leads to an effective accumulation of reduced S compounds (Table 4). The mixed station N contained a 10-fold higher content of reduced S compounds compared to the dynamic TRIS content in the sand flat sediments S I, S III. The amount of TRIS varied from spring to summer from 6 to 7.5 mol m^{-2}, whereas the TRIS content at the sand flat increased in summer 6-fold (from 0.7 up to 4.4 mol m^{-2}) at the lower (S I) and 2.5-fold (0.4 to 1 mol m^{-2}) at the upper position S III. To discuss inventory variations at the sand flat, it has to be considered, that the sediment surface of the stations SI and III undergoes intensive sediment reworking as a result of tidal induced hydrodynamic forcing.

Seasonal and spatial trends in AVS and CRS fractions were in general inversely correlated to those of reactive Fe_{HCl}. Correlation of SRR and dissolved Fe^{2+} in the pore water indicates that Fe reduction was coupled to sulfide oxidation. Reactive Fe was mobilized as ferrous Fe^{2+} in the zone of sulfate reduction and re-precipitates as Fe oxy(hydroxi)des (Fe_{HCl}) at the surface (Figure 7). The AVS pool showed usually an increasing trend with depth which reflected surface re-oxidation and the influence of oxygen penetration depth. The AVS pool at station N increased below 2 cm depth in spring 2002 whereas a higher recovery rate of 20 % AVS was found at the top layer in summer. On a short-time scale during 4 hours of incubation, re-oxidation processes were low at the mixed flat (N) but this finding pointed out that the burial rate of reduced sulfur on a long time scale was also superimposed by sulfide oxidation. In spring, the re-oxidation of AVS to Fe_{HCl} out competed H_2S fixation down to 4 cm depth at station S I. AVS formation increased subsequently with a corresponding decline of the Fe_{HCl} content. At station III, the total absence of AVS within the upper 15 cm indicated intensive re-oxidation processes and the Fe pool was completely converted to Fe_{HCl} and CRS (Figure 7). The relatively low concentrations of reduced S in the sandy sediment in spring reflects periods of high sediment oxidation influenced by deep O_2 penetration (Billerbeck et al. 2007; Walpersdorf et al., in prep.) and low microbial activity. During the hot summer of 2003 the oxidized surface zone was thinnest and AVS accumulated already in the surface layer at the sand flat stations S I and S III (Figure 7). Enhanced microbial sulfate reduction led to a complete transformation of reactive Fe to AVS and CRS at both sandy stations (Figure 7). Therefore, the Fe availability may become a process limiting factor for further sulfide fixation causing pyrite formation to cease at the sandy sediments. Despite a two times higher SRR at the upper position III in summer 2003, this station contained the lowest TRIS content (0.4-1 mol m^{-2}) compared to position S I (0.7-4.4 mol m^{-2}; Table 4). These observations underline that intensive

sulfate reduction was taking place in the oxygenated part of the sediment but without long-term preservation of the reduced S pool. The higher persistence of AVS at station S I was probably favored by the presence of finer grained and TOC richer layers at this position, which impede re-oxidation of reduced S by oxygen rich seawater.

Table 4: Overview of depth integrated sulfate reduction rates (upper 10 cm), the total reduced inorganic S (TRIS) content and reactive Fe_{HCl} content at the station D, N I and sandy stations S I, S III.

	S III	S I	N	D
SRR [mmol $m^{-2}d^{-1}$]				
spring	**0.7** ± 10.2	**2.1** ± 0.1	**11.1** ± 0.4	**21.4** ± 5
summer	**25.8** ± 1.9	**11.9** ± 0.9	**53.0** ± 20	**112.8** ± 69.3
TRIS [mol m^{-2}]				
spring	**0.4** ± 0.04	**0.7** ± 0.17	**6.0** ± 0.61	**14 ±** 5.7
june		0.7	**6.4** ± 1.9	/
summer	**1.0** ± 0.02	**4.4** ± 0.7	**7.5** ± 0.77	**2.2 ±** 1.6
sept.		**0.6**	**5.1**	**24 ±** 1.1
reactive Fe $_{HCl}$ [mol m^{-2}]				
spring	**0.01**	**0.02**	**0.10**	**0.39**
summer	**0**	**0**	**0.001**	**0.34**

Distribution of dissolved Fe

At the sediment surface, sulfides, such as hydrogen sulfide (H_2S), may also be re-oxidized microbially mediated or via direct reaction with O_2 and/or reactive metal oxides. Dissolved Fe^{2+} and Mn^{2+} in the pore water refer to an intense cycling of these metals in the surface sediment. The reduction of reactive solid Fe minerals by biogenic hydrogen sulfide (H_2S) leads to a release of Fe^{2+} into the pore water (Figure 8) which reflects the close interaction between the sedimentary Fe and S cycle. Highest concentrations of dissolved ferrous Fe were associated with the zone of intensive microbial activity and ranged during the sampling campaigns from 100-330 µM Fe^{2+} at the mixed station N and 20-180 µM Fe^{2+} at the sandy stations. Dissolved Fe and Mn diffuse upwards into the oxic zone near the surface where they are re-oxidized and re-precipitated as Mn- and Fe-oxy(hydrox)ides (Mn data presented in Bosselmann et al., in prep.). This short-scale cycle is reflected in the opposite vertical distribution of solid and dissolved metals (Figure 8). Reactive Fe_{HCl} typically shows enrichment at the sediment surface as a result of re-precipitation. Especially high microbial sulfate reduction in summer 2003 resulted in a complete reduction of Fe_{HCl} and the exhaustion of the reactive Fe pool.

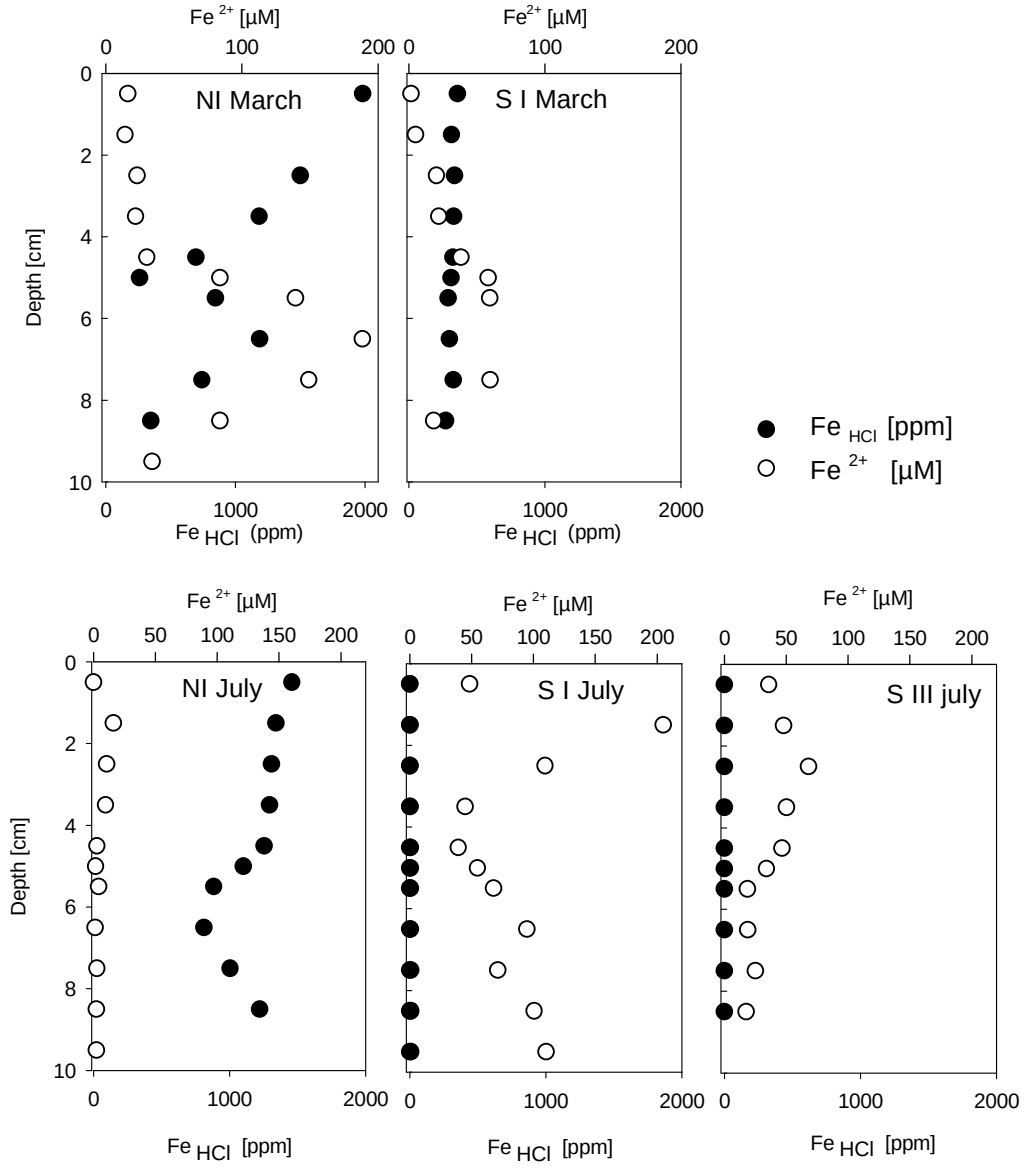

Figure 8: The vertical distribution of ferrous Fe in the pore water at station N, S I and S III, in spring and summer indicated the reduction of reactive Fe oxides.

Seasonal variation of areal sulfate reduction

Depth integrated SRR varied both temporally and spatially and were tightly related to sediment temperature. To compare the seasonal development of SRR for four different locations and two separate sampling events, rates presented in Figure 6 are integrated over the area of the surface 10 cm depth.

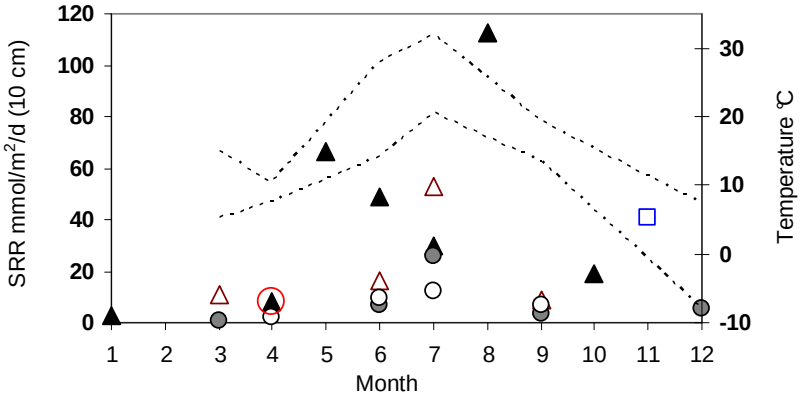

Figure 9: Sulfate reduction rates integrated over the upper 10cm depth (stations: D ▲, N Δ, S I O, S III ●, N II O (Batel, 2002, □ Peters, 2004) and seasonal maximum and minimum air temperature variations measured during the sampling campaign 2002 (dashed line).

The comparison of depth integrated SRR on a seasonal basis underlines the relation between temperature and microbial activity (Kristensen et al., 2000; Westrich & Berner, 1988). Remarkably high rates were observed in summer 2003, followed by the early summer month of June and the spring season, which corresponds to the annual temperature trend. The differences of SRR between the stations were most pronounced at the mud flat (D) (3-113 mmol m^{-2} d^{-1}) and the mixed flat station (N) (9-53 mmol m^{-2} d^{-1}). Smallest seasonal variations were observed at the sandy stations (2-26 mmol m^{-2} d^{-1}).

Discussion

Factors controlling S cycling in intertidal sediments

During this seasonal study with campaigns in spring, summer and autumn, SRR showed a distinct dependence consistent with depth and most notably with sediment type at different locations. This reflected the mutual effect of factors such as temperature, organic matter availability and redox conditions.

Compared to the stations with finer grained sediments, permeable sediments showed considerably high mineralization rates on a seasonal base and point out that the important role of marine sands for carbon and S cycling (Billerbeck et al., 2007; Werner et al., 2006). The mixed and muddy stations represent highly productive sediments where intensive sulfate reduction leads to high accumulation of reduced S (TRIS).

What was the main factor controlling this variability?

More detailed information about site specific differences was reflected by the spatial and vertical distribution of sulfate reduction at the different sites. The vertical profiles revealed that maximum activities of sulfate reducing bacteria occurred at the sediment surface of the upper 10 cm depth at all sites. Highest densities of sulfate reducing bacteria were found within the surface 5 cm depth at station S I in September 2002 (Ishii et al., 2004). The decreasing rates of sulfate reduction with depth cannot be attributed to limitation of sulfate. The only slightly decreasing trend of sulfate concentrations in the pore water of station N can be assigned to microbial consumption whereas no significant sulfate depletion could be observed at the sandy flats due to the continuous supply of sulfate from the overlying water. Only spots with anoxic surface conditions at station I showed spatially varying vertical sulfate concentrations. This was probably due to the observed low tide drainage of sulfide rich pore water downward the sand flat (Billerbeck et al., 2006a,b). Additionally, the embedded finer grained layers may have slowed down the re-supply of overlying seawater.

The measured microbial activity at station S I and the mixed flat (N) corresponds to the transition of rates found at other near shore sites including muddy and sandy sediments (e.g. Moeslund et al., 1994; Thamdrup et al., 1994; Böttcher et al., 2000; Llobet-Brossa et al., 2002). The development of the high sulfate reducing activity near the surface zone at all locations was probably fueled by the sedimentation and enrichment of organic matter in the upper sediment layers. The buried material undergoes rapid decomposition, which caused a decrease of TOC content with respect to core depth. In spring 2002, a 10-fold higher SRR at station N and D than on the sand flat cannot be attributed to the effect of temperature but to the high amount of available organic carbon as an important rate controlling factor for SRR in the surface sediments. However, the vertical distribution of microbial activity, especially in summer and autumn, showed decreasing SRR with only a small decline of organic carbon with depth at station N. Also, the TOC at the muddy station D leveled off to a content

of 1 % with increasing depth, which is still higher than maximum TOC amounts at the sand flat stations (Table 1). Thus, lower SRR with depth may have been caused by the shift of the reactive to the more refractory organic matter at depth (Henrichs & Reeburgh, 1987; Böttcher et al., 1997, 2000; Vosjan, 1974; Westrich & Berner, 1988). This trend can be explained by the preferential degradation of more easily decomposable fresh marine organic matter in the top sediments, which can be transported only by biological or physical processes in greater depths of non-permeable sediments. Organic matter of lower reactivity requires higher apparent activation energy (Ea) for decomposition (Westrich & Berner, 1988). Varying incubation temperatures reflected that temperature dependence of sulfate reduction varied between the different stations. Enhanced primary production and subsequent deposition of fresh and easily degradable organic matter from the water column in spring led to lowest activation energies in all investigated types of sediment (Table 4). Increasing Ea values in June and September at all stations, suggested that readily decomposable organic material had been consumed and the Ea increased with the age of the residual organic carbon. Higher Ea values required at station N compared to the relatively organic matter poor sandy locations confirmed the assumption that the stock of TOC was dominated by refractory organic matter (Table 4). Microbial sulfate reduction in the organic poor sandy locations is consequently stronger influenced by the input of reactive organic matter from the water column which was confirmed by higher Ea values required at station N compared to the organic matter poorer sandy locations (Table 4).

This is additionally influenced by the advective circulation of particulate and dissolved organic matter, electron acceptors and O_2 through the permeable sediments, which leads to an effective aerobic and anaerobic degradation (Shum & Sundby, 1996). In fine-grained sediment transport is often limited to diffusion, whereas in coarse sediments advection is an effective transport process across the sediment-water interface (Huettel & Gust 1992a,b; Huettel et al., 1996, Precht & Huettel, 2003; Precht et al., 2004). This is an effective filtration mechanism for organic carbon supplied into sandy sediments (D`Andrea et al., 2002, Huettel et al., 1996; de Beer et al., 2005) and may compensate the effect of higher TOC content and generally elevated microbial density in fine-grained sediments (Musat et al., 2006). In permeable sediments the rapid supply of oxidants and organic substrates likely controls the decomposition processes. Such an open system of permeable sands leads to an intensive element cycling and allows a rapid reaction to dynamic changes and functions as very efficient bio filter. The peak values of microbial activity at the sandy stations were often found in a greater depth than at station N, because particulate organic matter can be transported rapidly and deeper into the permeable sediment. This was also found for the vertical distribution of SRR at the Hausstrand of Sylt. Maximum rates were often measured in 4-14 cm depth (Werner et al., 2006). Intensified currents and wave movements induced by tidal flushing lead to a further enhancement of advective transport processes in sand flats. Advective flushing of sandy sediments has been shown to distribute algae into a significant sediment depth (e.g. Huettel et al., 1996; Huettel & Rusch, 2000). Intensive wave activity during low tide at the low water line of station S I supported the transport and accumulation of particulate organic matter into the porous sediment and led to higher contents of TOC at S I compared to position S III. In certain depths embedded finer grained layers caused localized higher TOC

concentrations. The rapid mineralization of carbon possibly creates a feedback mechanism whereby inorganic nutrients released by decomposition are rapidly available to the surface micro-algae community and stimulate its growth. Kostka (2002) observed that bioturbation in salt marsh sediments leads to a rapid Fe turn-over and stimulates sulfate reduction by decreasing sulfide concentrations through re-oxidation and thereby increasing sulfate levels. Thus it is likely that the turnover rates for organic matter were higher than expected for organic matter poorer sediments. Furthermore, the enhanced cycling of oxidants (Fe(III)), sulfate and inorganic nutrients released by decomposition are rapidly available to microbial communities and enhance the microbial turnover rates in sand flats. Howarth & Giblin (1983) showed that re-oxidation processes kept the concentration of dissolved sulfide low, which is thermodynamically favourable for sulfate reduction.

Comparable volumetric sulfate reduction rates were found in other intertidal sediments e.g. the sandy sediments of Königshafen (2-34 mmol m^{-2} d^{-1}, Kristensen et al., 2000), Westerhever (3-14 mmol m^{-2} d^{-1}, Böttcher et al., 2004) and List, Sylt (2-13 mmol m^{-2} d^{-1}, de Beer et al., 2005), Hausstrand, Sylt (0.03-39 mmol m^{-2} d^{-1}, Werner et al., 2006). Site specific differences of investigated sites were most clearly seen in the seasonal variations of areal SRR (Figure 9). Further investigations (N II) near the station N, in April 2002 and November 2002 by (Batel, 2003 and Peters, 2004) were in good agreement with SRR measured at station N (Figure 9). Microbial activity at station N II in November was two times higher than rates measured in September at N. This finding can be explained by the 2-5-fold higher TOC content within the surface 10 cm associated with a higher content of mud (Batel, 2003).

In intertidal sediments, transformation and exchange processes change periodically during exposure and inundation whereas conditions in permanently submerged subtidal sediments are more stable. The highly dynamic conditions in tidal systems enhanced the sediment mixing which stimulates microbial sulfate reduction. It also enhances the transport of reduced solutes to the surface where they can be re-oxidized and additionally causes a rapid re-supply of oxidants and particles to the deeper sediment. Hines & Jones (1985) and Berner & Westrich (1985) had also shown that sediment mixing and bioturbation resulted in enhanced microbial sulfate reduction. Enhanced ventilation by roots has also been shown to intensify sulfate reduction in Salt marsh sediments and can be compared to the tidal induced oxygen exchange (e.g. King, 1983, 1988; Kostka et al., 2002; Table 5).

In estuarine and shallow sea ecosystems, sulfate reduction has shown to be most active and may amount to 30 % ± 10 % of the global sulfate reduction (Skyring, 1987). With increasing distance from the coastal region, the input of terrestrial organic matter to the sediments decreases and mineralization processes mainly take places under oxic conditions in the water column. Therefore lower SRR were found in continental and deep sea sediments (e.g. Lein, 1983; Jørgensen, 1982; Boetius et al., 2000, Table 6).

Table 5: Comparison of depth integrated SRR from this study to rates reported in other Intertidal, subtidal and other marine coastal sediments.

Reference	Location	Sediment type	SRR mmol m^{-2} d^{-1}	
Christensen, 1989	US; Gulf of Maine,32-290m		0.006	subtidal
King et al., 1985	USA, South Carolina,Great Sippewissett Marsh, august	sandy-silt	107	saltmarsh
King, 1988	USA, South Carolina	sandy-silt	5-94	saltmarsh
Kostka et al., 2002	USA, Georgia,	clay-rich silt	56-200	saltmarsh
Aller & Yingst, 1980	USA, Long Island Sound, 15-34 m depth, calculated rates	silty clay	29-39	subtidal
Thamdrup et al., 1994	Denmark, Aarhus Bay, 16m depth	silty mud	2-13	subtidal
Moeslund et al., 1994	Denmark, Aarhus Bay, 16m depth	silty mud	4-13	subtidal
Thode-Andersen & Jørgensen, 1989	Denmark, Aarhus Bay, 12-41m depth	silty mud	1-3,8	subtidal
Thode-Andersen & Jørgensen, 1989	Denmark, Aarhus Bay, depth, Kysing - Hjarbaek Fjord	fine sand	16-22	subtidal
Thamdrup et al., 1994;	Denmark, Aarhus Bay, 16m depth	silty mud	4.7	subtidal
Jensen et al., 2003	Denmark, Kattegat, Belt Sea, 10-56m depth	fine grained	1.8-5.4	subtidal
		sand	0.4-2.7	subtidal
Sørensen & Jørgensen, 1987	Denmark, Kattegat, 33m depth	mixed	1	subtidal
Jørgensen & Bak, 1991	Denmark, Kattegat, 33m depth	sand-mixed	2.2	subtidal
Oenema, 1990	Netherlands, Eastern Sheldt	fine sand	14-68	tidal
Skyring & Lupton, 1986	Australia, Lake Eliza (hypersaline lake)	fine grained	7-198	lake
Kristensen et al., 2000	Sylt, Königshafen	fine sand	2-20	tidal
Werner et al., 2006	Sylt, Hausstrand	sand	0.2-19.3	tidal
de Beer et al., 2005	Sylt, Hausstrand	sand	0.01-13	tidal
Böttcher et al., 2004	Intertidal North Sea, Wadden Sea, Westerhever	sand	3-14	tidal
Böttcher et al., 2000	Dangast	mud	11	tidal
Batel, 2003	Intertidal North Sea, Wadden Sea, Neuharlingersiel	mixed	20-63	tidal
Peters, 2004	Intertidal North Sea, Wadden Sea, Neuharlingersiel	mixed	20,3	tidal
This study	Intertidal North Sea, Wadden Sea, Janssand	sand	1-26	tidal
This study	Intertidal North Sea, Wadden Sea, Neuharlingersiel	mixed	6-53	tidal
This study, Böttcher et al., in prep.	Intertidal North Sea, Wadden Sea, Dangast	mud	3-113	tidal

Model prediction

Varying incubation temperatures showed that temperature is a significant controlling factor for microbial activity. Strong temperature variations were measured at the surface of intertidal sediments. Therefore, it is important to consider this factor for the estimation of biogeochemical process rates under such dynamic environmental conditions in intertidal surface sediments. Sulfate reducing bacteria are able to adjust readily to temperature variations (Westrich & Berner, 1988; Thamdrup et al., 1998; Rabus et al., 2002, 2006). Sass et al. (2003) investigated the influence of seasonal changes on microbial communities of sulfate reducing bacteria in sediments from Neuharlingersiel. No distinct evidence was found that bacteria belonging to different temperature groups dominate at different seasons.

The temperature modulation points out that approximation by applying an average temperature derived from daily max- and minimum temperatures was not sufficient to represent the diurnal temperature range in intertial sediments. The influence of tidal flushing and exposure led to a highly dynamic temperature variation which influences instantaneously microbial activity. Furthermore, the vertical temperature profiles reflected that within the surface 10-15 cm of the sediment steep

temperature gradients developed and oscillated diurnally. To determine particular daily SRR in intertidal surface sediments, the temperature movement during 24 hours confirmed to be an important factor for microbial activity which needs to be considered. The presented model prediction is a helpful application to estimate the response of microbial activity during the daily temperature variations under the influence of the tidal dynamics. SRR predicted from the temperature model, reflected that rate calculations based on the average daily temperature would lead to overestimations of microbial activity which were found to range from 10 % up to 100 %. Therefore, the vertical distribution of temperature with depth should be taken into account for predictions of microbial activity and the connected element, carbon and S cycling in intertidal surface sediments.

Sulfide oxidation

In addition to the mineralization process of organic matter, sulfate reduction also plays a major role in sediment geochemistry with respect to the chemistry and metabolism of sulfide (King, 1988). The interaction between sedimentary Fe and S redox processes at the sediment surface reflects the close connection between the Fe and S cycles. The measured rates of sulfate reduction, including the separation of the radio-labelled S pools, pointed out that reduced sulfide undergoes a rapid diagenetic transformation and was not permanently trapped in the sediment. Only a small part of microbial sulfate reducing activity was detectable and maintained in the incubated sediment cores. The results demonstrated that especially at the sediment surface, where the highest activity of sulfate reducing bacteria occurred, abiotic re-oxidizing processes superimposed the bacterial sulfide production. The measured relative $AV^{35}S$ recoveries indicated that sulfide oxidation led to an underestimation of 40-90 % of gross rates at the sand flat. Tidal flushing resulted in oxygenation of permeable surface sediments and intensified sediment re-suspension. This leads to a stimulation of subsurface Fe and S cycling in intertidal sediments. Thus, the measured SRR especially at the surface (0-4 cm) of the sandy sediment have been underestimated up to 90 % and reflect only gross but no net rates of sulfate reduction. But even at the mixed station SRR were superimposed by re-oxidation processes and underestimated up to 10-40 %. This is consistent with findings by Jørgensen (1987) that less than 10 % of the produced H_2S is preserved in coastal sediments. Further comparable results were found in subtidal sediments (e.g. Thøde-Andersen & Jørgensen, 1989, Denmark; Lein, 1983, Baltic Sea). Highest recovery rates > 80 % were for instance measured in highly reduced coastal mud (Westrich, 1983) and lowest values were found in oxidized sediments of the continental shelf (Ivanov et al., 1976, Christensen, 1989). These observations underline, that intensive sulfate reduction was taking place in the oxygenated part of the sediment and that re-oxidation process led to a rapid turnover. These findings showed that improved knowledge of sulfide oxidation processes on a short time scale during incubation is important for accurate measurements of sulfate reduction.

The close coincidence of sulfate reduction and mobilization of Fe **(III) and Mn (IV) as Fe^{2+} and Mn^{2+}** into the pore water accompanied by the increase of Fe sulfides indicated that to a large extent the Fe reduction was coupled to sulfide oxidation (Pyzik & Sommer, 1981; Giblin & Howarth, 1984, Luther et

al., 1992). The connection between the S and metal cycling is reflected by the inverse vertical distribution of reactive Fe oxides (Fe_{HCl}) and the content of Fe sulfides. Reactive Fe (Fe_{HCl}) is mobilized as ferrous Fe^{2+} in the zone of sulfate reduction and re-precipitates as Fe oxy(hydroxi)des (Fe_{HCl}) at the surface. This proves the assumption that even below the O_2 penetration depth abiotic sulfide oxidation can become a competing process to the biogenic sulfide production in the sediment. The reactive part of the Mn_{HCl} and Fe_{HCl} phases provided an oxidizing reservoir to scavenge or oxidize H_2S. Additionally, intensive re-oxidation processes of Fe- and/or reduced S compounds effected that only gross but no net sulfate reduction was reflected in the pore water profiles. The solid Fe and Mn phases serve as important redox buffer in intertidal sediments (Morse, 1999)

Total reduced inorganic sulfur

The pool size of TRIS and especially AVS showed a dynamic seasonal response at all investigated stations. The abiotic re-oxidation processes led to a rapid turnover of reduced S compounds. The lower TRIS content of the sandy location compared to the station N was primarily due to enhanced chemical re-oxidation processes. Especially at the sandy station III a short residence time of reduced S compounds indicated that intensive re-oxidation processes must have taken place at the sandy sediments. The oxidative S cycling in the advection-driven sandy sediments was more dynamic compared to the diffusive dominated mixed sediments. The AVS pool usually showed an increasing trend with depth which reflected surface re-oxidation and the influence of O_2 penetration depth. The relatively low pools of reduced S in the sandy sediment in spring were related to periods of high sediment oxidation influenced by deep O_2 penetration (Walpersdorf et al., in prep.) and low microbial activity. During the hot summer in 2003, the pool of reactive Fe_{HCl} at the sandy stations S I, S III was consumed completely and converted to AVS and CRS, at both sandy stations (Figure 7). The AVS pools build up to concentrations 10-times higher than in all other months during our investigations. Therefore, the Fe availability became a process limiting factor for further sulfide fixation and pyrite formation probably ceased in the sandy sediments. The limited availability of reactive Fe phases or intermediate S species prevented a permanent fixation of sulfide into the thermodynamically more stable pyrite (Berner, 1970; Sweeney & Kaplan, 1973). Böttcher et al. (1997) showed that extreme events e.g. artificial organic matter burial, which leads to enhanced microbial sulfate reduction and increasing TRIS pool, are not preserved in intertidal sediments on a long time scale. The well-documented conversion of FeS_2 would involve the reaction of FeS with intermediate states of reduced S such as elemental S or polysulfides (Berner, 1970; Rickard, 1975; Goldhaber & Kaplan, 1974). The formation of these intermediate S species have been found to be low in highly reducing sediments and controlled by the availability of oxidants (e.g. Middelburg, 1991; Howarth & Jørgensen, 1984). Therefore, the restricted availability of reactive Fe phases and S intermediates may have limited the formation of pyrite via FeS.

Summary

In the present study seasonal variations in the activity of sulfate-reducing bacteria were investigated in different intertidal sediment types of the temperate coastal zone of the southern North Sea. On a seasonal base, organic poor permeable sediments showed considerably high mineralization rates and reflected that the role of marine sands for carbon and S cycling has been underestimated so far. Reduced S compounds undergo a fast chemical sulfide oxidation at the highly oxygenated sand flat surface. The mixed and muddy stations represent highly productive sediments where intensive sulfate reduction provided high inventories of reduced S compounds. This indicates that besides temperature, the availability of reactive organic matter as the main SRR-controlling factors in the investigated intertidal flats.

The surface of intertidal sediments is influenced by highly dynamic temperature conditions. Therefore, the variation of temperature should be taken into account for predictions of microbial activity. The presented model prediction is a helpful application to estimate the response of microbial sulfate reduction during the daily temperature variations under the influence of the tidal dynamics.

References

Afonso, M. and W. Stumm, 1992, The reductive dissolution of iron(III)(hydr)oxides by hydrogen sulfide: Langmuir, 8: 1671-1676.

Aller, R. C. and P. D. Rude, 1988, Complete oxidation of solid phase sulfides by manganese and bacteria in anoxic marine sediments: Geochimica et Cosmochimica Acta, 52: 751-765.

Aller, R. C., 1994, The Sedimentary Mn Cycle in Long-Island Sound - Its Role as Intermediate Oxidant and the Influence of Bioturbation, O_2 and $C_{(Org)}$ Flux on Diagenetic Reaction Balances: Journal of Marine Research, 52: 259-295.

Batel, S., 2003, Biogeochemische Umsatzprozesse in einem tidalen Oberflächensediment der südlichen Nordsee: Diploma Thesis, CvO Universität Oldenburg, 112 p.

Benner, S. G., D. W. Blowes, C. J. Ptacek and K. U. Mayer, 2002, Rates of sulfate reduction and metal sulfide precipitation in a permeable reactive barrier: Applied Geochemistry, 17: 301-320.

Berner, R. A., 1970, Sedimentary pyrite formation: American Journal of Science, 268: 1-23.

Berner, R. A. and J. T. Westrich, 1985, Bioturbation and the early diagenesis of carbon and sulfur: American Journal of Science, 285: 193-206.

Berner, R. A., 1989, Biogeochemical cycles of carbon and sulfur and their effect on atmospheric oxygen over phanerozoic time: Paleogeogr. Paleoclimatol. Palaeoecol, 75: 97-122.

Billerbeck, M., U. Werner, K. Bosselmann, E. Walpersdorf and M. Huettel, 2006a, Nutrient release from an exposed intertidal sand flat: Marine Ecology Progress Series, 316: 35-51.

Billerbeck, M., U. Werner, L. Polerecky, E. Walpersdorf, D. de Beer and M. Huettel, 2006b, Surficial and deep pore water circulation governs spatial and temporal scales of nutrient recycling in intertidal sand flat sediment: Marine Ecology Progress Series, 326: 61-76.

Billerbeck, M., H. Røy, K. Bosselmann and M. Huettel, 2007, Benthic photosynthesis in submerged Wadden Sea intertidal flats: Estuarine Coastal and Shelf Science, 71: 704-716.

Boetius, A., T. Ferdelman and K. Lochte, 2000, Bacterial activity in sediments of the deep Arabian Sea in relation to vertical flux: Deep Sea Research Part II, 47: 2835-2875.

Böttcher, M. E., A. Rusch, T. Hopner and H. J. Brumsack, 1997, Stable sulfur isotope effects related to local intense sulfate reduction in a tidal sandflat (southern North Sea): Results from loading experiments: Isotopes in Environmental and Health Studies, 33: 109-129.

Böttcher, M. E., B. Hespenheide, E. Llobet-Brossa, C. Beardsley, O. Larsen, A. Schramm, A. Wieland, G. Böttcher, U. G. Berninger and R. Amann, 2000, The biogeochemistry, stable isotope geochemistry and microbial community structure of a temperate intertidal mudflat: an integrated study: Continental Shelf Research, 20: 1749-1769.

Böttcher, M. E., B. Hespenheide, H. J. Brumsack and K. Bosselmann, 2004, Stable isotope biogeochemistry of the sulfur cycle in modern marine sediments: I. Seasonal dynamics in a temperate intertidal sandy surface sediment: Isotopes in Environmental and Health Studies, 40: 267-283.

Canfield, D. E., 1989, Reactive iron in marine sediments: Geochimica et Cosmochimica Acta, 53: 619-632.

Canfield, D. E., B. Thamdrup and J. W. Hansen, 1993, The anaerobic degradation of organic matter in Danish coastal sediments: Iron reduction, manganese reduction and sulfate reduction: Geochimica et Cosmochimica Acta, 57: 3867-3883.

Christensen, J. P., 1989, Sulfate reduction and carbon oxidation rates in continental shelf sediments, an examination of offshelf carbon transport: Continental Shelf Research, 9: 223-246.

Cline, J. D., 1969, Spectrophotometric determination of hydrogen sulfide in natural waters: Limnology and Oceanography, 14: 454-458.

D'Andrea, A. F., R. C. Aller and G. R. Lopez, 2002, Organic matter flux and reactivity on a South Carolina sandflat: The impacts of porewater advection and macrobiological structures: Limnology and Oceanography, 47: 1056-1070.

Davison, W. and H. Zhang, 1994, In-Situ Speciation Measurements of Trace Components in Natural-Waters Using Thin-Film Gels: Nature, 367: 546-548.

de Beer, D., F. Wenzhofer, T. G. Ferdelman, S. E. Boehme, M. Huettel, J. E. E. van Beusekom, M. E. Böttcher, N. Musat and N. Dubilier, 2005, Transport and mineralization rates in North Sea sandy intertidal sediments, Sylt-Rømø Basin, Wadden Sea: Limnology and Oceanography, 50: 113-127.

De Vitre, R. R. and W. Davison, 1993, Manganese particles in freshwater: In: H. P. van Leeuwen and J. Buffle (eds), Environmental Particles, 2: Boca Raton, Lewis: 317-352.

Delafontaine, M. T., A. Bartholomä, B. W. Flemming and R. Kurmis, 1996, Volume-specific dry POC mass in surficial intertidal sediments: a comparison between biogenic muds and adjacent sand flats: Senckenbergiana maritima, 26: 167-178.

Dellwig, O., K. Bosselmann, S. Kölsch, M. Hentscher, J. Hinrichs, M. E. Böttcher, R. Reuter and H.-J. Brumsack, 2007, Sources and fate of manganese in a tidal basin of the German Wadden Sea: Journal of Sea Research, 57: 1-18.

Fossing, H. and B. B. Jørgensen, 1989, Measurement of Bacterial Sulfate Reduction in Sediments - Evaluation of a Single-Step Chromium Reduction Method: Biogeochemistry, 8: 205-222.

Fossing, H. and B. B. Jørgensen, 1990, Oxidation and reduction of radiolabeled inorganic sulfur compounds in an estuarine sediment, Kysing Fjord, Denmark: Geochimica et Cosmochimica Acta, 54: 2731-2742.

Froelich, P. N., G. P. Klinkhammer, M. L. Bender, N. A. Luedtke, G. R. Heath, D. Cullen, P. Dauphin, D. Hammond, B. Hartman and V. Maynard, 1979, Early oxidation of organic matter in pelagic sediments of the eastern equatorial Atlantic: suboxic diagenesis: Geochimica et Cosmochimica Acta, 43: 1075-1090.

Giblin, A. and R. W. Howarth, 1984, Pore water evidence for a dynamic sedimentary iron cycle in salt marshes: Limnology and Oceanography, 29: 47-63.

Goldhaber, M. B. and I. R. Kaplan, 1974, The sulfur cycle: In: E. D. Goldberg (eds), The Sea, Wiley, p. 569-655.

Henrichs, S. M. and W. S. Reeburgh, 1987, Anaerobic mineralization of marine sediments organic matter. Rates and the role of anaerobic processes in the carbon economy: Geomicrobiology Journal, 5: 191-238.

Hertweck, G., 1995, Distribution patterns of characteristic sediment bodies and benthos populations in the Spiekeroog backbarrier tidal flat area, southern North Sea. Results of survey of tidal flat structure 1988-1992: Senckenbergiana maritima, 26: 81-94.

Hines, M. E. and G. E. Jones, 1985, Microbial biogeochemistry in the sediments of Great Bay, New Hampshire: Estuarine Coastal and Shelf Science, 20: 729-742.

Howarth, R. W. and A. Giblin 1983, Sulfate reduction in the salt marshes at Sapelo Island, Georgia: Limnology and Oceanography, 28: 70-82.

Howarth, R. W. and B. B. Jørgensen, 1984, Formation of ^{35}S-labelled elemental sulfur and pyrite in coastal marine sediments (Limfjorden and Kysing Fjord, Denmark) during short-term $^{35}SO_4^{2-}$ reduction measurements: Geochimica et Cosmochimica Acta, 48: 1807-1818.

Huettel, M. and G. Gust, 1992a, Impact of Bioroughness on Interfacial Solute Exchange in Permeable Sediments: Marine Ecology Progress Series, 89: 253-267.

Huettel, M. and G. Gust, 1992b, Solute Release Mechanisms from Confined Sediment Cores in Stirred Benthic Chambers and Flume Flows: Marine Ecology Progress Series, 82: 187-197.

Huettel, M., W. Ziebis and S. Forster, 1996, Flow-induced uptake of particulate matter in permeable sediments: Limnology and Oceanography, 41: 309-322.

Huettel, M. and A. Rusch, 2000, Transport and degradation of phytoplankton in permeable sediment: Limnology and Oceanography, 45: 534-549.

Ishii, K., M. Mussmann, B. J. MacGregor and R. Amann, 2004, An improved fluorescence in situ hybridization protocol for the identification of bacteria and *archaea* in marine sediments: FEMS Microbiology Ecology, 50: 203-212.

Ivanov, M. V., A. Y. Lein and E. V. Kashparova, 1976, Intensity of formation and diagenetic transformation of reduced sulfur compounds in sediments of the Pacific Ocean: In: Nauka (eds), The biogeochemistry of diagenesis of ocean sediments: Moskau, p. 171-178.

Jakobsen, R. and D. Postma, 1999, Redox zoning, rates of sulfate reduction and interactions with Fe-reduction and methanogenesis in a shallow sandy aquifer, Rømø, Denmark: Geochimica et Cosmochimica Acta, 63: 137-151.

Johnson, K. S., W. M. Berelson, K. H. Coale, T. L. Coley, V. A. Elrod, W. R. Fairey, H. D. Iams, T. E. Kilgore and J. L. Nowicki, 1992, Manganese Flux from Continental-Margin Sediments in a Transect through the Oxygen Minimum: Science, 257: 1242-1245.

Jørgensen, B. B., 1977, The sulfur cyle of a coastal marine sediment (Limfjorden, Denmark): Limnology and Oceanography, 22: 814-832.

Jørgensen, B. B., 1982, Mineralization of organic matter in the sea bed - the role of sulphate reduction, 296: 643-645.

Jørgensen, B. B. and S. D'Hondt, 2006, Ecology - A starving majority deep beneath the seafloor: Science, 314: 932-934.

Kallmeyer, J., T. G. Ferdelman, A. Weber, H. Fossing and B. B. Jørgensen, 2004, A cold chromium distillation procedure for radiolabeled sulfide applied to sulfate reduction measurements: Limnology and Oceanography: Methods, 2: 171-180.

King, G. M., 1983, Sulfate reduction in Georgia salt marsh soils: An evaluation of pyrite formation by use of ^{35}S -and ^{55}Fe-tracers: Limnology and Oceanography, 28: 987-995.

King, G. M., 1988, Patterns of sulfate reduction and the sulfur cycle in a South Carolina salt marsh: Limnology and Oceanography, 33: 376-390.

Kostka, J. E. and G. W. Luther, 1994, Partitioning and speciation of solid phase iron in saltmarsh sediments: Geochimica et Cosmochimica Acta, 58: 1701-1710.

Kostka, J. E., A. Roychoudhury and P. Van Cappellen, 2002, Rates and controls of anaerobic microbial respiration across spatial and temporal gradients in saltmarsh sediments: Biogeochemistry, 60: 49-76.

Kristensen, E., J. Bodenbender, M. H. Jensen, H. Rennenberg and K. M. Jensen, 2000, Sulfur cycling of intertidal Wadden Sea sediments (Königshafen, Island of Sylt, Germany): sulfate reduction and sulfur gas emission: Journal of Sea Research, 43: 93-104.

Lehmann, C. and R. Bachofen, 1999, Images of concentrations of dissolved sulfide in the sediment of a lake and implications for internal sulfur cycling: Sedimentology, 46: 537-544.

Lein, A. Y., 1983, Biogeochemistry of the anaeerobic diagenesis of recent Baltic Sea sediments: Ecol. Bull, 35: 441-461.

Llobet-Brossa, E., R. Rabus, M. E. Böttcher, M. Könneke, N. Finke, A. Schramm, R. L. Meyer, S. Grötzschel, R. Rosselló-Mora and R. Amann, 2002, Community structure and activity of sulfate reducing bacteria in an intertidal surface sediment: a multi-method approach: Aquatic Microbial Ecology, 29: 211-226.

Lovley, D. R., 1991, Dissimilatory Fe(III) and Mn(IV) Reduction: Microbiological Reviews, 55: 259-287.

Lovley, D. R., 1997, Microbial Fe(III) Reduction in subsurface environments: FEMS Microbiology Reviews, 20: 305-313.

Luther, G. W., J. E. Kostka, T. M. Church, B. Sulzberger and W. Stumm, 1992, Seasonal Iron Cycling in the Salt-Marsh Sedimentary Environment - the Importance of Ligand Complexes with Fe(II) and Fe(II) in the Dissolution of Fe(III) Minerals and Pyrite, Respectively: Marine Chemistry, 40: 81-103.

Middelburg, J. J., 1991, Organic-Carbon, Sulfur and Iron in Recent Semi-Euxinic Sediments of Kau Bay, Indonesia: Geochimica et Cosmochimica Acta, 55: 815-828.

Moeslund, L., B. Thamdrup and B. B. Jørgensen, 1994, Sulfur and Iron Cycling in a Coastal Sediment - Radiotracer Studies and Seasonal Dynamics: Biogeochemistry, 27: 129-152.

Morse, J. W., 1999, Sulfides in Sandy Sediments: New Insights on the Reactions Responsible for Sedimentary Pyrite Formation: Aquatic Geochemistry, 5: 75-85.

Musat, N., U. Werner, K. Knittel, S. Kolb, T. Dodenhof, J. E. E. van Beusekom, D. de Beer, N. Dubilier and R. Amann, 2006, Microbial community structure of sandy intertidal sediments in the North Sea, Sylt-Rømø Basin, Wadden Sea: Systematic and Applied Microbiology, 29: 333-348.

Peters, L., 2004, Zur Biogeochemie eines Sedimentkerns aus dem Mischwatt der südlichen Nordsee: Diploma Thesis, CvO Universität Oldenburg, 113 p.

Precht, E. and M. Huettel, 2003, Advective pore-water exchange driven by surface gravity waves and its ecological implications: Limnology and Oceanography, 48: 1674-1684.

Precht, E., U. Franke, L. Polerecky and M. Huettel, 2004, Oxygen dynamics in permeable sediments with wave-driven pore water exchange: Limnology and Oceanography, 49: 693-705.

Pyzik, A. J. and S. E. Sommer, 1981, Sedimentary iron monosulfides: Kinetics and mechanism of formation: Geochimica et Cosmochimica Acta, 45: 687-698.

Rabus, R., V. Bruchert, J. Amann and M. Konneke, 2002, Physiological response to temperature changes of the marine, sulfate reducing bacterium *Desulfobacterium autotrophicum*: FEMS Microbiology Ecology, 42: 409-417.

Rickard, D., 1975, Kinetics and mechanisms of pyrite formation at low temperatures: American Journal of Science, 275: 636-652.

Rusch, A., H. Topken, M. E. Böttcher and T. Höpner, 1998, Recovery from black spots: results of a loading experiment in the Wadden Sea: Journal of Sea Research, 40: 205-219.

Saager, P. M., J. P. Sweerts and H. J. Ellermeijer, 1990, A Simple Pore-Water Sampler for Coarse, Sandy Sediments of Low Porosity: Limnology and Oceanography, 35: 747-751.

Sass, H., H. Rütters, R. Schledjewski and E. Freese, 2003, Forschungszentrum Terramare, Berichte Nr.12, Biogeochemistry of Tidal Flats, Bonn, Delmenhorst, Forschungszentrum Terramare, p. 99-101.

Shum, K. T. and B. Sundby, 1996, Organic matter processing in continental shelf sediments--the subtidal pump revisited: Marine Chemistry, 53: 81-87.

Skyring, G. W. and F. S. Lupton, 1986, Anaerobic microbial activity in organic-rich sediments of a coastal lake: Abstract 12th Int. Sedi. Cong., Canberra Australia.

Skyring, G. W., 1987, Sulfate reduction in coastal ecosystems: Geomicrobiology Journal, 5: 295-374.

Skyring, G. W., 1988, Acetate as the main energy substrate for the sulfate-reducing bacteria in Lake Eliza (South Australia) hypersaline sediments: FEMS Microbiology Letters, 53: 87-93.

Stookey, L. L., 1970, Ferrozine - a New Spectrometric Reagent for Iron: Analytical Chemistry, 42: 779-781.

Sweeney, R. E. and I. R. Kaplan, 1973, Pyrite Framboid Formation; Laboratory Synthesis and Marine Sediments: Economic Geology, 68: 618-634.

Thamdrup, B., K. Finster, J. W. Hansen and F. Bak, 1993, Bacterial Disproportionation of Elemental Sulfur Coupled to Chemical-Reduction of Iron or Manganese: Applied and Environmental Microbiology, 59: 101-108.

Thamdrup, B., H. Fossing and B. B. Jørgensen, 1994, Manganese, Iron and Sulfur Cycling in a Coastal Marine Sediment, Aarhus Bay, Denmark: Geochimica et Cosmochimica Acta, 58: 5115-5129.

Thamdrup, B., J. W. Hansen and B. B. Jørgensen, 1998, Temperature dependence of aerobic respiration in a coastal sediment: FEMS Microbiology Ecology, 25: 189-200.

Thamdrup, B., 2000, Bacterial manganese and iron reduction in aquatic sediments: Advances in Microbial Ecology, 16: 41-84.

Thøde-Andersen, S. and B. B. Jørgensen, 1989, Sulfate reduction and the formation of ^{35}S-labeled FeS, FeS_2 and S_0 in coastal marine sediments: Limnology and Oceanography, 34: 793-806.

Trudinger, P. A., 1992, Bacterial sulfate reduction: current status and possible origin: In: M. Schidlowski, S. Golubic, M. M. Kimberley, D. M. McKirdy and P. A. Trudinger (eds), Early organic evolution: Berlin, Springer, p. 367-377.

Viollier, E., P. W. Inglett, K. Hunter, A. N. Roychoudhury and P. Van Cappellen, 2000, The ferrozine method revisited: Fe(II)/Fe(III) determination in natural waters: Applied Geochemistry, 15: 785-790.

Vosjan, J. H., 1974, Sulphate in water and sediment of the Dutch Wadden Sea: Netherlands Journal of Sea Research, 8: 208-213.

Walsh, J. J., 1991, Importance of continental margins in the marine biogeochemical cycling of carbon and nitrogen, Nature, 350: 53-55.

Werner, U., L. Polerecky, E. Walpersdorf, U. Franke, M. Billerbeck, M. E. Böttcher, T. G. Ferdelman and D. de Beer, 2003, Forschungszentrum Terramare Berichte Nr.12, Bonn; Delmenhorst, Forschungszentrum Terramare, p. 122-125.

Werner, U., M. Billerbeck, L. Polerecky, U. Franke, M. Huettel, J. E. E. van Beusekom and D. de Beer, 2006, Spatial and temporal patterns of mineralization rates and oxygen distribution in a permeable intertidal sand flat (Sylt, Germany): Limnology and Oceanography, 51: 2549-2563.

Westrich, J. T. and R. A. Berner, 1988, The effect of temperature on rates of sulfate reduction in marine sediments: Geomicrobiology Journal, 6: 99-117.

Wilms, R., H. Sass, B. Köpke, H. Köster, H. Cypionka and B. Engelen, 2006, Specific bacterial, archaeal and eukaryotic communities in tidal-flat sediments along a vertical profile of several meters: Applied and Environmental Microbiology, 72: 2756-2764.

Wollast, R., 1991, The coastal organic carbon cycle: fluxes, sources and sinks: In: M. R. F. C. Mantoura, J. M. Martin and R. Wollast (eds), Ocean margin processes in global change: London, John Wiley & Sons, p. 365-382.

Zhang, H. and W. Davison, 1999, Diffusional characteristics of hydrogels used in DGT and DET techniques: Analytica Chimica Acta, 398: 329-340

Dynamics of manganese in intertidal surface sediments.

K. Bosselmann, M. E. Böttcher, H. J. Brumsack, M. Billerbeck

In preparation

Abstract

In this study, we investigated the seasonal dynamics of the Mn cycling and it's interconnection to the Fe and S cycles in intertidal surface sediments of the North Sea. To quantify the exchange of dissolved Mn and Fe across the sediment-water interface, a combination of pore water, solid phase geochemistry and benthic flux measurements were performed in different sediment types. From the pore water profiles, it becomes evident that processes in the top 15 cm of the surface sediments are most important for Mn cycling and are controlling the metal flux across the sediment-water interface. Highest Mn^{2+} fluxes were measured at the mixed station N I due to the generally higher iron and manganese contents and microbial activities compared to sandy sediments. Gradients and concentrations of dissolved Mn in the pore water responded to the seasonal variation of microbial sulfate reduction and to changes in the reservoir of reactive metal oxides. This revealed the importance of chemical reduction of MnO_2 by biogenic sulfide in near-surface sediments. The decline of the Mn_{HCl} and Fe_{HCl} inventory indicated that, especially during the warmer months, manganese (Mn) escaped from the sediment by diffusion, advection and biological activity into the water column whereas the reactive Fe_{HCl} pool was re-precipitated or fixed in the sediment as sulfide. The comparison between measured flux rates and pool size variations indicated that more than 90 % of released Mn^{2+} was recycled and re-precipitated from the water column to the sediment. The dominance of Mn^{2+} release during spring and summer leads to a decrease of the sedimentary Mn_{HCl} inventory. Therefore, the flux of dissolved Mn^{2+} out of the sediment was larger than the external supply from the overlying water and was not balanced by re-sedimentation as observed during the colder months. Decreasing reductive conditions within the sediment during autumn and winter lead to lower release rates and the major part of the Mn cycling was restricted to the sediment. The external input of Mn oxide enriched particles from the water column replenished the sedimentary Mn_{HCl} pool during these months.

Introduction

Coastal marine sediments are characterized by input of terrestrial organic matter (Berner, 1989). In near shore waters, high nutrient concentrations lead to increased phytoplankton growth which generates up to 30 % of the total oceanic primary production (Walsh, 1991; Wollast, 1991). Intertidal areas, in particular represent a very dynamic and highly biologically productive transition zone between the terrestrial and marine ecosystem, e.g. the Wadden Sea. This system is influenced by solute and particle exchange between the coastal environments and the adjacent open North Sea mainly driven by the tidal water movement and freshwater inlets (Moore et al., 2002; Burnett et al., 2003). However, biogeochemical processes controlling element cycling in this unique environment are still poorly understood. Intertidal sediments are characterized by tidal and seasonal fluctuations of biological, chemical and physical properties and transformation processes at the sediment-water interface. Therefore, a variety of processes occurs particularly at the sediment-water interface driving the biogeochemical cycling of redox sensitive metals as manganese (Mn) and iron (Fe).

Mn functions as an essential micronutrient for phytoplankton as it is involved in photosynthesis and component of enzymes and proteins. Water column concentrations of dissolved Mn (Mn^{2+}) are elevated in the Wadden Sea compared to the open North Sea and showed seasonality with highest Mn concentrations during summer time (Dellwig et al., 2007). In addition to the seasonal effect, a shorter tidally induced cycling was observed with concentrations distinctly increasing towards low tide, suggesting that besides the freshwater input back-barrier intertidal flats may act as important bioreactors and temporal sources of dissolved Mn in the Wadden Sea (Dellwig et al., 2007).

Within the sediment, Mn and Fe act as important terminal electron acceptors for the oxidation of organic matter. In the sequence of redox processes, microbial Mn and Fe reduction begins after depletion of oxygen (O_2) and nitrate but before net sulfate reduction (Thamdrup, 2000). Mn and Fe can be re-circulated through various redox processes (e. g. Thamdrup et al., 1994; Canfield et al., 1993). The oxidation and reduction of Mn (III), (IV) occurs typically by direct chemical reaction with e.g. reduced Fe and sulfide or indirectly mediated by chemoautotrophic and heterotrophic biological activity (Lovley, 1991; Nealson & Myers, 1992; Thamdrup et al., 1994). Therefore, sulfate reduction is likely involved in Mn mobilization via chemical reduction of Mn oxides by sulfide (Burdige, 1993) resulting in a short scale metal cycling at the sediment surface with enrichment of oxidized Mn and Fe precipitates. This indicates the close coupling between the biogeochemical processes of metal and sulphur cycle (Burdige & Nealson, 1986). The biogeochemical cycling of Mn is controlled by redox transformations involving dissolved Mn^{2+} and insoluble oxides and oxy(hydroxid)es of Mn (III), (IV) (e.g. Stumm & Morgan, 1995; Neretin et al., 2003; Zopfi et al., 2001; Millero, 1991). Oxidized Fe is readily reduced by H_2S (Pyzik & Sommer, 1981).

Equ. 1: $2\ FeOOH + H_2S \rightarrow 2\ Fe^{2+} + S^o + 4\ OH^-$

and H_2S and ferrous Fe become electron donors for Mn oxides and thus function as control for the accumulation of dissolved sulfide in the sediments (Equ.2 and 3; Goldhaber & Kaplan, 1974; Canfield, 1989). The oxidation of Mn^{2+} by NO^{3-} plays a minor role in the investigated sediments (Luther et al., 1997).

Equ. 2: $MnO_2 + H_2S \rightarrow Mn^{2+} + S^0 + 2\ OH^-$

Equ. 3: $MnO_2 + 2\ Fe^{2+} + 2\ H_2O \rightarrow Mn^{2+} + 2\ FeOOH + 2\ H^+$

In chemical experiments FeS and FeS_2 were also oxidized by MnO_2. The oxidation of FeS_2 produces a variety of sulphur intermediates as (e.g. trithionate, tetrathionate; Schipper & Jørgensen, 2001).

Equ. 4: $4.5\ MnO_2 + FeS + 7H^+ \rightarrow 4.5\ Mn^{2+} + SO_4^{2-} + Fe(OH)_3 + 2\ H_2O$

Equ. 5: $MnO_2 + 7.5\ FeS_2 + 11\ H^+ \rightarrow 7.5\ Mn^{2+} + 2\ SO_4^{2} + Fe(OH)_3 + 4\ H_2O$

Promoted by the presence of sulfide agents such as Fe and Mn oxy(hydroxi)des the microbial disproportionation of S_0 to sulfate and sulfate was observed as follows (Thamdrup et al., 1993; Böttcher et al., 2001; Böttcher & Thamdrup, 2001; Lovley & Phillips, 1994):

Equ. 6: $4H_2O + 4S_0 \rightarrow 3H_2S + SO_4^{2-} + 2H^+$

Equ. 7: $3H_2S + 3MnO_2 \rightarrow 3Mn^{2+} + 3S_0 + 6OH^-$

Equ. 8: $S_0 + 3MnO_2 + 4H^+ \rightarrow SO_4^{2-} + 3Mn^{2+} + 2H_2O$

Following Mn reduction, Mn^{2+} may precipitate as a reduced authigenic mineral mainly mixed MnCa-carbonates (Jakobsen & Postma, 1999; Böttcher 1998) or may be adsorbed to clay minerals. After upward transport, it is partly re-precipitated as oxidic phases at or close to the surface sediment or escapes to the overlying water due to slow oxidation rates (Middelburg et al., 1987; Aller, 1994). In contrast, differences in reaction kinetics and thermodynamics i.e. faster oxidation rates of Fe^{2+} and oxidation of Fe^{2+} by oxidized Mn impede the diffusion of dissolved Fe into the overlying water (e.g. Balzer, 1982; Postma, 1993; Lovley & Phillips, 1988).

High sulfate reduction rates in the absence of accumulating sulfide are indicative for a very efficient re-oxidation of dissolved sulfide and are partly a consequence of the interaction between the metal and sulphur cycles (Thamdrup et al., 1994; Böttcher et al., 2004; de Beer et al., 2005). If reactive Fe is available in sufficient amounts, parts of the sulfide will react to form Fe sulfide minerals (Pyzik & Sommer, 1981). A distinct seasonal peak of microbial activity in summer caused more pronounced reducing conditions which favoured the reduction of solid Mn oxy(hydroxi)de phases to soluble Mn^{2+}. The effect of temperature and organic matter content on microbial activity and corresponding Fe cycling in the investigated intertidal surface sediments has been demonstrated by studies of microbial sulfate reduction (Böttcher et al., 1998, 2000, 2004; Bosselmann et al., 2003, in prep.). Abiotic reductions with inorganic compounds are competing processes for microbial mediated reduction and difficult to distinguish. Bacterial Mn and Fe reduction inhibits and competes with sulfate reduction

when a sufficient amount of reactive metal oxides is available (Lovley & Phillips, 1987; King, 1990) as well as Mn reduction can partially inhibit Fe reduction (Lovley & Phillips, 1987; Myers & Nealson, 1988; Thamdrup et al., 1994). Sulfide oxidation reactions involving metal oxides and reduced sulphur species lead to complex pathways of anaerobic sulphur cycling. Many processes take place simultaneously, depending on the overall redox chemistry and the availability of electron donors and acceptors in different sediment types and are therefore difficult to quantify.

In this study, the cycles of Mn and fluxes across the sediment-water interface were investigated to quantify process rates in order to understand the role of the benthic biogeochemistry on element cycling and interactions between Mn, Fe, and sulphur (S) in surface sediments (Böttcher et al., 2004; Bosselmann et al., in prep.). Therefore, element dynamics were investigated on a seasonal basis at study sites covering a range of intertidal sediments differing in biological activities and physico-chemical properties (organic matter and metal content, grain size, permeability and porosity).

Material and Methods

Study areas

The study sites are located in the intertidal area of Spiekeroog Island in the southern North Sea (Figure 1) and were chosen to include a range of sediments with different sedimentological and geochemical properties (grain size, organic matter and metal content, permeability and porosity) and biological activities (Table 1). The tides in this area are semi-diurnal. The tidal flats of Neuharlingersiel (N I) and Janssand (S I + S III) represent intertidal mixed and sandy sediments respectively. As a muddy site, a mud flat in the close-by Jade Bay (Site (D)angast; Figure 1) has been investigated on a seasonal basis. About 50 m away from the sampling location N I, two separate sampling events were performed in April and November 2002 only. This station (N II) is characterized by a slightly higher content of finer grained sediment compared to station N I, which was washed in by the adjacent outflow of a land reclamation area (further details, see Batel, 2003; Peters, 2004).

The Janssand flat is characterized by a slope of 1.6 cm m^{-1} in average toward the low water line and is covered by a water column of approximately 1.5 to 2 m during high tide. Sampling occurred along a transect which included 4 positions, but the lower sand flat position near the low water line (S I) and the upper sand flat site (S III, approximately 45 m upslope the sand flat) were chosen as the main study areas (Figure 1). The upper parts of this tidal flat become exposed to air for about 6 to 7.5 hours, the lower position falls dry for 3-4 hours during low tide. Hertweck (1995) observed that low macrofaunal abundance at exposed sides such as the Janssand sand flat is due to enhanced current velocities. During our investigations only a random occurrence of *Arenicola marina* and *Nereis diversicolor* was found. During summer, we observed a 6-fold decrease in *Arenicola marina* fecal mounds at a station close to the tidal channel compared to a station on top of the sand flat (Billerbeck, pers. communication). At the position near the waterline, layers of finer grained sediment were found in various depths. High current velocities because of the adjacent channel, leads to a permanent reworking of the sediments at the Janssand station.

The intertidal flat of Neuharlingersiel which becomes exposed for about 6-7 hours during low tide (Billerbeck et al., 2006a,b) represents mixed sediment of various grain size classes (Table 1). The Dangast station is influenced by fluvial input of the Weser river and is comparable to an estuarine system (Figure 1). The tidal cycles lead to an inundation time of about 7 hours and an exposure time of about 5 hours. The top 10 cm of the sediment were dominated by the mud fraction (Table 1; see Böttcher et al., 2000; Llobet-Brossa et al., 2002).

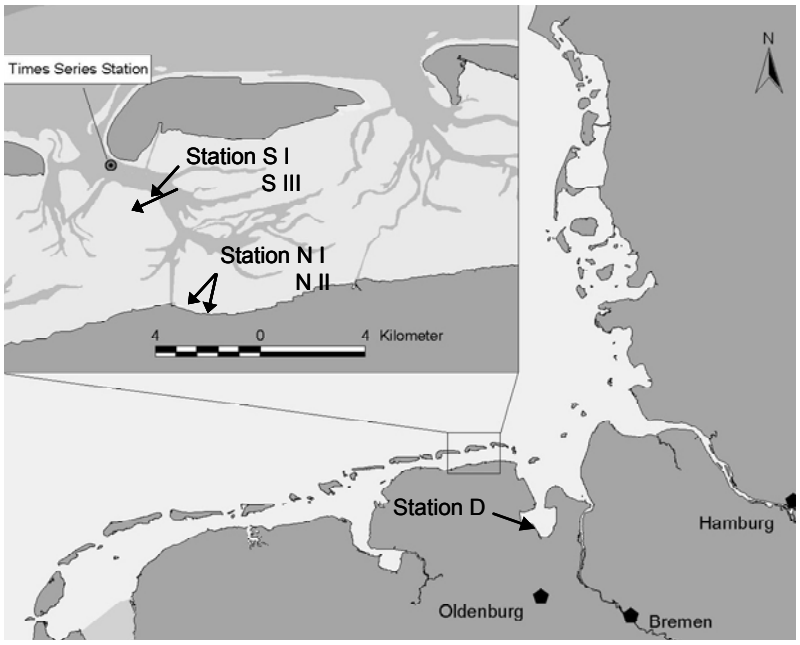

Figure 1: Location of the study area, in the back-barrier tidal area of Spiekeroog island, Wadden Sea, Germany.

Methods

Several parallel sediment cores (PC tubes; 3.6 to 10 cm in width; 20-40 cm in length) were sampled in an area of about 1 m^2 during low tide. The investigations were carried out in the field (in-situ) as well as by laboratory analyses and incubations. Sediment cores and interstitial waters were typically analyzed down to about 15 cm depth for a number of parameters: SRR, TOC, TIC, SO_4, Fe^{2+}, Mn^{2+}, reactive Fe (III), Mn (III), salinity, water content, grain size.

Two parallel sediment cores were analyzed in 1 cm intervals for porosity by measuring wet density (weight of a known volume) and water content (drying at 105 °C for 24 h weight constancy). The pore water temperature was measured in-situ with a digital sensor (GTH 1150 digital thermometer). Total Carbon (TC) was measured from freeze-dried samples using a CNS element analyzer (Fison Instruments, NA 1500, Series 2) and total inorganic carbon (TIC) on a CM 5012 CO_2 coulometer with a CM 5130 acidification module (UIC). Total organic carbon (TOC) content was calculated from the difference of TC and TIC. Freeze-dried sediment samples were pre-treated with H_2O_2 (30 %) and washed with distilled water, subsequently dried and analyzed by laser deflection (Fritsch Analysette 22) to determine grain size distribution. Microbial SRR were measured by the whole-core tracer incubation technique (Fossing & Jørgensen, 1989; Kallmeyer et al., 2004). Sediment cores were transported to the laboratory under in-situ temperature and dark conditions for further processing. Two parallel cores were stored in darkness at the daily maximum and minimum in-situ temperatures for about 10-12 hours. Carrier-free $^{35}SO_4^{2-}$- radiotracer solution (~200 kBq) was injected in 1 cm intervals down to 15 cm. After 4 h incubation in the dark, the sediment cores were sliced into 1 cm sections and immediately mixed with 10 ml of a 20 % Zinc Acetate solution to interrupt the microbial processes and to fix sulfates. Radioactivity of ^{35}S was determined using a Packard Liquid scintillation analyzer

(2500IR). The cold two-step distillation procedure was used to recover acid volatile sulphur (AVS = $FeS + HS^-$) and chromium reducible sulphur (CRS = $FeS_2 + S^0$) from the sediment. In contrast, the samples from Neuharlingersiel (March 2002) were analysed using the hot one step distillation (Fossing & Jørgensen, 1989).

The total reduced inorganic sulphur (TRIS) pool was calculated from the individual AVS and CRS measurements by the methylene blue method (Cline, 1969), using a Shimadzu UV-160A Spectrophotometer.

The extractable fraction of Fe and Mn were extracted from freeze-dried sediment using buffered dithionite-citrate acetic acid solution (Canfield, 1989) and 0.5 M HCl, respectively (Thamdrup et al., 1994; Kostka & Luther, 1994). Extraction with HCl for 1 hour is selective for the amorphous or poorly crystallized Fe- and Mn oxide and carbonate phases, while citrate-dithionite solution additionally liberates minor amounts of amorphous Fe-containing silicates (Canfield, 1989). Both extraction methods showed comparable contents of reactive Fe phases (for further details see chapter 2). Therefore, only data of HCl extractable Fe (Fe_{HCl}) are shown. The amount of reactive Fe_{HCl} was calculated from the difference between the HCl leachable Fe and the AVS fraction. Fe was determined spectrophotometrically using reducing Ferrozine (Ferrozine reagent with 1 % hydroxylamine-hydrochloride; Stookey, 1970; Viollier et al., 2000) whereas Mn was quantified by flame atomic absorption spectroscopy (Perkin Elmer AAS).

After sectioning the core in a glove box under inert gas atmosphere, pore waters were separated from the sediments in April 2004 by centrifugation (centrifuge tube; Saager et al., 1990) through membrane filters (Millipore, Amicon Bioseperations, PVDF-membrane 0.45 µm). The salinity of the pore water samples was measured with a hand-refractometer (Atago, SI Mill-E). An aliquot of the pore water was kept frozen for the determination of sulfate using a Dionex LC30 DX 500, WATERS Ion liquid chromatograph. The concentration of dissolved Fe^{2+} was measured immediately after filtration using Ferrozine reagent with 1 % hydroxylamine-hydrochloride (Stookey, 1970). Another aliquot of pore water was acidified (2 % HNO_3, suprapure quality) and the concentrations of dissolved Fe^{2+} and Mn^{2+} were measured after appropriate dilution by ICP-OES (Perkin Elmer Optima 3000 XL) with Scandium as an internal standard or by ICP-MS (Thermo Finnigan MAT ELEMENT). For parallel high resolution measurements of dissolved Fe (Fe^{2+}) and Mn (Mn^{2+}) in the pore water the technique of diffusive equilibration in thin films (DET; Davison & Zhang, 1994; Zhang & Davison, 1999) was used. Solutes equilibrate with the water of the hydrogels which were inserted in the sediment cores for 24 hours. After removal, the hydrogel was sliced in 0.5 cm intervals and re-equilibrated for 24 hours with HNO_3 (2 % suprapure quality). Figure 2 shows that pore water concentrations sampled by DET were in agreement with usual extracted samples. Discrepancies refer to sediment heterogeneity which may be balanced by diffusion with increasing depth. PROFILE (Berg, 1998) calculated Mn^{2+} fluxes were generally low in September and variations between compared pore water profiles showed fluxes of 5.8E-5 µmol m^{-2} h^{-1} sampled by DET and 7.3E-5 µmol m^{-2} h^{-1} for squeezed pore water at station N I. Fluxes at station S I varied form 3.56E-8 µmol m^{-2} h^{-1} for DET profiles and 2.67E-9 µmol m^{-2} h^{-1} (Figure 2).

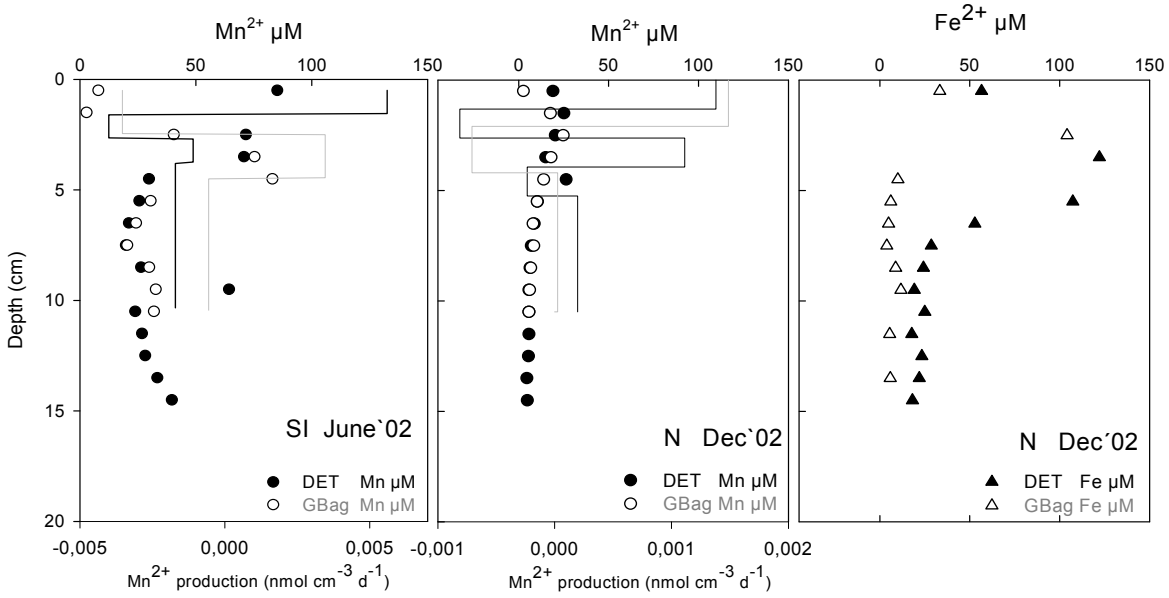

Figure 2: Comparison of dissolved Mn and Fe sampled by using diffusive equilibration in thin films (DET) and a glovebag (GBag).

The PROFILE program of Berg et al. (1998) allows a numerical interpretation of pore water profiles and enables the calculation of fluxes across the sediment water interface and net production and consumption for distinct depths. A series of possible fits are compared through the statistical F-test. For our predictions the influence of factors like bioturbation and irrigation were neglected and steady state conditions were assumed because the original pore water profile re-established rapidly after perturbation by advective and diffusive transport processes. The objective was to identify zones of Mn reduction and re-precipitation that provide an estimation of reactive zone corresponding to the measured fluxes. For the indication of saturation processes, data from pore water of station N II and sediment incubations (Batel, 2003; Peters, 2004) have been modelled by PHREEQE-C, a thermodynamic ion-association model (Batel, 2003; Peters, 2004; Parkhurst et al., 1980; Parkhurst, 1995). For the application of PHREEQE, the ionic strength of seawater has to be considered to prevent an overestimation of the activity coefficients.

In-situ flux measurements were performed using cylindrical benthic chambers (19 cm diameter, 3.5 l volume). To simulate a natural advective flow through the surface layer of the sediment, a rotating disc (15 cm diameter, 20 rpm) produced a radial pressure gradient (Huettel & Gust, 1992a,b; Huettel & Rusch, 2000). Two transparent and two or four opaque chambers were deployed to estimate the influence of O_2, nutrient, and metal exchanges at the sandy stations and station N. O_2 concentrations were measured within each chamber with fibre optic microoptodes inserted through the chamber lid or measured by the Winkler (1888) method. After inundation all chambers were sampled in hourly intervals with a syringe via a 1 m Tygon^{TM} tube connected to a sampling port in the chamber lid. Additionally, samples of ambient seawater were taken at each sampling interval. The sampled water volume was replaced with ambient seawater via a further port in the chamber lid.

Results

Selected biogeochemical sediment properties

Table 1 gives an overview about biogeochemical properties of the investigated sites. The sandy stations I and III consisted of well sorted fine grained sand. The water content ranged from 16-21 % at the upper sand flat station S III. Sediments at the lower station S I contained finer grained layers in various depths, and showed corresponding higher water contents of 18-27 %.

Table 1: Overview about sediment biogeochemical properties of the different locations range over the surface 10 cm.

	S I				S III				N I				N II	D					
sampling date	07.06.02	01.10.02	22.07.03	26.03.04	20.03.02	07.06.02	01.10.02	22.07.03	05.04.02	20.06.02	10.10.02	04.08.03	25.11.02	15.04.98	20.05.98	16.06.98	21.07.98	20.08.98	14.10.89	15.01.99
Average 10 cmbsf																				
Temp [°C]	15-25	11-16	20-31	7-10	7-15	15-25	11-16	20-31	7-15	18-31	15-20	22-32	6-11	further information see Böttcher et al., in prep.						
Grain size [%vol]																				
[<2µm]				1.1%				0.6%				6%					15,6%			
[<63µm]				3.1%				1.0%				21.3%					84,1%			
[<580µm]				95.7%				98.3%				72.7%					0,5%			
TOC [%]	0.08-0.2	0.04-0.1	0.06-0.2	0.02-0.3	0.02-0.09	0.003-0.0	0.03-0.1	0.02-0.13	0.4-1.2	0.4-0.6	0.3-0.5	0.4-0.7	0.5-2.6	1-3.3		1,4-3,5		3-3,2		
SO_4 [mM]	23-26	25-26	12-27	21-25	23-30	25-27	22-30	26-29	n.d.	23-26	22-24	22-30	18-24	17-21		17-21	18-26	16-19	22-24	
H_2O [%]	18-20	18-22	18-27	19-28	19-21	17-18	16-21	18-21	22-40	21-30	23-29	21-33	37-84	30-75		55-72		55-63	19-66	
Salinity [psu]	30-31	32-33	30-33	28-31	28-30	32-33	33-35	33-34	n.d.	28-32	28-30	30-32	24-25			26-27		22-23,5		

High variations of sulfate concentrations were observed in the pore water of S I. The vertical distribution of pore water sulfate below oxic surface sediments decreased from 25-22 mM with depth. Spatially restricted spots with anoxic surface conditions exhibited differing vertical pore water profiles (Bosselmann et al., in prep). In contrast, dissolved sulfate concentrations at S III remained constant with depth during all sampling campaigns. The mixed sediments of station N I consisted of various grain size classes. The surface 10 cm of the sediment at station N II contained a higher proportion of mud, due to the wash in from the adjacent land reclamation areas (Table 1). The inflow of freshwater was also reflected by a salinity of 24-25 psu and low sulfate concentrations of 18-24 mM. The salinity at station N I varied from 22 to maximum surface values of 34 psu in summer. Salinities below the typically found 33 psu of the German Bight (Dellwig et al., 2007) are due to the mixture with freshwater which is discharged to the Wadden Sea by floodgates (e.g. Neuharlingersiel) and rivers (e.g. Weser near Dangast), especially during the rainy seasons in spring and autumn. The grain sizes at the Dangast station (D) were dominated by a mud fraction (Table 1). The high capacity of clay minerals to adsorb organic matter is typically reflected by a positive correlation to the TOC content (Delafontaine et al., 1996; Böttcher et al., 2000).

Solid phase manganese

All investigated stations experienced regular periods of loss and gain in the inventory of reactive Mn_{HCl} (Figure 3). Highest seasonal variations in the Mn_{HCl} pool size occurred within the top 3 cm layer. The surface enrichment reached highest Mn_{HCl} amounts of up to 800 ppm at the muddy station D in April,

which decreased to 200-300 ppm in 5-10 cm depth. Surface Mn_{HCl} contents decreased to a minimum of 300 ppm in August. At the mixed station N I, highest surface amounts of Mn_{HCl} were 4 times lower with contents of 200 ppm in spring 2002. The Mn_{HCl} pool depleted from 110 ppm in June to 60 ppm in September and increased again up to 130 ppm until December. Below 5 cm depth, the Mn_{HCl} pool size showed only low variability which ranged around an average amount of 30 +/- 10 ppm. Compared to station N I (mixed sediment), the sandy station S III revealed an up to 10 times lower and station S I a 3-5 times lower Mn_{HCl} pool size. Surface variation at S I ranged from lowest values of 20 ppm in September to 50-60 ppm in December and April. Peak values of 60 ppm were found in 3 cm depth in June and 130 ppm in 5 cm depth in December. This was associated to imbedded layers of finer grained material. Furthermore, transport and accumulation of suspended matter deeper into the permeable sediment may have been supported by intensive wave activity at this station during low tide. The upper sandy position III reached maximum surface amounts of 40 ppm in June, followed by 25 ppm in march and lowest amounts of 3 ppm in summer 2003, increasing again to 13-17 ppm from September to December (Figure 3).

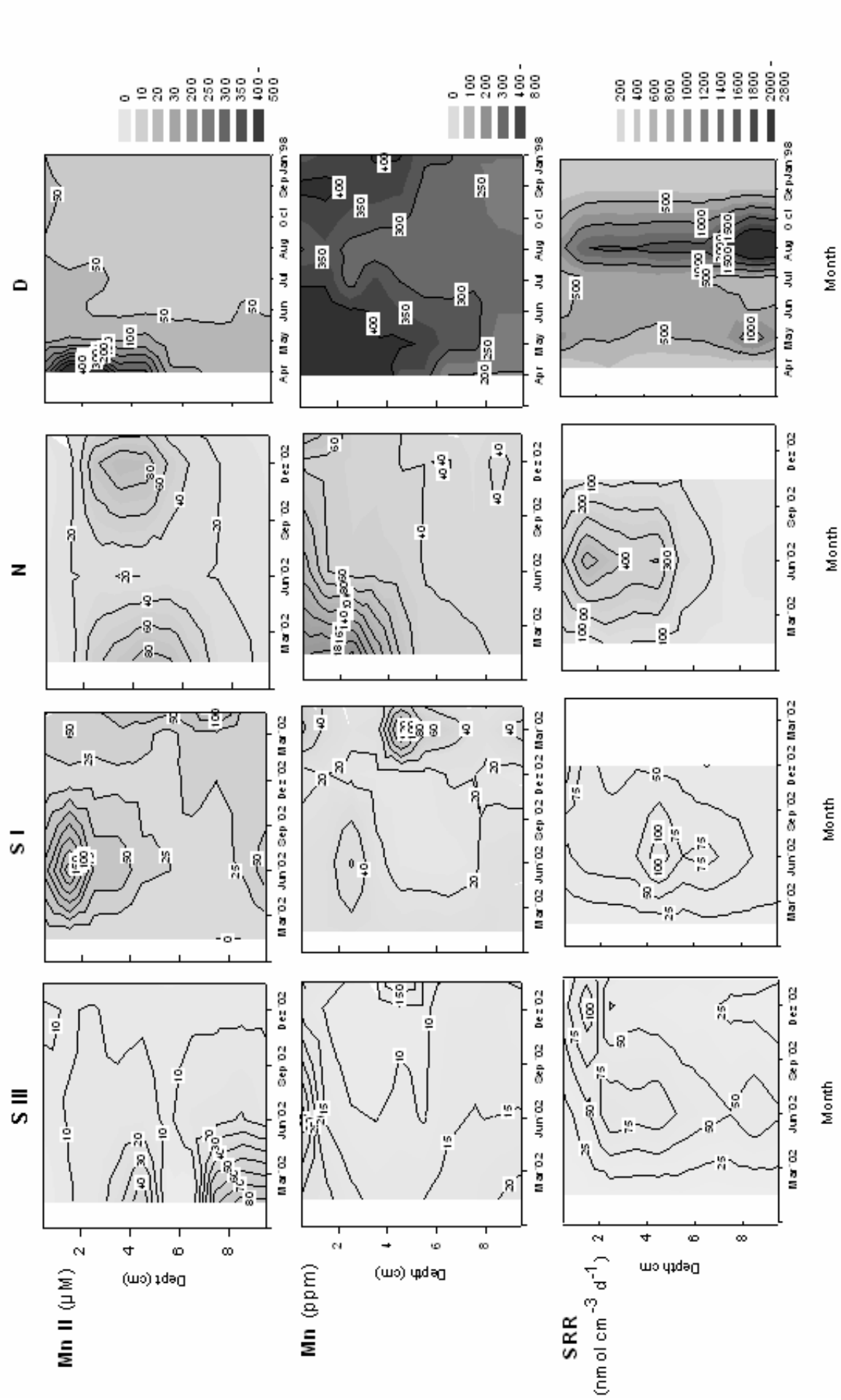

Figure 3: The seasonal depth distribution of dissolved Mn^{2+} and reactive Mn_{HCl} pool inventory. Both showed seasonal correspondence to microbial sulfate reduction.

Table 2: Average solid Fe_{HCl} and Mn_{HCl} inventory of the top 0-1 and 0-10 cm and relationship of Fe/Mn.

	N				S I			S III				D			
	Depth [cm]	Mn [mg/kg]	Fe [mg/kg]	Fe/Mn	Mn [mg/kg]	Fe [mg/kg]	Fe/Mn	Mn [mg/kg]	Fe [mg/kg]	Fe/Mn		Depth [cm]	Mn [mg/kg]	Fe [mg/kg]	Fe/Mn
March ´02	0-1	179	2000	**11**	32	358	**11**	24	230	**10**	**March `98**	0-1	796	1665	**2**
	0-10	98	1582	**21**	29	316	**11**	18	269	**15**		0-10	395	940	**2**
June ´02	0-1	111	1533	**14**	29	397	**14**	38	345	**9**	**June ´98**	0-1	444	1815	**4**
	0-10	49	1201	**27**	26	350	**15**	15	269	**20**		0-10	340	1500	**4**
Sep. ´02	0-1	57	1259	**22**	16	289	**18**	13	265	**20**	**Oct. ´98**	0-1	413	1923	**5**
	0-10	44	1253	**30**	17	302	**17**	10	223	**22**		0-10	310	1300	**4**
Dec. ´02	0-1	129	1446	**11**	63	712	**11**	18	255	**14**	**Jan. ´99**	0-1	329	982	**3**
	0-10	35	1051	**27**	51	519	**13**	12	257	**20**		0-10	290	997	**3**
July ´03	0-1	156	1118	**9**	36	0	**22**	3	0	**69**	**July ´98**	0-1	390	1791	**5**
	0-10	55	1168	**25**	12	374	**36**	5	267	**55**		0-10	280	1330	**5**

The reactive Mn_{HCl} inventory (Table 2) was up to 10 times smaller than the reactive Fe_{HCl} pool at the mixed (N) and sand flat (S I, III) stations, and showed different seasonal dynamics within the upper 15 cm. The muddy station D revealed a notably higher Mn_{HCl} inventory due to the high capacity of the mud fraction to absorb Mn. The Fe_{HCl} inventory showed comparable amounts to station N. The Mn_{HCl} inventory was related to the HCl leachable Fe pool (Fe_{HCl}) which was not acid volatile sulphur fraction (FeS) corrected, to point out that the main Fe cycling is restricted by sulfide fixation to the sediment. On a seasonal basis, the relation of Fe/Mn reflects the different reaction kinetics and thermodynamics i.e. slower oxidation rates of Mn^{2+} compared to Fe^{2+} and oxidation of Fe^{2+} by oxidized Mn (Stumm & Morgan, 1981; Lovley & Phillips, 1988).

For instance, the Fe/Mn relation showed at all stations the highest seasonal amplitude in the surface 5 cm of the sediment (Table 2). The increasing Fe/Mn relation at station D reflects that, compared to the Fe pool, the Mn content decreases much stronger during the warmer months. At station N, Mn enrichment developed at the surface 3 cm in spring leading to a low Fe/Mn ratio of 13 compared to highest values up to 29 in September when Mn was depleted. Stronger seasonal amplitudes of gain and loss were found in the sandy sediments. Highest Fe/Mn ratios in summer 2003 reflected the stronger decrease of Mn_{HCl} compared to the Fe_{HCl} pool (S III 63, S I 29). Lowest Fe/Mn relations in spring (11-13) reflected the re-establishment of the Mn inventory. This indicates that, especially during the warmer months, Mn was released from the sediment by diffusion into the water column whereas the reactive Fe_{HCl} pool was re-precipitated or fixed in the sediment as sulfide. Compared to the Mn_{HCl} contents the $Fe_{HCl+AVS}$ pool showed only small seasonal variations because the Fe cycle was restricted to the sediment.

Dissolved manganese

Solute transfer across the sediment-water interface is typically dominated by molecular diffusion, which leads to the establishment of steep pore water gradients. The gradients of dissolved Fe^{2+} and Mn^{2+} observed in the pore water point at an intense cycling of these metals in the surface sediment. The reduction of reactive solid Fe and Mn minerals by biogenic hydrogen sulfide leads to a release of Fe^{2+} and Mn^{2+} into the pore water (Figure 3, 4). At the sediment surface, sulfides, such as hydrogen

sulfide (H_2S), may also be re-oxidized via direct or microbial mediated reaction with O_2 and/or reactive metal oxides. Therefore, highest concentrations of dissolved Fe and Mn were related to the zone of microbial activity and differed depending on sediment type and season.

During the sampling campaigns, dissolved Fe^{2+} and Mn^{2+} concentrations in the pore water of station D ranged from 10-500 µM Mn^{2+} and 3-330 µM Fe^{2+}. Highest concentrations were found in spring and lowest in winter (January). Zones of intensive metal reduction were established within the surface 5-10 cm, which were less pronounced during autumn and winter. Mn reduction, calculated with PROFILE reached highest rates of 53 µmol m^{-2} h^{-1} near the surface in April and ranged from 2 to 0.2 µmol m^{-2} h^{-1} within the top 10 cm depth during the rest of the year.

At station N, maximum Mn^{2+} concentrations of 190 µM were found within the surface layer during summer, while winter values were distinctly lower (46 µM). Spring and autumn data showed peak values (80-90 µM) deeper in the sediment which correspond to zones of intensive sulfate reduction. Low ferrous Fe concentrations in July 2003 indicate the rapid precipitation of Fe^{2+} as sulfide and the limited re-supply of reactive Fe oxides. High amounts of up to 330 µM Fe^{2+} were found in December followed by 170-180 µM in March and June. The depth distribution reflects the correspondence of dissolved Fe^{2+} and Mn^{2+} maxima to the zone of microbial sulfate reduction within the surface 5 cm. The PROFILE modelled Mn reduction rates in productive zones ranged at station N I from 0.03 µmol m^{-2} h^{-1} (0-2 cm) in June and 1.3 µmol m^{-2} h^{-1} (2-6 cm) in March up to 9.1 µmol m^{-2} h^{-1} in July.

Pore water profiles at station N II showed a steep Mn^{2+} concentration gradient in the surface layer in April and highest Mn^{2+} reduction rates in November within the top 8 cm. Subsequently increasing Fe^{2+} concentrations indicate the influence of Mn reduction by Fe^{2+} (Figure 4). PROFILE calculated Mn reduction resulted in rates of 120-140 µmol m^{-2} h^{-1} (0-2 cm and 5-8 cm) in November and 44 µmol m^{-2} h^{-1} (0-4 cm) in April.

The PHREEQE model reflects potential saturation processes for rhodocrosite ($MnCO_3$) and aragonite ($CaCO_3$) in the pore water of station N II in April. The November profile indicates the potential precipitation of rhodocrosite ($MnCO_3$) and aragonite ($CaMg(CO_3)_2$ which both was probably inhibited by a high partial pressure of CO_2 (Batel, 2003). Precipitation of siderite ($FeCO_3$) was of less importance in the zone of sulfate reduction and increased slightly below 7 cm depth in November (for further details see Peters, 2004; Batel, 2003).

At the lower sand flat station S I, highest Mn^{2+} concentrations were measured in April (100 µM) and June (180 µM) whereas lowest values were found in the warmer months of July (20 µM) and September (30 µM). Dissolved Fe reached high surface concentrations of 200 µM in summer 2003 and lowest values in December (20 µM). In April and June maximum Fe^{2+} amounts reached 60-90 µM. This indicates that re-oxidation of Fe^{2+} by Mn-oxides superimposed the mobilization of ferrous Fe and Fe^{2+} only increased when the pool size of Mn-oxides had depleted as a result of intensive sulfate reduction. PROFILE modeled Mn^{2+} production zones showed a rate of 2.4 µmol m^{-2} h^{-1} (0-1 cm) in summer which decreased to values below 0.002 µmol m^{-2} h^{-1} during the year. At station S I, the

development of puddles filled with anoxic pore water – so called `black spots` indicated localized release of sulfidic pore water draining off the sloping sand flat. As a result of embedded finer grained layers at station S I, water flow followed preferential pathways through the sediment which were reflected by high spatial variations in dissolved Fe^{2+} and Mn^{2+} concentrations. The local drainage of anoxic pore water at station S I could be observed during all seasons.

Lowest Mn^{2+} concentrations were measured at the sand flat station S III. A steep increase with depth was found in March and reached highest concentrations up to 80 µM in 10 cm depth. Dissolved Mn concentrations varied between 2-20 µM in June, September and December and reached lowest values of 2 µM in July 2003. In contrast, ferrous Fe reached high surface concentrations of 70 µM in summer 2003. The enhanced input and mineralization of reactive organic matter in July and September caused peak values of 2-12 µM at the sediment surface, whereas highest microbial activity shifted to greater depths of 5-14 cm in March June and September (Figure 3, 4). A steep increase of Fe^{2+} with maximum values of 180 µM appeared in 8 cm depth in December. Mn reduction modeled by PROFILE revealed low rates of 0.07 µmol m^{-2} h^{-1} (0-6 cm) in March and only 7E-05 µmol m^{-2} h^{-1} (0-2 cm) during summer. Furthermore, Fe and Mn pore water profiles showed an overlap in the zones of highest reduction rates and indicating the importance of Mn reduction via ferrous Fe^{2+} (Figure 3; Postma, 1985; Burdige et al., 1992; Myers & Nealson, 1988). Therefore, the depletion of reactive Mn oxides during summer leads to increasing Fe^{2+} concentrations accompanied by low Mn^{2+} liberation in the pore water (Figure 4, Table 2).

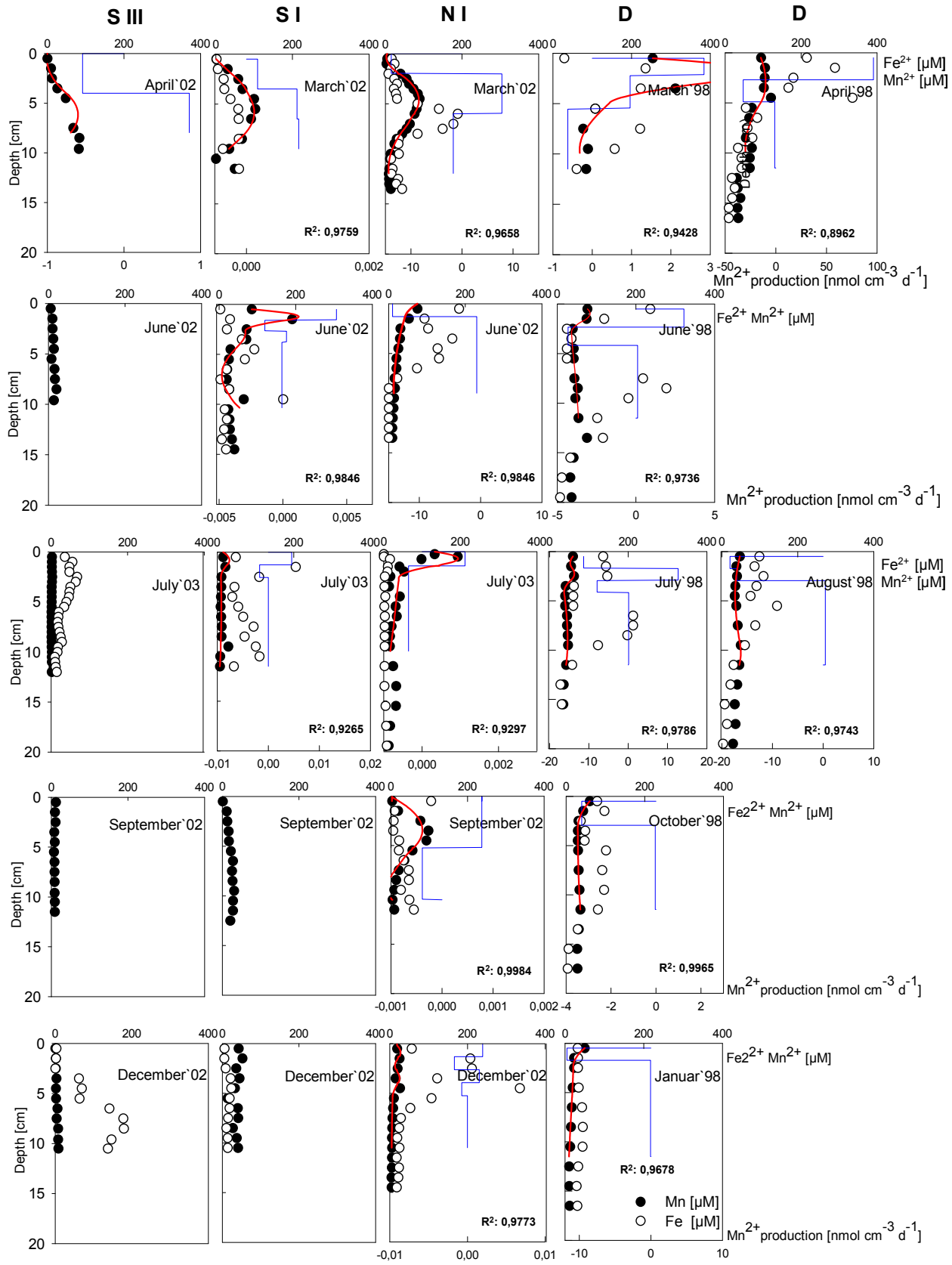
S III
S I
N I
D
D
April`02
March`02
March`02
March`98
April`98
June`02
June`02
June`02
June`98
July`03
July`03
July`03
July`98
August`98
September`02
September`02
September`02
October`98
December`02
December`02
December`02
Januar`98
R²: 0,9759
R²: 0,9658
R²: 0,9428
R²: 0,8962
R²: 0,9846
R²: 0,9846
R²: 0,9736
R²: 0,9265
R²: 0,9297
R²: 0,9786
R²: 0,9743
R²: 0,9984
R²: 0,9965
R²: 0,9773
R²: 0,9678
Depth [cm]
Fe2+ [µM]
Mn2+ [µM]
Mn2+ production [nmol cm-3 d-1]
Mn [µM]
Fe [µM]

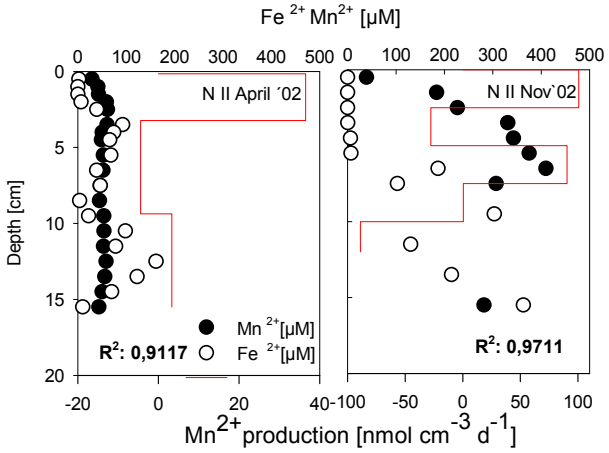

Figure 4: Vertical distribution of dissolved Fe^{2+} (open circles) and Mn^{2+} (filled circles) in the pore water (no Fe^{2+} data at available during April, June and September at station S I and/or III; sampled by *DET technique and pore water squeezing (*PW); data station D from Böttcher et al., 2000).

Benthic chamber experiments

Table 3: Mean fluxes of dissolved Mn^{2+} (± SD) and O_2 fluxes determined by using transparent and opaque benthic flux-chambers. O_2 fluxes were calculated from start-end concentrations of the incubations.

Fluxes µmol m^{-2} h^{-1}	**N**				**S I**				**S III**			
	light		**dark**		**light**		**dark**		**light**		**dark**	
	Mn^{2+}	**O_2**	**Mn^{2+}**	**O_2**	**Mn^{2+}**	**O_2**	**Mn^{2+}**	**O_2**	**Mn^{2+}**	**O_2**	**Mn^{2+}**	**O_2**
March ´02	21 ± 11 (n=2)	-903	7 ± 7 (n=2)	-1169					0 (n=2)	482	3,4 ± 3,4 (n=2)	-676
June ´02	34 ± 18 (n=2)	-2159	49 ± 6 (n=2)	-2483					42 ± 42 (n=2)	94	13 ± 13 (n=2)	-1394
June ´02	39 ± 18 (n=2)		54 ± 14 (n=2)									
Sept ´02	0 (n=2)	-1613	0 (n=2)	-2098					0,6 ± 0,2(n=2)	668	0 (n=2)	-617
July´03	78 ± 78 (n=2)	-2191	93 ± 92 (n=4)	-2901	92 ± 26 (n=2)	-662	289 ± 237(n=4)	-1472	1 ± 1 (n=2)	1942	2 ± 2 (n=4)	-1456

Mn fluxes showed considerable high differences between replicate deployments (Table 3). Nevertheless, differences between stations and seasons could be identified. Lower solubility and faster oxidation kinetics of Fe^{2+} generally lead to a low diffusive Fe flux out of the sediment. Therefore, no fluxes of dissolved Fe could be detected during the benthic chamber incubations.

The O_2 concentration in the overlying water and the penetration depths partly control the sedimentary Mn cycling. Transparent and opaque chambers were deployed to estimate the influence of benthic O_2 exchange in light with photosynthetic activity and in dark conditions when respiratory processes prevail (Figure 5; Table 3). O_2 concentrations in the water column ranged from 3500 µmol m^{-2} h^{-1} in spring to 2600-2200 µmol m^{-2} h^{-1} in June and July and increased up to 2900 µmol m^{-2} h^{-1} in September. O_2 was expected to decrease in the dark chambers whereas in the light chambers O_2 was produced by photosynthesis. In contrast, we found, that at station N I and the lower sandy station S I O_2 depletion occurred in both the dark and transparent chambers during all seasons investigated. Most pronounced differences between O_2 consumption (OCR) and production rates in light and dark were measured at station S III (Table 3). In the dark, O_2 was consumed efficiently by respiration and

re-oxidation of reduced substances released into the chamber water. Therefore, O_2 consumption, showed highest rates during June and summer. OCR at station N I were about 2 times higher compared to the sand flat stations. Maximum Mn fluxes in July were 27 times higher at station N I whereas SRR were only 2-fold higher related to station S III. But 10 fold higher SRR in March caused 5 times higher Mn^{2+} release rates at station N I compared to station S III (Table 3, Figure 3). This indicated that the in general higher O_2 penetration depth at the sandy station S III (Billerbeck et al., 2006a,b; Walpersdorf et al., in prep.) acts as a barrier for Mn outfluxes.

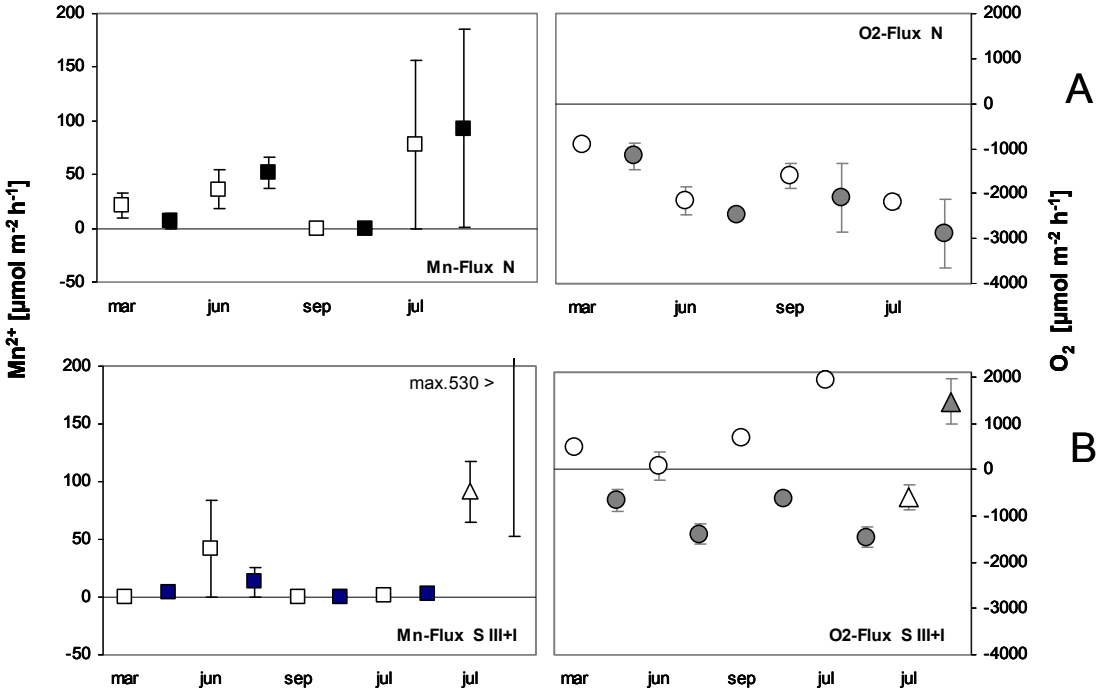

Figure 5: Mean fluxes (± SD) of dissolved Mn^{2+} (cubes) and O_2 (circles) fluxes determined by using transparent and opaque benthic flux-chambers, A: Station , N I and B: Station S III and I (triangles).

Furthermore, a remarkable rise of Mn^{2+} concentrations was observed at the sandy sites during the last 2 hours of incubation in the dark but also in the light chambers. The effect was, most pronounced at station I (Figure 6) where, release rates of 48 µmol m^{-2} h^{-1} increased up to 430 µmol m^{-2} h^{-1} soon after the upper flat became exposed. This indicates a larger contribution of advection to the measured Mn release as a direct consequence of the onset of a continuing drop of the water level shortly after slack tide. This caused a general pore water flow along the hydraulic gradient towards the low water line where pore water discharge zones emerged (Nielsen, 1990; Billerbeck et al., 2006). A further hint for enhanced pore water seepage in these zones are characteristic puddles filled with sulfidic pore water, so called `black spots`, which were visible during low tide. As a result of embedded finer grained layers at station S I, water flow followed preferential pathways with higher permeability through the sediment resulting in a spatial variability of pore water discharge in this release zone.

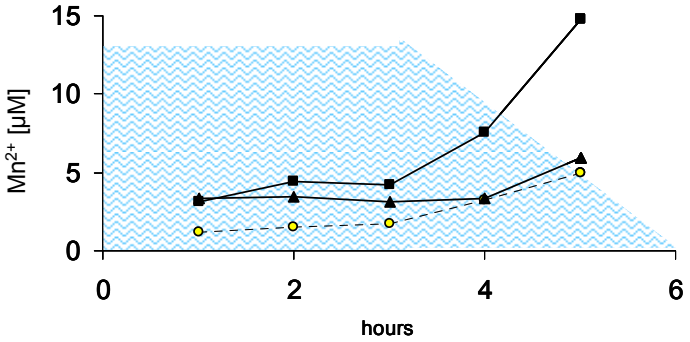

Figure 6: At station S I, Mn^{2+} concentrations increased after the dropping water level exposed the top of the sand plate, here average values of 2 transparent (circles), 4 opaque chambers (filled symbols) are shown for July 2003.

Table 4: Average fluxes (dark and light) of dissolved Mn^{2+} across the sediment-water interface. Determined by using benthic flux-chambers and compared to calculated fluxes by Berg's model and applying the surficial pore water gradients to Fick`s first law of diffusion.

Flux rate Mn^{2+}	**N**			**N II**	**S I**	**S III**	**D**		
[µM m^{-2} h^{-1}]	Chamber	Berg	Fick`s Law	Berg	Chamber	Chamber		Berg	Fick`s Law
March`02	17±15	0.3	1.6			3.4 ± 3.4	**April`98**	56.9	2.5
April`02							**May`98**	3.3	0.1
June`02	45±24	0.5	0.9			55 ± 28.8	**June`98**	2.3	0.1
Sept.`02	0					0.6 ± 0.2	**Oct `98**	3.4	0.08
Nov`02				145.8					
July`03	93 ± 92	4	14.8		286 ± 240	3.4 ± 1.1	**July`98**	1.6	0.02
							Aug`98	1.6	0.04

The PROFILE model provides a good description of the measured Mn^{2+} profiles in the pore water for the mixed (N) and muddy (D) sediments. The calculated Mn^{2+} production zones reflect that the flux of dissolved Mn out of the sediment is only a small fraction of the total reduced pool in the sediment. The estimated Mn reduction rates pointed out that in fact 20-44 % of the reduced Mn^{2+} does not escape and thus reflected that an important part of the Mn cycle takes place within the sediment (Figure 4, Table 4).

But PROFILE calculations also showed that the model can not reproduce the release rates of Mn^{2+} measured by benthic chamber incubations, which were orders of magnitude higher (Table 4). This large difference between measured and calculated fluxes may be explained by the relatively coarse centimetre wise resolution of the pore water data. Another reason may be that pore water data are the net result of all processes occurring in the sediment at a given time. Sediment cores were sampled during low tide when any exchange is restricted. Therefore, calculated surface fluxes consist only of a few data points which is probably not detailed enough to represent the actual surface gradient.

Therefore, release rates were additionally calculated by applying concentration gradients at the sediment-water interface to Fick´s First Law:

$$\textbf{Equ. 4: } J_{sed} = -\Phi * D_{sed} * dC/dx$$

$$\textbf{Equ. 5: } D_{sed} = D^{sw} / \theta^{2}$$

(θ=tortuosity, Φ=porosity, D=diffusion coefficient, C=concentration, x=depth)

A negative flux indicates a decreasing Mn^{2+} concentration from the sediment upward to the sediment surface layer, due to re-oxidation of dissolved Mn^{2+} near the sediment-water interface (Table 4). The calculated release rates by Fick`s Law showed that at station N I only 2-19 % of the measured rates due to diffusive flux.

Discussion

Data analysis from investigations of pore water, solid phase geochemistry, microbial sulfate reduction rates and benthic chamber incubations performed in different sediment types verified characteristic reactive zones and coupled processes supporting Mn reduction and consecutive Mn^{2+} release.

Manganese reduction

From the pore water profiles, it becomes evident that the top 15 cm of the surface sediments are most important for Mn cycling and are controlling the metal flux across the sediment-water interface. Gradients and concentrations in pore water responded to the seasonal variation of microbial sulfate reduction and the reservoir of reactive metal oxides (Figure 4). Accordingly, highest Mn reduction rates were found in the mud (station D) and mixed flat (station N I, N II), where Mn_{HCl} contents ranged from 40-800 ppm (Table 2). Furthermore, Mn reduction rates were influenced to a different extent by seasonal conditions depending on the sediment type. A comparison between the stations pointed out that Mn reduction showed less pronounced seasonal variations at station D and relatively constant vertical distribution during the year. Enhanced surface Mn^{2+} concentrations in spring are due to the input of fresh organic matter (Figure 4). The high Mn oxide inventory at station D provides a reservoir for rapid Mn re-supply. Therefore, fine grained Mn rich sediments, in general, are for a lesser extent controlled by the input of reactive Mn from the water column as observed at the sandy locations (station S I, S III), where the Mn_{HCl} decreased from 40 to 5 ppm at station S III (Table 2). Pore water depth distribution of Mn^{2+} also reflected a more pronounced seasonal effect at station N I (Figure 4). The influence of spring and autumn algae blooms enhanced maximum Mn reduction rates within the upper 6 cm and extremely high temperatures up to 32 °C during summer caused a steep surficial gradient of Mn^{2+} (Figure 4) in the sediments. In June and December Mn^{2+} profiles showed a homogeneous depth distribution at this station. Pore water profiles at the upper sand flat station S III indicate that the liberation of Mn was limited by both, the availability of Mn oxides during warmer months and relatively low microbial activity. The results demonstrated that especially at the sediment surface, where the highest activity of sulfate reducing activity occurred, abiotic re-oxidizing processes superimposed the bacterial sulfide production and consecutively Mn reduction. The relatively low rates of Mn^{2+} reduction and release (Table 4) at the sandy Station S III reflects high sediment oxidation influenced by enhanced O_2 supply due to deep oxygen penetration and low microbial activity (Billerbeck et al., 2006; Walpersdorf et al., in prep.). The vertical distribution of Mn^{2+} at S I does not necessarily reflect the seepage of Mn. Measurements below anoxic spots revealed locally, high concentrations of Mn^{2+} probably due to the lateral draining of anoxic pore water downward the sand flat which was postulated by Billerbeck et al., 2006a. Furthermore, those imbedded fine grained layers may function as sources for locally enhanced Mn^{2+} concentrations.

Laboratory incubations performed by Batel et al. 2003 confirmed this assumption as discussed above.

The general shape of the Mn^{2+} profile closely resembles that of the microbial sulfate reduction rate (Figure 3, 4). This demonstrates the importance of chemical reduction of MnO_2 by biogenic sulfide in near-surface sediments. But in the same zone liberation of Fe^{2+} was also detected and corresponded to the microbial sulfide production. Pore water profiles showed a typical depth distribution of increasing Fe^{2+} concentrations below the Mn^{2+} maximum, which indicated the Mn reduction by ferrous Fe (Figure 4). Therefore it is not possible to distinguish the bacterial Mn reduction from abiotic reduction processes by Fe^{2+} and H_2S from the pore water profiles alone.

Therefore and as a step further, experimental lab incubations were performed with the aim to separate the different reduction pathways from each other and to quantify potential process rates which would be hampered by competing reactions under in-situ conditions. To assess rates of dissimilatory Fe and Mn reduction and the coupling to the sulphur cycling, the experiments were performed over 4 weeks as summarized below (for further details see Batel, 2003, Batel et al., in prep.).

Sediments from station N II were incubation in gas-tight plastic bags and different experimental set ups were chosen:

A: addition of molybdate to inhibit microbial sulfate reduction

B: addition of molybdate and ferrozine to inhibit SRR and chemical reduction of Mn IV by Fe^{2+}

C: addition of manganese dioxide

In untreated sediments, 90 % of carbon oxidation is due to sulfate reduction and only 10 % amount to metal reduction. Inhibition of SRR by molybdate (A) allows the estimation that metal reduction may account for 95 % of carbon mineralization if concurrent sulfate reducing processes are eliminated (Batel, 2003). Fe and Mn reduction may have been taken over by sulfate reducing bacteria (Lovley et al., 1993). The additional complexation of dissolved Fe^{2+} by ferrozine (B) demonstrated that, 40 % of carbon mineralization may be performed via dissimilatory Mn reduction. This pointed out that, dissimilatory Mn reduction potentially may become an important mineralization process. The PHREEQE model showed that carbonate precipitation is a further sink for Mn^{2+} in the investigated sediments and may have superimposed Mn reduction rates calculated by concentrations of dissolved Mn in the pore water (Peters, 2004; Batel, 2003; Batel et al., in prep). Furthermore, the experimental laboratory incubations indicated that the addition of MnO_2 (C) leads to a decrease of SRR of 79 % in support of metal reduction (Batel, 2003). High MnO_2 concentrations can partly inhibit the activity of sulfate- and iron reducers (King, 1990; Myers & Nealson, 1988). The occurrence of Fe and Mn reduction has been found to depend preliminary on the availability of Mn oxides and reactive, poorly crystalline Fe oxide, respectively (Myers & Nealson, 1988; Thamdrup, 2000; Thamdrup & Dalsgaard, 2000). Therefore, Mn reduction in coastal sediments was generally expected to be of minor importance in carbon oxidation because of the relative low availability of Mn oxides (Thamdrup, 2000). Their study showed that dissimilatory Fe and Mn reduction becomes an important process in sediments with Fe- and Mn-oxide concentrations greater than 10 µmol cm^{-3}, respectively. Applied to

the different study sites, these findings imply that Mn reduction could potentially take over 50-100 % of the total carbon oxidation at station D and N II, up to 40 % at station N I and is of minor importance at the sandy stations S I and III. The potential contribution of Fe reduction amounts to 75-90 % at station N I and N II respectively, and 2-18 % at the sand flat stations (S I, S III).

The acquired Mn reduction rates from the different Wadden Sea sediments correspond well to reported values for other coastal sediments underlying an oxic water column, as Slomp, 1997 (southern North Sea and Skagerrak); van der Zee et al., 2003 (German Bight, see Table 5). A comparison to continental margin rates shows that Mn reduction rates in intertidal sediments were generally lower. In contrast to steady state conditions in subtidal sediments, e.g. Skagerrak, wave action and tidal currents in intertidal sediments cause enhanced sediment mixing. Sediment reworking stimulates the Mn cycling in several ways. Mixing increases the transport of reduced solutes to the surface where they can be re-oxidized and additionally enhances the oxidation state of surface sediments. This rapid re-oxidation induced by tidal dynamics is responsible for higher re-oxidation and therefore lower Mn reduction rates compared to other continental margin sediments. This assumption was also reflected by the PROFILE calculated Mn^{2+} production and consumption zones. The diffusion of dissolved manganese out of the sediment is only a small fraction of what is reduced within the sediment. The estimated Mn reduction rates pointed out that in fact 20-44 % of the reduced Mn^{2+} does not escape and thus indicated that an important part of the Mn cycle takes place within the sediment.

Other factors influencing manganese flux

The tidal hydrodynamics lead generally to a well oxygenated water column which is responsible for rapid re-oxidation and adsorption processes of dissolved Mn after diffusing out of the sediment (Aller, 1994). Therefore, the influence of the oxygen concentration in the overlying water and the penetration depths was expected to be a main factor influencing Mn^{2+} release rates. Benthic chamber incubations at station S III revealed oxygen consumption in the dark chambers and an increase in the light ones, but oxygen concentrations had no visible influence on the Mn release rates (Table 3). In contrast, the comparison of Mn fluxes between transparent and opaque chambers showed that at station N I and the lower sandy station S I oxygen was consumed in both the dark and transparent chambers during all investigated seasons. Therefore the O_2 concentration in the overlying water does not appear to dominate the Mn inventory dynamics. Rather, we found that during the warmer period high amounts of oxygen were consumed by benthic mineralization and re-oxidation of reduced solutes and promotes Mn^{2+} release (Table 3). Consequently, the observed Mn release rates showed a stronger response to biogenic sulfide production than to the sedimentary oxygen demand and availability in the overlying water. Mn^{2+} oxidation by oxygen is a relatively slow process (Sung & Morgan, 1981). This indicates that Mn oxidation was mainly mediated by light induced photo-oxidation as well as microbial Mn oxidation (Emerson et al., 1982; Tebo & Emerson, 1986; Sunda & Huntsman, 1994; Nico et al., 2002). Aller 1994 also found that the loss of sedimentary Mn is associated to the input of organic carbon and connected mineralization processes rather before a lowering of O_2 concentrations proceeded.

Highest Mn^{2+} fluxes were measured at the mixed station N I which is due to the generally higher iron and manganese contents and microbial activities. Compared to the sandy station, Mn reduction rates were higher as a result of an enhanced microbial sulfide production (Figure 4). This was additionally proven by the response of Mn^{2+} fluxes to increasing sulfate reduction rates during the warmer months. During the colder season, the input of organic matter is low and the oxic zone extends to a greater depth, which was also reflected by the deeper zones of Mn^{2+} production in the sediment (Figure 5). Therefore, the Mn flux shifts seasonally from an external cycle in summer, when Mn^{2+} can diffuse out of the sediment, to an internal cycle restricted to the sediment. At the sand flat stations tidal flushing causes that 10-40 % and 40-90 % of the reduced iron sulfides were rapidly re-oxidized at station N I and at station S III respectively (Bosselmann et al., in prep). The intensive oxygenation of surface sands enhanced re-oxidation processes and leads to distinctly lower Mn^{2+} release.

Release rates measured at station S I considerably exceeded rates reported in other studied sand flats (e.g. Epping et al., 1998; Slomp, 1997; Table 5). The sloping sand flat led to visible pore water drainage from the tidal flat during low tide. Zones of high pore water release were reflected by the development of puddles filled with sulfidic pore water so called `black spots` at the seepage zone during low tide. As a result of embedded finer grained layers at station S I, water flowed on preferential pathways through the sediment which led to a spatial variability of pore water discharge in this release zone during low tide.

Measured and calculated flux data at station N I and S III were consistent with investigations in related environments. Mn release rates measured in sediments under subtidal conditions e.g. Skagerak showed Mn fluxes comparable to the studied mud -and mixed station (D, N) and confirmed the relation of Mn reduction rates to Mn content and microbial sulfate reduction in the sediments in contrast to aerobic processes (e.g. Thamdrup et al., 1994; Canfield, 1993; Table 5). Generally, benthic Mn fluxes were observed to decrease with increasing water depth in continental sediments (Johnson et al., 1992) due to decreasing input of terrestrial organic matter to the sediments with increasing distance from the coastal region. Mineralization processes mainly takes places under oxic conditions in the water column. Therefore also lower SRR were found in continental and deep sea sediments (e.g. Lein, 1983; Jørgensen, 1982; Boetius et al., 2000; Table 5). Furthermore, the terrestrial input is an important source for Mn in the coastal regions. The freshwater environment of the study area is also rich in Mn as a result of mobilisation from soils and diffusion out of organic matter rich sediments in the hinterland (Dellwig et al., 2007). Freshwater is commonly discharged to the Wadden Sea via the flood-gate e.g. Neuharlingersiel and by rivers. Considerable Mn release rates were e.g. measured in the Weser estuary (0,3 - 383 µmol m^{-2} h^{-1}; Skowaronek et al., 1994; Table 5).

The calculated release rates in our case may to some extent underestimate in-situ release rates, due to neglected factors like e.g. bioturbation, lateral transport or draining effects through tidal forcing, but pointed out the close interaction of hydrodynamic, geochemical and biological processes. As discussed above, sediment mixing enhances the metal and sulphur cycling by transporting Mn oxides and organic matter into deeper and reduced zones. The stimulating influence of this sediment mixing on Mn reduction was demonstrated by Aller, 1990, 1994 (Panama Basin sediments) and enhanced

SRR by King, 1988 in salt marsh sediments. Presumably the continual resuspension of the sediment caused a translocation of metabolizable organic matter and enhances the transport of reduced solutes to the surface where they can be re-oxidized and additionally causes a rapid re-supply of oxidants and particles to the deeper sediment.

While in submerged sediments diffusional processes and pore water advection govern a permanent sediment-water exchange, processes in intertidal sediments change periodically during exposure and inundation. Exchange processes are reduced to a minimum during low tide. Dropping water levels initiate a flow of pore water along a hydraulic gradient towards release zones in form of tidal channels and drainage gullies (Billerbeck et al., 2006a, Nielsen 1990). Benthic chamber experiments revealed that highest amounts of manganese were released from the tidal flat as soon as the regressing inundation caused a sufficient hydraulic gradient, developed between the pore water level within exposed sand flats and the decreasing water level (Billerbeck et al., 2006a). Pore water flow measurements confirmed this assumption. At station S III in march 2004, pore water flow velocity in 5 cm depth documented an increase during the last 2.5 hours of exposure which due to a gradual drop of the water level (Billerbeck et al., 2006a). At the lower sandy station S I fluxes in the benthic chambers showed highest discharge during the last 1.5 hours of incubation when the upper part of the sand flat was already exposed (this study and Billerbeck et al., 2006). These findings pointed out that the measurement only of one-dimensional transport processes leads to an underestimation of pore water exchange and are not sufficient to comprise the complete discharge of solutes. Additional measurements of lateral transport processes are needed.

Table 5: Comparison of Mn reduction rates and fluxes from this study to other studies in North Sea and continental margin sediments.

Reference	Location, depth, season	Method	Sediment type	Mn red.rate $\mu mol*m^{-2}*h^{-1}$	Mn flux rate $\mu mol*m^{-2}*h^{-1}$
Skowaronek et al., 1994	Germany, Weser estuary, intertidal, seasonal	Lab Incubations	/	/	0.3 - 383.6
Slomp, 1997	south+northern North Sea, 19-90m depth, Feb.+ Aug.	Model calculation	sand	0.16-19.2	0 - 19.2
Slomp, 1997	Skagerrak, 40-330m depth, Feb.+ Aug.	Model calculation	silt	7.1-15.4	5 - 12.5
Canfield, 1993	Skagerrak, 10-700m depth, Sept.	Lab Incubations	clay	1500	5.8-11.7
Sundby & Silverberg, 1985	Gulf of the St Lawrence, 300-400m depth, June	Model calculation	mud	12.9-192.5	3.8-25
Thamdrup et al., 1994	Denmark, Aarhus Bay, 16m depth, seasonal	Calculated flux	silt	95.8	7.1- 32.5
Johnson et al., 1992	California margin, 95-1000m depth,	Benthic chambers	/	/	0.005-0.3
Aller, 1980	Long Island Sound, seasonal	Box-cores	silty-clay	23.8-191.7	
Aller, 1994	Long Island Sound, seasonal	Lab Incubations	sand+silty-clay	/	17.9- 91.7
Epping et al., 1998	North Sea, Frisian island Texel, July	Lab Incubations	sand	/	02.05.1935
Hunt, 1983	USA, Road Island, Narragansett Bay, seasonal	Benthic chambers	mixed	/	0.6 - 42.9
Aller & Benninger, 1981	Long Island Sound, seasonal	Box-cores	sand-silty -clay	/	16.7
Aguilar & Nealson 1994	New York, Oenida lake	Benthic chambers	/	/	8.3 - 57.5
van der Zee et al., 2003	North Sea, German Bight, seasonal	Model calculation	silty	8 - 59.8	0.2 - 19.2
van der Zee et al., 2001	Iberian Continental Margin, 100-5000m depth, Aug.+May	Model calculation	clastic	0.04-1.5	0.04 -1.5
Kristiansen et al., 2002	Denmark, Island Fyn, Sept.	Lab Incubations	sand	/	29-200
Stodian et al., 2000	Baltic Sea, Nordrügensche Bodden, seasonal	Lab Incubations	sand-mud	0.18-3.3	2.3-39.0
Peters, 2004	Intertidal North Sea, Wadden Sea, Neuharlingersiel II, April	PROFILE model	mixed	35.8	/
Batel, 2003	Intertidal North Sea, Wadden Sea, Neuharlingersiel II, Nov.	PROFILE model	mixed	111.3	145.8
This study	Intertidal North Sea, Wadden Sea, Dangast (D), seasonal	PROFILE model	mud	0.2-52.6	1.6-56.9
This study	Intertidal North Sea, Wadden Sea, Janssand (S I), July	Benthic chambers	sand	7E-07- 2.4	286
This study	Intertidal North Sea, Wadden Sea, Janssand (S III), seasonal	Benthic chambers	sand	7E-06- 0.1	0.6 - 55
This study	Intertidal North Sea, Wadden Sea, Neuharlingersiel, seasonal	Benthic chambers	mixed	0.03-9.3	17 - 93

Mn –cycling

Surface enrichment of Fe- and Mn oxy(hydroxi)des reflects that Fe and Mn are continuously re-cycled from the reduced state back to the oxides and with this, available for further reduction. All of the stations investigated showed seasonal shifts between periods of loss and gain in the inventory of reactive Mn_{HCl} which were most pronounced within the surface 3 cm layer. Dissolved iron and manganese diffuse upwards into the oxic zone near the surface where they are re-oxidized and re-precipitated as manganese- and iron-oxy(hydrox)ides. This short-scale cycle is reflected in the opposite vertical distribution of solid and dissolved metals (Figure 3). Results for sandy and mixed stations S I, III and N I showed that the reactive Mn_{HCl} inventory was usually 10 times smaller than the Fe_{HCl} pool. The higher Mn_{HCl} inventory at station D is correlated to enhanced mud content. Here, different reaction kinetics of Fe and Mn were reflected by differing seasonal variations of the inventory and most pronounced within the upper 5 cm. The solid iron inventory showed only low seasonal variations in comparison to the manganese pool. This was reflected by the seasonal pattern of the Fe/Mn ratio. Highest Fe/Mn relation in summer 2003 indicated a much stronger decrease in Mn_{HCl} than in the Fe_{HCl} pool. Lowest Fe/Mn relations in the colder seasons documented the re-establishment of the Mn inventory (Table 2). Strong seasonal amplitudes of gain and loss were found in the sandy sediments due to the generally lower content of Mn and Fe and enhanced advective transport processes in permeable sediments. Highest seasonal amplitudes were observed in the surface 0-5 cm at the mixed station N I but this zone extended down to 10 cm depth at the permeable stations S I and III. Higher sediment mixing and deeper penetration of particles into permeable sediments causes a higher mineralization rate and also increases the metal cycling in sandy compared to finer grained sediments. A declining Mn_{HCl} and Fe_{HCl} inventory indicated that, especially during the warmer months, manganese escaped from the sediment by diffusion, advection and biological activity into the water column whereas the reactive $iron_{HCl}$ pool was re-precipitated or fixed in the sediment as sulfide (Bosselmann et al., in prep.). This reflects a seasonal shift from internal cycling in the sediments to an external cycle connected to the water column. Furthermore, Mn-oxides are reduced by the reaction with Fe^{2+}. Therefore, the oxidation of Fe^{2+} by Mn-oxides acts as a barrier to the upward diffusion of dissolved iron on the way to the sediment-water interface (Figure 4). In contrast, the Fe_{HCl} inventory showed lower seasonal variations compared to the Mn_{HCl} content which reflected that the most important part of the Fe pool is restricted to the sediment.

Balance

The seasonal response of the sedimentary Mn_{HCl} pool revealed highest loss during spring and summer and decreased again during the colder months. The correlation of Mn fluxes to microbial sulfate reduction (r=0.9797) and temperature (r=0.4591) respectively, pointed out that the main seasonal factor (beneath factors like e.g. Mn availability) on Mn cycling was the rate of sulfate reduction which is in turn controlled by temperature. A direct correlation of Mn fluxes to the temperature variations as found for the Weser estuary by Skowronek et al., 1994, was probably superimposed by tidal cyclicity which caused high temperature variations (see chapter 2).

From March to August, the rate of daily Mn_{HCl} depletion amounted to 82-1320 µmol m^{-2} d^{-1} at station S III and 408-2232 µmol m^{-2} d^{-1} at station N I (Figure 7A) which means a pool size reduction of 56 % at station N I and up to 42 % at the sandy stations S I, S III. However, the net loss of the sedimentary Mn_{HCl} (which was detected with benthic chambers, Figure 7C) amounts to 5-43 µmol m^{-2} d^{-1} at station N II and 1-3 µmol m^{-2} d^{-1} at station S III (Figure 7C). This indicated that more than 90 % of released Mn^{2+} was recycled back in the water column and re-precipitated to the sediment (Figure 7B). The domination of Mn release during spring and summer leads to a depletion of the sedimentary Mn_{HCl} inventory. Therefore, the flux of dissolved Mn^{2+} out of the sediment was larger than the external supply from the overlying water and was not balanced by re-sedimentation as observed during the colder months (Figure 7A, calculated daily input). Particulate matter in the water column displayed a seasonal behaviour with increasing absorbed Mn content during summer and low Mn amounts during the colder months (Dellwig et al., 2007). Decreasing reductive conditions within the sediment during autumn and winter leads to lower release rates and a major part of the Mn cycling was restricted to the sediment. The external input of Mn oxide enriched particles from of the water column generated during these months a replenishment of the sedimentary Mn_{HCl} pool. Dellwig et al., 2007, found that from winter to summer the particulate Mn concentration in the water column increased by a factor of nearly 2. Therefore, it can be concluded that especially during temperate seasons the Mn inventory of tidal flat sediments form a very important source for Mn and is replenished to a certain degree by the higher freshwater contribution during rainy fall and winter. Dellwig et al., 2007 estimated that freshwater discharge can explain more than 90 % of the total Mn inventory in the Wadden Sea water column during phases of high rain fall and reduced microbial activity during winter time. Intensive re-suspension of particles into the surface sediment was caused by storm events, which occurred quite often during the autumn and spring seasons (Eisma & Kalf, 1987; Jago et al., 1993; Böttcher et al., in prep.).

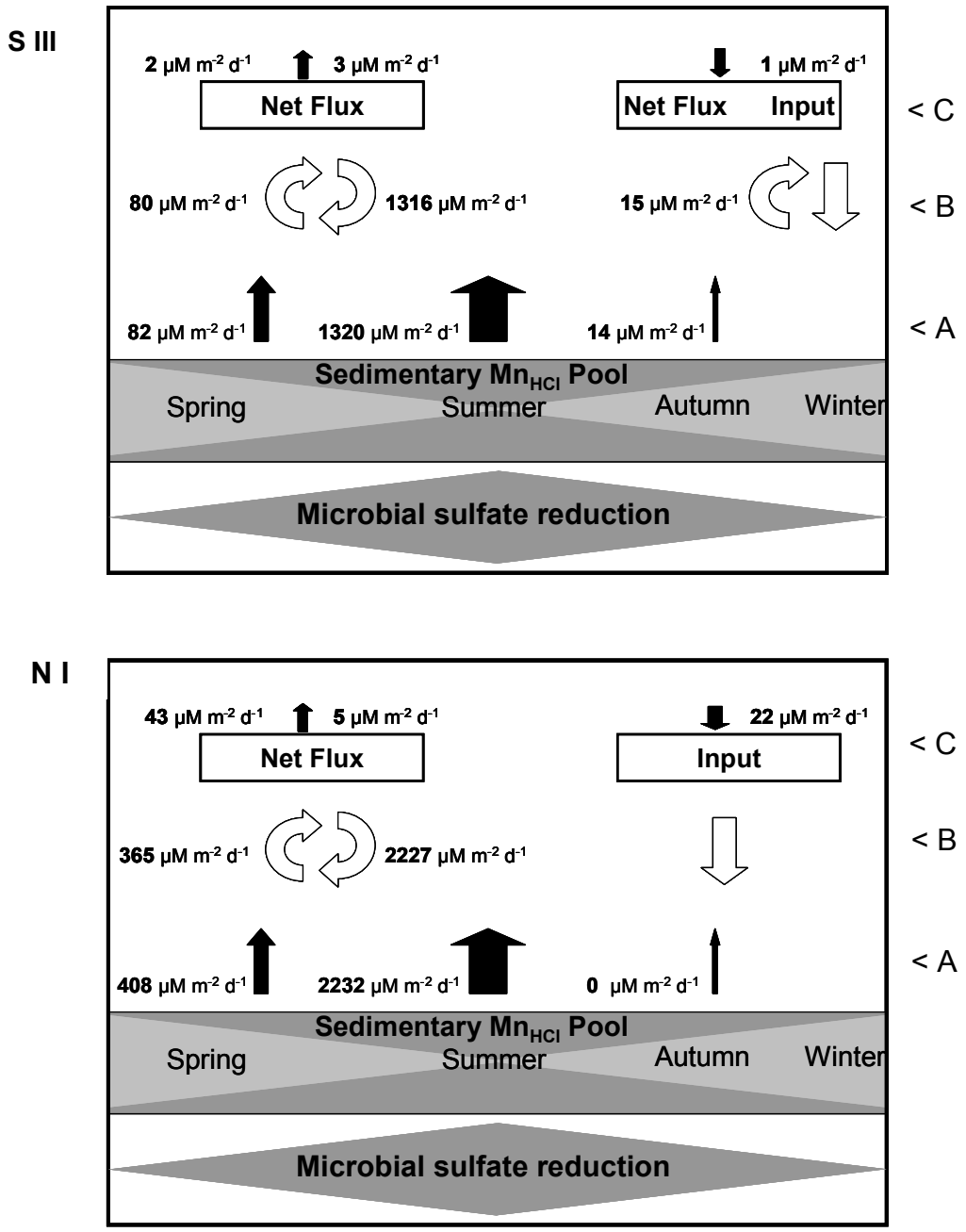

Figure 7: Fluxes of Mn in µmol m^{-2} d^{-1} calculated by benthic flux measurement and changes in sedimentary Mn_{HCl} pool size at station S III and N I.

The tidal area of the Lower Saxony Wadden Sea of 1411 km^2 consists to 80 % of sands, 12 % mixed and 8 % muddy sediments (including 1.6 % mussel beds; Meyer & Ragutzki, 1999). Extrapolation of the measured Mn flux to the area of the particular sediment type allows a rough estimation of total Mn^{2+} release for this Wadden Sea area. Daily Mn^{2+} fluxes at the sandy stations ranged from 14-1320 mmol km^{-2} d^{-1} which suggests a Mn^{2+} release of 16-1500 mol d^{-1} for an area of 1131 km^2. The

maximum flux up to 6864 mmol km^{-2} d^{-1} measured at the seepage zones (station S I) was neglected in this calculation because the extent of these seepage areas is not quantified yet.

From tidal mixed sediments 0-2232 mmol km^{-2} of dissolved Mn discharges during a day. Extrapolated to an area of 169 km^{-2}, maximum Mn release amounts to 377 mol d^{-1}. The model based calculated Mn flux suggests for the muddy sediments a Mn^{2+} release of 860-2670 mmol km^{-2} d^{-1} at station N II and 38-1366 mmol km^{-2} d^{-1} at station D, which means, referred to an area of 89 km^{-2} a discharge of 3-122 mol Mn^{2+} d^{-1}. Rough estimations of Mn^{2+} discharge rates averaged during all seasons (assumed that comparable environmental conditions prevail) would amount to 136-13011 mol d^{-1} which means a yearly Mn discharge of 2.5-7 million mol a^{-1} into the water column of the Lower Saxony Wadden Sea (Table 6). It has to be considered, that this assumption is based on benthic chambers experiments which allow only flux measurements during inundation of the tidal flats and discharge rates during exposure of tidal flats are missing.

Table 6: Sediment types at the Lower Saxony Wadden Sea and extrapolated Mn flux for this area.

Location			Mn Flux [mmol km^{-2} d^{-1}]			
	%	km^2	spring	june	summer	autumn
sand: S III	80.1	1131	82	1320	82	14
S I					6864	
mixed: N I	12.0	169	408	1080	2232	0
mud: D	6.3	89	1366	55	38	82
mussel bed	1.6	23				
			Mn Flux total area [mol d^{-1}]			
total area		**1412**	2620	3466	668	136
					13011	
total area per a			**2 500 000 - 7 000 000**		**mol a^{-1}**	

Summary

The seasonal distribution of dissolved and solid Mn indicated an intensive Mn cycling within the surface 15 cm of intertidal sediments. Furthermore, the relationships of Mn to other biogeochemical processes were reflected by the close connection to microbial sulfate reduction and Fe reduction. The influence of seasonal conditions was indicated by the close response to microbial sulfate reduction. Besides advective and bioturbating transport processes, sediment redox conditions influence the extent of internal and external Mn cycling. Highest Mn^{2+} discharge rates were measured at the mixed flat (station N I) and at the seepage zone at the sand flat (station S I). A distinct seasonal trend with maximum Mn^{2+} discharge rates in summer is evidently owing to increasing microbial activity and more pronounced reducing conditions, which favours the reduction of solid Mn oxide phases to soluble Mn^{2+}. Therefore, it can be concluded that especially during temperate seasons the Mn inventory of tidal flat sediments form a very important source for Mn and is replenished to a certain degree by the higher freshwater contribution during rainy fall and winter. These findings indicate that the Wadden Sea sediments act as an important Mn source for the North Sea.

References

Aguilar, C. and K. H. Nealson, 1994, Manganese Reduction in Oneida Lake, New-York - Estimates of Spatial and Temporal Manganese Flux: Canadian Journal of Fisheries and Aquatic Sciences, 51: 185-196.

Aller, R. C., 1980, Diagenetic processes near the sediment-water interface of Long Island Sound II Fe and Mn: Advances in Geophysics, 22: 351-415.

Aller, R. C., 1990, Bioturbation and manganese cycling at the sediment-watr interface.: Philosophical Transactions of the Royal Society of London Series a Mathematical Physical and Engineering Sciences, A 331: 51-68.

Aller, R. C., 1994, The Sedimentary Mn Cycle in Long-Island Sound - Its Role as Intermediate Oxidant and the Influence of Bioturbation, O_2, and $C_{(Org)}$ Flux on Diagenetic Reaction Balances: Journal of Marine Research, 52: 259-295.

Aller, R. C., and L. K. Benninger, 1981, Spational and temporal patterns of dissolved ammonium, manganese, and silica fluxes from bottom sediments of Long Island Sound, USA: Journal of Marine Research, 39: 295-314.

Aller, R. C. and P. D. Rude, 1988, Complete oxidation of solid phase sulfides by manganese and bacteria in anoxic marine sediments: Geochimica et Cosmochimica Acta, 52: 751-765.

Balzer, W., 1982, On the distribution of iron and manganese at the sediment/water interface: thermodynamic versus kinetic control: Geochimica et Cosmochimica Acta, 46: 1153-1161.

Bartoli, M., D. Nizzoli, P. Viaroli, E. Turolla, G. Castaldelli, E. A. Fano and R. Rossi, 2001, Impact of Tapes philippinarum farming on nutrient dynamics and benthic respiration in the Sacca di Goro: Hydrobiologia, 455: 203-212.

Batel, S., 2003, Biogeochemische Umsatzprozesse in einem tidalen Oberflächensediment der südlichen Nordsee: Diploma Thesis, CvO Universität Oldenburg, 112 p.

Batel, S., K. Bosselmann and M. E. Böttcher, 2008, Anaerobic reactions in a muddy intertidal surface sediments: Results from incubation experiments and pore water modeling: in prep.

Berg, P., N. Risgaard-Petersen and S. Rysgaard, 1998, Interpretation of measured concentration profiles in sediment pore water: Limnology and Oceanography, 43: 1500-1510.

Berner, R. A., 1989, Biogeochemical cycles of carbon and sulfur and their effect on atmospheric oxygen over phanerozoic time: Paleogeogr. Paleoclimatol. Palaeoecol, 75: 97-122.

Billerbeck, M., H. Røy, K. Bosselmann and M. Huettel, 2007, Benthic photosynthesis in submerged Wadden Sea intertidal flats: Estuarine Coastal and Shelf Science, 71: 704-716.

Billerbeck, M., U. Werner, K. Bosselmann, E. Walpersdorf and M. Huettel, 2006a, Nutrient release from an exposed intertidal sand flat: Marine Ecology Progress Series, 316: 35-51.

Billerbeck, M., U. Werner, L. Polerecky, E. Walpersdorf, D. de Beer and M. Huettel, 2006b, Surficial and deep pore water circulation governs spatial and temporal scales of nutrient recycling in intertidal sand flat sediment: Marine Ecology Progress Series, 326: 61-76.

Böttcher, M. E., 1998, Manganese(II) partitioning during experimental precipitation of rhodochrosite-calcite solid solutions from aqueous solutions: Marine Chemistry, 62: 287-297.

Böttcher, M. E., 2001, Sulfur isotope fractionation in the biogeochemical sulfur cycle of marine sediments: Isotopes in Environmental and Health Studies, 37: 97-99.

Böttcher, M. E., B. Hespenheide, H. J. Brumsack and K. Bosselmann, 2004, Stable isotope biogeochemistry of the sulfur cycle in modern marine sediments: I. Seasonal dynamics in a temperate intertidal sandy surface sediment: Isotopes in Environmental and Health Studies, 40: 267-283.

Böttcher, M. E., B. Hespenheide, E. Llobet-Brossa, C. Beardsley, O. Larsen, A. Schramm, A. Wieland, G. Böttcher, U. G. Berninger and R. Amann, 2000, The biogeochemistry, stable isotope geochemistry, and microbial community structure of a temperate intertidal mudflat: an integrated study: Continental Shelf Research, 20: 1749-1769.

Böttcher, M. E., B. Thamdrup, M. Gehre and A. Theune, 2005, S^{-34}/S^{-32} and O^{-18}/O^{-16} fractionation during sulfur disproportionation by Desulfobulbus propionicus: Geomicrobiology Journal, 22: 219-226.

Böttcher, M. E., B. Thamdrup and T. W. Vennemann, 2001, Oxygen and sulfur isotope fractionation during anaerobic bacterial disproportionation of elemental sulfur: Geochimica et Cosmochimica Acta, 65: 1601-1609.

Bosselmann, K., M. E. Böttcher, M. Billerbeck, E. Walpersdorf, A. Theune, D. de Beer, M. Huettel, H. J. Brumsack and B. B. Jørgensen, 2003, Iron-sulfur-manganese dynamics in intertidal surface sediments of the North Sea., Bonn, Delmenhorst, Forschungszentrum Terramare, 32-35.

Burdige, D. J., 1993, The Biogeochemistry of Manganese and Iron Reduction in Marine-Sediments: Earth-Science Reviews, 35: 249-284.

Burdige, D. J., S. P. Dhakar and K. H. Nealson, 1992, Effects of Manganese Oxide Mineralogy on Microbial and Chemical Manganese Reduction: Geomicrobiology Journal, 10: 27-48.

Burdige, D. J. and P. E. Kepkay, 1983, Determination of bacterial manganese oxidation rates in sediments using an in-situ dialysis technique I. Laboratory studies: Geochimica et Cosmochimica Acta, 47: 1907-1916.

Burdige, D. J. and K. H. Nealson, 1986, Chemical and microbial studies of sulfide mediated manganese reduction: Geomicrobiology Journal, 4: 361-387.

Burnett, W. C., H. Bokuniewicz, M. Huettel, W. S. Moore and M. Taniguchi, 2003, Groundwater and pore water inputs to the coastal zone: Biogeochemistry, 66: 3-33.

Canfield, D. E., 1989, Reactive iron in marine sediments: Geochimica et Cosmochimica Acta, 53: 619-632.

Canfield, D. E., B. Thamdrup and J. W. Hansen, 1993, The Anaerobic Degradation of Organic-Matter in Danish Coastal Sediments - Iron Reduction, Manganese Reduction, and Sulfate Reduction: Geochimica et Cosmochimica Acta, 57: 3867-3883.

Cline, J. D., 1969, Spectrophotometric determination of hydrogen sulfide in natural waters: Limnology and Oceanography, 14: 454-458.

Davison, W. and H. Zhang, 1994, In-Situ Speciation Measurements of Trace Components in Natural-Waters Using Thin-Film Gels: Nature, 367: 546-548.

de Beer, D., F. Wenzhofer, T. G. Ferdelman, S. E. Boehme, M. Huettel, J. E. E. van Beusekom, M. E. Bottcher, N. Musat and N. Dubilier, 2005, Transport and mineralization rates in North Sea sandy intertidal sediments, Sylt-Rømø Basin, Wadden Sea: Limnology and Oceanography, 50: 113-127.

De Vitre, R. R. and W. Davison, 1993, Manganese particles in freshwater: In: H. P. van Leeuwen, and J. Buffle (eds), Environmental Particles, 2: Boca Raton, Lewis, 317-352.

Delafontaine, M. T., A. Bartholomä, B. W. Flemming and R. Kurmis, 1996, Volume-specific dry POC mass in surficial intertidal sediments: a comparison between biogenic muds and adjacent sand flats: Senckenbergiana Maritima, 26: 167-178.

Dellwig, O., K. Bosselmann, S. Kölsch, M. Hentscher, J. Hinrichs, M. E. Böttcher, R. Reuter and H.-J. Brumsack, 2007, Sources and fate of manganese in a tidal basin of the German Wadden Sea: Journal of Sea Research, 57: 1-18.

Eisma, D. and J. Kalf, 1987, Distribution, organic content and particle size of suspended matter in the north sea: Netherlands Journal of Sea Research, 21: 265-285.

Emerson, S., S. Kalhorn, L. Jacobs, B. M. Tebo, K. H. Nealson and R. A. Rosson, 1982, Environmental oxidation rate of manganese(II): bacterial catalysis: Geochimica et Cosmochimica Acta, 46: 1073-1079.

Epping, E. H. G., V. Schoemann and H. de Heij, 1998, Manganese and iron oxidation during benthic oxygenic photosynthesis: Estuarine Coastal and Shelf Science, 47: 753-767.

Fossing, H. and B. B. Jørgensen, 1989, Measurement of Bacterial Sulfate Reduction in Sediments - Evaluation of a Single-Step Chromium Reduction Method: Biogeochemistry, 8: 205-222.

Goldhaber, M. B. and I. R. Kaplan, 1974, The sulfur cycle: In: E. D. Goldberg (eds), The Sea, Wiley, 569-655.

Hertweck, G., 1995, Distribution patterns of characteristic sediment bodies and benthos populations in the Spiekeroog backbarrier tidal flat area, southern North Sea. Results of survey of tidal flat structure 1988-1992.: Senckenbergiana maritima, 26: 81-94.

Huettel, M. and G. Gust, 1992a, Impact of Bioroughness on Interfacial Solute Exchange in Permeable Sediments: Marine Ecology Progress Series, 89: 253-267.

Huettel, M. and G. Gust, 1992b, Solute Release Mechanisms from Confined Sediment Cores in Stirred Benthic Chambers and Flume Flows: Marine Ecology Progress Series, 82: 187-197.

Huettel, M. and A. Rusch, 2000, Transport and degradation of phytoplankton in permeable sediment: Limnology and Oceanography, 45: 534-549.

Hunt, C. D., 1983, Variability in the benthic flux in coastal marine ecosystems resulting from temperature and primary production: Limnology and Oceanography, 28: 913-923.

Jago, C. F., A. J. Bale, M. O. Green, M. J. Howarth, S. E. Jones, I. N. McCave, G. E. Millward, A. W. Morris, A. A. Rowden and J. J. Williams, 1993, Resuspension Processes and Seston Dynamics, Southern North-Sea: Philosophical Transactions of the Royal Society of London Series a-Mathematical Physical and Engineering Sciences, 343: 475-491.

Jakobsen, R. and D. Postma, 1999, Redox zoning, rates of sulfate reduction and interactions with Fe-reduction and methanogenesis in a shallow sandy aquifer, Rømø, Denmark: Geochimica et Cosmochimica Acta, 63: 137-151.

Jensen, M. M., B. Thamdrup, S. Rysgaard, M. Holmer and H. Fossing, 2003, Rates and regulation of microbial iron reduction in sediments of the Baltic-North Sea transition: Biogeochemistry, 65: 295-317.

Johnson, K. S., W. M. Berelson, K. H. Coale, T. L. Coley, V. A. Elrod, W. R. Fairey, H. D. Iams, T. E. Kilgore and J. L. Nowicki, 1992, Manganese Flux from Continental-Margin Sediments in a Transect through the Oxygen Minimum: Science, 257: 1242-1245.

Jørgensen, B. B., 1977, The sulfur cyle of a coastal marine sediment (Limfjorden, Denmark). Limnology and Oceanography, 22: 814-832.

Jørgensen, B. B., 1982, Mineralization of organic matter in the sea bed - the role of sulphate reduction, 296: 643-645.

Kallmeyer, J., T. G. Ferdelman, A. Weber, H. Fossing and B. B. Jørgensen, 2004, A cold chromium distillation procedure for radiolabeled sulfide applied to sulfate reduction measurements: Limnology and Oceanography: Methods, 2: 171-180.

King, G. M., 1988, Patterns of sulfate reduction and the sulfur cycle in a South Carolina salt marsh: Limnology and Oceanography, 33: 376-390.

King, G. M., 1990, Effects of added manganic and ferric oxides on sulfate reduction and sulfide oxidation in intertidal sediments: FEMS Microbiology Letters, v. 73, p. 131-138.

Kostka, J. E. and G. W. Luther, 1994, Partitioning and speciation of solid phase iron in saltmarsh sediments: Geochimica et Cosmochimica Acta, 58: 1701-1710.

Kristiansen, K. D., E. Kristensen and M. H. Jensen, 2002, The influence of water column hypoxia on the behaviour of manganese and iron in sandy coastal marine sediment: Estuarine Coastal and Shelf Science, 55: 645-654.

Llobet-Brossa, E., R. Rabus, M. E. Böttcher, M. Konneke, N. Finke, A. Schramm, R. L. Meyer, S. Grötzschel, R. Rossello-Mora and R. Amann, 2002, Community structure and activity of sulfate-reducing bacteria in an intertidal surface sediment: a multi-method approach: Aquatic Microbial Ecology, 29: 211-226.

Lovley, D. R., 1991, Dissimilatory Fe(III) and Mn(IV) Reduction: Microbiological Reviews, 55: 259-287.

Lovley, D. R. and E. J. P. Phillips, 1987, Competitive Mechanisms for Inhibition of Sulfate Reduction and Methane Production in the Zone of Ferric Iron Reduction in Sediments: Applied and Environmental Microbiology, 53: 2636-2641.

Lovley, D. R. and E. J. P. Phillips, 1988, Manganese inhibition of microbial iron reduction in anaerobic sediments: Applied and Environmental Microbiology, 53: 145-155.

Lovley, D. R. and E. J. P. Phillips, 1994, Novel Processes for Anaerobic Sulfate Production from Elemental Sulfur by Sulfate-Reducing Bacteria: Applied and Environmental Microbiology, 60: 2394-2399.

Lovley, D. R., E. E. Roden, E. J. P. Phillips and J. C. Woodward, 1993, Enzymatic iron and uranium reduction by sulfate reducing bacteria: Marine Geology, 113: 41-53.

Luther, G. W., B. Sundby, B. L. Lewis, P. J. Brendel and N. Silverberg, 1997, Interactions of manganese with the nitrogen cycle: Alternative pathways to dinitrogen: Geochimica et Cosmochimica Acta, 61: 4043-4052.

Magni, P. and S. Montani, 2006, Seasonal patterns of pore-water nutrients, benthic chlorophyll a and sedimentary AVS in a macrobenthos-rich tidal flat: Hydrobiologia, 571: 297-311.

Meile, C. and P. Van Cappellen, 2003, Global estimates of enhanced solute transport in marine sediments: Limnology and Oceanography, 48: 777-786.

Meyer, C. and G. Ragutzki, 1999, KFKI Forschungsvorhaben Sedimentverteilung als Indikator für morphodynamische Prozesse., Norderney, Niedersächsisches Landesamt für Ökologie, 43.

Meysman, F. J. R., O. S. Galaktionov, B. Gribsholt and J. J. Middelburg, 2006, Bio-irrigation in permeable sediments: An assessment of model complexity: Journal of Marine Research, 64: 589-627.

Middelburg, J. J., G. J. De Lange and C. H. van Der Weijden, 1987, Manganese solubility control in marine pore waters: Geochimica et Cosmochimica Acta, 51: 759-763.

Millero, F. J., 1991, The oxidation of H_2S in the Chesapeake Bay: Estuarine, Coastal and Shelf Science, 33: 521-527.

Moffett, J. W., 1994, A radiotracer study of cerium and manganese uptake onto suspended particles in Chesapeake Bay: Geochimica et Cosmochimica Acta, 58: 695-703.

Moore, W. S., J. Krest, G. Taylor, E. Roggenstein, S. Joy and R. Lee, 2002, Thermal evidence of water exchange through a coastal aquifer: implications for nutrients fluxes: Geophys. Res. Lett., 29:10.1029.

Myers, C. R. and K. H. Nealson, 1988, Microbial reduction of manganese oxides: Interactions with iron and sulfur: Geochimica et Cosmochimica Acta, 52: 2727-2732.

Nealson, K. H. and C. R. Myers, 1992, Microbial Reduction of Manganese and Iron - New Approaches to Carbon Cycling: Applied and Environmental Microbiology, v. 58, p. 439-443.

Neretin, Y. A., 2003, Groups of hierarchomorphisms of trees and related Hilbert spaces: Journal of Functional Analysis, 200: 505-535.

Nico, P. S., C. Anastasio and R. J. Zasoski, 2002, Rapid photo-oxidation of Mn(II) mediated by humic substances: Geochimica et Cosmochimica Acta, 66: 4047-4056.

Nielsen, P., 1990, Tidal Dynamics of the Water-Table in Beaches: Water Resources Research, 26: 2127-2134.

Parkhurst, D. L., 1980, PHREEQE-A computer program for geochemical caculations: U.S. Geol. Surv. Water Resour. Inv., 219: 80-96.

Parkhurst, D. L., 1995, User`s guide to PHREEQUE: a computer model for speciation, reaction-path, advective-transport an inverse geochemical calculations: U.S. Geol. Surv. Water Resour. Inv., 143: 95-4227.

Peters, L., 2004, Zur Biogeochemie eines Sedimentkerns aus dem Mischwatt der südlichen Nordsee: Diploma Thesis, CvO Universität Oldenburg, 113.

Postma, D., 1985, Concentration of Mn and separation from Fe in sediments-I. Kinetics and stoichiometry of the reaction between birnessite and dissolved Fe(II) at 10°C: Geochimica et Cosmochimica Acta, 49: 1023-1033.

Postma, D., 1993, The reactivity of iron oxides in sediments: A kinetic approach: Geochimica et Cosmochimica Acta, 57: 5027-5034.

Pyzik, A. J. and S. E. Sommer, 1981, Sedimentary iron monosulfides: Kinetics and mechanism of formation: Geochimica et Cosmochimica Acta, 45: 687-698.

Saager, P. M., J. P. Sweerts and H. J. Ellermeijer, 1990, A Simple Pore-Water Sampler for Coarse, Sandy Sediments of Low Porosity: Limnology and Oceanography, 35: 747-751.

Schippers, A. and B. B. Jørgensen, 2001, Oxidation of pyrite and iron sulfide by manganese dioxide in marine sediments: Geochimica et Cosmochimica Acta, 65: 915-922.

Schippers, A. and B. B. Jørgensen, 2002, Biogeochemistry of pyrite and iron sulfide oxidation in marine sediments: Geochimica et Cosmochimica Acta, 66: 85-92.

Skowronek, F., J. Sagemann, A. Dahmke and H. D. Schulz, 1994, Austrag von gelöstem Cu, Ni, Cd und Mn aus Schlicksedimenten im Weserästuar, NW-Deutschland: In: J. Matschullat, and G. Müller (eds), Geowissenschaften und Umwelt, Springer Verlag.

Slomp, C. P., J. F. P. Malschaert, L. Lohse and W. VanRaaphorst, 1997, Iron and manganese cycling in different sedimentary environments on the North Sea continental margin: Continental Shelf Research, 17: 1083-1117.

Sørensen, J. and B. B. Jørgensen, 1987, Early diagenesis in sediments from Danish coastal waters: Microbial activity and Mn-Fe-S geochemistry: Geochimica et Cosmochimica Acta, 51: 1583-1590.

Stookey, L. L., 1970, Ferrozine - a New Spectrometric Reagent for Iron: Analytical Chemistry, 42: 779-781.

Stumm, W.,and J. J. Morgan, 1981, Aquatic Chemistry: New York, Wiley & Sons.

Sunda, W. G. and S. A. Huntsman, 1994, Photoreduction of manganese oxides in seawater: Marine Chemistry, 46: 133-152.

Sundby, B. and N. Silverberg, 1985, Manganese flux in the benthic boundary layer: Limnology and Oceanography, 30: 374-382.

Sung, W. and J. J. Morgan, 1981, Oxidative removal of Mn(II) from solution catalysed by the γ-FeOOH (lepidocrocite) surface: Geochimica et Cosmochimica Acta, 45: 2377-2383.

Tebo, B. and S. Emerson, 1986, Microbial manganese(II) oxidation in the marine environment: a quantitative study: Biogeochemistry, 2: 149-161.

Thamdrup, B., 2000, Bacterial Manganese and Iron Reduction in Aquatic Sediments: In: B. Schink, (eds), Advances in Microbial Ecology, 16: New York, Kluwer Academic/Plenum Publishers, 41-84.

Thamdrup, B. and T. Dalsgaard, 2000, The fate of ammonium in anoxic manganese oxide-rich marine sediments: Geochimica et Cosmochimica Acta, 64: 4157-4164.

Thamdrup, B., K. Finster, J. W. Hansen and F. Bak, 1993, Bacterial Disproportionation of Elemental Sulfur Coupled to Chemical-Reduction of Iron or Manganese: Applied and Environmental Microbiology, 59: 101-108.

Thamdrup, B., H. Fossing and B. B. Jørgensen, 1994, Manganese, Iron, and Sulfur Cycling in a Coastal Marine Sediment, Aarhus Bay, Denmark: Geochimica et Cosmochimica Acta, 58: 5115-5129.

Van Cappellen, P. and Y. Wang, 1995, Metal cycling in surface sediments: Modeling the interplay of transport and reaction: In: H. E. Allen (eds), Metal contaminated Aquatic sediments: Michigan, Ann Arbor Press.

van der Zee, C. and W. van Raaphorst, 2004, Manganese oxide reactivity in North Sea sediments: Journal of Sea Research, 52: 73-85.

van der Zee, C., W. van Raaphorst and E. Epping, 2001, Absorbed Mn^{2+} and Mn redox cycling in Iberian continental margin sediments (northeast Atlantic Ocean): Journal of Marine Research, 59: 133-166.

van der Zee, C., W. van Raaphorst, W. Helder and H. de Heij, 2003, Manganese diagenesis in temporal and permanent depositional areas of the North Sea: Continental Shelf Research, 23: 625-646.

Viollier, E., P. W. Inglett, K. Hunter, A. N. Roychoudhury and P. Van Cappellen, 2000, The ferrozine method revisited: Fe(II)/Fe(III) determination in natural waters: Applied Geochemistry, 15: 785-790.

Walsh, J. J., 1991, Importance of continental margins in the marine biogeochemical cycling of carbon and nitrogen, 350: 53-55.

Winkler, L. W., 1888, Die Bestimmung des im Wasser gelösten Sauerstoffes.: Ber. dtsch. chem. Ges, 21: 2843-2855.

Wollast, R., 1991, The coastal organic carbon cycle: fluxes, sources, and sinks: In: M. R. F. C. Mantoura, J. M. Martin and R. Wollast (eds), Ocean margin processes in global change: London, John Wiley & Sons, 365-382.

Yeats, P. A., B. Sundby and J. M. Bewers, 1979, Manganese recycling in coastal waters: Marine Chemistry, 8: 43-55.

Zhang, H. and W. Davison, 1999, Diffusional characteristics of hydrogels used in DGT and DET techniques: Analytica Chimica Acta, 398: 329-340.

Zhang, J.-Z. and F. J. Millero, 1993, The products from the oxidation of H_2S in seawater: Geochimica et Cosmochimica Acta, 57: 1705-1718.

Zopfi, J., T. G. Ferdelman, B. B. Jørgensen, A. Teske and B. Thamdrup, 2001, Influence of water column dynamics on sulfide oxidation and other major biogeochemical processes in the chemocline of Mariager Fjord (Denmark): Marine Chemistry, 74: 29-51.

An in situ 2D Photopaper Technique to monitor spatial sulfide distribution in surface sediments.

K. Bosselmann, M. E. Böttcher, A. Theune, E. Walpersdorf

In preparation

Abstract

A monitoring technique to visualize the 2D spatial distribution of dissolved sulfide has been tested in the laboratory and applied to intertidal surface sediments under in-situ conditions. The technique is based on the fixation of dissolved hydrogen sulfide as black silver-sulfide (Ag_2S) in the active layer of photographic paper, modified after Lehmann & Bachofen, 1999. The accumulation of Ag_2S can be measured densitometrically by using a flat bed scanner and evaluated using commercial imaging software. The color change is quantitatively related to the amount of Ag_2S. Here, we present the further development and evaluation of the technique by performance of calibration experiments and a comparison with gross microbial sulfate reduction rates measured with $^{35}SO_4^{2-}$ radiotracer (Kallmeyer et al., 2004). The 2D Photopaper Technique was deployed within the top 15 cm in different types of intertidal sediments, where high activities of sulfate reducing bacteria have been found (Bosselmann & Böttcher, in prep.).

Introduction

Microbial sulfate reduction is a key process in the biogeochemical sulfur cycling and plays an important role in the overall oxidation of organic matter (Jørgensen, 1982). In intertidal sediments, highest sulfate reduction rates were found in the suboxic zone of the top surface sediments (Kristensen et al., 2000; Böttcher et al., 2000, 2004; Bosselmann & Böttcher, in prep.). Dissolved sulfate is reduced to H_2S which further shows a variety of reactions in the surface sediments. Dissolved sulfide may diffuse out of the sediment and/or can be reoxidized in the sediment by microbial- and chemical processes and/or may further react to iron sulfides (Jørgensen, 1982; Canfield, 1989). Generally, variation in dissolved sulfide concentrations provides important biogeochemical information about the microbial sulfate reducing activity at the sediment surface and is closely coupled to the burial and cycling of sedimentary sulfur (S), iron (Fe), and manganese (Mn) compounds. Only about 10 % of the sulfide produced by microbial sulfate reduction is permanently buried into the sediment, while about 90 % of the reduced sulfide is re-oxidized back to sulfate (Jørgensen, 1977, 1982). Most of the sulfides precipitate more or less permanently in the sediment as iron sulfides FeS and FeS_2, if reactive Fe phases are available. Reactive Fe phases represent the pools readily available for reduction by H_2S or microbes (Canfield, 1989; Thamdrup et al., 1994; Kostka & Luther, 1994). Due to the high-recycling efficiencies of reactive Mn- and Fe oxy(hydroxi)des, these metals function as electron shuttles on a short scale metal cycling at the sediment-water interface.

Several methods are used for measuring dissolved sulfide in situ. Microelectrodes (Kühl et al., 1998; Jeroschewski et al.,1996) allow to measure concentrations at high spatial resolution (depth), but in 1 dimensional micro scale profiles only.

Reeburgh & Erickson (1982) used a so called ‘dipstick’ sampler` prepared with lead acetate that is fixed in polyacrylamid-gel but not completely immobilized. The blackening of the dipstick samplers was measured after retrieval by densitometry from a negative photograph. Radioisotope images of microbial sulfide production were produced by Krumholz et al. (1997) by means of pieces of oxidized silver foil as ^{35}S-sulfide traps called ‘silver foil technique’. Another in-situ technique that is based on the technique of diffusive gradients in thin films (DGT, Davison & Zhang, 1994) was developed by Teasdale et al. (1999). The dissolved sulfide diffuses through a layer of polyacrylamid gel and then reacts with silver iodide (AgI), incorporated at the surface of a second gel, to form Ag_2S. In addition to the densitometry measurement, this method allows elution and subsequent measurement of sulfide by colorimetry. The prepared gel samplers are purchasable but have to be deoxygenated before deployment (Jézéquel et al., 2007; Motelica et al., 2003; DeVries & Wang, 2003).

In the present study, we optimized an imaging technique developed by Lehmann & Bachofen (1999), called `sulfur print`. These authors used metal lances covered with photographic paper to monitor sulfide distributions in the water column and surface sediments of a sulfidic lake. The system was

successfully applied in the water column (Lehmann & Bachhofen, 1999). For the use in sediments, however, pushing the lance into the sediment caused significant potential disturbance of the sedimentary structure and the associated biogeochemical zonation. To avoid this, we modified the deployment technique to reduce the disturbance of the sediment. In advancement of the method of Lehmann & Bachofen (1999), we will present results of a systematic calibration procedure and will give specifications especially for the lower limits of detection and quantitative application. Furthermore, we compare the results of the S images with corresponding measurements of sulfate reduction rates that were measured using the whole-core $^{35}SO_4^{2-}$ tracer incubation technique (Kallmeyer et al., 2004) and analyzed sulfide concentrations in the pore waters after Cline (1969) and in situ with microsensors (Jeroschewski et al., 1996; Kühl et al., 1998). To evaluate and adapt this technique to a variety of sediment types and the influence of different hydrodynamic conditions, the 2D Photopaper Technique was deployed in sandy and mixed intertidal sediments. The sampling sites were chosen to include a range of sediments representing different biological activities, sedimentological and geochemical properties (grain size, organic matter and metal content, permeability and porosity).

In contrast to 1D-measurements of dissolved sulfide in the interstitial water, the 2D Photopaper Technique provides the impression of a 2 dimensional structure, and is able to reveal internal patterns of sulfide distribution and net production rates. The measuring procedure is based on densitometry of the optical density of color changes and can be performed with freeware. This procedure provides a high spatial resolution in two dimensions combined with a high reproducibility. The photopapers can be stored for months without visible change. The 2D Photopaper Technique is less time consuming to apply than other in situ techniques and allows a rapid analysis.

Material and Methods

In this study, we used commercial photographic paper (Ilford, Multigrade IV-RC de Luxe; 10x15 cm). A 9 micron emulsion layer contains mixed silver halide crystals as binding agent with a total amount of approximately 0.165 mg cm^{-2} silver (Fa. Ilford, written communication, 2007). Brownish-black silver sulfide is readily formed in the emulsion layer when dissolved sulfide from the interstitial water reacts with the silver chlorobromide in the gel. The reaction $\mathbf{2Ag^+ + S^{2-} \rightarrow Ag_2S}$ is the basic reaction in the photography because Ag_2S is chemically very stable over time. Above pH 7, the main form of sulfide in aqueous solution is $HS^-_{(aq)}$ and the equilibration time with H_2S(aq) and S^{2-} is rapid (Millero et al., 1986; Hershey et al., 1988). Therefore, the pH was measured at the beginning and end of the calibration procedure to ensure that the pH values of the calibration solution were above 7.

As opposed to grayscale in black and white photography images, the development of silver sulfide creates a typical monochromatic image in shades of brown called 'sepia tone' (Daguerre, 1988). Resin coated photopaper is sufficiently resistible to be deployed in a solution medium for a few days (Lehmann & Bachofen, 1999). In a dark room, the photographic paper was attached to the inner wall of a black foil coated polycarbonate core liner by means of double face photostrip. Sediment sampling using core liners is proved to minimize disturbance compared to the set up used previously (Lehmann & Bachofen 1999). The liner was closed by rubber lids to protect the paper from light. During deployment and retrieval a black plastic bag covered the core liner to prevent exposure to light.

The immersion time varied from 1 to 24 hours, depending on the concentration of sulfide in the sediment. To achieve an optimized result, several core liners were deployed and retrieved after different time intervals. For fixation of the S prints after retrieval, the papers were immersed for 10 minutes into a 1 M sodium-thiosulfate solution, washed for further 10 minutes in a water bath and subsequently dried in air. The fixing bath leads to a removal of excessive silver halogenide according to:

$$\mathbf{Ag\ Cl\ Br + 2\ Na_2S_2O_3 \rightarrow Na_3(Ag(S_2O_3)_2) + NaBr + NaCl}$$

$$\mathbf{2\ Ag\ Cl\ Br + 5\ Na_2S_2O_3 \rightarrow 2\ Na_3(Ag(S_2O_3)_2) + 2\ NaBr + 2\ NaCl}$$

The degree of Ag_2S accumulation was determined by means of a flat bed scanner and evaluated with free imaging software (**Scion Image©;** Scion Corporation). This software allows to select user defined regions of the image and performs average optical density measurements for a chosen area. The images were recorded as 8-bit gray-scale tagged image file format (TIFF files). Pixels are represented by 8-bit unsigned integers, produce 256 shades of grey with pixels with 0 and 255 being displayed as white and black, respectively.

A calibration for the densitometric measurements was performed by exposing photographic paper to a range of 10-1000 µM sodium sulfide (Na_2S*9H_2O) solutions and different incubation times. The range

of darkening varied from light to dark brown depending on the concentration of sulfide in the solution and immersion time. The sulfide stock solution was prepared by dissolving Na_2S*9H_2O in deoxygenated water (purging the water with N_2-gas before addition of sulfide). Dissolved sulfide concentrations were measured with the methylene-blue method (Cline, 1969). Circles of photographic paper were attached to the bottom of syringes which were filled with sulfide stock solution. Sulfide losses were minimized by using gas tight glass syringes filled without any headspace. The syringes were placed in a shaker to ensure a homogeneous distribution of the S print. Each syringe was sampled for sulfide measurements at the beginning and end of the incubation time to quantify uptake and possible loss of sulfide by oxidation or degassing/volatilization of dissolved sulfide.

Two testing procedures were performed to verify a potential influence of inferences with Fe- and Mn oxy(hydroxid)es which may lead to an overestimation of sulfide concentrations. Formations of brownish Fe- and Mn-oxy(hydroxid)es during sediment deployment, as observed by Teasdale et al. (1999), were quantified by a leaching procedure of retrieved S images. To leach out possible incorporations of Fe- and Mn oxy(hydroxid)es, S images were exposed to 1 M hydrogen chloride solution for 60 min. The comparison of densitometric measurements before and after HCl-leaching showed that the possible interference caused only a slight discoloration from brown to bluish or the complete disappearance of faint colorations which can be neglected after conversion to grayscale images. This variation can be neglected according to the standard deviation of 3 replicate measurements. To further test potential artifacts caused by the precipitation of metal oxy(hydroxid)es in the photographic layer originating from dissolved pore water Fe and Mn, stripes of photographic paper were immersed in 1 mM $FeCl_2$, $FeSO_4$, and $MnCl_2$ solution for 1 and 24 hours. Incubation tests showed that only 24 hours incubation in 1mM $MnCl_2$ solution caused a brownish discoloration which would account for/corresponding to an average sulfide concentration of 29 µM. Discoloration due to the incorporation of dissolved Fe is also neglectable after conversion to grayscale image. We therefore suggest to add a cleaning step with hydrochloric acid to prevent minor interferences prior to the application of this technique in sediments with a suboxic zone with accumulation of dissolved Mn or Fe.

Inferences with humic acids were found to be important in suspensions up to 2 % (Lehmann & Bachofen, 1999). Concentrations of humic acids in the investigated locations are considerably lower (Lovley & Woodward, 1996) and hence can be neglected. Exposure to light as it occurs at the sediment water interface can be easily identified on the photopaper since it can be distinguished from the brownish silver-sulfide by its bluish-purple coloration.

Results and Discussion

Calibration procedures

Sulfide accumulation was investigated by exposing photographic paper to a series of 10-1000 µM sodium sulfide (Na_2S) solutions. A series of duplicate measurements were performed for each sulfide concentration. The incubation times ranged from 15 minutes up to 24 hours. Density measurements were obtained by triplicate analysis of selected square-centimeters of the scanned calibration images (Figure 1).

Figure 1: Sulfide images, exposed to 0.3 mM di-sodium-sulfide solution for calibration after 0, 0.15, 1, 2, 6, 12 and 24 hours.

Variation of standard deviation of the duplicate calibration measurements was highest at concentrations below 10 µM, which can be explained by loss of sulfide by oxidation, volatilization or adsorption. Maximum variations of ± 5 pixel cm^{-2} were found, corresponding to a concentration of ± 3 µM cm^{-2} sulfide. Duplicate measurements of sulfide concentrations from 300-1000 µM revealed a maximum standard deviation of ± 2 pixel cm^{-2} or ± 2.7 µmol cm^{-2} sulfides. The lower detection limit for a 24 hours deployment was reached at 10 µM sulfide. Concentrations above 50 µM sulfide yielded reliable results, with a standard deviation of ± 1,04 pixel cm^{-2} equal to a concentration of ± 2.6 µmol cm^{-2} sulfide (Figure 2). A saturation of the grey scale intensity for the densitometric measurement was reached after 8 hours of deployment in 1000 µM sulfide solution (std. dev.: ± 1.8 pixel cm^{-2}; 2.7 µmol cm^{-2} sulfide). Consequently, reliable measurements can be obtained for concentrations (detection limits ranged) from above 10 µM for 24 hour incubation to more than 1000 µM with appropriate shorter deployment times.

The calibration experiments showed that the mean intensities of darkening were quantitatively related to the amount of Ag_2S (Figure 1).

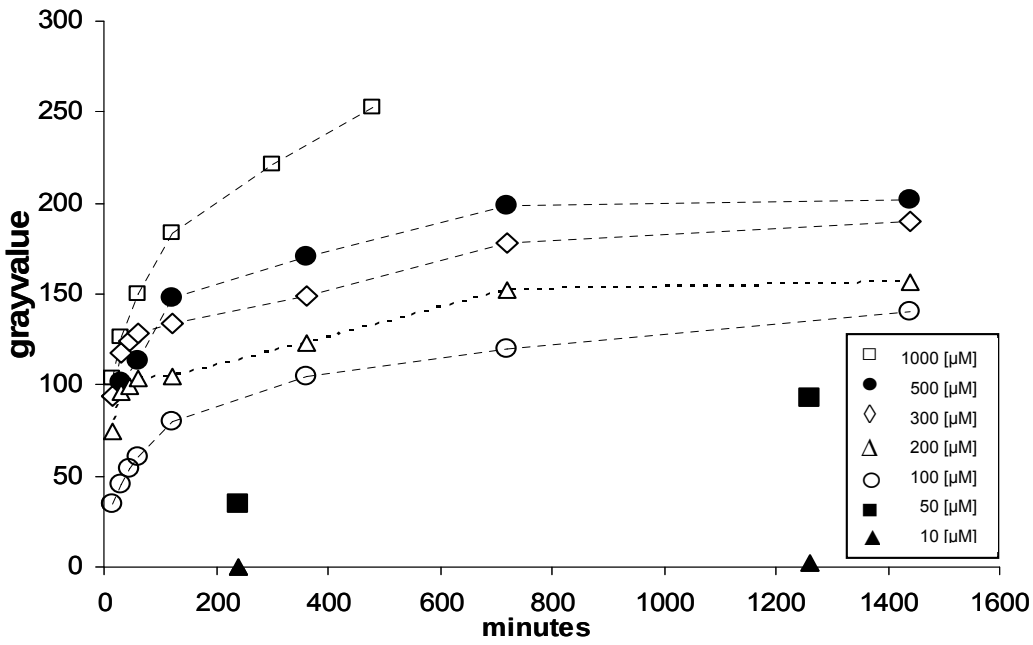

Figure 2: Time-dependent evolution of the average grayscale density of different sulfide concentrations versus incubation time.

The correlation between sulfide concentration and gray-scale-density showed a systematic logarithmic relationship (Figure 3). The *Scion Image* software works on the basis of the Lambert-Beer law and provides a logarithmic dependence between the transmission of light through a substance and the concentration of the substance. *Scion Image* converts grey values to optical density values using following function:

Equ. 3: OD = log10 (255/255-gray values).

According to Lambert-Beer's law, concentration is proportional to optical density (OD). The density of a point is the log ratio of incident light upon it and transmitted light through it. $OD = Log_{10} (I_o T^{-1})$. The mean data were fitted according the equation y = a ln (b x).

Equ. 4: y = 41,828*ln(x) + 251,65.

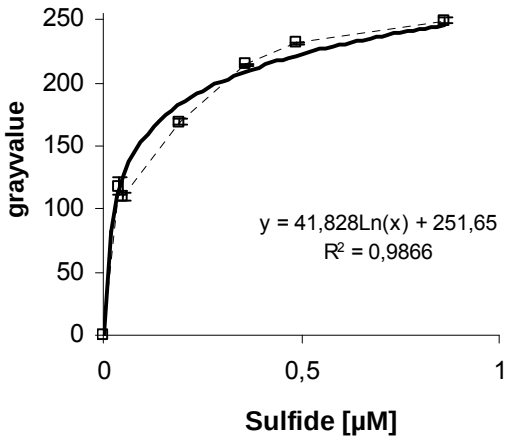

Figure 3: Relation of mean densitometric measurement and concentration of the sulfide calibration solutions.

This finding may indicate that the method is more sensitive at low concentrations than at higher concentrations. A similar relation was also found by measurements of diffusive thin films (Teasdale et al., 1999). Teasdale et al. compared their densitometry results with corresponding chemical measurements and ascribed this to an `optical` effect because of limited visible reactive particles at the surface layer. AgS particles further away from the interface may lead to an incomplete measurement by densitometry analysis. Sulfide concentrations up to 1000 µM showed reliable results and this assumption was not confirmed by our calibration experiments.

Field deployment

The 2D Photopaper Technique was deployed in different types of intertidal sediments located in the German Wadden Sea. The sampling sides were chosen to include a range of sediments representing different biological activities, sedimentological and geochemical properties (grain size, organic matter and metal content, permeability and porosity, for further information see Bosselmann et al., in prep.). Besides, the influence of temperature, the amount and quality of organic matter and metals are further process-controlling factors for the sulfate reduction rate. In the tidal back-barrier area of Spiekeroog island, our sites Neuharlingersiel (N) and Janssand (S I + III) represent intertidal mixed and sandy sediments, respectively. The Janssand flat is characterized by a slowly ascending slope of about 60 cm over a difference of 50 m between the highest position on the top (S III) and down to near the waterline (S I) at low tide (further details, see Bosselmann & Böttcher, in prep.).

Sulfate reduction rates, measured in spring, summer and autumn and presented in (Figure 4B) along with the scanned 2D Photopaper images (Figure 4AB). The images provide a 2 dimensional impression of the spatial variation of dissolved sulfide concentrations in situ.

Photopaper images deployed in spring in the sand flat sediments showed that low concentrations of sulfide remain close to the limit of detection, even after 24 hours of deployment. This corresponds to

the observed low sulfate reduction rates (Figure 4A, B). The accumulation maximum of sulfide 8 cm depth corresponds to an average amount of 20 µmol cm^{-2}. Pore water measurements of dissolved sulfide are not available.

At the mixed flat, sulfate reduction reached 10 times higher rates (Figure 4B). Photopaper images reflect that dissolved sulfide increased below 4 cm depth and showed different zones of sulfide production. Sulfide prints account to maximum amounts from 350-500 µmol cm^{-2} (Figure 4A).

In summer, a shorter deployment time (2-5 hours) was chosen to prevent reaching the saturation limit for the densitometric measurement. Despite maximum SRR in the surface layer of the top sand flat station S III, the photopaper image shows that sulfide reached only low concentrations which correlates to 17-600 µmol cm^{-2} and increased downwards to concentrations of up to 450 µmol cm^{-2} (Figure 4A, B). Compared to microsensor measurements, dissolved sulfide concentrations ranged from 0-520 µmol cm^{-2} and showed consistent depth distributions to the S image. At the position near the waterline, sulfide showed a more heterogeneous distribution, which reflects the irregular distribution of organic matter and confirms that a 1-dimensional measurement would not be sufficient to represent the processes occurring within this sediment. A sharp increase of peak sulfide concentrations up to 5000 µmol cm^{-2} responded to the zone where highest sulfate reduction rates were measured. Pore water sulfide concentrations amount to 2 µmol cm^{-2} at the surface and up to 920 µmol cm^{-2} deeper in the sediment.

In autumn peak rates of sulfate reduction at the sand flat S I was found deeper in the sediment (~6 cm below the surface). The photopaper image visualized a heterogeneous sulfide distribution within the surface 5 cm depth which were also reflected by duplicate measurements of sulfate reduction rates by using the whole core incubation technique. Highest sulfide concentrations ranged from 200-400 µmol cm^{-2} (Figure 4A, B). Sulfide concentrations measured by microsensors in the pore water amount to 0-400 µmol cm^{-2}. The S print of the mixed flat indicated a sulfide rich zone below 4 cm depth, according to concentrations of 200-400 µmol cm^{-2} (Figure 4A) which corresponds to 250-640 µmol cm^{-2} sulfide in the pore water.

Variances between calculated sulfide concentrations and pore water measurements point out that the S fixation on the photopaper is superimposed by rapid sulfide oxidation or precipitation processes. During the deployment time only free sulfide reacts with the active photographic layer and indicated the net sulfide production. Therefore, the 2D Photopaper Technique is an adequate monitoring tool for the mean retention time of free sulfide and allows a semi-quantitative impression of sulfide production and consumption zones. Furthermore, pore water showed lower sulfide concentrations than those measured by microsensors. This probably due to rapid re-oxidation of sulfide during pore water squeezing and the small scale spatial variability of dissolved sulfide which is assessed with microsensors and also visible in the photopaper prints. A remarkable feature is, that particles of mussel shells were illustrated by sharp white contours on the S print (Figure 4A). Furthermore, the high resolution of the photopaper images permits detailed information of textural changes as reflected by the distribution of sand size particles at the sand flat stations (Figure 4A).

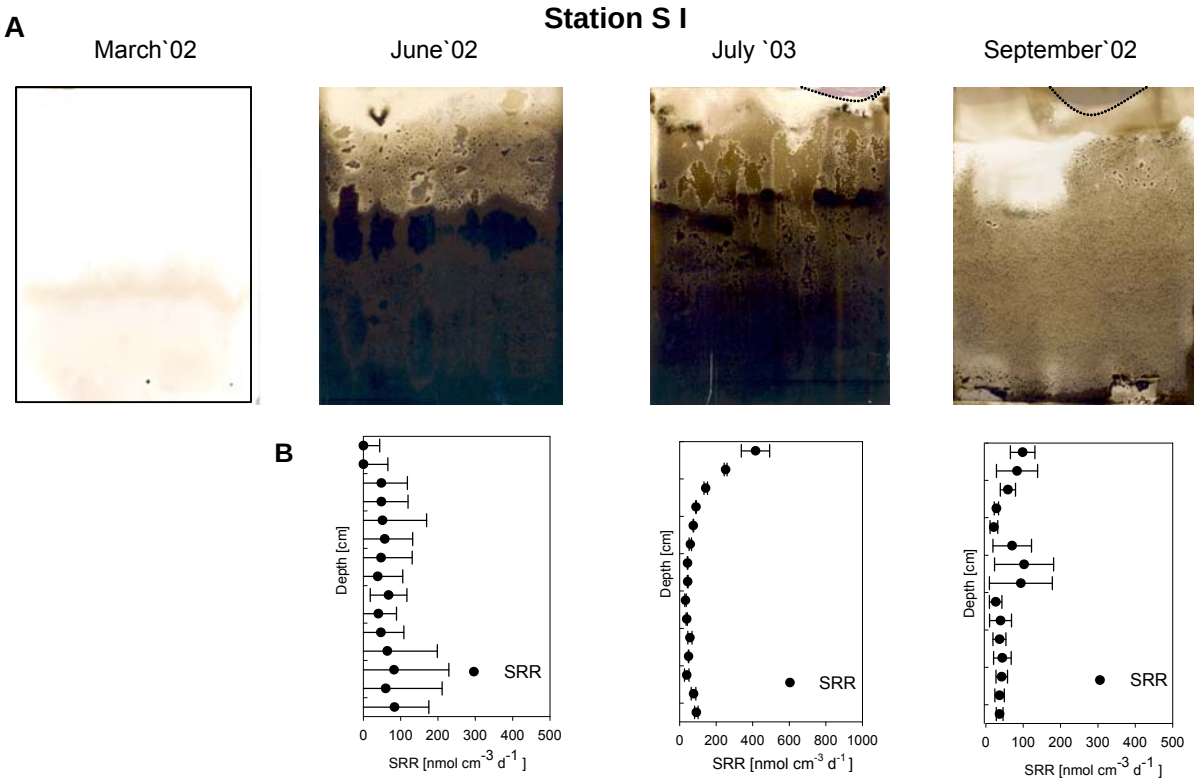
Station S I
A
March`02
June`02
July `03
September`02
B
Depth [cm]
SRR
SRR [nmol cm-3 d-1]

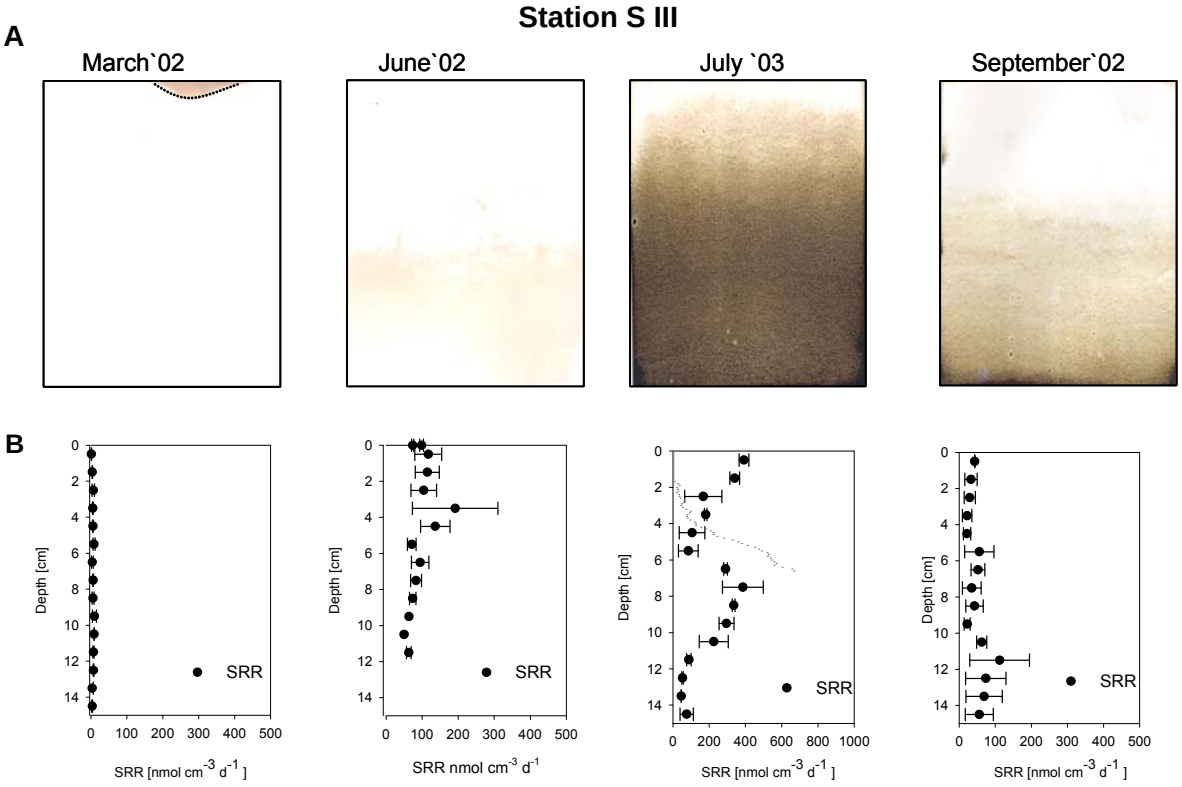
Station S III
A
March`02
June`02
July `03
September`02
B
Depth [cm]
SRR
SRR [nmol cm-3 d-1]
SRR nmol cm-3 d-1

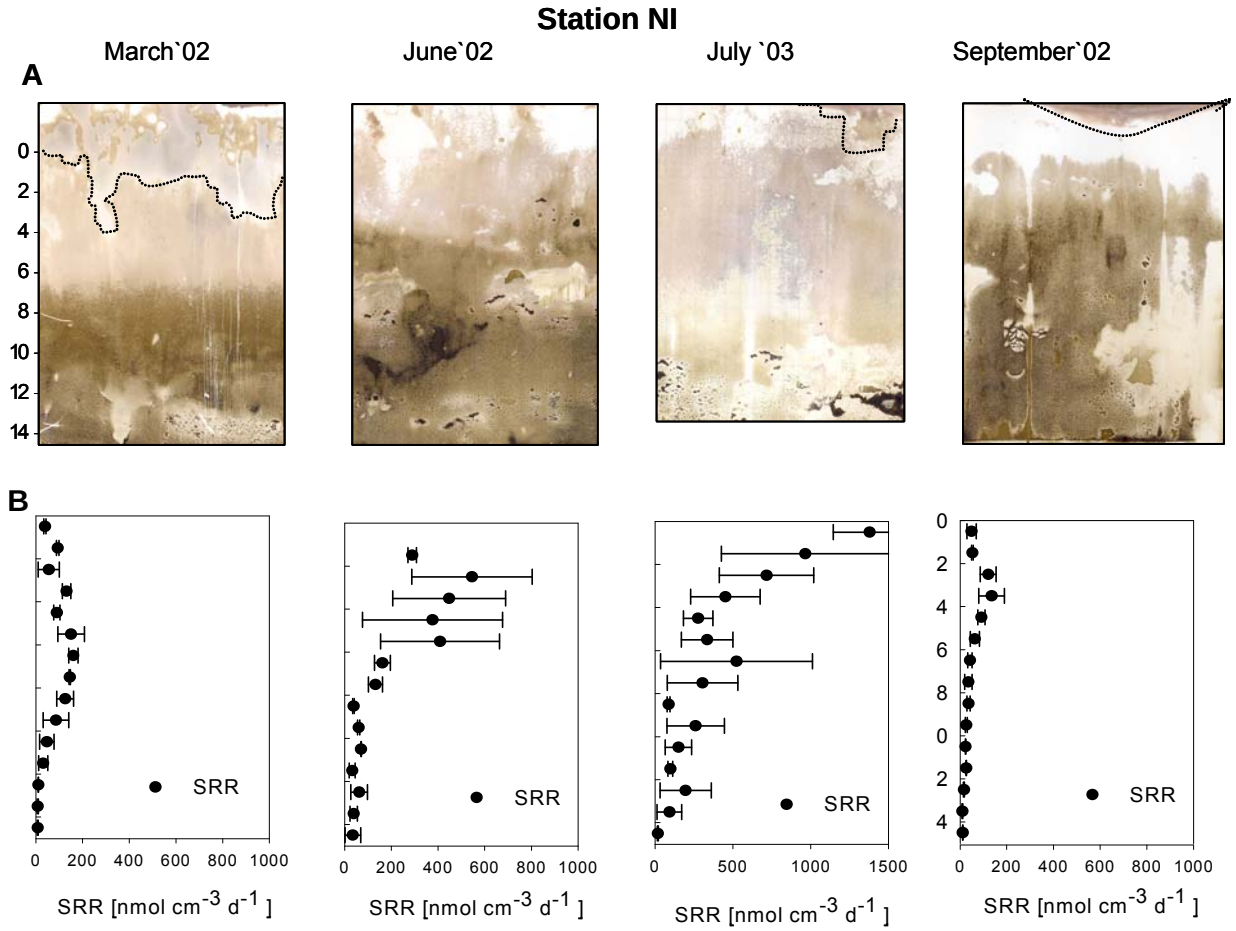

Figure 4: **A** : Spatial distribution of sulfide production monitored by the 2-D photo paper technique
B : Sulfate reduction rates [nmol cm^{-3} d^{-1}] by the whole core incubation.

Conclusions

The comparison of S prints at different sediment sites confirmed that sulfide production in the sandy sediments from Janssand were much lower than in the mixed sediment of Neuharlingersiel (Bosselmann & Böttcher, in prep.). Comparative measurements of sulfate reduction rates using the whole-core $^{35}SO_4^{2-}$ tracer incubation technique (Kallmeyer et al., 2004) reflected that the zones of sulfide production and depletion are readily apparent in the S prints of the sediment profiles and also illustrate the influence of different hydrodynamic conditions for the S cycling (Figure 4). Compared to SRR, the S prints from the sand flat pointed out that intensive sulfate reduction took place in the oxygenated part of the sediment, but abiotic re-oxidizing processes superimposed the bacterial sulfide production. Consequently, the abiotic sulfide oxidation was faster than the diffusion into the reactive layer of the photographic paper. Pore water sulphate concentration remained constant throughout the surface 15 cm depth and indicated deep exchange and efficient mixing with tidal bottom waters and fast re-oxidation of hydrogen sulfide (Bosselmann & Böttcher, in prep). As an effect of tidal flushing, permeable surface sediments are flushed with oxygen rich water which stimulates subsurface S-cycling in intertidal sediments. But even at the mixed station anaerobic re-oxidation by oxidized Fe and/or Mn phases may become competing processes (Aller & Rude, 1988; Fossing & Jørgensen, 1990; Afonso & Stumm, 1992).

Therefore, the 2D Photopaper Technique provides information about the retention time of hydrogen sulfide at a high spatial resolution, which was rapidly re-oxidized especially at the sand flat surface. Furthermore, visualization of spatial sulfide distribution indicated a stronger bioturbation activity in the mixed sediment than in the sandy sediments with a more homogenous (depth) zonation of microbial activity. The very heterogeneous distribution of sulfide, especially at the position near the waterline, confirms that a 1-dimensional measurement would not be sufficient to represent the heterogeneity of processes within this sediment. In addition to the expected 2-dimensional impression of sulfide distribution, the detailed resolution of the photopaper images permits information of textural changes visualizing details of internal sediment structures as grain sizes and particles as mussels (Figure 4). Measured sulfide concentrations in the pore water showed good agreements with sulfide accumulation determined by densitometric photopaper images. The application of the Photopaper Technique in the field has been proven to show reliable results in various sediment types.

Complementary to the investigations made by Lehmann & Bachofen 1999, a further evaluation of the technique was performed by the calibration experiments. The calibration experiments showed that the mean intensities of darkening were quantitatively related to the amount of Ag_2S (Figure 2,3). The sensitivity of this method allows detection of concentrations from 50 µM for 24 hour incubation to more than 1000 µM with appropriate shorter deployment times. Duplicate measurements offered reliable and reproducible results with a maximum standard deviation of $\pm$ 2 pixel cm^{-2} equal to the concentration of $\pm$ 2.7 µmol cm^{-2} sulfide. A saturation of the grey scale intensity for the densitometric measurement was reached after 8 hours of deployment in 1000 µM sulfide solution. Two testing

procedures were performed to verify a potential influence of inferences with Fe- and Mn oxy(hydroxid)es. Results showed that the possible interference caused only a slight discoloration which is according to the standard deviation of 3 replicate measurements and can therefore be neglected after conversion to grayscale images. This procedure confirmed to be appropriate for easy and rapid in situ application in the field and easy hand able utilization in the lab, afterwards.

References

Aller, R. C. and P. D. Rude, 1988, Complete oxidation of solid phase sulfides by manganese and bacteria in anoxic marine sediments: Geochimica et Cosmochimica Acta, 52: 751-765.

Böttcher, M. E., B. Hespenheide, H. J. Brumsack and K. Bosselmann, 2004, Stable isotope biogeochemistry of the sulfur cycle in modern marine sediments: I. Seasonal dynamics in a temperate intertidal sandy surface sediment: Isotopes in Environmental and Health Studies, 40: 267-283.

Böttcher, M. E., B. Hespenheide, E. Llobet-Brossa, C. Beardsley, O. Larsen, A. Schramm, A. Wieland, G. Böttcher, U. G. Berninger and R. Amann, 2000, The biogeochemistry, stable isotope geochemistry, and microbial community structure of a temperate intertidal mudflat: an integrated study: Continental Shelf Research, 20: 1749-1769.

Bosselmann, K. and M. E. Böttcher, in prep., Microbial sulfate reduction in intertidal surface sediments of the southern North Sea: Seasonal and spatial dynamics, and controlling factors.

Canfield, D. E., 1989, Reactive iron in marine sediments: Geochimica et Cosmochimica Acta, 53: 619-632.

Canfield, D. E., B. Thamdrup and J. W. Hansen, 1993, The Anaerobic Degradation of Organic-Matter in Danish Coastal Sediments - Iron Reduction, Manganese Reduction, and Sulfate Reduction: Geochimica et Cosmochimica Acta, 57: 3867-3883.

Cline, J. D., 1969, Spectrophotometric determination of hydrogen sulfide in natural waters: Limnology and Oceanography, 14: 454-458.

Daguerre, L. J. M., 1988, Das Daguerreotyp und das Diorama, oder genaue und authentische Beschreibung meines Verfahrens und meiner Apparate zu Fixirung der Bilder der Camera obscura und der von mir bei dem Diorama angewendeten Art und Weise der Malerei und der Beleuchtung / von Louis Jacq. Mandé Daguerre., Nachdr. d. Ausg. Stuttgart, Metzler, 1839: Stuttgart, Metzler, 67.

Davison, W. and H. Zhang, 1994, In-Situ Speciation Measurements of Trace Components in Natural-Waters Using Thin-Film Gels: Nature, 367: 546-548.

DeVries, C. R. and F. Wang, 2003, In Situ Two-Dimensional High-Resolution Profiling of Sulfide in Sediment Interstitial Waters: Environ. Sci. Technol.,. 37: 792-797.

Afonso, M.D. and W. Stumm, 1992, The reductive dissolution of iron (III)(hydr)oxides by hydrogen sulfide: Langmuir, 8: 1671-1676.

Fossing, H. and B. B. Jørgensen, 1990, Oxidation and reduction of radiolabeled inorganic sulfur compounds in an estuarine sediment, Kysing Fjord, Denmark: Geochimica et Cosmochimica Acta, 54: 2731-2742.

Hershey, J. P., T. Plese and F. J. Millero, 1988, The pK for the dissociation of H_2S in various ionic media: Geochimica et Cosmochimica Acta, 52: 2047-2051.

Jeroschewski, P., C. Steuckart and M. Kühl, 1996, An Amperometric Microsensor for the Determination of H_2S in Aquatic Environments: Anal. Chem., 68: 4351-4357.

Jézéquel, D., R. Brayner, E. Metzger, E. Viollier, F. Prevot and F. Fievet, 2007, Two-dimensional determination of dissolved iron and sulfur species in marine sediment pore-waters by thin-film based imaging. Thau lagoon (France): Estuarine, Coastal and Shelf Science, 72: 420-431.

Jørgensen, B. B., 1977, The sulfur cycle of a coastal marine sediment (Limfjorden, Denmark). Limnology and Oceanography, 22: 814-832.

Jørgensen, B. B., 1982, Mineralization of organic matter in the sea bed-the role of sulphate reduction, 296: 643-645.

Kallmeyer, J., T. G. Ferdelman, A. Weber, H. Fossing and B. B. Jørgensen, 2004, A cold chromium distillation procedure for radiolabeled sulfide applied to sulfate reduction measurements: Limnology and Oceanography: Methods, 2: 171-180.

Kostka, J. E. and G. W. Luther, 1994, Partitioning and speciation of solid phase iron in saltmarsh sediments: Geochimica et Cosmochimica Acta, 58: 1701-1710.

Kristensen, E., J. Bodenbender, M. H. Jensen, H. Rennenberg and K. M. Jensen, 2000, Sulfur cycling of intertidal Wadden Sea sediments (Königshafen, Island of Sylt, Germany): sulfate reduction and sulfur gas emission: Journal of Sea Research, 43: 93-104.

Krumholz, L. R., J. P. McKinley, G. A. Ulrich and J. M. Suflita, 1997, Confined subsurface microbial communities in Cretaceous rock: Nature, 386: 64-68.

Kühl, M., C. Steuckart, G. Eickert and P. Jeroschewski, 1998, A H_2S microsensor for profiling biofilms and sediments: application in an acidic lake sediment: Aquatic Microbial Ecology, 15: 201-209.

Lehmann, C. and R. Bachofen, 1999, Images of concentrations of dissolved sulphide in the sediment of a lake and implications for internal sulfur cycling: Sedimentology, 46: 537-544.

Lovley, D. R. and J. C. Woodward, 1996, Mechanisms for chelator stimulation of microbial Fe(III)-oxide reduction: Chemical Geology Chemical And Biological Control On Mineral Growth And Dissolution Kinetics, American Chemical Society Meeting, 132: 19-24.

Millero, F. J., 1986, The thermodynamics and kinetics of the hydrogen sulfide system in natural waters: Marine Chemistry, 18: 121-147.

Motelica-Heino, M., C. Naylor, H. Zhang and W. Davison, 2003, Simultaneous Release of Metals and Sulfide in Lacustrine Sediment: Environ. Sci. Technol., 37: 4374-4381.

Reeburgh, W. S. and R. E. Erickson, 1982, A ´dipstick´ sampler for rapid continuous chemical profiles in sediments: Limnology and Oceanography, 27: 556-559.

Teasdale, P. R., S. Hayward and W. Davison, 1999, In situ, High-Resolution Measurement of Dissolved Sulfide Using Diffusive Gradients in Thin Films with Computer-Imaging Densitometry: Anal. Chem., 71: 2186-2191.

Thamdrup, B., H. Fossing and B. B. Jørgensen, 1994, Manganese, Iron, and Sulfur Cycling in a Coastal Marine Sediment, Aarhus Bay, Denmark: Geochimica et Cosmochimica Acta, 58: 5115-5129.

Source and fate of manganese in a tidal basin of the German Wadden Sea

O. Dellwig, K. Bosselmann, S. Kölsch, M. Hentscher, J. Hinrichs, M.E. Böttcher, R. Reuter, H.J. Brumsack

This chapter is published in Journal of Sea Research:

57 (2007), 1-18

ELSEVIER

In Collaboration with the Royal Netherlands Institute for Sea Research

Journal of Sea Research 57 (2007) 1 – 18

JOURNAL OF SEA RESEARCH

www.elsevier.com/locate/seares

Sources and fate of manganese in a tidal basin of the German Wadden Sea

O. Dellwig [a,*], K. Bosselmann [b,1], S. Kölsch [a], M. Hentscher [a], J. Hinrichs [a], M.E. Böttcher [b,2], R. Reuter [c], H.-J. Brumsack [a]

[a] *Microbiogeochemistry, Institute for Chemistry and Biology of the Marine Environment, Carl von Ossietzky University of Oldenburg, D-26111 Oldenburg, Germany*

[b] *Department of Biogeochemistry, Max Planck Institute for Marine Microbiology, Celsiusstr. 1, D-28359 Bremen, Germany*

[c] *Marine Physics, Institute of Physics, Carl von Ossietzky University of Oldenburg, D-26111 Oldenburg, Germany*

Received 16 January 2006; accepted 27 July 2006
Available online 9 August 2006

Abstract

Dissolved and particulate Mn concentrations were investigated on a seasonal scale in surface waters of the NW German Wadden Sea (Spiekeroog Island) in 2002 and 2003. As the Wadden Sea forms the transition zone between the terrestrial and marine realms, Mn was analysed in coastal freshwater tributaries and in the adjoining German Bight as well. Additionally, sediments and porewaters of the tidal flat sediments were analysed for Mn partitioning and microbial activity.

Dissolved Mn concentrations show strong tidal and seasonal variation with elevated concentrations during summer at low tide. Summer values in the Wadden Sea (av. 0.7 μM) are distinctly higher than in the central areas of the German Bight (av. 0.02 μM), suggesting a possible impact of the Wadden Sea environment on the Mn budget of the North Sea. Seasonality is also observed for particulate Mn in the Wadden Sea (winter av. 800 mg kg^{-1}; summer av. 1360 mg kg^{-1}). Although particles are relatively Mn-poor during winter, the high SPM load during this season causes elevated excess concentrations of particulate Mn, which in part exceed those of the dissolved phase. Therefore, winter values cannot be ignored in balance calculations for the Wadden Sea system.

Porewater Mn concentrations differ depending on sediment type and season. Maximum concentrations are found in surface sediments at a mixed flat site (190 μM) during summer, while winter values are distinctly lower. This indicates that enhanced microbial activity owing to higher temperature during summer leads to increased reduction of Mn-oxides in surface sediments and enhances the corresponding diffusive and advective Mn flux across the sediment-water interface. Draining of Mn-rich porewaters from sediments is also documented by analyses of tidal creek waters, which are highly enriched in Mn during summer.

Furthermore, an important Mn source is freshwater discharged into the Wadden Sea via a flood-gate. The concentration of dissolved Mn in freshwater was highly variable during the sampling campaigns in 2002 and 2003, averaging 4 μM. In contrast, particulate Mn displayed a seasonal behaviour with increasing contents during summer. On the basis of salinity variations in the Wadden Sea, the total amount of Mn contributed to the Wadden Sea via freshwater was estimated. This balance shows the importance of the freshwater environment for the Mn inventory of the Wadden Sea. During winter the total Mn inventory of the

* Corresponding author. Present address: Baltic Sea Research Institute (IOW), Seestrasse 15, 18119 Rostock, Germany.
E-mail address: olaf.dellwig@io-warnemuende.de (O. Dellwig).
[1] Present address: University of Kiel, FTZ, 25761 Büsum, Germany.
[2] Present address: Baltic Sea Research Institute (IOW), Seestrasse 15, 18119 Rostock, Germany.

1385-1101/$ - see front matter
doi:10.1016/j.seares.2006.07.006

Wadden Sea water column may be explained almost completely by freshwater discharge, whereas in summer the porewater system forms the dominating source.

Keywords: Manganese; Tidal flat sediments; North Sea; Microbial activity; Sulphate reduction; Freshwater; Porewater

1. Introduction

Concentrations of dissolved manganese (Mn) in the North Sea are more than an order of magnitude higher than in the North Atlantic (Kremling, 1983, 1985; Tappin et al., 1995; Shiller, 1997). These elevated Mn concentrations have generally been explained by benthic fluxes from sediments during early diagenesis in North Sea sediments and riverine input (e.g. Duinker et al., 1979; Dehairs et al., 1989; Burton et al., 1993; Laslett, 1995; Tappin et al., 1995). However, tidal flats and salt marshes, which are highly dynamic systems due to tidal and seasonal fluctuations of biological, chemical, and physical parameters, can also have an impact on carbon, nutrient, and trace metal budgets of open marginal seas. Brasse et al. (1999), for instance, estimate that the amounts of dissolved inorganic carbon delivered to the German Bight from the Wadden Sea and rivers are of the same order of magnitude. The exchange between the coastal environment and the adjacent sea occurs directly via the tidal regime and to a much smaller extent by submarine groundwater discharge (e.g. Tappin et al., 1995 and references therein; Shaw et al., 1998; Moore et al., 2002; Burnett et al., 2003).

Although the tidal flats in the study area form the biologically productive transition zone between the terrestrial and marine realm, the processes controlling their geochemical variability are still poorly understood. For example, microbially induced reactions in the sediment and in the water column should influence the geochemical composition of suspended matter and water in the intertidal area, and, therefore, also the exchange of elements with the North Sea.

To date, geochemical investigations in the NW German Wadden Sea have mainly focussed on nutrients and environmentally crucial heavy metals within a specific grain-size fraction of the sediments (e.g. Schwedhelm and Irion, 1985; Recke and Förstner, 1988; Dellwig et al., 2000; Hinrichs et al., 2002), and the biogeochemistry of silty surface sediments (Böttcher et al., 2000). By contrast, data related to the chemical composition of the water column of the Wadden Sea and the adjoining freshwater environment are rare (e.g., Liebezeit et al., 1996; Hild, 1997; Dellwig et al., 2002).

The interdisciplinary Research Group 'BioGeoChemistry of Tidal Flats' was established by the Deutsche Forschungsgemeinschaft in 2001 and is coordinated by the ICBM to study the fundamental biological, chemical, and physical processes in the backbarrier tidal area of Spiekeroog Island. One of the research topics is focussed on an input/output balance of dissolved and particulate matter between the open North Sea and the tidal flats. Furthermore, the cycles of manganese, iron, and sulphur in different types of intertidal sediments are investigated in a quantitative manner in order to understand the role of the benthic biogeochemistry on element cycling in surface sediments and fluxes across the sediment-water interface (Böttcher et al., 2004).

In this contribution we present new data for dissolved and particulate Mn from several cruises (1997–2004) into the backbarrier tidal area of Spiekeroog Island and the German Bight. The study focuses on manganese, because its redox-sensitivity makes it a strong candidate as a useful tracer for water exchange between the biologically active Wadden Sea and the less active North Sea. Furthermore, Mn is of general importance, as it forms an essential micronutrient for phytoplankton (Davidson and Marchant, 1987; Fraustro da Silva and Williams, 1991) and the transfer of dissolved Mn to the particulate phase via microbial and photo-oxidation (Moffett, 1994; Nico et al., 2002) influences the cycles of other trace metals by scavenging (e.g. Feely et al., 1983; Koschinsky et al., 2003).

The major goal of this study is to explain the tidal and seasonal variation of Mn within the Wadden Sea water column and to elucidate the importance of individual sources, such as tidal flat sediments and small coastal

Fig. 1. a. Map of the study area showing the sampling sites in the Spiekeroog Island backbarrier area (time-series; asterisks) and in the German Bight. The bold line displays the separation between near-shore (SPM >5 mg^{-1}) and offshore samples (SPM <5 mg^{-1}). The grey arrow denotes the general flow direction in the German Bight. b. Detailed map of the Spiekeroog Island backbarrier area showing the time-series stations in the Otzumer Balje (OB) and in the central backbarrier area (CBA) as well as the porewater and tidal creek sampling sites (JS, NHS, GP). D1 and D2 mark two drift experiments with X denoting the end point of the drift experiment D1. c. Map of the freshwater sampling sites in the catchment area of the flood-gate in Neuharlingersiel.

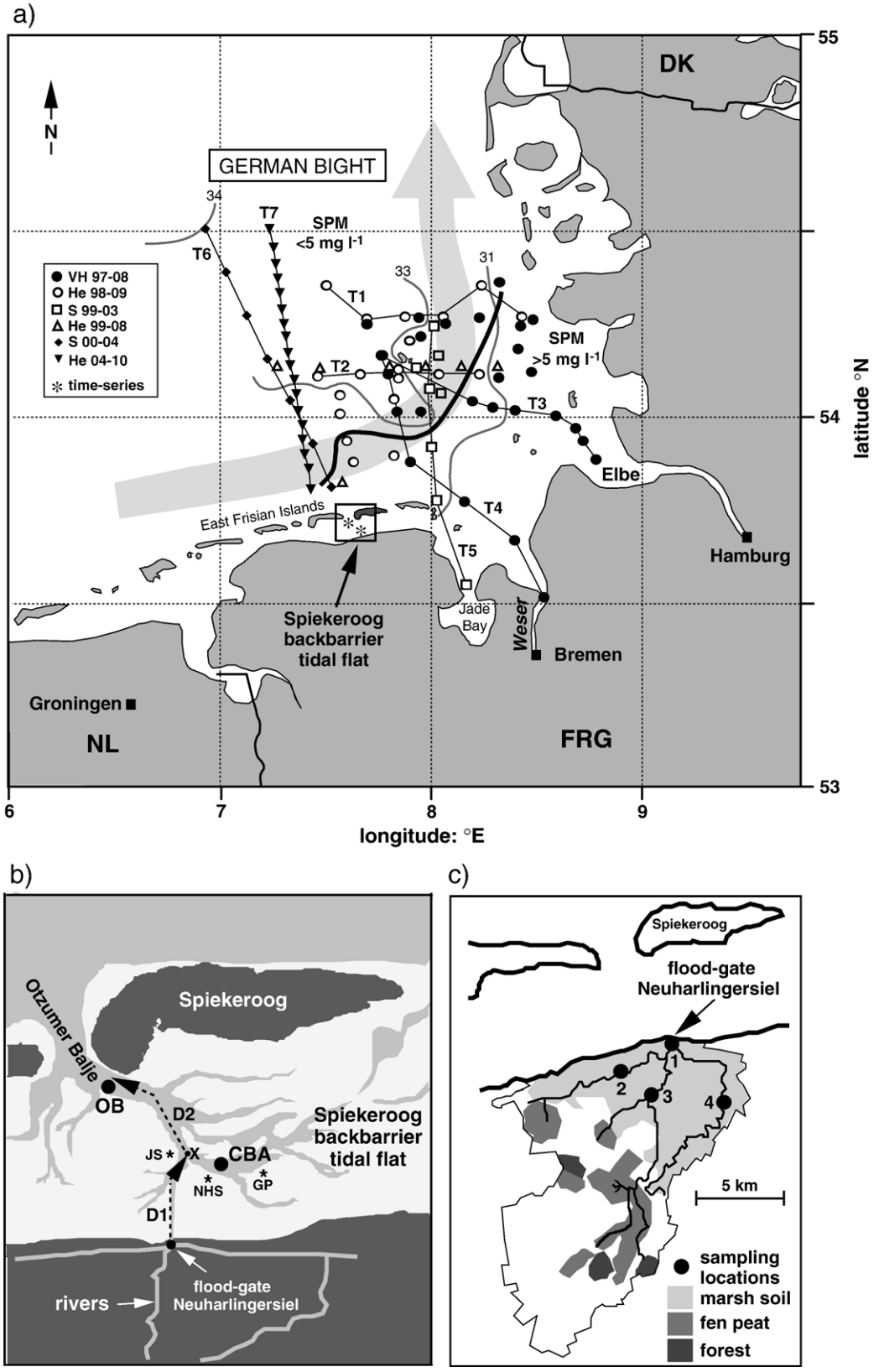
a)
N
GERMAN BIGHT
DK
NL
FRG
Groningen
Bremen
Hamburg
Elbe
East Frisian Islands
Spiekeroog backbarrier tidal flat
Jade Bay
Weser
T1
T2
T3
T4
T5
T6
T7
SPM <5 mg l-1
SPM >5 mg l-1
VH 97-08
He 98-09
S 99-03
He 99-08
S 00-04
He 04-10
time-series
34
33
31
55
54
53
6
7
8
9
latitude °N
longitude: °E
b)
Spiekeroog
Otzumer Balje
OB
D2
D1
JS
X
CBA
NHS
GP
Spiekeroog backbarrier tidal flat
rivers
flood-gate Neuharlingersiel
c)
Spiekeroog
flood-gate Neuharlingersiel
1
2
3
4
5 km
sampling locations
marsh soil
fen peat
forest

freshwater tributaries, for the Mn budget of the Wadden Sea system.

2. Geographical setting

The Wadden Sea of the southern North Sea stretches across a coastline of about 500 km from Den Helder in the Netherlands to Esbjerg in Denmark and covers an area of 9300 km^2 (Ehlers, 1994). The East-Frisian Wadden Sea amounts to about 15% of the entire area and is characterised by a mesotidal regime (tidal range 2.2–2.8 m). The formation of this system with its tidal flats and barrier Islands started about 7500 BP as a result of the Holocene sea-level rise (Streif, 1990) when the approaching North Sea transported Pleistocene sands and riverine sediments landwards. Today, the morphology of the coastline is largely determined by human activities, such as dike building, land reclamation, and drainage.

Fig. 1a shows the sampling locations in the Spiekeroog backbarrier tidal flats and the German Bight. The asterisks in the Spiekeroog backbarrier area indicate two time-series stations in the major tidal inlet (Otzumer Balje, OB) and in the central backbarrier area (CBA), which are shown in more detail in Fig. 1b. Sampling in the Spiekeroog backbarrier area was performed at intervals of 20 to 60 min for dissolved compounds and 60 min for particulates during nine cruises with the research vessel FK 'Senckenberg' in February 2002 and 2003, May 2002, April 2003, August 2002 and 2003, November 2002 and 2003, and January 2004.

Water samples from tidal creeks were taken during the cruises in the Spiekeroog backbarrier area on a sand flat (Janssand, JS, Fig. 1b) about one hour before low tide. At this location, sampling of porewaters and sediments for geochemical and microbiological investigations was carried out periodically by a Dutch tjalk (barge) (Böttcher and Jørgensen, 2005). In the present communication, results are presented from sampling campaigns in June 2002, December 2002, and July 2003. Sampling of the sandy site Gröninger Plate (GP) was performed once in July 2003. Geochemical results on the Gröninger Plate have been reported previously by Böttcher et al. (1998). Sediment and porewater sampling on a mixed flat close to Neuharlingersiel (NHS) was carried out during several campaigns between 2001 and 2004.

German Bight samples were collected during several cruises with RV 'Victor-Hensen' (August 1997), RV 'Senckenberg' (July 1998, March 1999, April 2000), and RV 'Heincke' (September 1998, August 1999; October 2004).

Freshwater samples were taken monthly between March 2002 and December 2003 at locations 2 to 4 in the catchment area of the flood-gate in Neuharlingersiel (Fig. 1c). At location 1 (flood-gate Neuharlingersiel) the sampling frequency was about 2 weeks.

3. Materials and methods

Suspended particulate matter (SPM) and water samples were collected from surface waters in the backbarrier tidal flat area (406 particulate samples, 658 water samples), in the German Bight (148), and in the freshwater environment (195). Depending on SPM contents, 0.15 to 1.25 L of water were filtered through pre-weighed Millipore Isopore© membrane filters (0.45 μm polycarbonate [PC], for multi-element analyses) and Whatman glass microfibre filters GF/F (0.7 μm glass fibre [GF], for TC and TIC analyses). Filters were rinsed with purified water, dried at 60 °C for 48 h and re-weighed for the determination of total SPM. Samples for analysis of dissolved metals were directly taken with pre-cleaned PE-syringes and 0.45 μm SFCA syringe filters. These samples were acidified to 1 vol. % HNO_3 in pre-cleaned PE-bottles. Tidal creek water samples (five samples for each cruise in the Wadden Sea) were taken directly with syringes and treated in the same way.

For multi-element analysis the PC filters were treated overnight with 1 ml HNO_3 and 2 ml $HClO_4$ in closed PTFE autoclaves (PDS-6; Heinrichs et al., 1986) at room temperature to oxidise organic matter. Then the filters were decomposed at 160 °C. SPM residues were digested in the same PTFE vessels at 180 °C after adding a mixture of 1 ml $HClO_4$ and 3 ml HF. After digestion the acids were evaporated at 180 °C, re-dissolved and fumed off three times with 2 ml half-concentrated HCl and diluted with 2 vol.% HNO_3 to a final dilution factor of 2500 to 5000. All acids were pre-cleaned by sub-boiling distillation, except for HF (suprapure quality).

Particulate Al and Mn were analysed by ICP-OES (Perkin Elmer Optima 3000XL), whereas dissolved Mn was measured by ICP-MS (Thermo Finnigan MAT ELEMENT). Dissolved Mn was determined directly from 25-fold diluted samples. The analytical procedure applied is similar to the method published by Rodushkin and Ruth (1997). For water samples of the cruises in February, April, and August 2003 the ICP-MS instrument was coupled to a desolvation unit (Aridus, Cetac). The difference between the two methods was 5% for dissolved Mn. Contamination effects were excluded by measurement of filter and onboard procedural blanks.

Table 1
Average concentrations, range (in brackets), and standard deviation (SD) of dissolved and particulate parameters for the Wadden Sea

	Wadden Sea winter	SD	Spring	SD	Summer	SD	Fall	SD
SPM [mg l^{-1}]	40.6 (18–151)	23.2	9.9 (4.1–36)	4.9	8.7 (2.6–68)	11.3	32.1 (12–104)	17.9
POC [%]	4 (2.3–5)	0.4	5.7 (3.7–11.4)	1.9	4.6 (3.3–9.1)	1.0	3.8 (3.1–4.9)	0.5
DOC [mM] *	0.24 (0.19–0.29)	0.03	0.21 (0.18–0.24)	0.01	0.21 (0.17–0.25)	0.02	0.21 (0.18–0.25)	0.02
CaO [%]	9.1 (7.2–9.9)	0.4	6.9 (4.9–8.3)	0.7	6.0 (4.5–8.7)	0.6	7.3 (6.0–8.4)	0.5
Al_2O_3 [%]	11.6 (8–12.7)	1.1	9.5 (7.1–11.5)	0.9	9.6 (7.1–11.5)	0.8	10.5 (8.2–12.5)	0.8
$Mn_{part.}$ [mg kg^{-1}]	795 (614–883)	54	1004 (677–1331)	153	1362 (746–2496)	303	930 (434–1113)	85
$Mn_{diss.}$ [μM]	0.07 (0.01–0.18)	0.04	0.3 (0.04–1.2)	0.24	0.7 (0.14–1.6)	0.27	0.08 (0.01–0.35)	0.05

* Data from the Wadden Sea cruises in 2002.

Total inorganic carbon (TIC) on GF-filters was determined coulometrically with a UIC instrument. Total carbon (TC) was determined from a parallel GF-filter by high temperature combustion and coulometric detection of CO_2 with a Ströhlein Coulomat 702. Particulate organic carbon (POC) was calculated as the difference of TIC and TC.

DOC measurements were performed on GF-filtrates by combustion and IR-detection with a multi N/C 3000 analyser (Analytik Jena). The filtrate was stored in brown glass bottles and acidified with semi-concentrated HCl (500 μl per 100 ml). The analysis was checked by measurements of K-hydrogenphthalate solutions containing 2 and 3 mg l^{-1} C. Precision and accuracy of all measurements were checked by parallel analysis of international and in-house reference materials. GSD-4, GSD-10 and our in-house shale standard TW-TUC were used as a reference for particulate samples, whereas reference seawater standards CASS-3 and CASS-4 (Canada) and riverine water reference material SLRS-3 (Canada) were used for dissolved samples. Precision (1σ) and accuracy were ≤4% for bulk parameter and ICP-OES measurements. For dissolved Mn precision and accuracy were 6.3% and 2.5%, respectively.

Extractable manganese (Mn_x) and iron were leached from freeze-dried sediments at room temperature (1 h; continuous agitation) with 0.5 M p.a. grade HCl. Mn was measured with a Perkin Elmer atomic absorption spectrometer and corrected for dissolved porewater Mn^{2+}. Porewater samples for dissolved Mn analyses were obtained on-board ship by centrifugation under nitrogen gas using centrifugation devices similar to the ones described by Saager et al. (1990), equipped with membrane filters (0.45 μm). Porewaters were analysed for major and trace elements by ICP-OES (Perkin Elmer Optima 3000XL). Additionally, gel samplers were applied in parallel to obtain high-resolution Fe and Mn porewater data. Benthic flux chambers were applied to measure element fluxes across the sediment-water interface (Bosselmann and Böttcher, unpublished data). Microbial sulphate reduction rates were measured using the whole-core incubation method. Carrier-free $^{35}SO_4^{2-}$ tracer was injected in the sediment core and incubated for 4 h. Tracer recovery after microbial conversion was measured in the acid volatile sulphur (AVS) and chromium reducible sulphur (CRS consisting of pyrite and S°) fractions. AVS and CRS were extracted from the sediments by a modified two-step distillation method (Fossing and Jørgensen, 1989; Kallmeyer et al., 2004).

CTD data were collected with a CTD probing system (Model OTS 1500, ME Meerestechnik-Elektronik, Germany) equipped with sensors for measuring pressure, conductivity and temperature. Salinity and density were calculated according to UNESCO standards (UNESCO, 1981).

Table 2
Average concentrations, range (in brackets), and standard deviation (SD) of dissolved and particulate parameters for the offshore samples of the German Bight

	German Bight (offshore) spring	SD	Summer	SD	Fall	SD
SPM [mg l^{-1}]	1.6 (1.1–4.9)	1.2	1.8 (0.6–4.8)	1.1	2.0 (0.6–4.8)	1.1
POC [%]	5.1 (4.1–7.5)	1.9	7.8 (4.8–17.6)	3.2	8.4 (4.9–14.8)	2.6
DOC [mM]	n.d.		n.d.		0.15 (0.12–0.19)	0.02
CaO [%]	9.3 (2.1–21)	4.9	7.6 (2.2–15.4)	2.6	7.0 (5.2–9.0)	0.9
Al_2O_3 [%]	10.4 (1.4–12.2)	4.2	8.4 (2.9–10.9)	1.9	9.2 (7.2–11.2)	1.2
$Mn_{part.}$ [mg kg^{-1}]	514 (111–1057)	316	1487 (835–2692)	423	970 (857–1088)	79
$Mn_{diss.}$ [μM]	0.02 (0.0036–0.047)	0.012	0.024 (0.014–0.07)	0.02	0.017 (0.009–0.028)	0.006

4. Results and discussion

4.1. The Wadden Sea

4.1.1. Particulate manganese

The backbarrier area of Spiekeroog Island is characterised by large amounts of suspended particulate matter (SPM) compared to values from the offshore regions of the German Bight (Tables 1 and 2). Moreover, during the time-series in the Wadden Sea a large variability in SPM concentrations is observed, which is modulated by the tidal regime and weather conditions. While maximum SPM concentrations occur during ebb and flood tide when current velocities are highest, minimum values are found at tidal slacks. Generally, a higher SPM load is seen in winter and fall due to stronger wave action and possibly less stable bio-aggregates, causing enhanced resuspension of inorganic particles. Investigations on particle size and abundance carried out by Simon et al. (2003) in the study area show a higher abundance of smaller particles in winter than in summer. For instance, the 30–100 μm fraction amounts to 70–90% in winter and only 30–60% in summer, whereas in summer the larger fractions are distinctly higher in abundance.

A significant difference between both sampling sites in the tidal inlet (Otzumer Balje OB) and the central backbarrier area (CBA) during the cruises in 2003 cannot be inferred from our data. Only at position CBA during the end of the cruise in August 2003, did SPM concentrations increase from on average 9 mg l^{-1} to a maximum value of 68 mg l^{-1} within 6 h due to increasing wind speed, reflecting the fast response of the Wadden Sea system to changing weather and hydrodynamic conditions.

Particulate Mn shows a pronounced seasonal behaviour with average contents increasing by a factor of nearly 2 from winter to summer (Table 1). The increasing contents of particulate Mn towards summer most likely result from oxidation of dissolved Mn followed by subsequent adsorption of MnO_x phases on particles. This transfer of dissolved Mn to the particulate phase is caused either by photochemical (Nico et al., 2002) and/or microbial processes (Moffett, 1994). Unfortunately our data do not allow differentiating between the two processes. According to Nico et al. (2002) the presence of dissolved organic compounds is required for elevated photochemical oxidation. These compounds act as catalysts and occur in sufficient amounts in the Wadden Sea environment as the DOC concentrations are comparatively high during the entire year (Table 1). Although solar intensity increases from winter to summer, its influence is limited in the turbid Wadden Sea water due to elevated SPM load. On the other hand, the difference in water temperature between winter and summer, which may exceed 20 °C, favours a more temperature-dependent and therefore microbially mediated process. Moffett (1994) also reported a strong seasonal dependence of Mn oxidation with extremely high rates in July and distinctly lower values in March. Measurements of Mn^{2+} oxidation rates in water samples from Saanich Inlet showed maximum rates of 3.5 to 12.1 nM h^{-1} (Tebo and Emerson, 1986). Taking into account an average residence time of the water mass in the backbarrier area of at least three tidal cycles, which is suggested by measurements of ^{223}Ra and ^{224}Ra as tracers of water exchange (Shaw, 2003) and numerical modelling (Stanev et al., 2003), the rates mentioned above lead to a production of 0.13 to 0.44 μM particulate Mn. Such values are within the range of Mn that is added to Wadden Sea SPM, as seen in excess Mn values in Fig. 3. Therefore, sufficient time seems to be available in the Wadden Sea for the microbial oxidation of dissolved Mn.

The seasonal increase of particulate Mn is also displayed in Fig. 2, which shows Mn/Al ratios of particles sampled during several Wadden Sea cruises. The normalisation to Al eliminates dilution effects mainly caused by carbonate and organic matter (TIC and POC in Table 1). Despite the seasonal rise in particulate Mn, Fig. 2 displays a tidal cyclicity for most cruises with a trend towards higher values during high tide. The highest Mn enrichment in SPM was observed in August 2003 during high tide (av. 2420 mg kg^{-1}) whereas low tide values (av. 1420 mg kg^{-1}) are distinctly lower. This difference is most likely due to settling of coarser Mn-poor particles during transport of water masses out of and into the backbarrier area. Thus, during the end of this cruise wind direction and speed changed from NE, Beaufort 2–3 to NW, Beaufort 5–6, which led to enhanced resuspension of sediment material in the backbarrier area. This assumption is basesd on distinctly higher SPM concentrations (max. 68 mg l^{-1}) and dramatically decreasing Mn contents (min. 750 mg kg^{-1}) as tidal flat surface sediments are comparatively Mn-poor owing to early diagenetic Mn-release (Hinrichs et al., 2002).

The Mn data discussed so far provide information on the geochemical composition of particles on a dry weight basis. However, knowledge on particulate Mn concentrations per water volume is required to assess the relevance of the particulate phase in comparison to the dissolved phase. This is particularly important as SPM contents vary on seasonal and tidal scales. Therefore, excess Mn concentrations were calculated, which reflect the amount of Mn added to SPM above the geogenic background. The excess fraction (Mn_{xs}) is calculated according to the following equations (average shale data

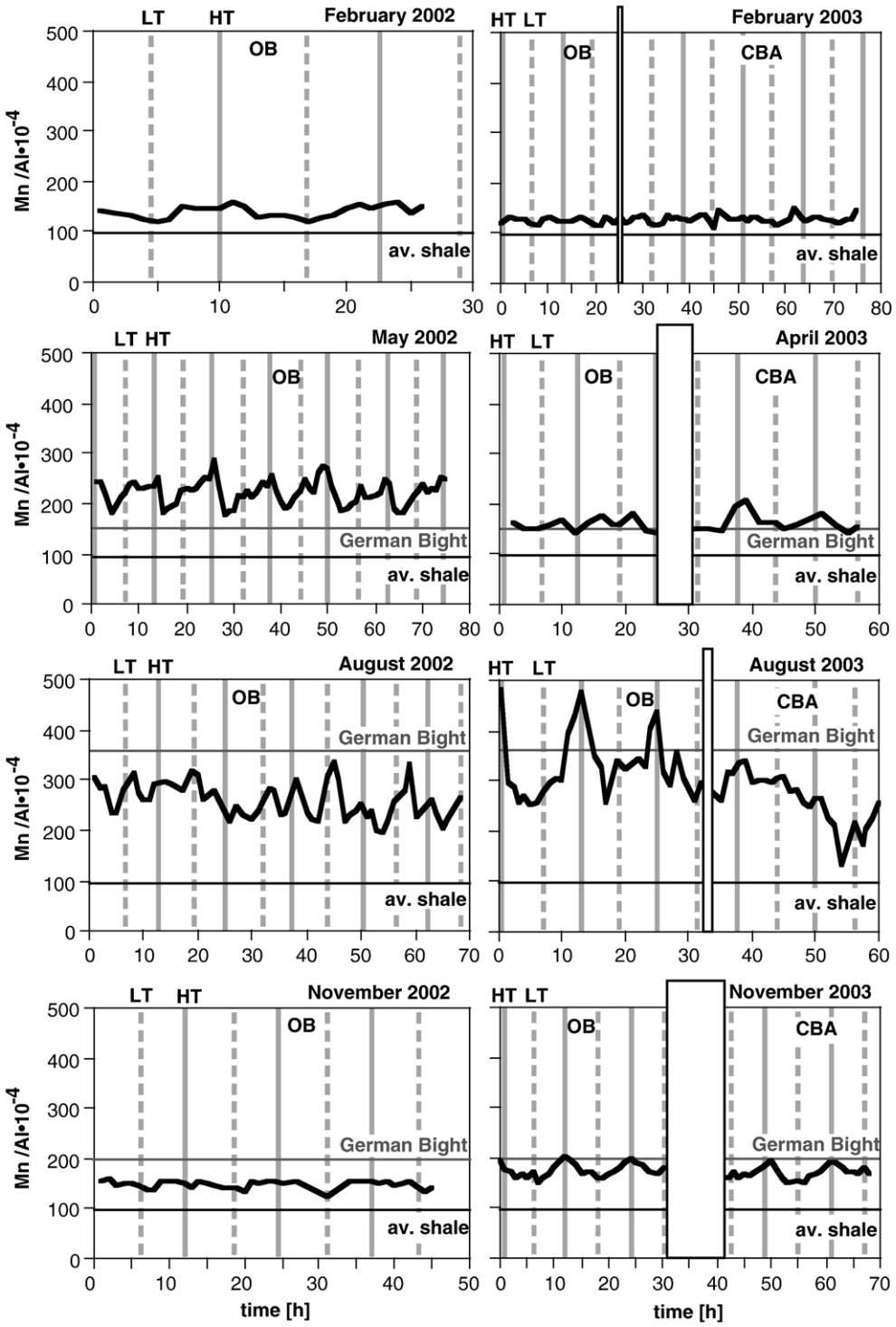

Fig. 2. Mn/Al-ratios of particles for the Wadden Sea cruises in 2002 and 2003. The black line marks the shale value after Wedepohl (1971) and the grey line indicates the average German Bight value for the corresponding seasons. The vertical grey and dashed lines denote high tide (HT) and low tide (LT). The abbreviations OB and CBA represent sampling in the tidal inlet (Otzumer Balje) and in the central backbarrier area (compare Fig. 1b).

from Wedepohl, 1971; Al: 8,9%, Mn: 850 mg kg^{-1}), where $Mn_{background}$ represents the geogenic background content of Mn:

$$Mn_{background} = (Mn/Al)_{shale} \times Al_{sample}$$
$$Mn_{xs} = Mn_{sample} - Mn_{background}$$

Mn_{xs} is then converted into volume specific Mn concentrations by multiplication by SPM concentrations.

In Fig. 3 the covariations of excess Mn concentrations ($Mn_{SPM,xs}$) with particulate Al are shown for the Wadden Sea cruises in 2002 and 2003. Mn excess values reflect seasonality by increasing slopes of the regression lines from winter to summer. As Al concentrations decrease from winter to summer in the Wadden Sea this behaviour is consistent with a higher Mn load of the particles during spring and summer. A further important feature that can be inferred from Fig. 3 is that winter and autumn, with their elevated SPM concentrations, cannot be neglected in elemental mass balances for the Wadden Sea system. Although the Mn contents of the particles in winter and autumn are lower than in the other seasons (Table 1), the high SPM load leads to considerable excess Mn concentrations per water volume. In winter and fall 2002 excess values in part even exceeded the concentrations observed during spring and summer (Fig. 3a). Furthermore $Mn_{SPM,xs}$ data from the winter season are distinctly higher than those of dissolved Mn, which documents the importance of particulate phases as a significant Mn carrier. On the other hand, during summer particulate Mn plays a less important role, as the concentrations of $Mn_{SPM,xs}$ are lower than dissolved Mn concentrations for the majority of samples.

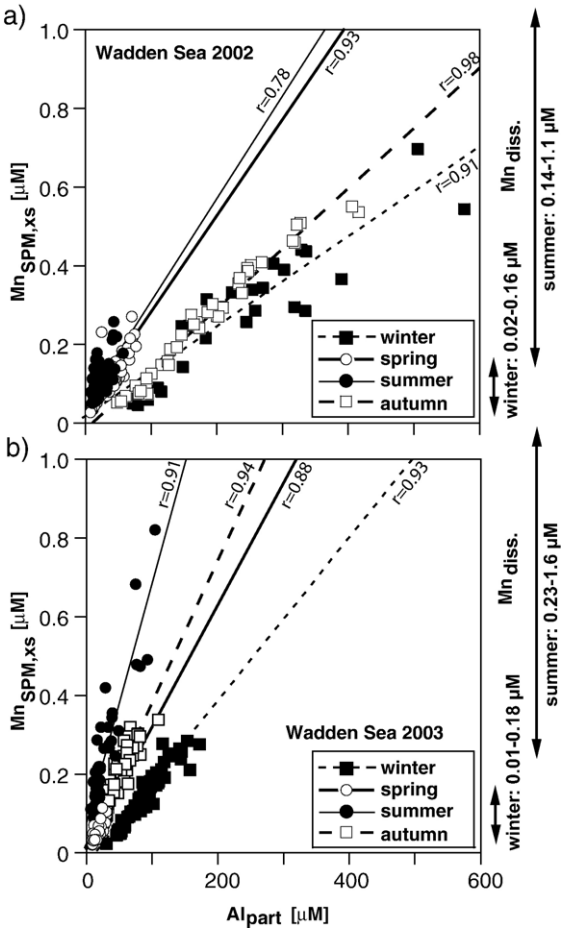

Fig. 3. Scatter plots of excess particulate Mn ($Mn_{SPM,xs}$) versus particulate Al for the Wadden Sea in 2002 and 2003. Excess Mn forms the Mn fraction that is added to particles in comparison to the geogenic background. Multiplication by SPM concentrations converts excess Mn into volume specific Mn concentrations. Correlation coefficients are given at the end of regression lines. The arrows display the range of dissolved Mn in winter and summer.

4.1.2. Dissolved manganese

The Wadden Sea is highly enriched in dissolved Mn in comparison with values of the German Bight (Tables 1 and 2) and the North Atlantic (0.001–0.002 µM, Shiller, 1997). Like the particulate phase, dissolved Mn in the Wadden Sea shows pronounced seasonal differences as well, with about ten times higher values in summer than in winter. In Fig. 4 the tidal patterns of dissolved Mn for the cruises in 2002 and 2003 are presented. In addition to the seasonal dependence, a tidal cyclicity is seen for all cruises with distinctly increasing values towards low tide, suggesting that backbarrier tidal flats act as important Mn sources. This is emphasised by the fact that during the cruises in 2003 dissolved Mn concentrations were distinctly higher at the location in the central backbarrier area (CBA) than in the tidal inlet (OB). On the one hand, site CBA is more strongly influenced by Mn-rich tidal creek waters, owing to its topography (lower water depth, narrow channel). On the other hand, site CBA is next to mixed flat sediments which contain a higher metal inventory than the sand flats close to site OB sand flats. Thus, the higher mud fraction leads to more intense metal cycling and the liberation of Mn to the bottom waters (Bosselmann et al., 2003). Another Mn source is the freshwater input through a flood gate in Neuharlingersiel (Fig. 1b) as discussed below.

4.2. Manganese sources

The Wadden Sea data presented so far show that Mn is significantly enriched in both dissolved and particulate phases. In order to explain these enrichments the elemental sources influencing the Wadden Sea system will be discussed in more detail. These sources are (i) the

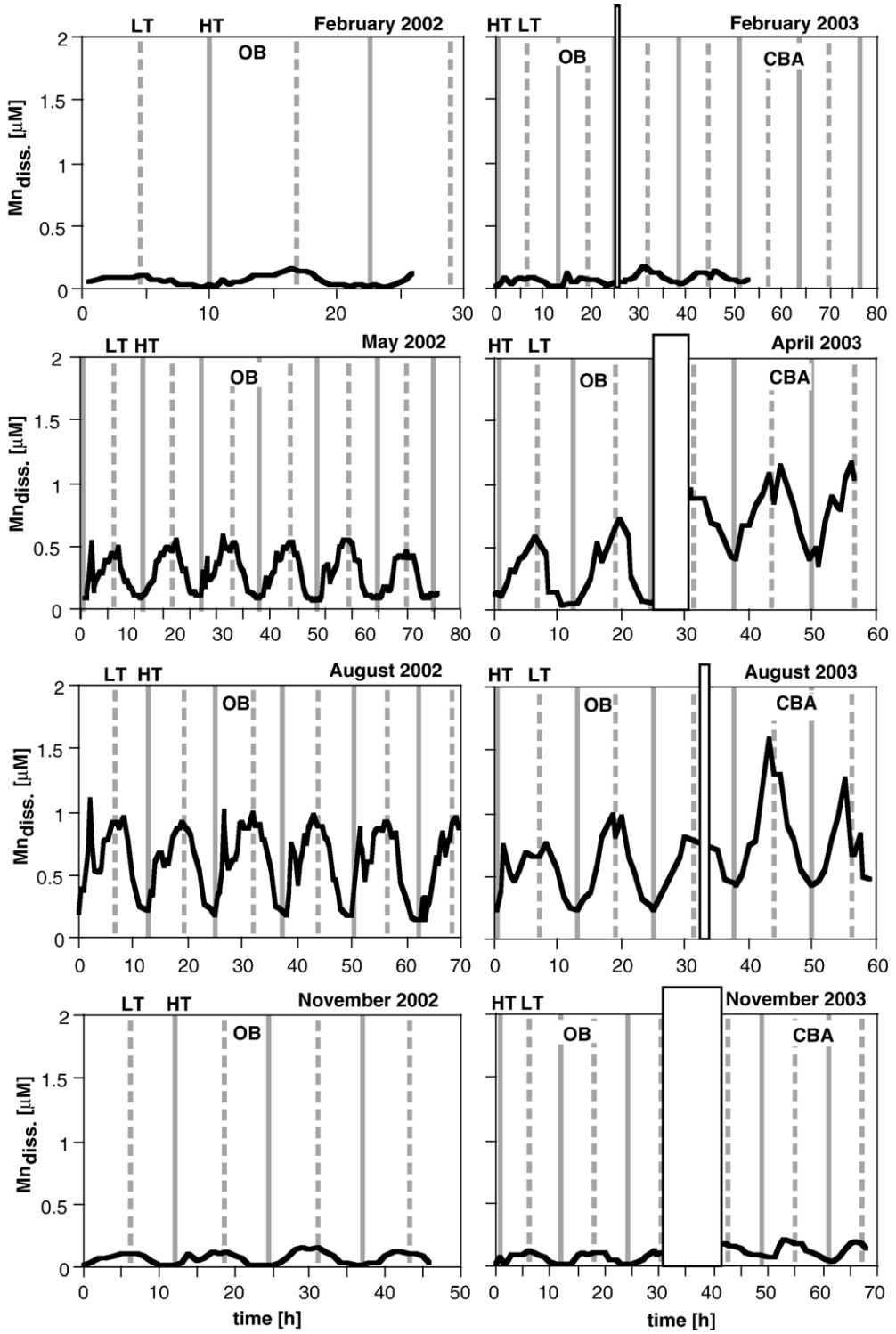

Fig. 4. Dissolved Mn for the Wadden Sea cruises in 2002 and 2003. The vertical grey and dashed lines denote high tide (HT) and low tide (LT). Abbreviations OB and CBA represent the sampling sites in the tidal inlet (Otzumer Balje) and in the central backbarrier area (compare Fig. 1b).

North Sea, (ii) the tidal flat sediments and corresponding porewaters, and (iii) the freshwater contributed to the Wadden Sea via the flood-gate at Neuharlingersiel.

4.2.1. The North Sea

In a comparison of the dissolved and particulate phases of the Wadden Sea and the German Bight (Tables 1 and 2) two substantial differences stand out. While the contents of particulate Mn stay at a level comparable to the Wadden Sea, concentrations of dissolved Mn in the German Bight are distinctly lower than Wadden Sea values. A comparison with published data of the North Sea is rather difficult to perform as the reported concentrations of dissolved Mn cover a wide range from 0.001 to 0.4 μM due to seasonal and spatial differences (Schmidt, 1980; Kremling, 1985; Burton et al., 1993; Hydes and Kremling, 1993; Laslett, 1995; Tappin et al., 1995). Nevertheless, the German Bight Mn values reported here are comparable to values measured off the Dutch and East-Frisian coast by Millward et al. (1998) and Tappin et al. (1995). Generally, dissolved Mn shows decreasing concentrations with increasing distance from the coast as seen in several transects from the coast towards the central German Bight. This finding can be explained by either dilution of Mn-rich coastal waters with offshore waters or by the bacterial Mn oxidation mentioned in Section 4.1.1.

Similar to the Wadden Sea results, particulate Mn also shows seasonal behaviour in the offshore regions of the German Bight (SPM <5 mg l^{-1}), i.e., increasing contents from spring to summer and decreasing values towards fall (Table 2). However, the Mn contents of offshore SPM are in parts extremely low during the spring cruises in comparison to the Wadden Sea. Dehairs et al. (1989) reported similar behaviour off the Belgian and Dutch coasts. They even observed depletion in particulate Mn during spring, whereas the other seasons showed elevated Mn contents. Although, the data from the German Bight presented here cover a wide range due to spatial and seasonal variations, a comparison with measurements of particulate Mn carried out by Kersten et al. (1990) and Tappin et al. (1995) in the southern North Sea reveals on average similar values.

Fig. 5a presents the Mn/Al ratios of SPM of several transects from the coast towards the outer German Bight

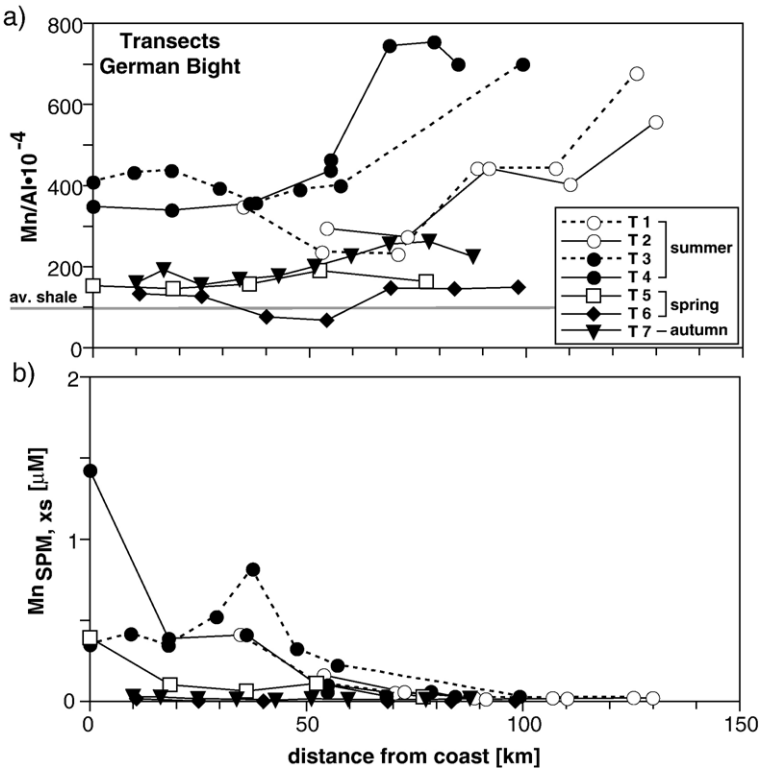

Fig. 5. (a) Mn/Al ratios of SPM for several transects from the coast towards the central area of the German Bight. The grey line indicates the average shale level after Wedepohl (1971). (b) Excess concentrations of particulate Mn ($Mn_{SPM,xs}$) for transects from the coast towards the central area of the German Bight.

(compare Fig. 1a). Generally, Mn/Al ratios increase with increasing distance from the shore during the summer transects (T1–T4), and less clearly so in autumn (T 7). Despite the settling of coarser Mn-poor particles during transport in the German Bight, the offshore increasing Mn contents are to a certain degree caused by the proceeding oxidation of dissolved Mn. The latter assumption is in accordance with the offshore decreasing concentrations of dissolved Mn mentioned above. However, as this effect gains in importance only further offshore, a significant influence on the Wadden Sea during normal weather conditions is rather unlikely. In addition, excess concentrations of particulate Mn (Fig. 5b) also decrease offshore due to the decreasing SPM load.

We conclude that the distinctly higher concentrations and the tidal signature of dissolved Mn in the Wadden Sea evidence that offshore waters do not form a significant Mn source for the Wadden Sea. The same is true for particulate Mn as SPM concentrations and, therefore, also the inventory of particulate Mn is comparatively low in offshore regions. Moreover, the Wadden Sea is more likely to act as an important Mn source for the North Sea in addition to riverine input.

4.2.2. Tidal flat sediments

Porewater Mn concentrations vary in the different sediment types (Figs. 6 and 7). A distinct maximum with values of up to about 40 μM is seen in the sand flat site Gröninger Plate (Fig. 6b), indicating an intense Mn cycling in the upper 10 cm of the sediment as described earlier by Böttcher et al. (2004). The general shape of the Mn^{2+} profile resembles that of microbial sulphate reduction rate (Fig. 6a). This is in agreement with the model of Böttcher et al. (2004), which considers the importance of chemical reduction of MnO_2 by biogenic sulphide in near-surface sediments, partially counterbalanced by the flux of oxygen from the sediment-water interface. Additional support arises from the observation that during short-term incubations most of the ^{35}S radiotracer is retrieved in the chromium reducible sulphur fraction (CRS), indicating re-oxidation of the acid volatile sulphur fraction (AVS) to elemental sulphur. In agreement with these findings, the reducible solid-phase Mn(IV) pool, as quantified by acid extraction, displays a maximum in the upper 4 cm of the sand flat (Fig. 6c). Water flow in the surface sediment and at the surface may lead to the advective flow of Mn-bearing water during water-coverage (e.g., Hüttel et al., 1998). A near-surface maximum-type behaviour for dissolved Mn was also found for the mixed flat site (Fig. 7a) where in addition higher concentrations were found during summer (up to 190 μM) compared to winter sampling campaigns. The latter trend was confirmed for the sand flat site Janssand, JS (Fig. 7b and c). This demonstrates that enhanced microbial activity due to higher temperature during summer months leads to an increased reduction of Mn oxides and may enhance the

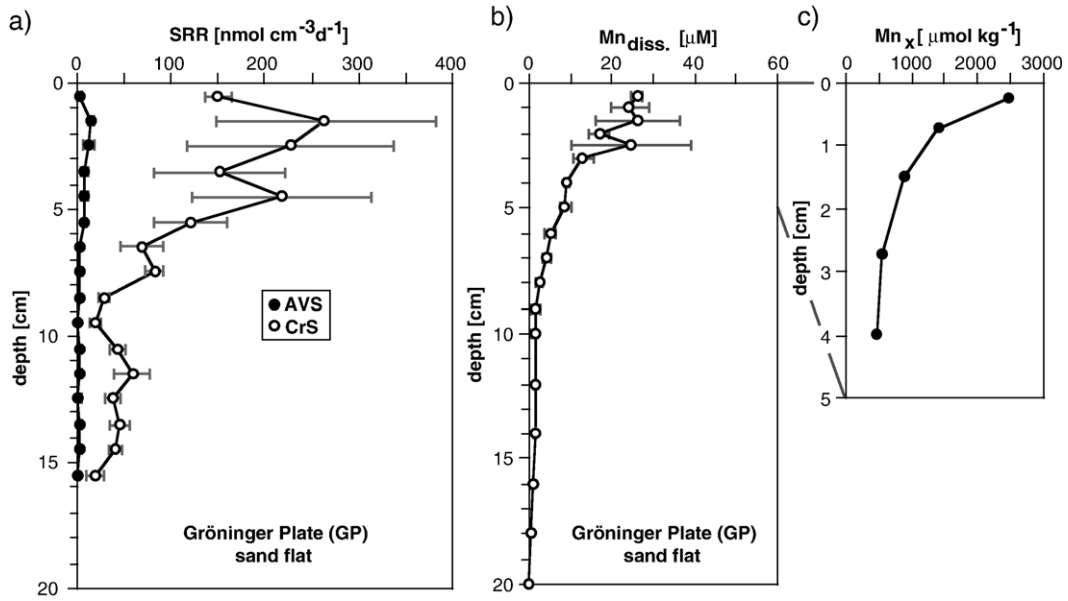

Fig. 6. (a) Sulphate reduction rates in porewaters (AVS = acid volatile sulphur; CrS = chromium reducible sulphur), (b) Mn porewater profile of two parallel cores, and (c) reactive Mn_x in a short sediment core from a sand flat site (Gröninger Plate GP) during summer 2003.

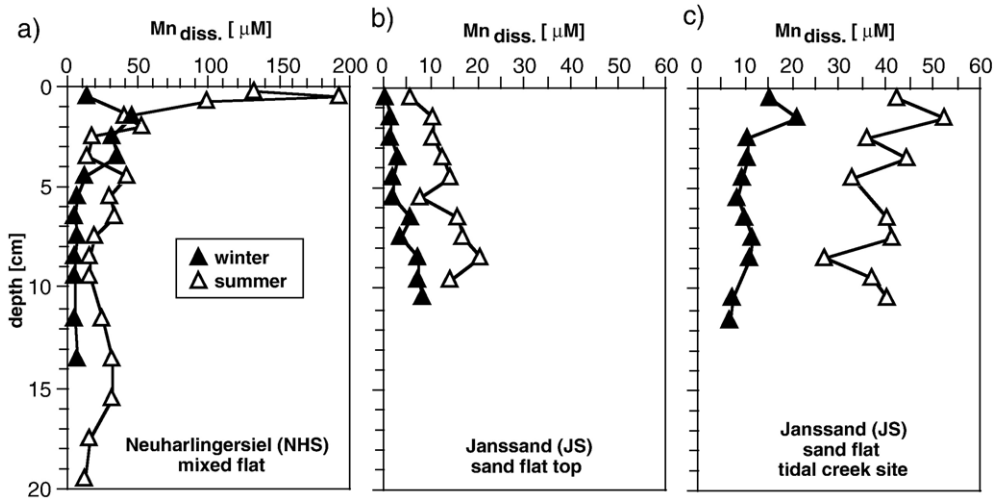

Fig. 7. Mn porewater profiles for mixed and sand flat sediments during winter and summer 2003. Porewater samples were obtained by centrifugation under N_2 atmosphere.

corresponding flux of Mn^{2+} across the sediment-water interface. The porewater profiles at the top sand flat (JS) positions show relatively low concentrations and a steady increase with depth. This indicates that the dissolved concentrations are limited by both the availability of Mn oxides (data not shown) and temperature-dependent microbial activity. Much higher concentrations are found at the JS site close to the tidal creek rim where a slight increase towards the surface is observed. This is due to the higher availability of metals in mixed sediment layers with sand and elevated mud (and metal) contents. All four sites presented may contribute Mn to the water column, except for the sandy top JS location. From the porewater profiles it becomes evident that the top 15 cm of the surface sediments are most important for Mn cycling and control the metal flux across the sediment-water interface. This is in agreement with the abundance of available reducible sedimentary Mn phases (Fig. 6c; Bosselmann and Böttcher, unpubl. data).

The effect of temperature and organic matter content on microbial activity in the intertidal surface sediments has been demonstrated by studies of microbial sulphate reduction (Böttcher et al., 1998, 2000, 2004; Bosselmann et al., 2003). Sulphate reduction rates (SRR) show a trend opposite to the accumulation of oxidised Mn in surface sediments, which implies that sulphate reduction is likely to be involved in Mn mobilisation via chemical reduction of Mn oxides by sulphide (Burdige, 1993). Highest SRR in the absence of accumulating sulphide are indicative of a highly efficient re-oxidation of dissolved sulphide and are partly due to coupling between the metal and sulphur cycles (Thamdrup et al., 1994; Böttcher et al., 2004; De Beer et al., 2005).

Besides areal metal fluxes into bottom water, also local drainage of Mn-rich porewaters from sediments is indirectly documented, for instance by the analysis of tidal creek waters. Fig. 8 shows the seasonal variation of dissolved Mn in tidal creeks of the Spiekeroog back-barrier area (Janssand JS, compare Fig. 1b). Mn is highly enriched in the tidal creeks in comparison with concentrations in the water column. Furthermore, a distinct seasonal trend with maximum values in summer is evident owing to increasing microbial activity and more pronounced reducing conditions, which favours the reduction of solid MnO_x phases to soluble Mn^{2+}. Therefore, it can be concluded that especially during spring and summer the tidal flat sediments form a very important source of Mn.

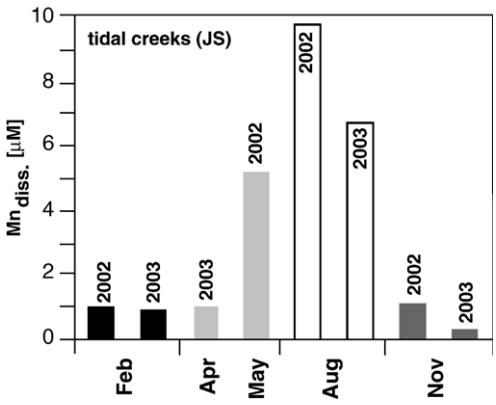

Fig. 8. Seasonal variations of dissolved Mn in tidal creek water from the Janssand sand flat site (JS).

4.2.3. The freshwater environment

Apart from direct rainfall over the tidal flat area the input through the flood-gate at Neuharlingersiel (Fig. 1b and c) forms the most important freshwater contribution to the study area. Depending on the water level, the freshwater discharge generally occurs about two hours before low tide when the flood-gate opens. In 2002 and 2003 phases of elevated rainfall occurred not only during winter and autumn but also in summer. The discharge rate, however, coincides with rainfall only in winter and autumn but not during the vegetation growth period in spring and summer.

The catchment area of the flood-gate encompasses about 125 km^2, which is almost twice as large as the backbarrier area of Spiekeroog Island (Fig. 1c). The northern part is characterised by the occurrence of cultivated marsh soils, whereas in the southern part fen peats and forests are more common. The flood-gate (location 1) is fed by three major water courses (locations 2–4), which in turn are linked to a multitude of small streams.

The geochemical composition of freshwater from the study area is controlled by the soil types present in the catchment area as well as by the proximity to the sea. Table 3 shows average values for salinity, pH, and several geochemical parameter of the sampling location at the flood-gate in Neuharlingersiel (location 1) and the three main water courses flowing towards the flood-gate (location 2–4). Except for location 3, the sampling sites 1, 2 and 4 show elevated salinities with a maximum value of 3.8 psu. At the flood-gate site (location 1) this is mainly caused by seawater intrusion during high tide due to small leakages of the gate. In contrast, locations 2 and 4 are most likely influenced by sea spray and seawater intrusion through filled former channels below the mainland dike. Thus, Holocene tidal channels may permit subterranean contact of the freshwater and seawater environments via tidal pumping (Dellwig et al., 2001). On the other hand, location 3 is to a higher degree influenced by small water courses from fen peats and forests in the southern part of the catchment area. These waters are comparatively low in pH due to humic and fulvic acids, which contribute considerably to the acidity of the water (Oliver et al., 1983).

Generally, all water courses of the study area are rich in dissolved Mn due to mobilisation from soils under reducing and acidic conditions (Viers et al., 1997) as well as diffusion from anoxic stream sediments (Table 3). In comparison to average world river water (Martin and Meybeck, 1979) dissolved Mn is on average highly enriched in the investigated freshwater courses by a factor of 25. However, dissolved Mn shows a large variability (1.1–8.9 μM) during the sampling period in 2002 and 2003 with no observable seasonality. This behaviour is due to several competing factors, e.g. seawater intrusions, microbial oxidation, and diffusion from sediments. Particulate Mn also displays a wide range (202 mg kg^{-1} to 8,063 mg kg^{-1}), which results from a different source rock composition as well as elevated microbial Mn oxidation during phases of water stagnation and low precipitation. In contrast to dissolved Mn, the particulate Mn phase displays a seasonal behaviour with increasing contents towards summer. For instance, Mn contents of the winter samples from the flood-gate (location 1) average 687 mg kg^{-1}, whereas the summer values are distinctly higher (2175 mg kg^{-1}). Such high values tend to coincide with decreases in dissolved Mn, which is in accordance with the process of microbial Mn oxidation (see Section 4.1.1.).

Taking into account the SPM load of the freshwater, the particulate Mn per water volume for location 1 is only 0.2 μM in winter and 1.4 μM in summer. Therefore, the dissolved phase (av. 4 μM) appears to be the most important Mn carrier for the freshwater, which is especially true during winter. Depending on tidal state and season the total Mn concentration of the freshwater is at most 400-fold higher than in the Wadden Sea. Therefore, the Mn contribution via the freshwater

Table 3
Average concentrations and range of dissolved and particulate parameters of the freshwater samples from the sampling campaigns between March 2002 and December 2003

Parameter	Location 1 (flood-gate)	SD	Location 2	SD	Location 3	SD	Location 4	SD
salinity [psu]	0.7 (0.1–3.8)	0.6	0.9 (0.4–3)	0.7	0.3 (0.2–0.4)	0.1	0.6 (0.2–2)	0.4
pH	7.8 (7.1–8.8)	0.4	7.5 (6.9–8.6)	0.4	7.3 (6.7–7.8)	0.3	7.7 (7.1–8.3)	0.3
DOC [mM]	1.2 (0.8–2.4)	0.2	1.1 (0.7–2.7)	0.5	1.1 (0.7–3.0)	0.6	1.3 (1.0–1.6)	0.2
$Mn_{diss.}$ [μM]	3.7 (2.0–8.4)	1.4	4.3 (2.0–8.9)	1.7	3.3 (1.7–6.1)	1.0	5.2 (1.1–8.8)	1.7
SPM [mg l^{-1}]	33 (8–173)	27	34 (8–101)	28	26 (7–69)	13	59 (14–116)	26
POC [%]	10 (5.7–22.6)	4.0	11.8 (7.6–23.4)	4.1	14.3 (8.8–18.5)	3.1	7.8 (4.1–12.8)	2.4
Al_2O_3 [%]	9.3 (3.7–14.7)	2.4	8.8 (4.5–11.7)	1.8	8.2 (5.9–11.3)	1.4	9.6 (6.9–14.7)	2.2
$Mn_{part.}$ [mg kg^{-1}]	2116 (312–8063)	1984	920 (226–4797)	1002	1164 (202–5115)	1130	1134 (277–3845)	814

during rainy periods cannot be neglected in mass balance calculations for the Wadden Sea system.

As mentioned the freshwater discharge commonly occurs about two hours before low tide. Although the concentration of dissolved Mn in the freshwater is highly variable over the entire year without a clear seasonal trend, the freshwater is distinctly enriched in Mn in comparison to seawater. In order to investigate the consequences of freshwater discharge into the Wadden Sea area after opening of the flood-gate, we performed two drifter experiments in February 2002 (D2) and March 2002 (D1).

The experiment (D1) in March started close to the flood-gate 30 min after opening. The drifter was carried along with the current of the freshwater lens and reached the central backbarrier area within 1.5 hours (X, Fig. 1b). During the drift experiment several samples were taken within the salinity gradient. Additionally, in May 2002 the freshwater outflow was sampled in the opposite direction against the water current from the end position of drift experiment D2 towards the flood-gate. Dissolved Mn reveals a non-conservative tendency as concentrations increase slightly in the salinity range of 2–10 (Fig. 9). At higher salinities Mn values show a distinct decrease due to mixing with relatively Mn-poor Wadden Sea water. This behaviour might reflect the transfer of particulate Mn to the dissolved phase due to changes of the physicochemical conditions in the low-salinity range. Such transfer has also been observed in

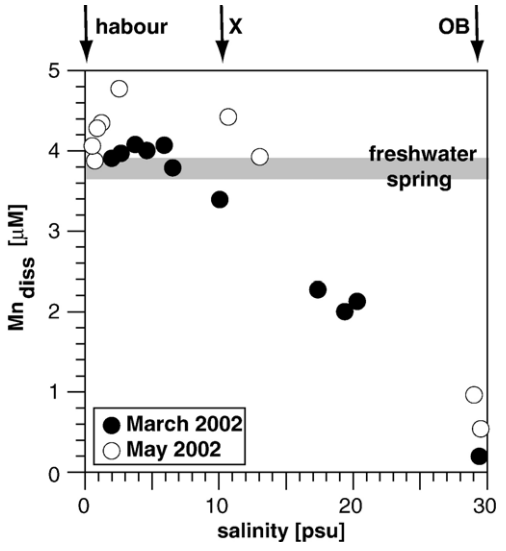

Fig. 9. Variations of dissolved Mn within the salinity gradient during two drift experiments in the central backbarrier area of Spiekeroog Island in March and May 2002. The grey bar indicates freshwater level in spring. The arrows mark the locations in the habour, at the end of drifting (X, compare Fig. 1b), and in the tidal inlet (OB).

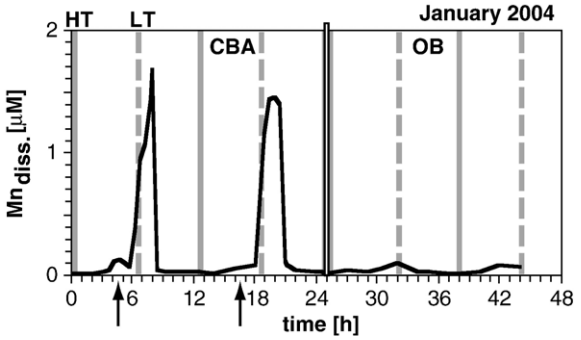

Fig. 10. Tidal variations of dissolved Mn during a cruise in January 2004 for the locations in the central backbarrier area (CBA) and in the tidal outlet (OB). The black arrows indicate opening of the flood-gate.

estuaries within the salinity range of 0–10 (e.g. Duinker et al., 1979; Boughriet et al., 1992; Balls et al., 1994).

An earlier drifter experiment (D2) was performed in February 2002 two hours after high tide to track the ebb current. The drifter started in the central backbarrier area, at a position almost identical to the endpoint of the drift experiment in March (Fig. 1b; X) and passed the location of the time-series stations in the Otzumer Balje (OB) two hours later. Overall, both drift experiments showed that freshwater, which is contributed via the flood-gate, does not reach the tidal inlet directly within one tidal cycle. Moreover, the freshwater is dispersed in the central backbarrier area during the subsequent flood tide and can only reach the tidal inlet strongly diluted during the following ebb tide. This behaviour was directly observed during a cruise in January 2004 (Fig. 10), when extremely high concentrations of dissolved Mn were observed twice about one hour after low tide at site CBA. The observed Mn concentration peaks reach half of the freshwater Mn level and correspond to a drop in salinity to 14–15 psu in the top metre of the water column. During the remaining time, salinity ranged between 30.4 psu (high tide) and 28.2 (low tide). Thus, the flood-gate opened two times and the discharged freshwater was transported towards the position CBA with the following flood tide, as shown by the drift experiments.

4.3. Manganese balance for the Wadden Sea

The discussion in Section 4.2. shows that both porewater and freshwater are potential Mn sources for the Wadden Sea water column. However, the question remains: which source is the dominant one? To answer this question salinity data are a helpful tool, because such data allow an estimation of the amounts of freshwater that are contributed to the Wadden Sea. In Table 4 the mean salinity and range are presented for the Wadden

Table 4
Balance for an estimate of the input of dissolved Mn via freshwater and porewater into the Wadden Sea area

	February 2002	May 2002	August 2002	November 2002	February 2003	April 2003	August 2003	November 2003
Mean salinity German Bight *	33.1	33.1	33.1	33.1	33.1	33.1	33.1	33.1
Salinity Wadden Sea	27.2 (26.2–28.4)	30.9 (30.5–31.1)	31.2 (30.8–31.4)	29.5 (28.7–30.2)	28.6 (27.5–29.7)	31.9 (31.2–33.2)	32.7 (32.4–32.9)	31.7 (30.2–32.0)
Δ Salinity	5.9	2.2	1.9	3.6	4.5	1.2	0.4	1.4
% Freshwater (flood-gate plus rainfall)	17.9	6.6	5.7	10.9	13.7	3.7	1.2	4.1
% Flood-gate input from total freshwater	44	35	26	26	53	54	79	30
% Freshwater (only flood-gate)	7.9	2.3	1.5	2.8	7.3	2.0	1.0	1.2
Dissolved Mn freshwater [μM]	4.2	3.7	4.1	3.5	4.2	3.7	4.1	3.5
Particulate $Mn_{xs.}$ freshwater [μM]	0.01	1.3	1.2	0.4	0.01	1.3	1.2	0.4
Dissolved Mn Wadden Sea [μM]	0.06	0.3	0.7	0.08	0.06	0.3	0.6	0.07
Particulate $Mn_{xs.}$ Wadden Sea [μM]	0.3	0.1	0.1	0.3	0.15	0.06	0.2	0.2
% Mn via freshwater	92	30	10	32	>100	26	7	17
% Mn via porewater	8	70	90	31	/	74	93	83

The calculations are based on data from the OB station in the major tidal outlet of the Spiekeroog backbarrier tidal flat.
* Average value from offshore cruises in the German Bight (range: 32.2–33.7).

Sea cruises in 2002 and 2003. Distinct differences are seen for the individual cruises. While in February 2002/2003 as well as in November 2002, a comparatively low mean salinity with high amplitudes was observed, the remaining cuises are characterised by an almost constant salinity on a higher level. Generally, salinity shows a tidal cyclicity with maximum values during high tide, when the influence of offshore water masses is most pronounced. One exception forms the cruise in August 2003, when the highest salinity values were measured at low tide. As the water temperature during that time partly exceeded 25 °C, this converse behaviour of salinity can be explained by elevated evaporation in the Wadden Sea. The consequences of evaporation on the following balance will be discussed below.

Except for this extreme situation, salinity in the Wadden Sea is mainly controlled by the freshwater input, which points towards a significant Mn input via freshwater in February 2002/2003 and November 2002, whereas during the other cruises the porewater contribution gained in importance. Table 4 presents a balance for Mn in order to estimate the importance of the freshwater and porewater inputs on the Mn inventory of the Wadden Sea water column. This balance is based on the assumption that the observed differences in salinity during the cruises result from the freshwater discharge via the flood-gate and rainfall in the tidal flat area. For the following calculations only data from the tidal inlet (OB) position were used. The percentage of the total freshwater input can be calculated from the difference between the salinity of the German Bight and the Wadden Sea. Taking into account the ratios of rainfall and flood-gate discharge for the time-period of the cruises plus two weeks, we inferred the percentage of freshwater input only via the flood-gate. Based on the total Mn concentration (dissolved and particulate) of the freshwater, the Mn input via freshwater can be calculated from the percentage of freshwater input. In addition, the difference between total Mn concentrations in the Wadden Sea and Mn input via freshwater provides an estimate of the porewater contribution.

The percentage of the Mn input via freshwater evidences the assumed importance of this source for the Mn budget of the Wadden Sea during winter. Thus, the total Mn concentration of the Wadden Sea water column in February 2002 and 2003 can be explained almost exclusively by freshwater discharge. Although the freshwater contribution was lower in February 2003, the lower SPM load in the Wadden Sea during that time led to a distinctly lower Mn concentration. This difference in SPM concentration was caused by an about two times higher wind speed in February 2002 than during the cruise in 2003. Even though the freshwater contribution was distinctly lower in May 2002, November 2002, and April 2003, about one third of the Mn in the Wadden Sea water column may have been due to freshwater input. In contrast, during the summer cruises in August 2002 and 2003 the Mn budget of the Wadden Sea water column was almost completely controlled by the porewater system, which corresponds with the seasonal variation of Mn in tidal creek waters (Fig. 8) as an example for local porewater drainage.

As mentioned, salinity was particularly high in the Wadden Sea in August 2003, with values close to those

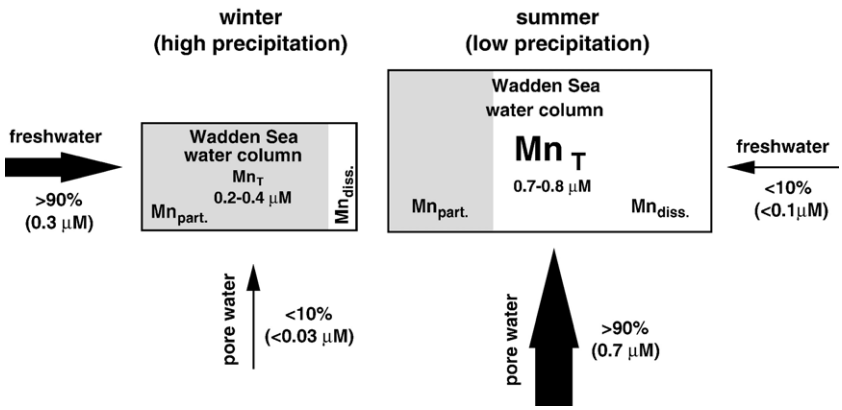

Fig. 11. Illustration of the relationship between freshwater and porewater importance for the Mn inventory of the Wadden Sea water column during winter and summer.

of the German Bight due to elevated evaporation. This evaporation tends to result in an underestimate of the freshwater contribution. However, in August 2003 we observed the lowest values in rainfall and freshwater discharge during the two-year sampling period. In comparison with the average freshwater discharge and rainfall in 2002 and 2003, the values of August 2003 amount to only 13% and 6%, respectively. Although there is some uncertainty, it can be disregarded in this context. Additionally, the fact that concentrations of dissolved Mn are very high in the Wadden Sea during summer while discharge rates of freshwater are low is in accordance with direct flux measurements at the sediment-water interface (Bosselmann and Böttcher, unpublished data).

The relationship between the extent of freshwater and porewater influence during winter and summer as extreme situations (spring and autumn are intermediate) is illustrated in Fig. 11. During phases of high precipitation and reduced microbial activity in winter the freshwater discharge can explain more than 90% of the total Mn inventory of the Wadden Sea water column. When increasing microbial activity in summer leads to distinctly higher amounts of Mn in the Wadden Sea, the freshwater discharge plays only a subordinate role and the Mn inventory is dominated by the porewater contribution. In addition, the ratio of dissolved and particulate Mn in the Wadden Sea water column is displayed in this scheme. While in winter the dominating Mn carrier is the particulate phase, during summer we observe the opposite trend due to seasonal variations in SPM concentration.

Although porewater forms the dominating Mn source in the Wadden Sea, this simple balance highlights the importance of the freshwater environment for the Mn budget of the Wadden Sea. As the tidal flat sediments are subject to a permanent diagenetic loss of Mn (especially in summer), it can be speculated that the Mn reservoir of the tidal flats is replenished to a certain degree by the freshwater contribution during the wet seasons in fall and winter. A further significant Mn input, however, may be suspended material from the near-coastal areas of the German Bight. Numerical modelling (Brink-Spalink et al., 2003) as well as sedimentological investigations (Santamarina Cuneo and Flemming, 2000) showed that during strong winds (>6 Bft) from NW an import of mud occurs in the backbarrier area which provides an additional Mn source after settling.

5. Conclusions

Surface waters of the Wadden Sea (Spiekeroog Island, NW Germany) are highly enriched in Mn in comparison with the central areas of the German Bight, which illustrates the importance of the coastal environment for the Mn inventory of the North Sea. Both dissolved and particulate Mn reveal distinct tidal and seasonal variations with maximum values in summer.

Excess concentrations of particulate Mn evidence that winter and autumn with their elevated SPM load cannot be neglected in mass balance calculations for the Wadden Sea system. The excess concentrations of particulate Mn partly even exceed concentrations in the dissolved phase in winter and fall.

Porewater Mn also shows a seasonal behaviour with highest concentrations at a mixed flat site during summer. This finding is due to enhanced microbial activity during warmer summer months, which leads to elevated reduction of Mn-oxides and Mn flux across the sediment-water interface. The draining of Mn-rich porewaters from the sediments is additionally confirmed

by analyses of tidal channel waters draining the intertidal plates during low tide.

For the Mn budget of the Wadden Sea, the freshwater discharge from small coastal tributaries plays an important role. On the basis of salinity variations in the Wadden Sea the amounts of total Mn contributed via freshwater are estimated. During winter the Mn inventory of the Wadden Sea water column is dominated almost completely by the freshwater input, while in summer the porewater system forms the prevailing source.

Acknowledgements

We wish to thank the crews of the research vessels RV 'Senckenberg', RV 'Heincke', and RV 'Victor Hensen' for active support during the cruises. Further thanks are due to Meteomedia Deutschland GmbH (Bochum, Germany) for providing meteorological data of the study area. Furthermore we are indebted to J. Meinen-Hieronimus (harbour officer at Neuharlingersiel) for supporting our work at the flood-gate. Two anonymous reviewers are thanked for their constructive comments. This study was funded by the Deutsche Forschungsgemeinschaft (DFG) through grants BR 775/14-1/2 and JO 307/4-1/2, and Max Planck Society, Munich.

References

Balls, P.W., Laslett, R.E., Price, N.B., 1994. Nutrient and trace-metal distributions over a complete semi-diurnal tidal cycle in the Forth Estuary, Scotland. Neth. J. Sea Res. 33, 1–17.

Bosselmann, K., Böttcher, M.E., Billerbeck, M., Walpersdorf, E., Theune, A., De Beer, D., Hüttel, M., Brumsack, H.-J., Jørgensen, B.B., 2003. Iron-sulfur-manganese dynamics in intertidal surface sediments of the North Sea. Ber. Forschungsz. Terramare 12, 32–35.

Böttcher, M.E., Jørgensen, B.B., 2005. Leben an der Grenze: Die alltägliche Sintflut. Einblicke 41, 19–21.

Böttcher, M.E., Oelschläger, B., Höpner, T., Brumsack, H.-J., Rullkötter, J., 1998. Sulfate reduction related to the early diagenetic degradation of organic matter and "black spot" formation in tidal sandflats of the German Wadden Sea: stable isotope (^{13}C, ^{34}S, ^{18}O) and other geochemical results. Org. Geochem. 29, 1517–1530.

Böttcher, M.E., Hespenheide, B., Llobet-Brossa, E., Beardsley, C., Larsen, O., Schramm, A., Wieland, A., Böttcher, G., Berninger, U.-G., Amann, R., 2000. Biogeochemistry, stable isotope geochemistry, and microbial community structure of a temperate intertidal mudflat: an integrated study. Cont. Shelf Res. 20, 1749–1769.

Böttcher, M.E., Hespenheide, B., Brumsack, H.-J., Bosselmann, K., 2004. Stable isotope biogeochemistry of the sulfur cycle in modern marine sediments: I. Seasonal dynamics in a temperate intertidal sandy surface sediment. Isotopes Environ. Health Stud. 40, 267–283.

Boughriet, A., Ouddane, B., Fischer, J.C., Wartel, M., Leman, G., 1992. Variability of dissolved Mn and Zn in the seine estuary and chemical speciation of these metals in suspended matter. Water Res. 26, 1359–1378.

Brasse, S., Reimer, A., Seifert, R., Michaelis, W., 1999. The influence of intertidal mudflats on the dissolved inorganic carbon and total alkalinity distribution in the German Bight, southeastern North Sea. J. Sea Res. 42, 93–103.

Brink-Spalink, G., Stanev, E.V., Wolff, J.-O., 2003. On numerical modelling of sediment dynamics in the East-Frisian Wadden Sea. Ber. Forschungsz. Terramare 12, 39–42.

Burdige, D.J., 1993. Biogeochemistry of manganese and iron reduction in marine sediments. Earth Sci. Rev. 35, 249–284.

Burnett, W.C., Bokuniewicz, H., Hüttel, M., Moore, W.S., Taniguchi, M., 2003. Groundwater and pore water inputs to the coastal zone. Biogeochemistry 66, 3–33.

Burton, J.D., Althaus, M., Millward, G.E., Morris, A.W., Statham, P.J., Tappin, A.D., Turner, A., 1993. Processes influencing the fate of trace-metals in the North Sea. Phil. Trans. R. Soc. Ser. A-Math. Phys. Eng. Sci. 343, 557–568.

Davidson, A.T., Marchant, H.J., 1987. Binding of manganese by Antarctic Phaeocystis pouchetti and the role of bacteria in its release. Mar. Biol. 95, 481–487.

De Beer, D., Wenzhöfer, F., Ferdelman, T.G., Boehme, S.E., Hüttel, M., Van Beusekom, J.E.E., Böttcher, M.E., Musat, N., Dubilier, N., 2005. Transport and mineralization in North Sea sandy intertidal sediments, Sylt-Rømø Basin, Wadden Sea. Limnol. Oceanogr. 50, 113–127.

Dehairs, F., Baeyens, W., Van Gansbeke, D., 1989. Tight coupling between enrichment of iron and manganese in North Sea suspended matter and sedimentary redox processes: evidence for seasonal variability. Estuar. Coast. Shelf Sci. 29, 457–471.

Dellwig, O., Hinrichs, J., Hild, A., Brumsack, H.-J., 2000. Changing sedimentation in tidal flat sediments of the southern North Sea from the Holocene to the present: a geochemical approach. J. Sea Res. 44, 195–208.

Dellwig, O., Watermann, F., Brumsack, H.-J., Gerdes, G., Krumbein, W.E., 2001. Sulphur and iron geochemistry of Holocene coastal peats (NW Germany): a tool for palaeoenvironmental reconstruction. Palaeogeogr. Palaeoclim. Palaeoecol. 167, 359–379.

Dellwig, O., Böttcher, M.E., Lipinski, M., Brumsack, H.-J., 2002. Trace metals in Holocene coastal peats and their relation to pyrite formation (NW Germany). Chem. Geol. 182, 423–442.

Duinker, J.C., Wollast, R., Billen, G., 1979. Behavior of Manganese in the Rhine and Scheldt Estuaries: 2. Geochemical Cycling. Estuar. Coast. Mar. Sci. 9, 727–738.

Ehlers, J., 1994. Geomorphologie und Hydrologie des Wattenmeeres. In: Lozan, J.L., Rachor, E., Von Westernhagen, H., Lenz, W. (Eds.), Warnsignale aus dem Wattenmeer. Blackwell Wissenschaftsverlag, Berlin, pp. 1–11.

Feely, R.A., Massoth, G.J., Paulson, A.J., Gendron, J.F., 1983. Possible evidence for enrichment of trace-elements in the hydrous manganese oxide phases of suspended matter from an urbanized embayment. Estuar. Coast. Shelf Sci. 17, 693–708.

Fossing, H., Jørgensen, B.B., 1989. Measurement of bacterial sulfate reduction in sediments – evaluation of a single-step chromium reduction method. Biogeochemistry 8, 205–222.

Fraustro da Silva, J.J.R., Williams, R.J.P., 1991. The Biological Chemistry of the Elements/The Inorganic Chemistry of Life. Clarendon Press, Oxford.

Heinrichs, H., Brumsack, H.-J., Loftfield, N., König, N., 1986. Verbessertes Druckaufschlußsystem für biologische und

anorganische Materialien. Zeitschr. Pflanzenernähr. Bodenk. 149, 350–353.
Hild, A., 1997. Geochemie der Sedimente und Schwebstoffe im Rückseitenwatt von Spiekeroog und ihre Beeinflussung durch biologische Aktivität. Ber. Forschungsz. Terramare 5, 1–33.
Hinrichs, J., Dellwig, O., Brumsack, H.-J., 2002. Lead in sediments and suspended particulate matter of the German Bight: natural versus anthropogenic origin. Appl. Geochem. 17, 621–632.
Hüttel, M., Ziebis, S., Forster, S., Luther III, G., 1998. Advective transport affecting metal and nutrient distribution and interfacial fluxes in permeable sediments. Geochim. Cosmochim. Acta 62, 613–631.
Hydes, D.J., Kremling, K., 1993. Patchiness in dissolved metals (Al, Cd, Co, Cu, Mn, Ni) in North-Sea surface waters—seasonal differences and influence of suspended sediment. Cont. Shelf Res. 13, 1083–1101.
Kallmeyer, J., Ferdelman, T., Weber, A., Fossing, H., Jørgensen, B.B., 2004. A cold chromium distillation procedure for radiolabeled sulfide applied to sulfate reduction measurements. Limnol. Oceanogr. Meth. 2, 171–180.
Kersten, M., Kienz, W., Koelling, S., Schröder, M., Förstner, U., 1990. Heavy Metal Contamination of suspended particulate matter and sediments of the North Sea. Vom Wasser 75, 245–272.
Koschinsky, A., Winkler, A., Fritsche, U., 2003. Importance of different types of marine particles for the scavenging of heavy metals in the deep-sea bottom water. Appl. Geochem. 18, 693–710.
Kremling, K., 1983. Trace-Metal Fronts in European Shelf Waters. Nature 303 (5914), 225–227.
Kremling, K., 1985. The distribution of cadmium, copper, nickel, manganese, and aluminium in surface waters of the open Atlantic and European shelf area. Deep-Sea Res. Part a-Oceanogr. Res. Pap. 32, 531–555.
Laslett, R.E., 1995. Concentrations of dissolved and suspended particulate Cd, Cu, Mn, Ni, Pb and Zn in surface waters around the coasts of England and Wales and in adjacent seas. Estuar. Coast. Shelf Sci. 40, 67–85.
Liebezeit, G., Behrends, B., Kraul, T., 1996. Variability of nutrients and particulate matter in backbarrier tidal flats of the East Frisian Wadden Sea. Senckenb. Marit. 26, 195–202.
Martin, J.M., Meybeck, M., 1979. Elemental mass-balance of material carried by major world rivers. Mar. Chem. 7, 173–206.
Millward, G.E., Morris, A.W., Tappin, A.D., 1998. Trace metals at two sites in the southern North Sea: results from a sediment resuspension study. Cont. Shelf Res. 18, 1381–1400.
Moffett, J.W., 1994. A radiotracer study of cerium and manganese uptake onto suspended particles in Chesapeake Bay. Geochim. Cosmochim. Acta 58, 695–703.
Moore, W.S., Krest, J., Taylor, G., Roggenstein, E., Joy, S., Lee, R., 2002. Thermal evidence of water exchange through a coastal aquifer: implications for nutrient fluxes. Geophys. Res. Lett. 29 (Art. No. 1704).
Nico, P.S., Anastasio, C., Zasoski, R.J., 2002. Rapid photo-oxidation of Mn(II) mediated by humic substances. Geochim. Cosmochim. Acta 66, 4047–4056.
Oliver, B.G., Thurman, E.M., Malcolm, R.L., 1983. The contribution of humic substances to the acidity of colored natural waters. Geochim. Cosmochim. Acta 47, 2031–2035.
Recke, M., Förstner, U., 1988. Geochemical investigations on heavy metals in anoxic and oxic sediments from the North Sea and the East Frisian Wadden Sea. Mitt. Geol.-Paläontol. Inst. Univ. Hamburg 65, 313–344.
Rodushkin, I., Ruth, T., 1997. Determination of trace metals in estuarine and sea-water reference materials by high resolution inductively coupled plasma mass spectrometry. J. Analyt. Atom. Spectrom. 12, 1181–1185.
Saager, P.M., Sweerts, J.-P., Ellermeijer, H.J., 1990. A simple pore-water sampler for coarse, sandy sediments of low porosity. Limnol. Oceanogr. 35, 747–751.
Santamarina Cuneo, P., Flemming, B.W., 2000. Quantifying concentration and flux of suspended particulate matter through a tidal inlet of the East Frisian Wadden Sea by acoustic doppler current profiling. In: Flemming, B.W., Delafontaine, M.T., Liebezeit, G. (Eds.), Muddy Coast Dynamics and Resource Management. Elsevier, Amsterdam, pp. 40–51.
Schmidt, D., 1980. Comparison of trace heavy-metals from monitoring in the German Bight and the southwestern Baltic Sea. Helgol. Meeresunters. 33, 576–586.
Schwedhelm, E., Irion, G., 1985. Schwermetalle und Nährelemente in den Sedimenten der deutschen Nordseewatten. Cour. Forschungsinst. Senckenberg 73, 1–119.
Shaw, T.J., 2003. Methods and models for estimating advective pore water exchange in tidal flats. Ber. Forschungsz. Terramare 12, 103–104.
Shaw, T.J., Moore, W.S., Kloepfer, J., Sochaski, M.A., 1998. The flux of barium to the coastal waters of southeastern USA: the importance of submarine groundwater discharge. Geochim. Cosmochim. Acta 62, 3047–3054.
Shiller, A.M., 1997. Manganese in surface waters of the Atlantic Ocean. Geophys. Res. Lett. 24, 1495–1498.
Simon, M., Lunau, M., Brinkhoff, T., Stevens, H., Rink, B., Dürselen, C., Grossart, H.-P., 2003. Tidal and seasonal variations in dynamics of microaggregates and associated bacterial communities in the German Wadden Sea. Ber. Forschungsz. Terramare 12, 105–108.
Stanev, E.V., Wolff, J.-O., Burchard, H., Bolding, K., Flöser, G., 2003. On the circulation in the East Frisian Wadden Sea: numerical modeling and data analysis. Ocean Dynam. 53, 27–51.
Streif, H., 1990. Das ostfriesische Küstengebiet. Gebrüder Borntaeger, Berlin.
Tappin, A.D., Millward, G.E., Statham, P.J., Burton, J.D., Morris, A.W., 1995. Trace-Metals in the Central and Southern North-Sea. Estuar. Coast. Shelf Sci. 41, 275–323.
Tebo, B.M., Emerson, S., 1986. Microbial manganese(II) oxidation in the marine environment: a quantitative study. Biogeochemistry 2, 149–161.
Thamdrup, B., Fossing, H., Jørgensen, B.B., 1994. Manganese, iron, and sulfur cycling in a coastal marine sediment, Aarhus Bay, Denmark. Geochim. Cosmochim. Acta 58, 5115–5129.
UNESCO, 1981. The Practical Salinity Scale 1978 and the International Equation of State of Seawater 1980. Tenth Report on the Joint Panel on Oceanographic Tables and Standards. UNESCO Tech. Pap. Mar. Sci. 36, UNESCO, Paris.
Viers, J., Dupre, B., Polve, M., Schott, J., Dandurand, J.-L., Braun, J.-J., 1997. Chemical weathering in the drainage basin of a tropical watershed (Nsimi-Zoetele site, Cameroon): comparison between organic-poor and organic-rich waters. Chem. Geol. 140, 181–206.
Wedepohl, K.H., 1971. Environmental influences on the chemical composition of shales and clays. In: Ahrens, L.H., Press, F., Runcorn, S.K., Urey, H.C. (Eds.), Physics and Chemistry of the Earth, vol. 8. Pergamon, Oxford, pp. 305–333.

Nutrient release from an exposed intertidal sand flat

M. Billerbeck, U. Werner, K. Bosselmann, E. Walpersdorf, M. Huettel

This chapter is published in

MARINE ECOLOGY PROGRESS SERIES

316: 35-51 2006.

Vol. 316: 35–51, 2006 | MARINE ECOLOGY PROGRESS SERIES
Mar Ecol Prog Ser | Published July 3

Nutrient release from an exposed intertidal sand flat

Markus Billerbeck[1,*], Ursula Werner[1], Katja Bosselmann[1], Eva Walpersdorf[2], Markus Huettel[3]

[1]Max Planck Institute for Marine Microbiology, Celsiusstrasse 1, 28359 Bremen, Germany
[2]Oceanlab, University of Aberdeen, Main Street, Newburgh, Aberdeenshire AB41 6AA, UK
[3]Department of Oceanography, Florida State University, West Call Street, Tallahassee, Florida 32306-4320, USA

ABSTRACT: We studied pore water seepage and associated nutrient release in the Janssand intertidal sand flat (North Sea) during exposure at low tide. The hydraulic gradient developing at ebb tide between the pore water level in the elevated sand flat and the water level in the tidal gully generated interstitial water flows toward the seepage zone with velocities ranging from 0.5 (March) to 0.9 cm h^{-1} (July). Pore water was discharged from an approximately 20 m wide zone near the seaward margin of the flat at rates of 2.4 (March) and 4.2 l m^{-2} d^{-1} (July). Nutrient and dissolved inorganic carbon (DIC) concentrations of the seepage water exceeded those measured in the pore water of the upper section of the flat by 10- and 5-fold, respectively. Nutrient effluxes through seepage reached 1100 and 7600 µmol m^{-2} d^{-1} for NH_4, 280 and 2500 µmol m^{-2} d^{-1} for PO_4 and 140 and 1700 µmol m^{-2} d^{-1} for $Si(OH)_4$ in March and July, respectively. Benthic flux chambers revealed that nutrients and DIC were released from the still submerged sediment as soon as the ebb tide exposed the upper section of the elevated flat. A conservative estimate based on our measurements suggests that 168 000 l (March) to 294 000 l (July) pore water are discharged each day from the sandy northeastern margin of the Janssand (3.5 km length, 70 000 m^2). Nutrients contained in this water corresponded to 6–25 kg d^{-1} (90 to 350 mg m^{-2} d^{-1}) carbon mineralized during March and 42–223 kg d^{-1} (600 to 3200 mg C m^{-2} d^{-1}) during July. Our study indicates that the Janssand intertidal flat does not accumulate organic matter but releases mineralization products that can account for all the organic matter that is potentially filtered through the permeable beds during a tidal cycle. Nutrient fluxes associated with seepage exceeded 5- to 8-fold those fluxes caused by the combined effects of diffusion, advection and bioirrigation during inundation, emphasizing the importance of sand flat drainage to the nutrient cycles in the Wadden Sea.

KEY WORDS: Intertidal flat · Drainage · Pore water flow velocity · Filtration · Nutrient flux

INTRODUCTION

Fine to medium sands prevail in the intertidal regions of the Wadden Sea, covering a total area of ca. 13 000 km^2 along the Dutch, German and Danish coasts (Flemming & Ziegler 1995, van Beusekom & de Jonge 2002). The relatively high permeability of these sands (10^{-12} to 10^{-11} m^2) allows inflow of water through the interstices as soon as pressure gradients caused by currents or water level changes are present. During inundation, the pore water exchange transports solutes (Huettel et al. 1998) and particles (Huettel et al. 1996, Pilditch et al. 1997) into and out of the upper layers of permeable sediment. Through the enhanced exchange of organic matter, electron acceptors and metabolic products (Ziebis et al. 1996, Huettel et al. 1998), such permeable sands become sites of high organic matter turnover (Huettel & Rusch 2000, D'Andrea et al. 2002). During ebb tide, pressure gradients develop between the pore water level within elevated, exposed sand flats and the decreasing water level of the Wadden Sea. In these sands, the pore water table drops slower than the seawater level (Nielsen 1990) because of the sediment's hydraulic impedance and capillary forces, and the ensuing pressure gradient leads to water release that fills the numerous drainage channels typi-

*Email: mbillerb@mpi-bremen.de

cal of intertidal flats (Nielsen 1990, Horn 2002). Such discharge of pore water has been recognized as an ecologically important process in studies covering coastal, submarine, groundwater discharge (Simmons 1992, Moore 1996, Taniguchi & Iwakawa 2004), wave dominated beaches (McLachlan & Illenberger 1986, Uchiyama et al. 2000, Ullman et al. 2003) and salt marshes (Howes & Goehringer 1994, Osgood 2000, Jahnke et al. 2003). For tide dominated intertidal flats, however, studies on drainage and associated solute releases are scarce. Le Hir et al. (2000) estimated from runnel-runoff velocities that intertidal mud flats on the French and British coasts discharged roughly 10 l m^{-2} $tide^{-1}$. In a tidal flat in Tokyo Bay, drainage has been suggested as a possible mechanism causing a drop in sedimentary water content during exposure (Usui et al. 1998). In contrast, Kuwae et al. (1998) concluded that pore water release in another intertidal flat in Tokyo Bay was small because the sediment remained nearly saturated during exposure. Likewise, Drabsch et al. (1999) suggested that tidal pumping and total water flux in a tidal flat (Manukao Harbour, New Zealand) was small because pore water flow velocities ranged only between 0.2 and 4.0 cm d^{-1}. However, visible pore water seepage from intertidal sand flats in the North Sea indicates that drainage may produce significant pore water release in more steeply sloping flats. Therefore, we initiated the present study, which investigated the magnitude of pore water release and implications of this drainage for sedimentary nutrient and dissolved inorganic carbon (DIC) release in permeable intertidal sand flats. Because benthic microalgae act as biological nutrient filters at the sediment–water interface (Sundbäck et al. 2000), we also assessed the effect of these organisms on nutrient release during inundation.

MATERIALS AND METHODS

Study site. The study was conducted during 2 field campaigns (July 2003 and March 2004) on the northeastern margin of the intertidal Janssand sandflat situated landward of the barrier island of Spiekeroog, North Sea (53° 44′ 07″ N, 007° 41′ 57″ E) (Fig. 1). Tides in this area are semi-diurnal, and the Janssand (11 km^2 area) is covered by approximately 1.5 to 2 m of water during high tide, becoming exposed to air for about 6 to 7.5 h during low tide. The Janssand tidal flat is almost level, except at the margin where the sediment surface slopes (1.6 cm m^{-1} over ca. 80 m, Fig. 2). We chose 4 study sites (A to D in Fig. 2), with most measurements conducted at the 'lower sand flat' site (Site D) near the edge of the Janssand and at the 'upper sand flat' site (Site A) about 45 m upslope from the mean low water line. All measurements and samplings are listed in Table 1, together with their respective locations on the tidal flat and associated tidal range. The Janssand is characterized by well sorted ($\sigma < 0.38$ phi), fine quartz sands with a mean grain size of 176 µm (assessed through dry-sieving). On the upper sand flat, permeability of the sediment surface layer (upper 15 cm), determined by constant head permeametry, is 7.2×10^{-12} m^2 (SD ± 0.6×10^{-12} m^2, n = 6, July 2003), which permits advective pore water flows (Huettel et al. 2003). At the lower sand flat site, the same layer is less permeable (5.2×10^{-13} m^2 [SD ± 0.3×10^{-13} m^2, n = 6]), because of imbedded mud lenses. Macrofaunal abundances are relatively low at the study site (Hertweck 1995). The Spiekeroog tide gauge within 2 km of the study site provided the data on water level changes.

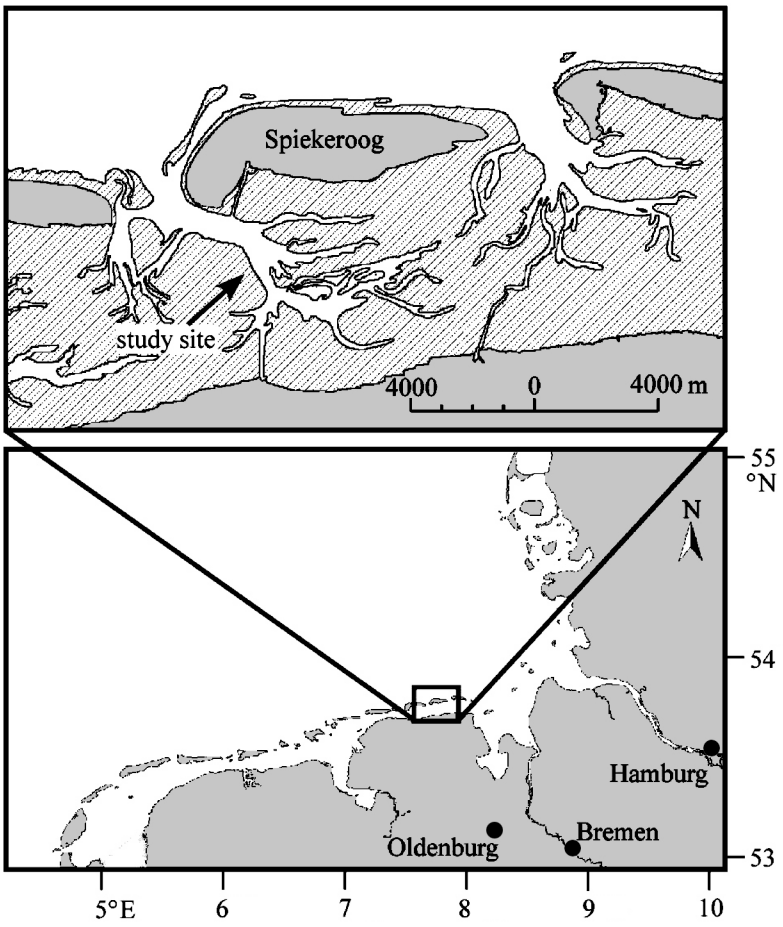

Fig. 1. Location of the study site, near the island of Spiekeroog, North Sea, Germany

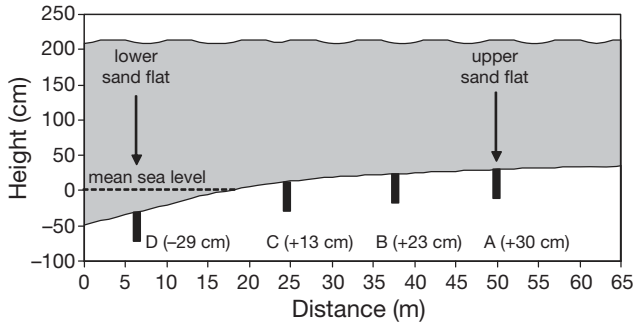

Fig. 2. Janssand tidal flat topography, as surveyed during July 2003, showing positions (cm) of Study Sites A–D relative to mean sea level. Shading indicates the mean high water; dashed line at zero water height marks the position of mean low water line during July 2003. An additional 10 to 15 m of the tidal flat was exposed during the March 2004 campaign due to wind conditions

Pore water level. To assess fluctuations of the pore water level within the sediment with change in the tidal water level, 4 acrylic pipes (20 cm long, 36 mm diameter) were vertically inserted into the sediment on a transect (A–D in Fig. 2) from the upper sand flat site (A) toward the lower sand flat site (D). The open lower ends of the pipes were covered with nylon mesh (63 µm) and their open upper ends were level with the sediment surface. The water table in the pipes was measured to the nearest 1 mm with a ruler throughout exposure of the respective sites, at 1 to 60 min intervals (Table 1).

Pore water flow velocity. The horizontal flow velocity of pore water was measured at the upper sand flat site by following the passage of a fluorescent dye tracer through the sediment with a buried linear array of 6 fiberoptic sensors, as described in Precht & Huettel (2004) (Fig. 3). The tracer solution was prepared by adding fluorescein dye to filtered seawater to an end concentration of 100 mg l^{-1} and adjusting it to the local pore water density. Prior to the first measurement, fluorescein dye solution was injected with a syringe into the sand, and subsequently dug out to visually determine the main flow direction of the pore water. Then a small incision was cut into the sediment at low tide to the desired depth, and the setup was carefully inserted and pushed horizontally several centimeters into the undisturbed part of the sediment. The sensor array orientation was horizontal to the sediment surface and roughly perpendicular to the low water line; other orientations did not show any measurable pore water flow. During the July 2003 campaign, pore water flow velocities were measured at 2, 5 and 10 cm sediment depth throughout exposure. These measurements were extended by four 10 cm intervals to a sediment depth of 50 cm during the March 2004 campaign. An additional measurement was conducted at 5 cm sediment depth about 30 m upslope on the upper sand flat site (+6 cm height) during the March campaign. Some measurements were continued during inundation of the tidal flat until re-exposure. All pore water flow velocity measurements were conducted during the transition from mean tide to neap tide for both campaigns. The average pore water flow velocity was calculated for all measurements from the time interval between the geometric centroids of the signal curves at consecutive sensors (Fig. 3). The average and standard deviation of flow velocity were derived for each deployment from individual velocity calculations between adjacent sensors in the 6-sensor array.

Table 1. Sampling and *in situ* measurements made during July 2003 and March 2004 field campaigns. Also shown are sites A to D where measurements were made, their tidal range, and their respective positions on the tidal flat. Positions of the sites A to D relative to mean sea level were +30, +23, +13, and –29, respectively (Fig. 2). Seepage measurements were made using open and rhombic meters; chamber measurements assessed solute fluxes and benthic primary production during inundation. Further details in 'Materials and methods'

Date (dd.mo.yr)	Tidal range (m)	Site characteristics				*In situ* measurements		
		Sediment	Seawater	Pore water	Pore water level	Pore water flow velocity	Chambers	Seepage
21.07.2003	2.7					A: 2 cm depth		
22.07.2003	2.6			A				
23.07.2003	2.3	Topography: A–D	D					
25.07.2003	2.2					A: 10 cm depth		
26.07.2003	2.5	Grain size: A			A,B,C,D	A: 5 cm depth		
27.07.2003	2.7	Permeability: A,D						
29.07.2003	3.0	Chl *a*: A	High tide				A	
30.07.2003	3.2	Chl *a*: D	High tide				D: –12 cm	
26.03.2004	3.0					A: 2 cm depth		D: –21 cm (open)
27.03.2004	2.8					A: 5 cm depth		D: –21 cm (open)
28.03.2004	2.5		High tide			A: 20 cm depth		D: –21 cm, –32 cm (open)
29.03.2004	2.3					A: 30 cm, 40 cm depths		A,C,D: –21 cm (open)
30.03.2004	1.9			A,D		A: 50 cm depth		D: –21 cm (rhombic)
31.03.2004	1.8					A+6 cm: 5 cm depth		

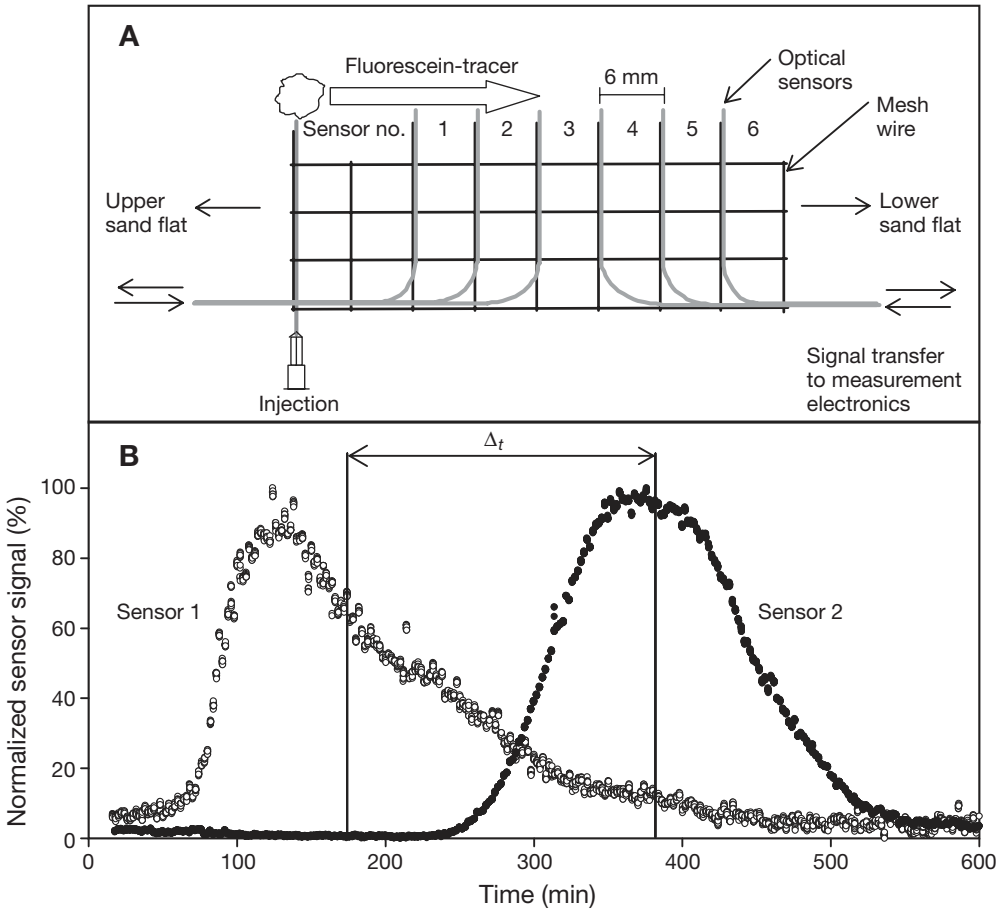

Fig. 3. (A) Setup of the 6 optical sensors used to measure pore water flow velocity (schematic, top view). (B) Fluorescence signals of 2 optical fibers and location of geometric centroids (vertical lines) used to calculate time span (Δt) between dye passage at respective sensor tips. Geometric centroids are located at cumulative 50% of the respective signal curve areas

Pore water seepage. Pore water discharge from the sloping margin of the tidal flat was quantified in March during exposure by measuring the volume of fluid collected at the end of 2 flow barriers (open seepage meter) that guided draining pore water into a container (Fig. 4). The open seepage meter consisted of two 5 cm wide plastic laths (100 cm length) inserted to a depth of 2 cm vertically into the sediment, with the 2 laths forming an angle of 130°. The resulting surface-water flow-barrier collected seepage water from a 1.8 m wide upslope section of the flat. At the meeting point of the 2 plastic laths, a plastic funnel with tubing was attached to collect the seeped pore water into a graduated cylinder. The amount of collected pore water was quantified to the nearest 1 ml, and filtered samples were transferred to plastic vials and kept frozen for later nutrient analysis. Up to 3 of these seepage meters were established along a transect (Sites A, C, D) and were ready for measurement within 20 min of exposure. The zones of pore water discharge upslope of the seepage meters could be identified from the 'glassy' appearance of the surface of the water saturated sediment, and their areal dimensions were recorded throughout the measurements. In order to verify the seepage measurements with the open seepage meter, an additional measurement was conducted by inserting 2 additional plastic laths opposite to the open seepage meter, isolating a rhombic area of 0.78 m^2 (Fig. 4). A good agreement between the seepage rates m^{-2} measured with the rhombic and open seepage meters was obtained for discharge zones extending less than 6 m above the open seepage meter. Discharge rates were calculated by dividing the collected pore water volume per unit time by the respective seepage area (Fig. 4) of the open or rhombic seepage meter.

Chamber flux measurements. During the July 2003 campaign, *in situ* measurements with stirred cylindrical chambers (19 cm inner diameter) were carried out to measure advective fluxes of oxygen, DIC and nutrients across the sediment–water interface. At the lower sand flat site, the chambers were also used to assess drainage discharge of solutes from the sediment. The chamber measurements were conducted on 2 consecutive days at the upper and lower sand flat sites. We deployed 3 transparent and 3 opaque chambers at each site, permitting assessment of benthic primary production during inundation. At the lower sand flat site, chamber incubations were longer (8 h) and water

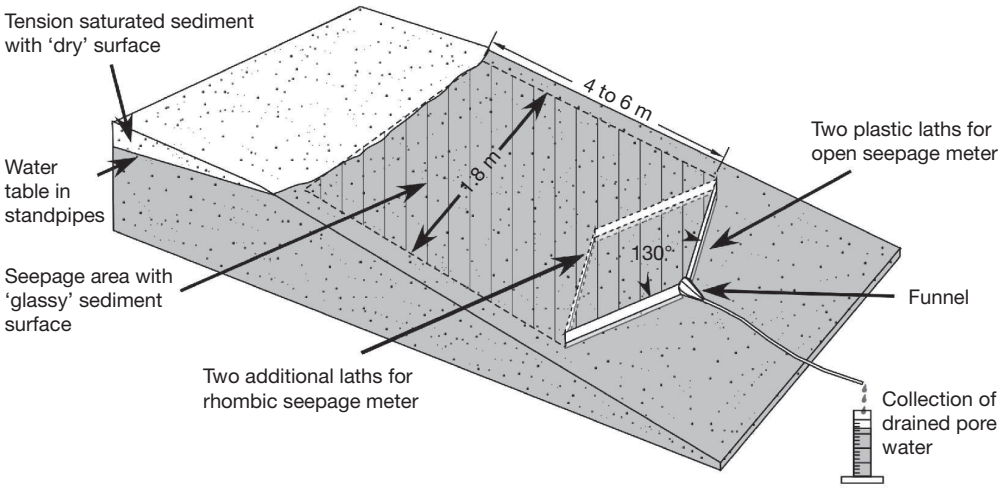

Fig. 4. Setup of open and rhombic seepage meters on the sloping sand flat. Discharge area was identified from the 'glassy' appearance of sediment surface upslope of the meter (hatched area), and spanned an area of 6 to 13 m^2 for the open and 0.78 m^2 for the rhombic seepage meters

depth deeper (2.3 m), than at the upper flat (4 h incubations, 1.5 m water depth). During the incubation period, water temperature varied by ≤1°C, while concentrations of nutrients, DIC and oxygen in the ambient seawater remained relatively constant. During low tide, the chambers were gently inserted to a sediment depth of 19 cm, and neoprene collars (20 cm diameter) were placed around them to prevent erosion. Upon inundation, the chambers were sealed with acrylic lids, each enclosing a water volume of 3.4 l and a sediment area of 0.028 m^2. Inside the chambers, a rotating disc (15 cm diameter, 20 rpm) producing a radial pressure gradient of 0.1 Pa cm^{-1} caused flushing of the upper sediment layer, thus mimicking natural advective pore water exchange (Huettel & Gust 1992, Huettel & Rusch 2000). Advective tracer and solute fluxes caused by this very low pressure gradient (corresponding to a gradient created by flow of 10 cm s^{-1} at 10 cm above the bed interacting with a sediment ripple of 0.5 cm height) should be considered conservative. Each lid had a sampling port and a small opening with a 1 m Tygon™ tubing coil attached to it to allow pressure equilibration between chamber and surrounding water and inflow of discharged pore water into the chambers. Oxygen concentrations inside each chamber were monitored every 2 min for 20 s with fiberoptic optodes (Klimant et al. 1995) inserted through the chamber lid. After closing the chambers, 20 ml of a 3 mol l^{-1} NaBr inert tracer solution was injected into 1 dark and 1 light chamber for the assessment of the depth of advective fluid exchange between overlying water and sediment (Forster et al. 1999). After the bromide tracer had mixed with the chamber water for 15 min, all chambers were sampled at hourly intervals (when water level and currents permitted). At each sampling, samples of ambient seawater were taken, and a total of 80 ml of water was drawn with a syringe from each chamber, of which the first 20 ml were discarded to compensate for the sampling tube volume (15 ml). At the end of the incubations, with the water level still above the chambers, sediment cores from the chambers treated with bromide tracer were retrieved with cut-off 60 ml syringes. The sediment cores were sliced into 0.5 cm sections within 30 min after retrieval and kept frozen until analysis. Benthic chamber measurements could not be carried out during March due to adverse weather conditions.

Sampling and analyses. For sedimentary chlorophyll *a* determination, samples of the upper 5 cm of the sand were divided into 0.5 cm sections for analysis according to Lorenzen (1967). For characterization of ambient seawater, samples collected at high tide and samples from gullies (ebb tide) were collected in plastic centrifuge tubes (glass vials for DIC and dissolved organic carbon, DOC) and filtered through 0.2 µm nylon syringe filters. Aliquots were either kept frozen (for nutrients, DOC) or preserved with mercury chloride (for DIC analysis). For POC and PN contents, samples were filtered onto pre-combusted Whatman® GFF filters and kept frozen. For pore water nutrient and DIC determinations, sediment cores were collected with 36 mm core liners shortly after exposure of the study sites and sectioned within an argon-flushed glove box to a depth of 20 cm at 1 cm intervals. Equivalent slices from 4 sediment cores were pooled and transferred to a small pressure container with an inert gas inlet and a pore water outlet. By flushing the container ca. 20 s with argon gas, the pore water was separated from the sediment matrix. After filtration through 0.2 µm nylon syringe filters, aliquots were frozen for nutrient analysis or preserved with saturated mercury chloride solution for subsequent DIC analysis. Bromide in the pore water was analyzed by ion chromatography with a Waters® anion-exchange column, using NaBr as a standard for calibration. Filters for POC and PN analysis were treated with a few drops of 1 mol l^{-1} HCl to remove inorganic carbon, prior to analysis on a Heraeus® CHNO-

rapid elemental analyzer with sulfanilamide as calibration standard. Nutrient analyses of silicate, phosphate, ammonium, nitrate and nitrite were performed spectrophotometrically with a Skalar continuous-flow-analyzer according to Grasshoff et al. (1999). DIC was determined by flow injection analysis (Hall & Aller 1992) or coulometric titration on a UIC CM5012 (for chamber water). Seawater DOC analysis was performed by high temperature, catalytic oxidation on a Shimadzu™ TOC-5050A analyzer and obtained by subtracting the measured DIC concentration from the measured total DC. Oxygen concentrations of chamber water were determined by Winkler titration and used for calibration of the chambers' oxygen optodes (for details see Klimant et al. 1995, Holst et al. 1997). Dilution of the chamber waters due to sampling was corrected by adding the difference of the solute inventory between the sampled and replaced volume to the chamber volume solute inventory. Solute fluxes were estimated by linear regression on concentration changes over time, or from start and end concentrations when linear regression was not applicable. Pore water concentrations and flux data were analyzed with a Wilcoxon-Mann-Whitney nonparametric *U*-test for pairwise comparisons at a 95% confidence level ($p < 0.05$).

RESULTS

Pore water level

The water level in the sediment changed when the Janssand became exposed at ebb tide (Fig. 5). At Sites A and B on the upper sand flat, the pore water level remained at the sediment surface during the first 2 h of exposure and dropped gradually thereafter, reaching its lowest point approximately 1.5 h after low tide. The pore water level then increased again with the rising tide, but never reached the sediment surface until re-inundation. At Site C, the pore water level remained high and did not drop at all at the lower sand flat position, Site D. At Site D, a pore water level at times above sediment elevation cannot be ruled out, as the open end of the standpipe was level with the sand surface. The maximum measured difference in pore water level between the upper (Site A) and lower (Site D) sand flat was 46 cm over a horizontal distance of 4300 cm.

Pore water flow velocity

The fiberoptical measurements revealed pore water flows directed toward the low water line over the measured sediment depth of 50 cm during exposure

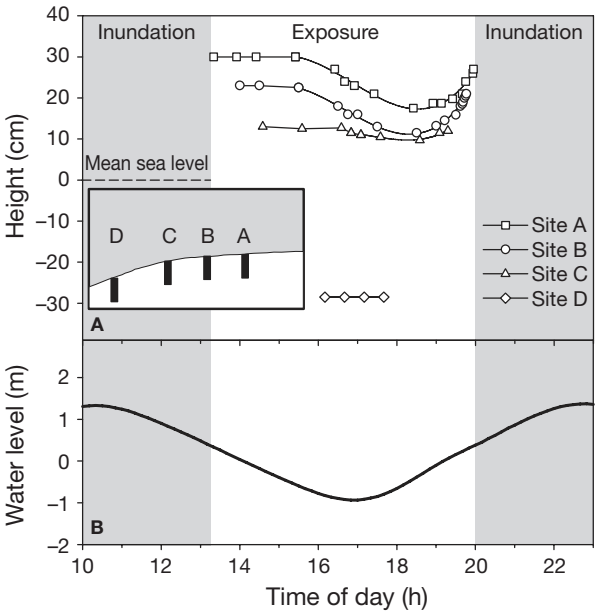

Fig. 5. (A) Response of pore water level, relative to mean sea level, to fluctuation in the tidal water level at Sites A–D (accuracy of ±1 mm) during average tidal range (pore water levels may differ for other tidal ranges). Trend lines were manually drawn through the data sets. Inset: schematic representation of locations of respective measurement sites on tidal flat (see also Fig. 2). Shading marks inundation period of upper sand flat site (Site A). (B) Tidal water level based on mean sea level

(Table 2). During July 2003, an average pore water flow velocity of 0.86 cm h^{-1} was measured, with similar velocities between 2 and 10 cm sediment depths (Table 2). This pore water flow started after the exposure of the tidal flat and continued for 6.5 h until the measuring position became inundated again. After submergence of the measuring position, a steady fluorescence signal remained for the seaward sensor during the entire inundation period (Fig. 6), and decreased rapidly once the tidal flat became exposed again. This

Table 2. Pore water flow velocities at different sediment depths at upper sand flat site during the July and March campaigns. Flow velocities at respective depths are given as average of measurements between consecutive sensors ± SD (n = 3–5)

Sediment depth (cm)	Flow velocity (cm h^{-1}) July 2003	March 2004
2	0.87 ± 0.32	0.68 ± 0.27
5	0.74 ± 0.23	0.61 ± 0.11
10	0.98 ± 0.13	
20		0.58 ± 0.25
30		0.62 ± 0.39
40		0.45 ± 0.17
50		0.32 ± 0.06
Average	0.86	0.54

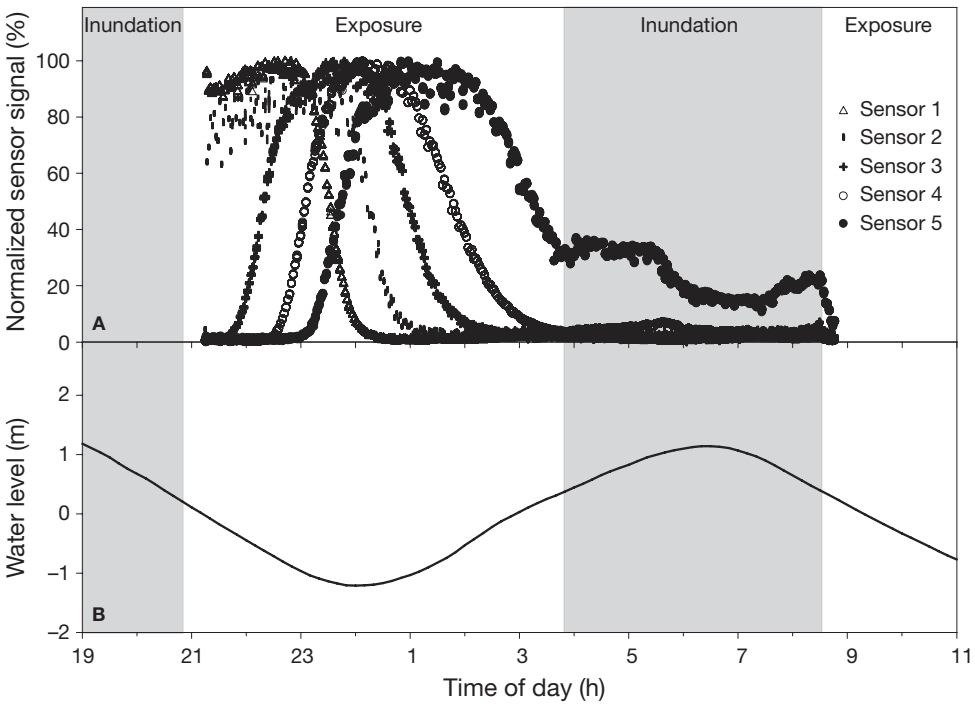

Fig. 6. (A) Tracer signal curves from velocity measurements of pore water flow in 2 cm sediment depth at the upper sand flat site in July 2003 (see also Table 2). Normalized signals (% of maximum signal) of 5 consecutive sensors are shown during exposure (white) and inundation (shaded) of the measuring position; Sensor 6 data could not be shown because of excessive data noise. (B) Tidal water level based on mean sea level

showed that the pore water flow ceased during submergence and resumed again after exposure. Other pore water flow measurements confirmed this finding (data not shown). During the March 2004 campaign, wind conditions resulted in up to 9 h long periods of exposure, compared to 7.5 h in July. Nevertheless, measured flow velocities in the upper 10 cm of the sediment (0.54 cm h^{-1}) were less than during the July campaign. In March, pore water flow velocities were similar down to a sediment depth of 30 cm, but decreased below this (Table 2). During both measuring campaigns, pore water flow velocities remained relatively constant for the duration of the exposure period. During most of the exposure period, puddles of water persisted on the almost level sediment surface 30 m upslope on the upper sand flat site (6 cm vertical gain), and no pore water flow could be detected during the first 6.5 h of exposure in March 2004. Pore water flow at 5 cm depth started within the last 2.5 h of exposure and coincided with a 'drying' of the sediment surface due to a gradual drop in the pore water table. In contrast, pore water flow was detected during the entire period of exposure in the steeper sloping, upper sand flat site.

Pore water seepage

Pore water was released from the sediment at the lower sand flat site during ebb tide, as quantified during the March 2004 campaign. At low tide, seepage was restricted to an area extending from the low water line to about 20 to 30 m up the slope, as indicated by its 'glassy' sediment surface. Discharge continued throughout the period of exposure. In 4 measurements with the open seepage meters, initial rates of seepage ranged between 0.7 and 3.0 l m^{-2} h^{-1}, decreasing to 0.1–0.4 l m^{-2} h^{-1} shortly before re-inundation (Fig. 7A). Measurements with the rhombic seepage meters recorded a comparable discharge. Nutrient concentrations of the discharged pore water increased over time for silicate, phosphate and ammonium, and decreased or remained constant for NOx (Fig. 7B). At similar rates of pore water seepage, the discharge of nutrients varied between measurements (Table 3).

Pore water solute and seawater concentrations

In July and March, we measured significant differences in the pore water nutrient and DIC concentrations between the upper and the lower Janssand sites (Wilcoxon-Mann-Whitney *U*-test, $p < 0.001$). At the lower sand flat site, where water drained from the Janssand sediment, pore water silicate, phosphate and ammonium concentrations exceeded the respective concentrations at the upper flat by about 1 order of magnitude during both measuring campaigns (Fig. 8). Likewise, pore water DIC concentrations at the lower site were 2- to 5-fold higher than at the upper site in July, and 5 to 6-fold higher in March (Fig. 9), reaching 20 mmol l^{-1} during both campaigns. Pore water solute

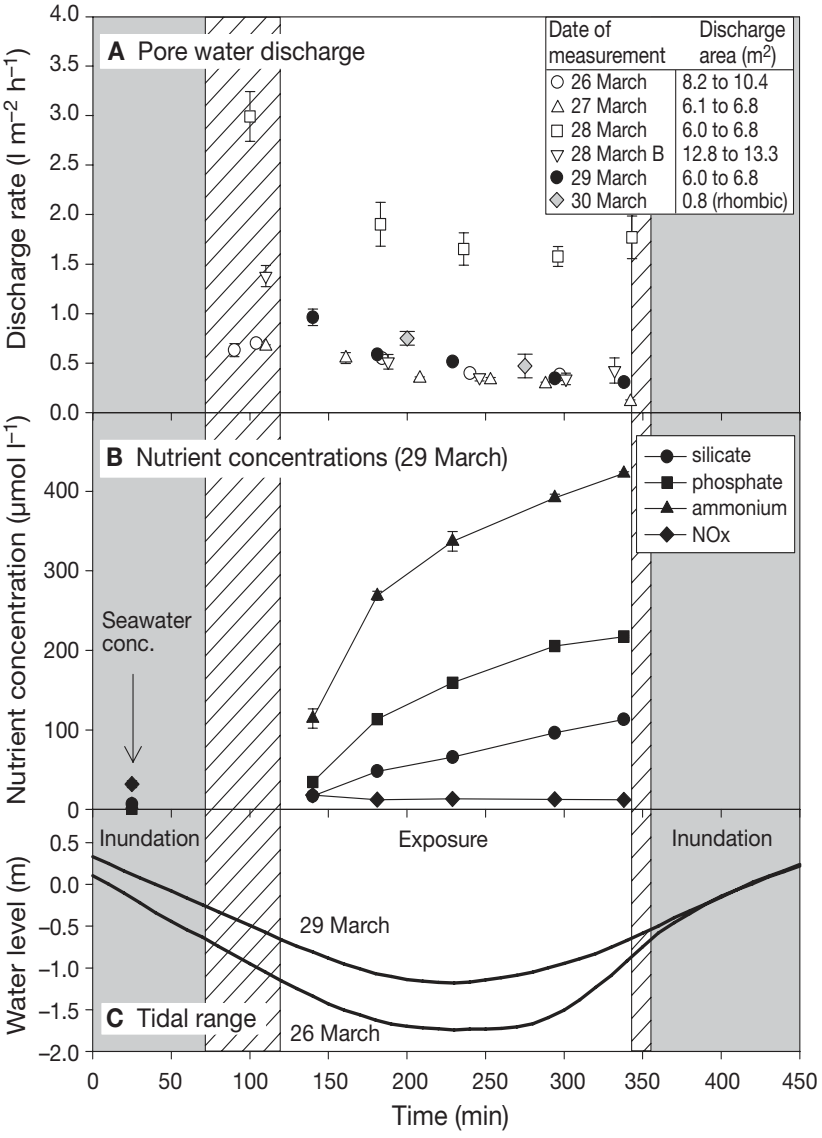

Fig. 7. (A) Mean (±SD) seepage rates of pore water during low tide during 5 consecutive days at the lower sand flat (n = 10) and associated sampling discharge areas (inset). (B) Nutrient concentrations of discharged pore water corresponding to measurement of 29 March (● in A; n = 3); all measurements were conducted within 20 m distance of each other and data are means (±SD). (C) Lines mark minimum and maximum range of water level between 26 March and 30 March measurements based on mean sea level; shading: inundation period on tidal flat; hatched area: period of inundation or exposure (depending on tidal range)

concentrations exceeded those of the ambient water by far (Table 4). Water column C:N ratios of POM averaged between 6 and 7, indicating fresh organic matter. During July 2003, the chlorophyll *a* inventory in the upper 5 cm of the sediment was similar for the upper (11.2 ± SD 1.9 µg g^{-1}, n = 20) and lower (10.4 ± SD 1.3 µg g^{-1}, n = 20) flat.

Chamber flux measurements

The bromide tracer was transported down to a sediment depth of 2 to 3 cm, revealing advective flushing of the incubated permeable sediment (Table 5). At the upper sand flat, phosphate was released from the sediment, while silicate was consumed. Concentrations of ammonium, nitrate and nitrite stayed below detection limits. Fluxes of DIC and oxygen reflected photosynthetic activity. Oxygen was produced in the transparent chambers (1500 to 2000 µmol m^{-2} h^{-1}) and consumed (1300 to 1600 µmol m^{-2} h^{-1}) in the opaque chambers, corresponding to an average gross photosynthetic production of 3300 µmol C m^{-2} h^{-1}. At the lower sand flat site, pore water started seeping from the sediment after the upper Janssand became exposed during ebb tide. In order to assess the contribution of seepage to the total solute release in the chambers, fluxes measured during inundation of the lower flat (0 to 6.5 h) were subtracted from the total fluxes recorded during the period of 1.5 h when the upper flat was exposed and seepage occurred at the lower site (6.5 to 8 h) (Table 5). During the first 6.5 h of the lower sand flat incubation, effluxes of silicate, phosphate and ammonium were observed in all but 1 chamber (Fig. 10). Fluxes of silicate and phosphate were slightly higher and ammonium fluxes were largely increased compared to the upper sand flat

Table 3. Discharge rate of nutrients (µmol m^{-2} h^{-1}) and seepage rate (l m^{-2} h^{-1}) of pore water; average of 4 measurements during the March 2004 campaign. Values are means (range)

Nutrient discharge			Seepage rate
Silicate	Phosphate	Ammonium	
0.94 (0.34–1.57)	0.13 (0.04–0.20)	3.59 (1.19–3.70)	0.38 (0.11–0.67)
100.76 (66.97–117.69)	196.15 (90.14–262.15)	724.45 (449.31–924.50)	1.98 (1.58–2.99)
10.23 (9.25–11.25)	19.97 (12.64–24.84)	205.55 (163.86–230.76)	0.60 (0.34–1.38)
29.06 (16.11–34.46)	63.59 (33.08–81.68)	140.61 (109.95–172.66)	0.54 (0.30–0.96)

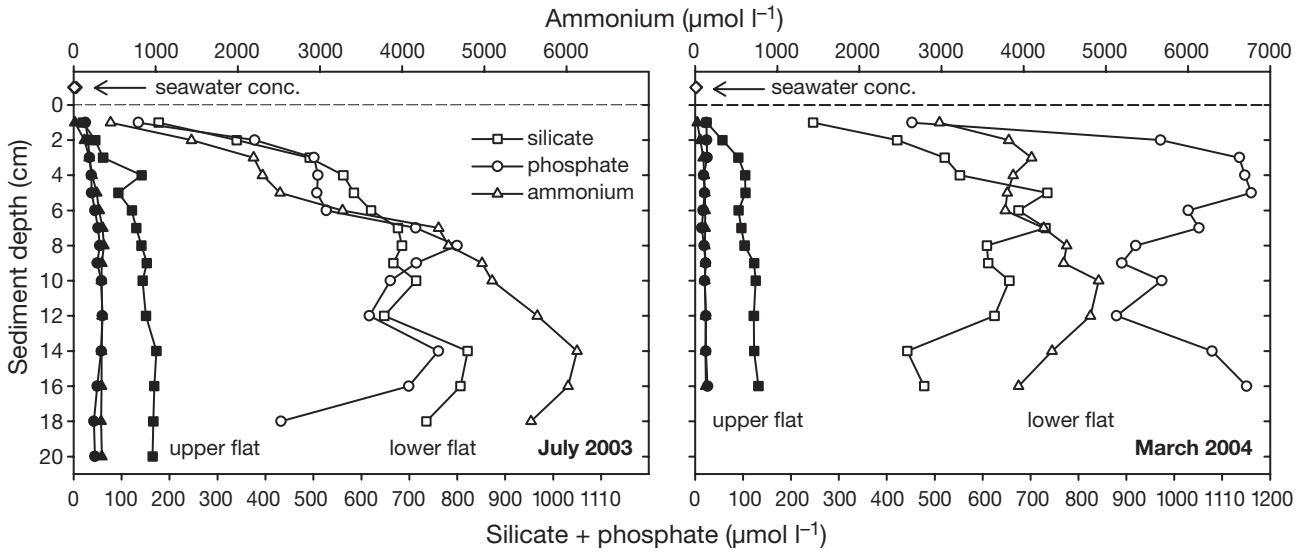

Fig. 8. Pore water concentrations of silicate, phosphate and ammonium in upper (filled symbols) and lower (open symbols) sand flat sites during July 2003 and March 2004. Concentrations in overlying seawater are shown above the dashed line

chamber measurements (Table 5). Concentrations for nitrate and nitrite always stayed below the detection limit. There was no visible influence of photosynthesis on oxygen fluxes (in contrast to the upper flat site (Wilcoxon-Mann-Whitney *U*-test, $p < 0.05$)), as oxygen was consumed to the same extent in dark and light chambers (Table 5). During the last 1.5 h (6.5 to 8 h) of the lower sand flat incubations, a significantly increased efflux of reduced solutes ($p < 0.05$) could be observed in all chambers (for silicate in 4 chambers) suggesting that pore water was released from the submerged margin of the Janssand when the upper section of the flat became exposed (Table 5). The venting port of the chambers permitted release of seepage water into the chambers. Irrespective of dark or light incubations, silicate, phosphate and ammonium concentrations in the chamber waters increased at a higher rate during this period (Fig. 10). The efflux of DIC increased up to 87 000 µmol m^{-2} h^{-1} compared to the initial 6.5 h period, and an increased consumption of oxygen in the opaque chambers was observed ($p < 0.05$). The fluxes of nutrients and DIC during the last 1.5 h exceeded the fluxes recorded prior to this period on average of 5 to 8-fold. Advection of pore water into the chambers due to the interaction of the chambers with waves and currents (Shinn et al. 2002) could be ruled out as the cause for this increase, since no increased pore water discharge into the chambers was measured shortly after submergence of the tidal flat, when strong tidal currents were present.

Table 4. Seawater characteristics at the study site during the March and July campaigns. Values are means ± SD

Parameter	July 2003	March 2004
Temperature (°C)	20.5–23.1	5.6–8.4
Salinity	31–32	29–31
Silicate (µmol l^{-1})	5.91 ± 0.51 (n = 4)	6.86 ± 2.63 (n = 4)
Phosphate (µmol l^{-1})	1.80 ± 0.27 (n = 4)	0.91 ± 0.76 (n = 4)
Ammonium (µmol l^{-1})	0.21 ± 0.07 (n = 4)	6.03 ± 4.11 (n = 4)
Nitrate + Nitrite (µmol l^{-1})	0.30 ± 0.02 (n = 4)	31.75 ± 4.45 (n = 4)
DIC (µmol l^{-1})	2082.82 ± 21.61 (n = 4)	2200.02 (n = 1)
DOC (mg l^{-1})	4.79 ± 1.98 (n = 5)	2.59 ± 1.48 (n = 6)
POC (mg l^{-1})	1.56 ± 0.13 (n = 2)	2.47 ± 0.06 (n = 3)
PN (mg l^{-1})	0.23 ± 0.01 (n = 2)	0.31 ± 0.03 (n = 3)

DISCUSSION

Our study highlights a process unique to intertidal, permeable sediments: the periodic release of concentrated nutrients through pore water seepage. This release is caused by the exposure of the sediments during ebb tide, which sets up a hydraulic pressure gradient between the pore water level and the seawater level (Nielsen 1990). The pressure gradient causes water flow through permeable sediment layers toward the seepage zone at the margin of the tidal flat, where pore water is released into tidal gullies. Re-inundation of the flat during flooding eliminates the pressure gradient, thereby discontinuing the seepage. In the following discussion, we contrast sediment–water exchange in subtidal and intertidal sand beds and discuss the characteristics of drainage release and its potential implications.

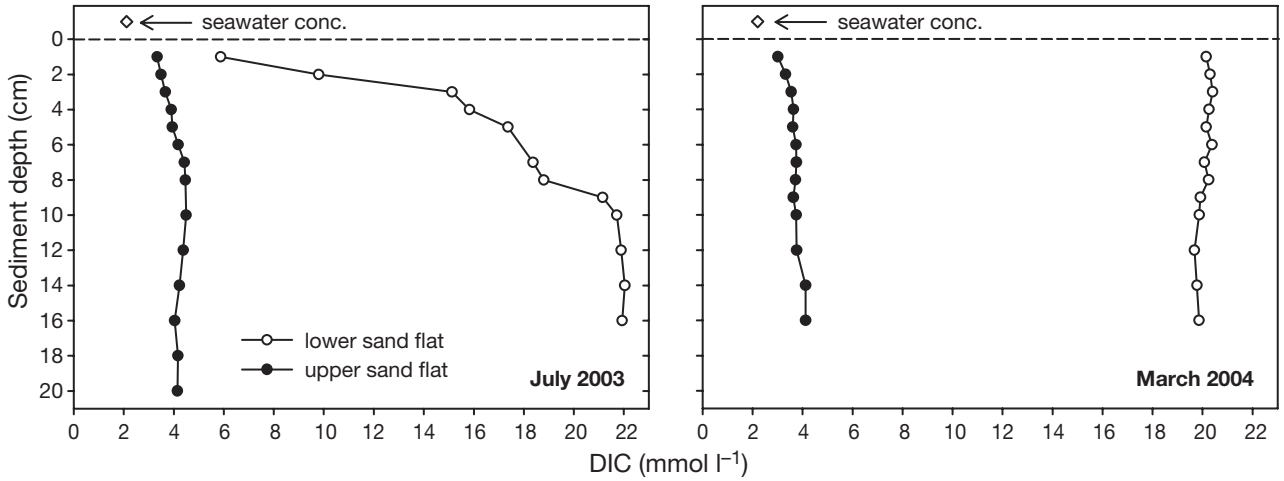

Fig. 9. Pore water dissolved inorganic carbon (DIC) concentration in upper (●) and lower (○) sand flat sites during July 2003 and March 2004. DIC concentration in overlying seawater is shown above dashed line

Sediment–water exchange in intertidal versus subtidal zones

Because of their draining mechanism, the sediment–water exchange of matter in intertidal sand flats distinctly differs from that in constantly submerged marine deposits during parts of the tidal cycle. While submerged, diffusion, pore water advection, and bioturbation govern sediment–water exchange in both subtidal and intertidal sandy beds. With the onset of exposure of the intertidal sediment during ebb tide, however, the exchange mechanisms in these sediments change abruptly. With little or no water being present above most of the sediment, diffusive and advective release of sedimentary materials and the activities of bioirrigating macrofauna are reduced to a minimum. The continuing drop of the water level initiates a decline in the water level in the sediment. A slow but directed pore water flow sets in, carrying solutes and small particles along the increasing

Table 5. Effluxes (positive values) and influxes (negative values) in µmol m^{-2} h^{-1} of nutrients, dissolved inorganic carbon (DIC) and oxygen in opaque and transparent chamber experiments conducted at the upper and lower sand flat sites in July 2003 (nd: not detectable). For fluxes calculated by linear regression, the r^2 is given in parentheses. All other fluxes were calculated from start–end concentrations. Chamber fluxes (advection + faunal activity + diffusion + drainage [where applicable]) and drainage fluxes ([flux 6.5 to 8 h] – [flux 0 to 6.5 h]) are given as average of 6 chambers, except for the average upper sand flat DIC flux, which was calculated from dark incubations only

Upper sand flat		Silicate 0–4 h	Phosphate 0–4 h	Ammonium 0–4 h	DIC 0–4 h	Oxygen 0–4 h
Opaque	1	–47 (0.70)	10 (0.30)	nd	4354 (0.89)	–1290 (0.95)
	2	2 (0.01)	60 (0.76)	nd	6824 (0.90)	–1642 (0.93)
	3	–60 (0.51)	28 (0.28)	nd	2513 (0.86)	–1469 (0.91)
Transparent	4	–56 (0.91)	nd	nd	1223	2050 (0.95)
	5	–46 (0.98)	–5 (0.56)	nd	747	1930 (0.90)
	6	–34 (0.74)	83 (0.72)	nd	4055	1493 (0.90)
Chamber flux		–40	29		4564	

Lower sand flat		0–6.5 h	6.5–8 h	0–6.5 h	6.5–8 h	0–6.5 h	6.5–8 h	0–6.5 h	6.5–8 h	0–6.5 h	6.5–8 h
Opaque	1	50 (0.45)	–166	12 (0.22)	178	92 (0.68)	576	1202 (0.98)	13792	–697 (0.95)	–1276 (0.87)
	2	285 (0.99)	2419	309 (0.97)	3070	1144 (0.98)	9449	12911 (0.85)	86993	–862 (0.92)	–5042 (0.98)
	3	–42 (1.00)	275	–1 (0.05)	58	–18 (0.31)	300	2623 (1.00)	17740	–1241 (0.95)	–3174 (0.86)
Transparent	4	35 (0.47)	836	55 (0.65)	794	391 (0.73)	3306	3199 (0.89)	28714	–646 (0.89)	–660 (0.54)
	5	158 (0.90)	767	155 (0.85)	1265	734 (0.96)	3455	6949 (0.96)	36594	–789 (0.88)	–1449 (0.62)
	6	108 (0.76)	–111	78 (0.91)	247	497 (0.96)	986	7540 (0.98)	36447	–695 (0.82)	–397 (0.19)
Chamber flux		99	670	101	935	473	3012	5737	36713		
Drainage flux			571		834		2539		30976		

hydraulic gradient toward the lower rim of the flat and the drainage gullies. Here, pore water release zones develop, similar to those in sandy beaches when a quickly falling tide decouples from the slower falling pore water table (Nielsen 1990, Horn 2002). Material release (except gases) from the exposed intertidal flats, thus, becomes mainly restricted to the seepage zones, and here the observed fluxes were significantly higher than interfacial fluxes recorded during inundation.

Our chamber experiments indicate that pore water was discharged in submerged parts of the tidal flat as soon as a sufficient hydraulic gradient was present. The pronounced increase in nutrient and DIC concentrations in all submerged chambers deployed on the lower flat site after the elevated upper flat became exposed reflected increased discharge of nutrient-rich seepage water into the chambers (the venting port of the chambers permitted slow fluid exchange) (Fig. 10, Table 5). We can exclude that enhanced metabolic activity at the lower site was the cause for these observed increases, because oxygen consumption rates measured during the first 6.5 h of chamber incubations (Table 5) and sulfate reduction rates (Billerbeck et al. in press) were similar at both study sites. A similar discharge of pore water into benthic chambers caused by tidal water level fluctuations was reported by Jahnke et al. (2003) for an intertidal salt marsh.

Different qualities of fluxes in submerged and exposed sediment

While in the subtidal and submerged intertidal, sediment–water fluxes may reflect seasonal changes in organic matter loading, biological activity and hydrodynamical forcings (Kristensen et al. 1997, D'Andrea et al. 2002, de Beer et al. 2005), the compositional changes of the seepage fluxes during exposure are governed by the length and biogeochemical characteristics of the pathways the pore water follows through the sediment. Although the measured drainage fluid velocity (March 0.54 cm h^{-1}, July 0.86 cm h^{-1}) exceeded transport by molecular diffusion by some orders of magnitude, about 16 to 29 tidal cycles are needed for pore water to travel 1 m through the sediment. Organic materials progressively degrade during passage through the sediment, with degradation of buried organic matter (e.g. microphytobenthos, macroalgae) contributing to the solute inventory of the pore water flow (Ehrenhauss et al. 2004). This may explain why the DIC and nutrient concentrations in the seepage water exceeded those in the pore water of the upper 20 cm of the upper flat by factors of 10 to 15. Furthermore, in contrast to the upper flat, the pore water nutrient and DIC concentrations of the lower flat did not show any seasonality, due to the long residence time, dispersion and mixing of the pore water in deeper layers of the tidal flat (Billerbeck et al. in press).

When integrated over areas exceeding several ripple wavelengths (few decimeters), the quality and quantity of solute fluxes from submerged sand beds is relatively homogeneous (Huettel 1990, Marinelli et al. 1998). In contrast, we observed large changes in the seepage solute concentrations draining from the exposed sand flat (Table 3). Draining of different sections and layers of the intertidal sand (while the water level falls and rises) produces variability in seepage water composition. Likewise, variation in fluxes between replicate chambers simultaneously deployed at the lower flat site suggests seepage heterogeneity on a relatively small spatial scale (Table 5). As a result of sediment heterogeneities (i.e. zones of different permeabilities), water flowed on preferential paths through the sand (Beven & Germann 1982, Harvey et al. 1995, DiCarlo et al. 1999), which led to spatial variability of seepage in the release zone. This variability was also reflected by black spots (<50 cm diameter) in the seepage zone, produced by local release of sulfidic pore water. Discharge rates for most measurements in the seepage zone, however, were similar (Fig. 7) when seepage was integrated over larger sediment areas as done by our seepage collectors (6 to 13 m^2 collection area).

Origin of seepage water

On average, 2.4 to 4.2 l m^{-2} d^{-1} of pore water was discharged on the lower sand flat site during spring and summer, respectively. The subsurface flows drained fluid from the sediment surface, water puddles that had remained on the surface gradually disappeared, and sections of the upper flat became visually 'dry'. The infiltration of surface water into the sediment carried oxygenated water (possibly O_2-oversaturated due to strong benthic photosynthesis: Revsbech et al. 1980, Revsbech & Jørgensen 1986), solutes and small particles into the sand (Huettel et al. 1998, Rusch et al. 2001, Ehrenhauss et al. 2004). Despite a continuous drop in the pore water level in the standpipes, the 'drying' of the sediment surface ceased with development of a water saturated capillary fringe (Gillham 1984, Turner & Nielsen 1997), extending upward from the pore water table to the sediment surface (Drabsch et al. 1999, Atherton et al. 2001).

Persistent water saturation of the sediment surface, while pore water flows and seepage continued, suggested fueling of the pore flows either through other sources (e.g. groundwater: Simmons 1992, Moore

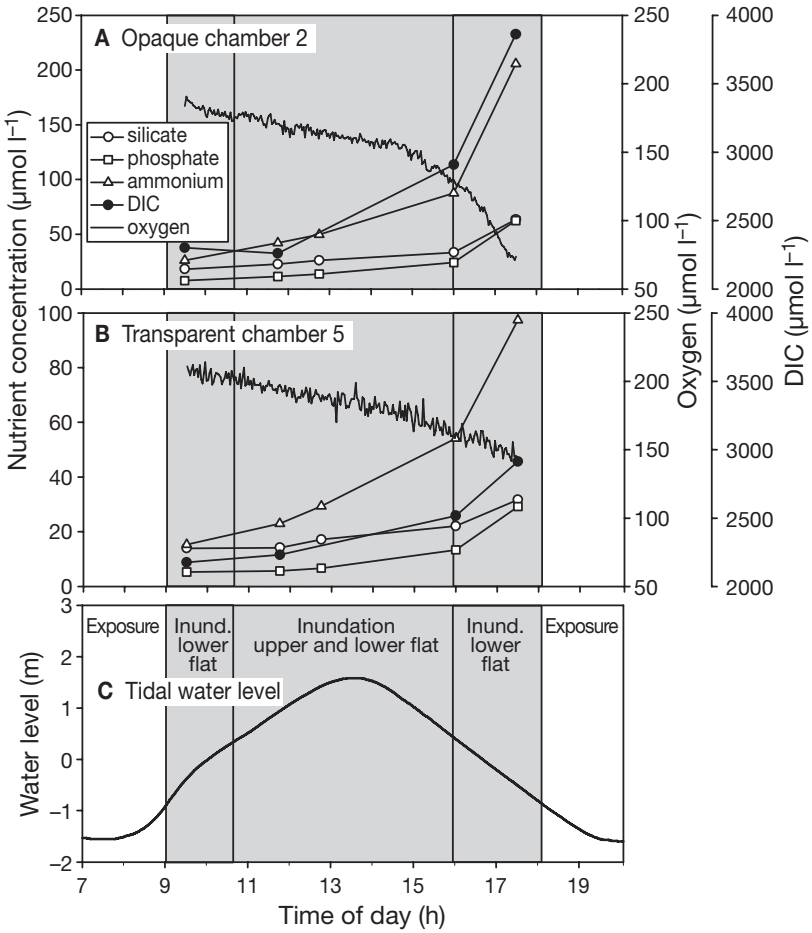

Fig. 10. Solute concentration changes at lower sand flat site measured in overlying water of (A) 1 opaque and (B) 1 transparent benthic chamber in July 2003. Shading marks the period of inundation for the upper and lower flats or lower flat only (delimited by vertical lines). (C) Tidal water level change based on mean sea level. Note the different scaling for nutrient concentrations in (A) and (B)

1996), or a gradual decrease in total tidal flat pore water volume through drainage. Terrestrial groundwater input is unlikely, since pore water chloride concentration remained nearly constant at seawater concentrations down to 4 m depth (Koelsch, pers. comm.) and salinity of the seepage water did not change. The gradual decrease in total pore water volume of the tidal flat without entrainment of air (which was never observed at the Janssand) would require shrinking of the tidal flat during exposure and subsequent swelling during inundation, resulting in small elevation changes of the tidal flat surface. Such oscillating changes in sediment elevation within a range of 1 to 3 mm due to changes in tidal water level have been detected in intertidal salt marshes (Paquette et al. 2004). We suggest that the seepage in Janssand also resulted in such pore volume changes, but that the resulting elevation changes would be smaller and difficult to detect. From each 1 m of the release zone (average 20 m wide), about 24 to 42 l of pore water were discharged per tidal cycle during March and July, respectively. These volumes would correspond to a sediment elevation change of 0.5 mm for March and 0.8 mm for July, assuming this volume was drained from the approximately 50 m wide zone adjacent to the release zone, where we observed water infiltration into the sediment. During reinundation, partial release of the capillary tension may initiate expansion of the pore space with simultaneous uptake of water.

Tidal filtration

Uptake and release of water during a tidal cycle represents a filtration process that characterizes the Janssand as a large biocatalytic sand filter (Fig. 11). From pore water release rates and seepage nutrient concentrations, we can roughly estimate the total filtration and potentially associated mineralization for the investigated section of tidal flat. During March, about 1.2 l m^{-2} pore water was discharged each tidal cycle from the release zone of the sand flat, assuming an average exposure time of 2 h per tide for that zone. On a length of 3.5 km on the northern and northeastern boundary of the Janssand tidal flat (see Fig. 1), the topography and sediment is similar to those at our study site. With an average width of the release zone of 20 m, a total of 168 000 l pore water was discharged each day from this area (ca. 70 000 m^2). In July, the drainage rates calculated based on the benthic chamber incubations were higher, producing on average 2.1 l m^{-2} $tide^{-1}$ (1.5 h discharge per tide) or a total discharge of 294 000 l d^{-1} for the 3.5 km long Janssand section. Assuming degradation of organic matter with a composition close to the Redfield ratio, the nutrient discharge associated with seepage would correspond to an average mineralization of about 200 mg m^{-2} organic carbon d^{-1} during March (356 mg C m^{-2} based on P, 86 mg C m^{-2} based on N) and 1600 mg C m^{-2} d^{-1} during July (3183 mg C m^{-2} d^{-1} based on P, 605 mg C m^{-2} d^{-1} based on N, 1115 mg C m^{-2} d^{-1} based on DIC). This corresponds to a roughly estimated yearly mineralization of 300 g C m^{-2} yr^{-1}. The observed low N:P ratios (3 to 4) may have resulted from a loss of NH_4^+ through coupled nitrification/denitrification or release of PO_4 from previously immobilized ironhydroxide-complexes, ensuing in the release of anoxic pore waters. It must be borne in mind, however, that the main

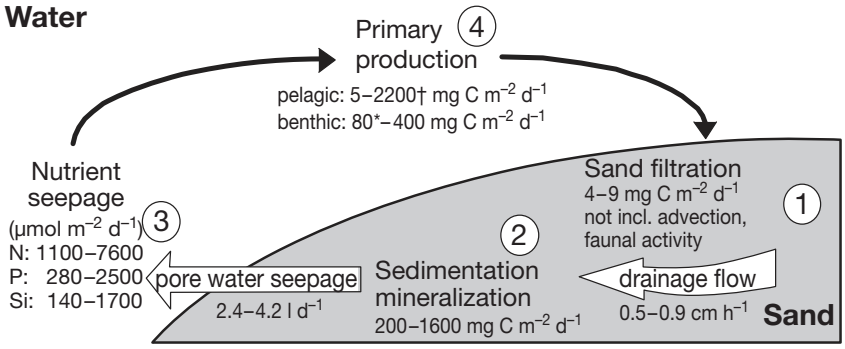

Fig. 11. Conceptual model of the Janssand filtration cycle. As a result of the hydraulic pressure gradient developing during low tide, water, suspended and dissolved matter infiltrates the sediment (1) and pore water flows through permeable sediment along the hydraulic gradient toward the tidal gully. Drainage flows transport substrates to the sedimentary microbial community, fueling mineralization (2) and carry metabolic products toward the seepage zone, where nutrient-enriched pore water is discharged (3). The seepage nutrients enhance primary production in the water column and on the sediments in the Wadden Sea (4). Replacement of discharged water volume with seawater during high tide filters organic matter into permeable sand (1) and the cycle starts anew. During inundation, additional organic matter is supplied to sediment by advection and faunal activity. *Billerbeck (unpubl., from March 2002); †gross water column production in the German Wadden Sea (from Tillmann et al. 2000)

body of the tidal flat acts as a seasonally independent nutrient source to the ecosystem through drainage (Billerbeck et al. in press). Therefore, the nutrients released from the lower flat may reflect mineralization processes occurring over long time spans and flow paths within the tidal flat. Nevertheless, the estimated mineralization rates are in the range of rates determined in both seasons for full tidal cycles on this tidal flat (967 and 2401 mg C m^{-2} d^{-1} for March and July, respectively (Billerbeck et al. in press).

Extrapolated to the 3.5 km long region of the Janssand tidal flat, the pore water discharge would amount to a total required organic carbon mineralization of 6 to 25 kg d^{-1} during March and 42 to 223 kg d^{-1} during July, based on ammonium and phosphate discharge, respectively (78.1 kg d^{-1} based on DIC fluxes in July). Assuming that 100% of the DOC and 50% of the POC in the overlying seawater (Table 4) is transported into the sediment, about 4 to 9 mg C m^{-2} d^{-1} are filtered into the 50 m wide infiltration zone as a consequence of drainage during March and July, respectively. This totals to 0.6 kg (March) or 1.6 kg (July) for the 3.5 km long Janssand section (175 000 m^2 infiltration area). These amounts can only account for a fraction of the mineralization required to produce the observed nutrient release. Fresh organic matter may be introduced to the sediment by advective infiltration during inundation (Huettel & Rusch 2000) and by filtering, bioirrigating and bioturbating fauna (Graf & Rosenberg 1997, Aller 2001). Buried mud lenses, such as those found in the lower flat, may be another source of organic matter and nutrients for this tidal flat. However, pore water nutrient concentrations did not reflect the location of these mud inclusions in the sediment cores. Probably the most important organic carbon source in this tidal flat is benthic primary production. Extrapolated to the total area of 245 000 m^2 of tidal flat that is influenced by infiltration and discharge, and assuming a 10 h light period during July, the average gross photosynthetic production of 3300 µmol C m^{-2} h^{-1} for the chamber incubations in the upper sand flat corresponds to a total organic carbon production of 97 kg d^{-1}. This rough estimate can account for about half of the carbon mineralization required to match the observed nutrient export during summer, but benthic primary production should be even higher during exposure of the tidal flat (Pinckney & Zingmark 1991).

Regardless of the origin of the organic matter, our estimate indicates that the Janssand intertidal flat does not accumulate organic matter, but releases mineralization products that can account for all the organic matter potentially filtered through the permeable beds by drainage during each tidal cycle, and for the material generated by benthic primary production. These findings suggest that these sands mineralize all organic matter that is introduced to the sediment, emphasizing their role as biocatalytic filter systems.

Potential significance of seepage

The pore water release locally affects the benthos and, on a larger spatial scale, the nutrient concentrations in the intertidal zone. In the vicinity of the seepage zone, the increased nutrient concentrations in the seepage water can support the benthic primary production; however, in July 2003, the chlorophyll *a* (chl *a*) inventory in the upper 5 cm of the sediment was similar for the upper and lower flat sites (10 to 11 µg g^{-1} chl *a* at both sites). Adverse effects of the seepage water may have masked the positive influence of nutrient enrichment. During summer, when seepage sulfide reached 1 mmol l^{-1}, the otherwise omnipresent diatoms were replaced by green flagellates and sulfide oxidizers (C.M. Burke & D. de Beer pers. comm.), and *Arenicola marina* fecal mounds in the release zone decreased from 3.6 m^{-2} on the upper flat to 0.6 m^{-2} on the lower flat (6-fold).

Table 6. Comparison of discharge volumes and nutrient release rates in this study with rates reported for other coastal systems

Location	Discharge rate (l m^{-2} d^{-1})	N discharge (µmol m^{-2} d^{-1})	P discharge (µmol m^{-2} d^{-1})	Si discharge (µmol m^{-2} d^{-1})	Method	Source
Beaches						
Alexandria dune field, South Africa	1000[a]	151857[a]	2065[a]		Darcy's law, nutrients	McLachlan & Illenberger (1986)
Threemile Beach, OR	3000–4500[a]				Darcy's law	McLachlan (1989)
Alexandria dune field, South Africa	157–328[a]	185714–400000[a]			Darcy's law, nutrients	Campbell & Bate (1998)
Kashima coast, Japan	283.5–405[a]	77676[a]	5132[a]	452626[a]	Darcy's law, nutrients	Uchiyama et al. (2000)
Cape Henlopen, DE	600–3200[a]	300000–1600000[a]	30000–160000[a]	140000–800000[a]	Darcy's law, nutrients	Ullman et al. (2003)
Submarine groundwater discharge						
Long Island, NY	10.0–70.0				Seepage meter	Bokuniewicz & Pavlik (1990)
Cape Cod, MA	24.0–72.0	300 mmol N m^{-3} yr^{-1}			Seepage meter	Giblin & Gaines (1990)
Florida Keys, FL	5.4–8.9	1.3–2.7 mol s^{-1}	0.5–1.0 mol s^{-1}		Seepage meter	Simmons (1992)
Wilmington, NC	6.0–20.0				Seepage meter	
Cherrystone Inlet, VA	0.48–88.6	3926.4			Seepage meter	Reay et al. (1992)
South Atlantic Bight	5.0				226 Ra-activity	Moore (1996)
Puck Bay, Baltic Sea	0.4				Nutrients, isotopes	Piekarek-Jankowska (1996)
Northeast Gulf of Mexico, FL	15.8–33.1				Seepage meter	Cable et al. (1997)
Florida Bay, FL	10.4–30.5	301.4	0.6		Seepage meter	Corbett et al. (1999)
Great Sippewissett, MA	9.8				226 Ra-activity	Charette et al. (2003)
Eckernfoerde Bay, Baltic Sea	0.5				Pore water modeling	Schlueter et al. (2004)
Osaka Bay, Japan	10.3–81.9				Seepage meter	Taniguchi & Iwakawa (2004)
Salt marshes						
Great Sippewissett, MA	12.0				Darcy's law	Hemond & Fifield (1982)
North Inlet, SC	15.2–168.0				Water balance	Agosta (1985)
Rhode River, MD	60[a]	45.7–62.1[a]	7.8–15.5[a]		Darcy's law, nutrients	Jordan & Correll (1985)
Pender County, NC	0.1–0.9				Seepage meter	Yelverton & Hackney (1986)
North Inlet, SC	7.8–28.0	344.4–615.6	6.5–15.8		Seepage meter	Whiting & Childers (1989)
Eagle Bottom, Carter Creek, VA	0.2–1				Darcy's law	Harvey & Odum (1990)
Great Sippewissett, MA	30.4	332.9			Seepage meter	Howes & Goehringer (1994)
North Inlet, SC	9.4–16.6				Salt balance	Morris (1995)
Phillips Creek, VA	0.4				Water balance	Harvey & Nuttle (1995)
Pritchards Island, SC	114.8	476.7	30.1		Seepage meter	Osgood (2000)
Hog Island, VA	120.2	531.5	189		Seepage meter	
Ringfield Marsh, VA	0.6–22.6	802.5			Salt balance	Tobias et al. (2001)
Satilla River Estuary, GA	0.4–0.6[b]	500 000			Benthic chambers	Jahnke et al. (2003)
Tidal flats						
Le Havre, Marennes-Oleron, France	20.0				Runnel-runoff velocity	Le Hir et al. (2000)
Humber Estuary, UK						
Island of Spiekeroog, Germany	2.4	1074	280	141	V-shaped laths (Mar)	This study
	4.2	7616	2503	1713	Benthic chambers (Jul)	

[a]Discharge m^{-1} shoreline; [b]localized discharge (l cm^{-2} d^{-1})

Most nutrients released through seepage are transported through the tidal gullies toward the North Sea (Niesel & Günther 1999), where they can fuel primary production seaward of the barrier islands. Tidal currents transport the organic matter produced within these highly net autotrophic coastal waters back to the Wadden Sea, where it is mineralized (Postma 1954, van Beusekom et al. 1999). Because the seepage becomes most active only near maximum low tide and the average width of the sand flat belt along the southern coast of the North Sea is 13 km (van Beusekom & de Jonge 2002), a large fraction of the nutrients will remain within the Wadden Sea, where they can enhance primary production of phytoplankton and microphytobenthos.

Thus, microalgal production, tidal flat filtration of this organic matter, mineralization within the intertidal sands and subsequent release of nutrients form a recycling loop, in which seepage plays an important role (Fig. 11). This coastal nutrient cycling resembles the mechanism of sediment–water column interaction proposed by Childers (1994) for salt marshes with tidal ranges exceeding 1 m. In the Janssand, nutrient fluxes associated with the seepage exceeded by 5- to 8-fold those fluxes caused by the combined effects of diffusion, advection and bioirrigation during inundation. The ecological importance of groundwater or pore water discharge and the associated export of metabolic products to the water column has been emphasized in studies covering submarine groundwater discharge, wave dominated beaches and salt marshes (Table 6). However, only a few data are available on drainage for intertidal flats. Nutrient export from the Janssand through seepage surpassed the release rates reported in most other studies (Table 6), emphasizing the ecological importance of the seepage process in intertidal sands and the need for further, more detailed studies on this subject.

Acknowledgements. We thank Martina Alisch for the assistance with field and laboratory work and also acknowledge the hospitality and help of the Plattboden ship crews during the cruises. We also thank Gaby Schüssler, Susanne Menger, Daniela Franzke and Sindy Pabel for their help with laboratory work and Cäcilia Wigand for the preparation of the oxygen optodes. This study would not have been possible without the technical assistance of Jens Langreder, Axel Nordhausen, Georg Herz, Alfred Kutsche, Paul Färber, Volker Meyer, and Harald Osmers. Thomas Badewien of the ICBM in Oldenburg and Waldmar Anton of the WSA Emden kindly provided tide gauge data. We appreciate the valuable comments of Antje Boetius, Perran Cook, Stefan Jansen, and Christian Wild on the manuscript. The comments of Professor V. de Jonge and 4 anonymous referees greatly helped to improve the manuscript. This study was supported by the Deutsche Forschungsgemeinschaft (DFG) within the research group 'Biogeochemistry of the Wadden Sea' (FG 432-5), coordinated by Jürgen Rullkötter. We are grateful to Bo Barker Jørgensen and Michael Böttcher for their support of this work and coordination of the sub-project 'Biogeochemical processes at the sediment-water interface of intertidal sediments'.

LITERATURE CITED

Agosta K (1985) The effect of tidally induced changes in the creekbank water table on pore water chemistry. Estuar Coast Shelf Sci 21:389–400

Aller RC (2001) Transport and reactions in the bioirrigated zone. In: Boudreau BP, Jørgensen BB (eds) The Benthic Boundary Layer. Oxford University Press, Oxford, p 269–301

Atherton RJ, Baird AJ, Wiggs GFS (2001) Inter-tidal dynamics of surface moisture content on a meso-tidal beach. J Coast Res 17:482–489

Beven K, Germann P (1982) Macropores and water flow in soils. Water Resour Res 18:1311–1325

Billerbeck M, Werner U, Polerecky L, Walpersdorf E, de Beer D, Huettel M (in press) Surficial and deep pore water circulation governs spatial and temporal scales of nutrient recycling in intertidal sand flat sediment. Mar Ecol Prog Ser

Bokuniewicz H, Pavlik B (1990) Groundwater seepage along a barrier-island. Biogeochemistry 10:257–276

Cable JE, Burnett WC, Chanton JP, Corbett DR, Cable PH (1997) Field evaluation of seepage meters in the coastal marine environment. Estuar Coast Shelf Sci 45:367–375

Campbell EE, Bate GC (1998) Tide-induced pulsing of nutrient discharge from an unconfined aquifer into an *Anaulus australis*-dominated surf-zone. Water S A 24:365–370

Charette MA, Splivallo R, Herbold C, Bollinger MS, Moore WS (2003) Salt marsh submarine groundwater discharge as traced by radium isotopes. Mar Chem 84:113–121

Childers DL (1994) Fifteen years of marsh flumes: a review of marsh–water column interactions in southeastern USA estuaries. In: Mitsch WJ (ed) Global wetlands: old world and new. Elsevier, Amsterdam, p 277–293

Corbett DR, Chanton J, Burnett W, Dillon K, Rutkowski C, Fourqurean JW (1999) Patterns of groundwater discharge into Florida Bay. Limnol Oceanogr 44:1045–1055

D'Andrea AF, Aller RC, Lopez GR (2002) Organic matter flux and reactivity on a South Carolina sandflat: the impacts of porewater advection and macrobiological structures. Limnol Oceanogr 47:1056–1070

de Beer D, Wenzhöfer F, Ferdelman TG, Boehme SE and 5 others (2005) Transport and mineralization rates in North Sea sandy intertidal sediments, Sylt-Rømø Basin, Wadden Sea. Limnol Oceanogr 50:113–127

DiCarlo DA, Bauters TWJ, Darnault CJG, Steenhuis TS, Parlange JY (1999) Lateral expansion of preferential flow paths in sands. Water Resour Res 35:427–434

Drabsch JM, Parnell KE, Hume TM, Dolphin TJ (1999) The capillary fringe and the water table in an intertidal estuarine sand flat. Estuar Coast Shelf Sci 48:215–222

Ehrenhauss S, Witte U, Bühring SL, Huettel M (2004) Effect of advective pore water transport on distribution and degradation of diatoms in permeable North Sea sediments. Mar Ecol Prog Ser 271:99–111

Flemming BW, Ziegler K (1995) High-resolution grain size distribution patterns and textural trends in the backbarrier environment of Spiekeroog Island (southern North Sea). Senckenb Marit 26:1–24

Forster S, Glud RN, Gundersen JK, Huettel M (1999) In situ study of bromide tracer and oxygen flux in coastal sediments. Estuar Coast Shelf Sci 49:813–827

Giblin AE, Gaines AG (1990) Nitrogen inputs to a marine embayment—the importance of groundwater. Biogeochemistry 10:309–328

Gillham RW (1984) The capillary-fringe and its effect on water-table response. J Hydrol (Anst) 67:307–324

Graf G, Rosenberg R (1997) Bioresuspension and biodeposition: a review. J Mar Syst 11:269–278

Grasshoff K, Kremling K, Ehrhardt M (1999) Methods of seawater analysis. Wiley-VCH, Berlin

Hall POJ, Aller RC (1992) Rapid, small-volume, flow injection analysis for ΣCO_2 and NH_4^+ in marine and freshwaters. Limnol Oceanogr 37:1113–1119

Harvey JW, Nuttle WK (1995) Fluxes of water and solute in a coastal wetland sediment. 2. Effect of macropores on solute exchange with surface water. J Hydrol 164:109–125

Harvey JW, Odum WE (1990) The influence of tidal marshes on upland groundwater discharge to estuaries. Biogeochemistry 10:217–236

Harvey JW, Chambers RM, Hoelscher JR (1995) Preferential flow and segregation of porewater solutes in wetland sediment. Estuaries 18:568–578

Hemond HF, Fifield JL (1982) Subsurface flow in salt-marsh peat—a model and field-study. Limnol Oceanogr 27:126–136

Hertweck G (1995) Distribution patterns of characteristic sediment bodies and benthos populations in the Spiekeroog backbarrier tidal flat area, southern North Sea. 1. Results of a survey of tidal flat structure. 1988–1992 Senckenb Marit 26:81–94

Holst G, Glud RN, Kühl M, Klimant I (1997) A microoptode array for fine-scale measurement of oxygen distribution. Sensors Actuators B 38:122–129

Horn DP (2002) Beach groundwater dynamics. Geomorphology 48:121–146

Howes BL, Goehringer DD (1994) Porewater drainage and dissolved organic carbon and nutrient losses through the intertidal creekbanks of a New England salt marsh. Mar Ecol Prog Ser 114:289–301

Huettel M (1990) Influence of the lugworm *Arenicola marina* on porewater nutrient profiles of sand flat sediments. Mar Ecol Prog Ser 62:241–248

Huettel M, Gust G (1992) Solute release mechanism from confined sediment cores in stirred benthic chambers and flume flows. Mar Ecol Prog Ser 82:187–197

Huettel M, Rusch A (2000) Transport and degradation of phytoplankton in permeable sediment. Limnol Oceanogr 45:534–549

Huettel M, Ziebis W, Forster S (1996) Flow-induced uptake of particulate matter in permeable sediments. Limnol Oceanogr 41:309–322

Huettel M, Ziebis W, Forster S, Luther GW (1998) Advective transport affecting metal and nutrient distributions and interfacial fluxes in permeable sediments. Geochim Cosmochim Acta 62:613–631

Huettel M, Røy H, Precht E, Ehrenhauss S (2003) Hydrodynamical impact on biogeochemical processes in aquatic sediments. Hydrobiologia 494:231–236

Jahnke RA, Alexander CR, Kostka JE (2003) Advective pore water input of nutrients to the Satilla River Estuary, Georgia, USA. Estuar Coast Shelf Sci 56:641–653

Jordan TE, Correll DL (1985) Nutrient chemistry and hydrology of interstitial water in brackish tidal marshes of Chesapeake Bay. Estuar Coast Shelf Sci 21:45–55

Klimant I, Meyer V, Kühl M (1995) Fiberoptic oxygen microsensors, a new tool in aquatic biology. Limnol Oceanogr 40:1159–1165

Kristensen E, Jensen MH, Jensen KM (1997) Temporal variations in microbenthic metabolism and inorganic nitrogen fluxes in sandy and muddy sediments of a tidally dominated bay in the northern Wadden Sea. Helgol Mar Res 51:295–320

Kuwae T, Hosokawa Y, Eguchi N (1998) Dissolved inorganic nitrogen cycling in Banzu intertidal sand-flat, Japan. Mangroves Salt Marshes 2:167–175

Le Hir P, Roberts W, Cazaillet O, Christie M, Bassoullet P, Bacher C (2000) Characterization of intertidal flat hydrodynamics. Cont Shelf Res 20:1433–1459

Lorenzen CJ (1967) Determination of chlorophyll and pheopigments: spectrophotometric equations. Limnol Oceanogr 12:343–346

Marinelli RL, Jahnke RA, Craven DB, Nelson JR, Eckman JE (1998) Sediment nutrient dynamics on the South Atlantic Bight continental shelf. Limnol Oceanogr 43:1305–1320

McLachlan A (1989) Water filtration by dissipative beaches. Limnol Oceanogr 34:774–780

McLachlan A, Illenberger W (1986) Significance of groundwater nitrogen input to a beach surf zone ecosystem. Stygologia 2:291–296

Moore WS (1996) Large groundwater inputs to coastal waters revealed by Ra-226 enrichments. Nature 380:612–614

Morris JT (1995) The mass-balance of salt and water in intertidal sediments—Results from North-Inlet, South Carolina. Estuaries 18:556–567

Nielsen P (1990) Tidal dynamics of the water table in beaches. Water Resour Res 26:2127–2134

Niesel V, Günther CP (1999) Distribution of nutrients, algae and zooplankton in the Spiekeroog backbarrier system. In: Dittmann S (ed) The Wadden Sea ecosystem—stability properties and mechanisms. Springer-Verlag, Berlin, p 77–94

Osgood DT (2000) Subsurface hydrology and nutrient export from barrier island marshes at different tidal ranges. Wetlands Ecol Manag 8:133–146

Paquette CH, Sundberg KL, Boumans RMJ, Chmura GL (2004) Changes in saltmarsh surface elevation due to variability in evapotranspiration and tidal flooding. Estuaries 27:82–89

Piekarek-Jankowska H (1996) Hydrochemical effects of submarine groundwater discharge to the Puck Bay (Southern Baltic Sea, Poland). Geogr Polon 67:103–119

Pilditch CA, Emerson CW, Grant J (1997) Effect of scallop shells and sediment grain size on phytoplankton flux to the bed. Cont Shelf Res 17:1869–1885

Pinckney J, Zingmark RG (1991) Effects of tidal stage and sun angles on intertidal benthic microalgal productivity. Mar Ecol Prog Ser 76:81–89

Postma H (1954) Hydrography of the Dutch Wadden Sea. Arch Néerl Zool 10:405–511

Precht E, Huettel M (2004) Rapid wave-driven advective pore water exchange in a permeable coastal sediment. J Sea Res 51:93–107

Reay WG, Gallagher DL, Simmons GM (1992) Groundwater discharge and its impact on surface-water quality in a Chesapeake Bay inlet. Water Resour Bull 28:1121–1134

Revsbech NP, Jørgensen BB (1986) Microelectrodes: their use in microbial ecology. In: Marshall KC (ed) Advances in microbial ecology. Vol 9. Plenum Press, London, p 293–352

Revsbech NP, Sorensen J, Blackburn TH, Lomholt JP (1980) Distribution of oxygen in marine sediments measured with microelectrodes. Limnol Oceanogr 25:403–411

Rusch A, Forster S, Huettel M (2001) Bacteria, diatoms and detritus in an intertidal sandflat subject to advective transport across the water–sediment interface. Biogeochemistry 55:1–27

Schlüter M, Sauter EJ, Andersen CE, Dahlgaard H, Dando PR (2004) Spatial distribution and budget for submarine groundwater discharge in Eckernförde Bay (Western Baltic Sea). Limnol Oceanogr 49:157–167

Shinn EA, Reich CD, Hickey TD (2002) Seepage meters and Bernoulli's revenge. Estuaries 25:126–132

Simmons GM Jr (1992) Importance of submarine groundwater discharge (SGWD) and seawater cycling to material flux across sediment/water interfaces in marine environments. Mar Ecol Prog Ser 84:173–184

Sundbäck K, Miles A, Göransson E (2000) Nitrogen fluxes, denitrification and the role of microphytobenthos in microtidal shallow-water sediments: an annual study. Mar Ecol Prog Ser 200:59–76

Taniguchi M, Iwakawa H (2004) Submarine groundwater discharge in Osaka Bay, Japan. Limnology 5:25–32

Tillmann U, Hesse KJ, Colijn F (2000) Planktonic primary production in the German Wadden Sea. J Plankton Res 22:1253–1276

Tobias CR, Harvey JW, Anderson IC (2001) Quantifying groundwater discharge through fringing wetlands to estuaries: seasonal variability, methods comparison, and implications for wetland–estuary exchange. Limnol Oceanogr 46:604–615

Turner IL, Nielsen P (1997) Rapid water table fluctuations within the beach face—implications for swash zone sediment mobility. J Coast Engin 32:45–59

Uchiyama Y, Nadaoka K, Rolke P, Adachi K, Yagi H (2000) Submarine groundwater discharge into the sea and associated nutrient transport in a sandy beach. Water Resour Res 36:1467–1479

Ullman WJ, Chang B, Miller DC, Madsen JA (2003) Groundwater mixing, nutrient diagenesis, and discharges across a sandy beachface, Cape Henlopen, Delaware (USA). Estuar Coast Shelf Sci 57:539–552

Usui T, Koike I, Ogura N (1998) Tidal effect on dynamics of pore water nitrate in intertidal sediment of a eutrophic estuary. J Oceanogr 54:205–216

van Beusekom JEE, de Jonge VN (2002) Long-term changes in Wadden Sea nutrient cycles: importance of organic matter import from the North Sea. Hydrobiologia 475: 185–194

van Beusekom JEE, Brockmann UH, Hesse KJ, Hickel W, Poremba K, Tillmann U (1999) The importance of sediments in the transformation and turnover of nutrients and organic matter in the Wadden Sea and German Bight. Dtsch Hydrogr Z 51:245–266

Whiting GJ, Childers DL (1989) Subtidal advective water flux as a potentially important nutrient input to southeastern USA saltmarsh estuaries. Estuar Coast Shelf Sci 28:417–431

Yelverton GF, Hackney CT (1986) Flux of dissolved organic carbon and pore water through the substrate of a *Spartina alterniflora* marsh in North Carolina. Estuar Coast Shelf Sci 22:255–267

Ziebis W, Huettel M, Forster S (1996) Impact of biogenic sediment topography on oxygen fluxes in permeable sediments. Mar Ecol Prog Ser 140:227–237

Editorial responsibility: Howard I. Browman (Associate Editor-in-Chief), Storebø, Norway

Submitted: September 16, 2005; Accepted: March 7, 2006
Proofs received from author(s): June 6, 2006

Benthic photosynthesis in submerged Wadden Sea intertidal flats

M. Billerbeck, H. Røy, K. Bosselmann, M. Huettel

This chapter is published in

ESTUARINE COASTAL AND SHELF SCIENCE

71 (3-4): 704-716 FEB 2007

Available online at www.sciencedirect.com
ScienceDirect
Estuarine, Coastal and Shelf Science 71 (2007) 704–716
ESTUARINE COASTAL AND SHELF SCIENCE
www.elsevier.com/locate/ecss

Benthic photosynthesis in submerged Wadden Sea intertidal flats

Markus Billerbeck*, Hans Røy, Katja Bosselmann[1], Markus Huettel[2]

Microbial Habitats, Max Planck Institute for Marine Microbiology, Celsiusstrasse 1, 28359 Bremen, Germany

Received 16 June 2006; accepted 22 September 2006
Available online 7 November 2006

Abstract

In this study we compare benthic photosynthesis during inundation in coarse sand, fine sand, and mixed sediment (sand/mud) intertidal flats in the German Wadden Sea. In situ determinations of oxygen-, DIC- and nutrient fluxes in stirred benthic chamber incubations were combined with measurements of sedimentary chlorophyll, incident light intensity at the sediment surface and scalar irradiance within the sediment. During submergence, microphytobenthos was light limited at all study sites as indicated by rapid response of gross photosynthesis to increasing incident light at the sea floor. However, depth integrated scalar irradiance was 2 to 3 times higher in the sands than in the mud. Consequently, gross photosynthesis in the net autotrophic fine sand and coarse sand flats during inundation was on average 4 and 11 times higher than in the net heterotrophic mud flat, despite higher total chlorophyll concentration in mud. Benthic photosynthesis may be enhanced in intertidal sands during inundation due to: (1) higher light availability to the microphytobenthos in the sands compared to muds, (2) more efficient transport of photosynthesis-limiting solutes to the microalgae with pore water flows in the permeable sands, and (3) more active metabolic state and different life strategies of microphytobenthos inhabiting sands.

Keywords: benthic photosynthesis; tidal flats; inundation; light availability; advective transport; Germany; North Sea; Wadden Sea

1. Introduction

Microphytobenthos contributes significantly to total primary production in intertidal ecosystems (MacIntyre et al., 1996; Underwood and Kromkamp, 1999). Benthic microalgae are a central component supporting the coastal food chain (Middelburg et al., 2000; Herman et al., 2001), they influence oxygen and nutrient fluxes across the sediment water interface (Bartoli et al., 2003; Tyler et al., 2003) and they are critical for coastal sea bed dynamics through stabilization of sediments by their extracellular polymeric substances (Smith and Underwood, 1998; Widdows et al., 2000; Yallop et al., 2000). Biomass, light- and CO_2 availability have been identified to determine microphytobenthic production (Admiraal et al., 1982; MacIntyre et al., 1996; Barranguet et al., 1998). Nutrients are often not a limiting factor in intertidal sediment (Barranguet et al., 1998; Serôdio and Catarino, 2000; Migne et al., 2004) as the microphytobenthos can assimilate nutrients from both the overlying water and the sediment pore water (MacIntyre et al., 1996; Cahoon, 1999).

In the intertidal regions of the German Wadden Sea, sandy sediments are predominant, while muddy sediments are restricted to relatively narrow low energy zones close to the coastline (Flemming and Ziegler, 1995). Muddy sediments exhibit high rates of benthic primary production (Pomeroy, 1959; Leach, 1970) and tend to have a higher microphytobenthic biomass than sandy sediments (Colijn and Dijkema, 1981; de Jong and de Jonge, 1995). Nevertheless, primary production in intertidal sand flats can be equally high as in mud flats during low tide exposure (Barranguet et al., 1998). In the dynamic intertidal habitat, high microphytobenthic productivity

* Corresponding author.
E-mail addresses: mbillerb@mpi-bremen.de (M. Billerbeck), hroey@mpi-bremen.de (H. Røy), bosselmann@ftz-west.uni-kiel.de (K. Bosselmann), mhuettel@ocean.fsu.edu (M. Huettel).
[1] Present address: Forschungs- und Technologiezentrum Westküste (FTZ), Hafentörn 1, 25761 Büsum, Germany.
[2] Present address: Department of Oceanography, Florida State University, West Call Street, Tallahassee, FL 32306-4320, USA.

0272-7714/$ - see front matter © 2006 Elsevier Ltd. All rights reserved.
doi:10.1016/j.ecss.2006.09.019

can be sustained by regular resuspension events that keep the algal standing stock below the maximum carrying capacity of the system (Blanchard et al., 2001). Resuspension of benthic algae is more likely in high-energy environments like sand flats. More frequent mixing events and higher degradation rates in sand than in mud cause a higher turnover of algal biomass in intertidal sandy sediment of the Dutch Wadden Sea (Middelburg et al., 2000). Therefore, high benthic productivity can possibly be more effectively sustained in sandy sediments than in muds.

As a result of the frequently highly turbid water near the coast, light is the principal limiting factor for primary production in the water column of the Wadden Sea (Veldhuis et al., 1988; Tillmann et al., 2000; Colijn and Cadee, 2003) and may also limit benthic photosynthesis. Therefore, in several studies, microphytobenthos production in intertidal sediments has been assumed to be mostly restricted to the exposure period (e.g. Serôdio and Catarino, 2000; Guarini et al., 2002; Migne et al., 2004). However, photosynthetic production of benthic microalgae can be sustained at low light intensities of about 5–10 μmol photons m^{-2} s^{-1} (Cahoon, 1999 and references therein). Furthermore, the early studies of Cadee and Hegeman (1974, 1977) suggest that benthic primary production takes place also during inundation. Asmus (1982) showed that the microphytobenthos contributed 68% to total primary production during inundation of a sand flat in Sylt, Germany, in an area where water is relatively clear (Asmus et al., 1998).

Light limitation during flooding is possibly more severe over mud flats than sand flats, as fine sediments are more easily resuspended by waves and currents and have much longer settling times than sand. Motile benthic microalgae migrate into the sediment surface layer during inundation to prevent erosion (Janssen et al., 1999; Mitbavkar and Anil, 2004) and consequentially depend on the light availability within the sediment. Light is typically more effectively absorbed in muddy sediment than in sand (Haardt and Nielsen, 1980; Kühl et al., 1994). Thus, benthic microalgae in sand flats may profit from a higher light availability within the sediment as compared to the microphytobenthos in mudflats.

The production of benthic microalgae can be limited by CO_2 availability (Admiraal et al., 1982; Rasmussen et al., 1983). Intense CO_2 assimilation of microphytobenthos can result in pH values above 9 within the photic zone of the sediment (Revsbech and Jørgensen, 1986) and reduced free CO_2 concentrations limiting primary production (Rasmussen et al., 1983; Cook and Røy, 2006). Recent laboratory and field studies suggest that this CO_2 limitation can be relieved by increased advective flushing of the photic zone (Cook and Røy, 2006; Wenzhöfer et al., in preparation).

We hypothesize that during inundation, benthic photosynthesis may be enhanced in intertidal sand flats as compared to mud flats due to higher light availability, more effective solute transport to the algae counteracting CO_2 and nutrient limitation and ensuing more active metabolic state of the microalgal community. We tested this hypothesis by conducting light and dark incubations with advection chambers in coarse, fine, and mixed sand/mud intertidal sediments of the German Wadden Sea. Interpretations of the flux recordings were supported by concurrent measurements of sedimentary chlorophyll, in situ incident light intensity and scalar irradiance within the sediment.

2. Methods

2.1. Study sites

In situ measurements and sampling were carried out in two intertidal sand flats and one mixed sand/mud flat in the German Wadden Sea (Fig. 1). The coarse sand site was located on the sand flat "Hausstrand" (55°00′53″ N, 008°26′17″ E) on the island of Sylt. The fine sand site on the intertidal flat "Janssand" (53°44′07″ N, 007°41′57″ E) and the mixed flat near Neuharlingersiel (53°42′09″ N, 007°42′33″ E) were both situated in the backbarrier area of the island of Spiekeroog. Henceforth, the Sylt, Janssand and Neuharlingersiel sites are denoted as coarse sand, fine sand and mud site, respectively. During high tide, the coarse sand and fine sand sites are covered by 1.5–2 m of water, the mud site by 1–1.5 m of water. Investigations took place during spring, summer and autumn 2002, and Summer 2003 (Table 1). In situ measurements with benthic chambers were not possible during winter due to frozen sediments and adverse weather conditions.

2.2. Sediment characteristics

Grain size was analysed by dry-sieving the top 10 cm of the sediment and classified according to Wentworth (1922). Permeability was determined with the constant head method (Klute and Dirksen, 1986) for the top 15 cm of the sediment at the two sandy sites and for the top 4 cm at the mud site. Sediment samples for total carbon (TC) and total inorganic carbon (TIC) measurements were sectioned into 1 cm intervals and stored frozen.

2.3. Chlorophyll analysis

For the measurement of chlorophyll, the top 10 cm of the sediment at the two sandy sites were sectioned in 0.5 cm intervals down to 5 cm depth, and in 1 cm intervals below. At the mud site, the top 5 cm of the sediment were sectioned in 0.2–0.5 cm intervals down to 2 cm depth, and in 0.5 cm intervals below. During spring 2002, the upper 5 cm of the sediment at the mud site were pooled. All sediment samples for chlorophyll analysis were kept frozen and dark until analysis.

2.4. Light measurements in the sediment

A microsensor for scalar irradiance measurement was prepared by placing a 70 μm spherical diffuser on the tapered tip of a 100 μm optical glass fibre (Kühl and Jørgensen, 1992). The same sensor was used for all profiles and connected to a photo-multiplier tube with custom support electronic. Light profiles within the sediment were measured in the laboratory

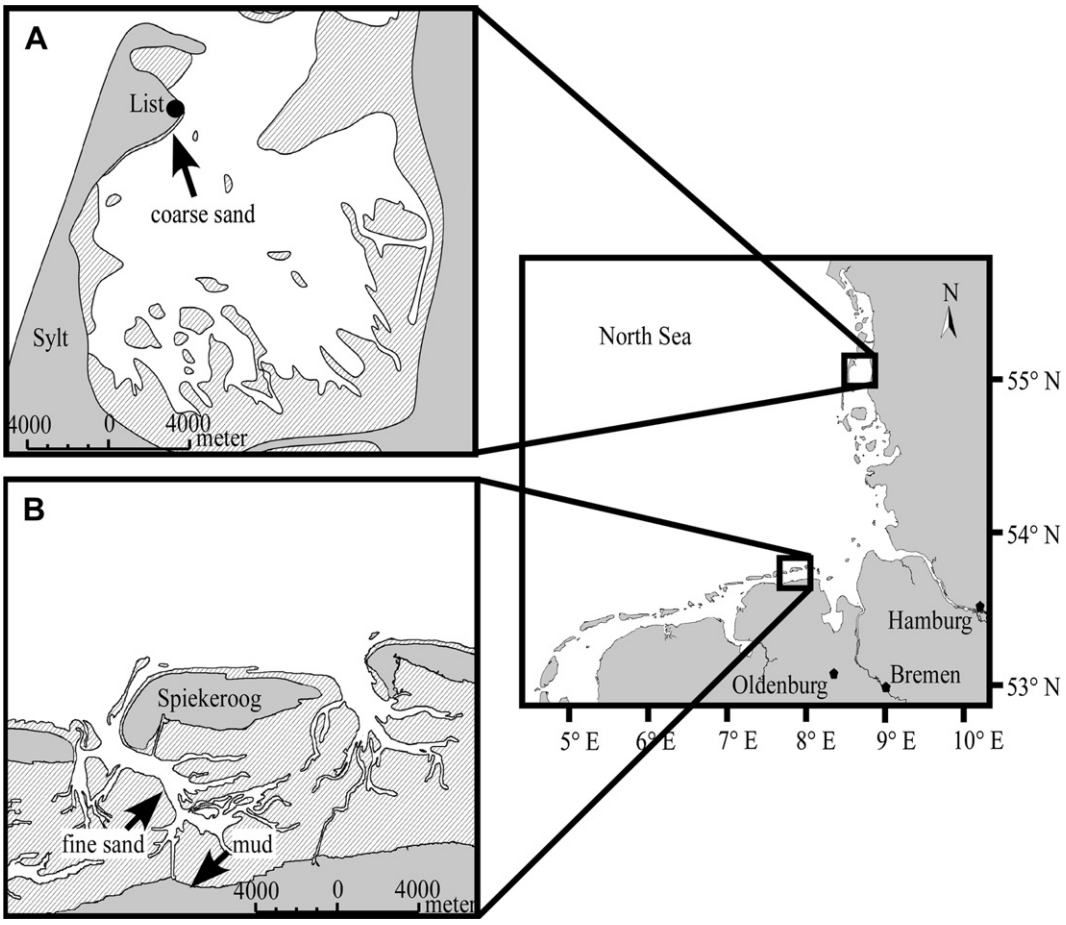

Fig. 1. Intertidal study sites in the German Wadden Sea. (A) The coarse sand site. (B) The fine sand and mixed sand/mud site.

Table 1
Sampling and in situ benthic chamber incubations during the measurement campaigns at the three study sites. Numbers denote replicate measurements (dark/light incubations for benthic chambers)

Campaigns	Sediment parameters			Benthic chambers				
	Permeability	TOC	Chlorophyll	Oxygen	DIC	Nutrients	Br-tracer	Incident light
Coarse sand								
Spring 2002 16./17.04.02	12	13	4	5/4 Optodes	2/2	4/4		1 Only 17.4.
Summer 2002 18./22.08.02	15	13	4	4/2 Winkler		4/2	5	1
Fine sand								
Spring 2002 13.03.02		10		3/2 Optodes	2/2	2/2		
Summer 2002 07.06.2002	9	10	4	2/2 Winkler		2/2	5	1
Autumn 2002 25./26.09.02		10	2	5/4 Optodes	3/2	4/2	5	1
Summer 2003 29.07.2003	6	8	2	3/3 Optodes	3/3	3/3	2	1
Mud								
Spring 2002 04.04.2002	3	10	4 top 0–5 cm	2/2 Winkler		2/1	2	
Summer 2002 19.06.2002		8	4	2/2 Winkler		2/2	4	1
Autumn 2002 30.09.2002		8	2	3/2 Optodes		2/1		1
Summer 2003 02.08.2003		8	2	3/2 Optodes	2/2	2/2		1

in sediment cores (36 mm diameter) from all study sites. The sediment surface was uniformly illuminated with two white light sources placed opposite from each other at 20° zenith angle. The light intensity within the sediment is given normalized to the incident irradiance.

2.5. Benthic chamber incubations

In situ incubations with cylindrical benthic chambers (19 cm inner diameter) were conducted to measure fluxes of oxygen, DIC and nutrients across the sediment water interface. Two transparent and two opaque chambers were used in one or two deployments (Table 1) at each study site. During summer 2003, three transparent and three opaque chambers were used. The stirring of the chamber water by a rotating disc (15 cm diameter) at 20 rpm induces advective flow through the surface layer of permeable sediment (Huettel and Gust, 1992a,b). During low tide, the chambers were placed onto the respective sediment, with the walls of the chambers penetrating down to a sediment depth of 19 cm. After inundation, the chambers were sealed with transparent or opaque lids, each enclosing a water volume of 3.4 L and a sediment area of 0.028 m^2. Twenty milligrams of a 3 mol L^{-1} NaBr inert tracer solution was then injected into each chamber for the assessment of the advective fluid exchange between enclosed sediment and overlying water (Forster et al., 1999). During most incubations (see Table 1), the oxygen concentration inside each chamber was monitored every 2 min for 20 s with fibre-optic optodes inserted through the chamber lid. For oxygen, nutrient and DIC analysis, a total of 80–140 ml volume of chamber water was sampled in 0.5–1 h intervals via a flexible tube (15 ml volume) with one end attached to a sampling port on the chamber lid and the other end reaching above the maximum water level. The first 20 ml of each sample was discarded to account for the sampling tube volume. The sampled water was replaced with ambient seawater via a second port in the chamber lid. Additionally, samples of ambient seawater were taken at each sampling interval. Samples for nutrient analysis were filtered through 0.2 μm nylon syringe filters into plastic vials and kept frozen until analysis. DIC samples were stored without headspace in glass vials and preserved with a saturated mercury chloride solution (end concentration 0.01%) in a refrigerator until analysed in the laboratory. At the end of the chamber incubations, with the water level still above the chambers, sediment cores were retrieved with cut off 60 ml syringes for bromide tracer analysis. The sediment cores were sliced in 0.5 cm intervals (0.2 cm intervals at the mud site) within 30 min after retrieval and kept frozen. Incident light at the sediment surface during the chamber incubations was measured with an Onset® photometric light logger that was sealed watertight into a transparent acrylic tube and positioned close to the sea floor (Table 1). The data, logged in lumen m^{-2}, were transformed into μmol Quanta m^{-2} s^{-1} by calibrating the light logger within the acrylic tube against a Licor® LI-250A quantum light meter in the laboratory.

2.6. Analytical procedures

The sediment samples for TC and TIC analysis were freeze-dried and ground in the laboratory. Sample aliquots were then transferred into tin-cups for TC measurements and analysed with a Heraeus CHNO-rapid elemental analyser using sulphanilamide as a calibration standard. TIC sample aliquots were measured by coulometric titration on a UIC CM5012 and TOC was calculated by subtracting TIC from TC. Pigments were extracted in the laboratory by sonification of sediment subsamples in 10 ml 90% acetone and subsequent measurement of the supernatant on a Shimadzu® UV-160 A spectrophotometer before and after acidification. Phaeopigment concentrations were then calculated according to Lorenzen (1967). Because concentrations of chlorophyll degradation products were very low at the two sandy sites and in some cases produced erroneous results when used for the calculation of chlorophyll *a*, pigment concentrations were given as total chlorophyll (absorption at 665 nm without acidification) for all study sites. For the analysis of bromide, the pore water of the sediment samples was extracted by centrifugation and 100 μl of the pore water then analysed by ion chromatography with a Waters anion-exchange column, using NaBr as a standard for calibration. Nutrient analysis of silicate, phosphate, ammonium, nitrate, and nitrite were performed spectrophotometrically with a Skalar® Continuous-Flow-Analyzer according to Grasshoff et al. (1999). In the following, NO_x fluxes denote the sum of nitrate and nitrite fluxes. Chamber water DIC was determined in the laboratory by flow injection analysis using freshly prepared $NaHCO_3$ calibration standards (Hall and Aller, 1992). In Summer 2003, DIC was measured by coulometric titration on a UIC® CM5012. Oxygen concentrations of the chamber water were determined by Winkler titration and used for calibration of the chamber oxygen optodes (Klimant et al., 1995; Holst et al., 1997). The dilution of the chamber waters due to the sampling was corrected by adding the difference of the solute inventory between the sampled and replaced volume to the chamber volume solute inventory. All solute fluxes are given as calculated from start and end concentrations (lowest end concentration for oxygen was 46 μmol L^{-1} in mud incubations).

3. Results

3.1. Sediment characteristics

At the coarse and fine sand sites, the mud fraction (<63 μm) was below 0.2%, while reaching 12.5% at the mixed sand/mud site. As a consequence, the sediment was highly permeable at the coarse sand, permeable at the fine sand and almost impermeable at the mud site (Table 2). The sandy sites were organic poor, with TOC contents of 0.1% or less in the upper 10 cm of the sediment, whereas the TOC content ranged between 0.5% and 0.7% at the mud flat.

Table 2
Sediment parameters, permeability (top 15 cm at sandy sites, top 4 cm at mud site) and percentage of TOC per sediment weight (top 10 cm) at the three study sites. The standard deviation ($n = 3$–15 for permeability, $n = 8$–11 for TOC) is given in parentheses

	Coarse sand	Fine sand	Mud
Median grain size (μm)	380	176	139
Sorting	Very well	Well	Moderately
Permeability (m^2)			
Spring 2002	4.0×10^{-11} (0.3)		6.0×10^{-14} (0.2)
Summer 2002	3.9×10^{-11} (0.3)	9.0×10^{-12} (0.8)	
Autumn 2002			
Summer 2003		7.2×10^{-12} (0.6)	
TOC (%)			
Spring 2002	0.06 (0.02)	0.05 (0.02)	0.71 (0.28)
Summer 2002	0.08 (0.04)	0.06 (0.01)	0.51 (0.08)
Autumn 2002		0.06 (0.02)	0.52 (0.12)
Summer 2003		0.08 (0.03)	0.56 (0.10)

3.2. Tracer transport

The stirring of the benthic chambers generated an advective flushing of the upper sediment layer. Reflecting the different permeabilities at the three study sites, the tracer was transported down to a sediment depth of 7.0 cm (SD ± 1.6, $n = 5$) in the coarse sand, 2.3 cm (SD ± 0.5, $n = 12$) in the fine sand and 1.3 cm (SD ± 0.4, $n = 6$) at the mud site.

3.3. Light availability in the sediment

Light distributions within the sediment of the three study sites are shown in Fig. 2. The increase above the sediment surface of the coarse and fine sand is due to reflection by the quartz sand. The irradiance peak below the surface is due to multiple scattering within the sediment. These features are less pronounced at the mud site due to less reflection and higher light absorption of the mud. The depth integrated scalar irradiance in the coarse sand was factor 3.45 higher and in the fine sand factor 2.04 higher than in the mud.

3.4. Sediment total chlorophyll

Total chlorophyll concentrations decreased with sediment depth at the three study sites and were generally higher at the muddy site than at the two sandy sites (Fig. 3). Total chlorophyll in the uppermost cm of the sediment was on average 185 mg m^{-2} (range 176–194 mg m^{-2}) in the coarse sand, 150 mg m^{-2} (range 134–172 mg m^{-2}) in the fine sand and 291 mg m^{-2} (194–356 mg m^{-2}) in the mud during the study seasons. At the two sandy sites, phaeophytin was never detectable in the top 3 cm and did not exceed 10% of the total chlorophyll below. At the mud site, phaeophytin was present at all sediment depths reaching up to 18% of total chlorophyll in the uppermost cm of the sediment and up to 38% below.

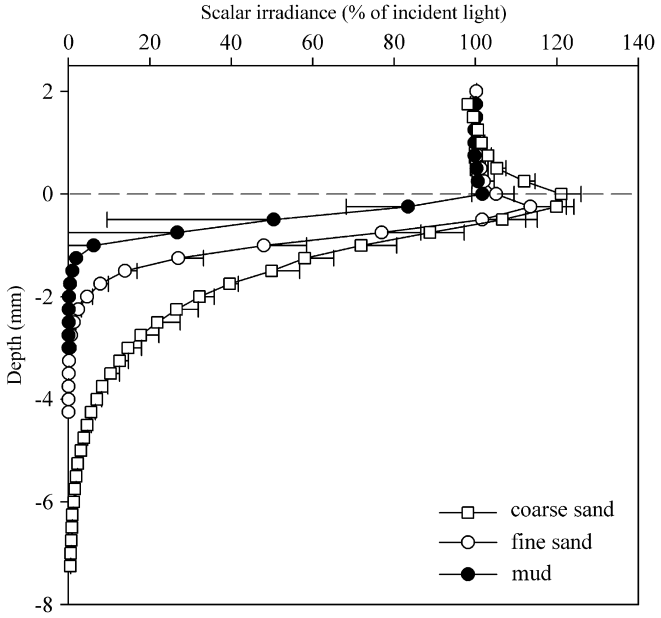

Fig. 2. Depth profiles of scalar irradiance normalized to incident light at the coarse sand, fine sand and mud site. Error bars indicate standard deviation of 3–6 measurements.

3.5. Oxygen and DIC fluxes

Oxygen and DIC fluxes revealed that benthic microalgae photosynthesized during inundation at all stations during all seasons (Fig. 4). Despite the higher total chlorophyll concentrations in the upper sediment layer of the mud site, areal gross photosynthesis was about 4-fold higher in the fine sand and 10-fold higher in the coarse sand compared to the mud site (Table 3). Fig. 5 shows the direct response of areal gross photosynthesis rates to the changing incident light regime at all study sites. During Summer 2002, areal gross photosynthesis rates in the coarse sand were much higher than those in the fine sand and mud, despite similar or even lower in situ photon flux at the coarse sand site compared to the two other sites (Fig. 5). The high photosynthetic activity at the two sandy study sites led to an efflux of oxygen during daytime inundation, whereas the oxygen produced at the mud site was completely consumed within the sediment (Fig. 4A). Production in the water column measured with in situ bottle incubations during July 2003 at the fine sand and mud sites was less than 3% of the benthic production.

3.6. Nutrient fluxes

Benthic photosynthesis affected the chamber nutrient fluxes (Fig. 6). While phosphate and ammonium were generally released from the sediment in the dark incubations, the light chamber fluxes indicated an uptake of inorganic nutrients by the microphytobenthos (Fig. 6B, C). Silicate was generally released in the dark incubations at all sites and the light fluxes indicated photosynthetic assimilation of silicate in the fine sand (Fig. 6A). Nitrate + nitrite (NO_x) was usually taken up by the sediment in both dark and light incubations during all

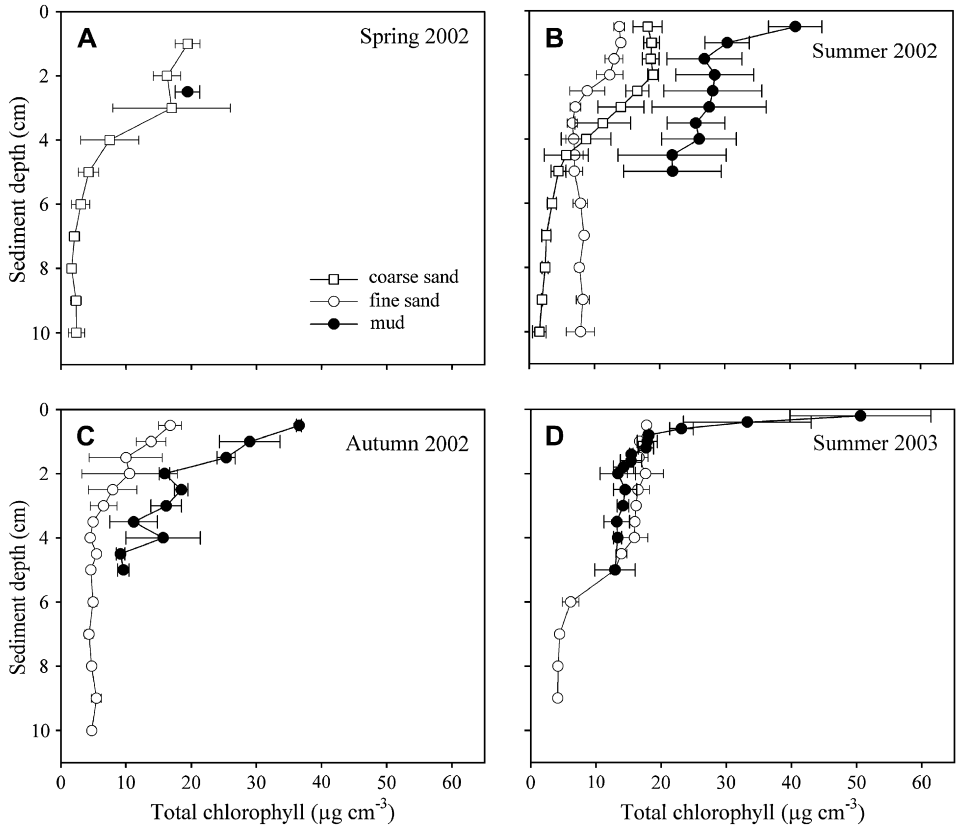

Fig. 3. Total chlorophyll concentration of the sediment at the study sites (µg cm^{-3}) with the standard deviation ($n = 2–4$) as error bars.

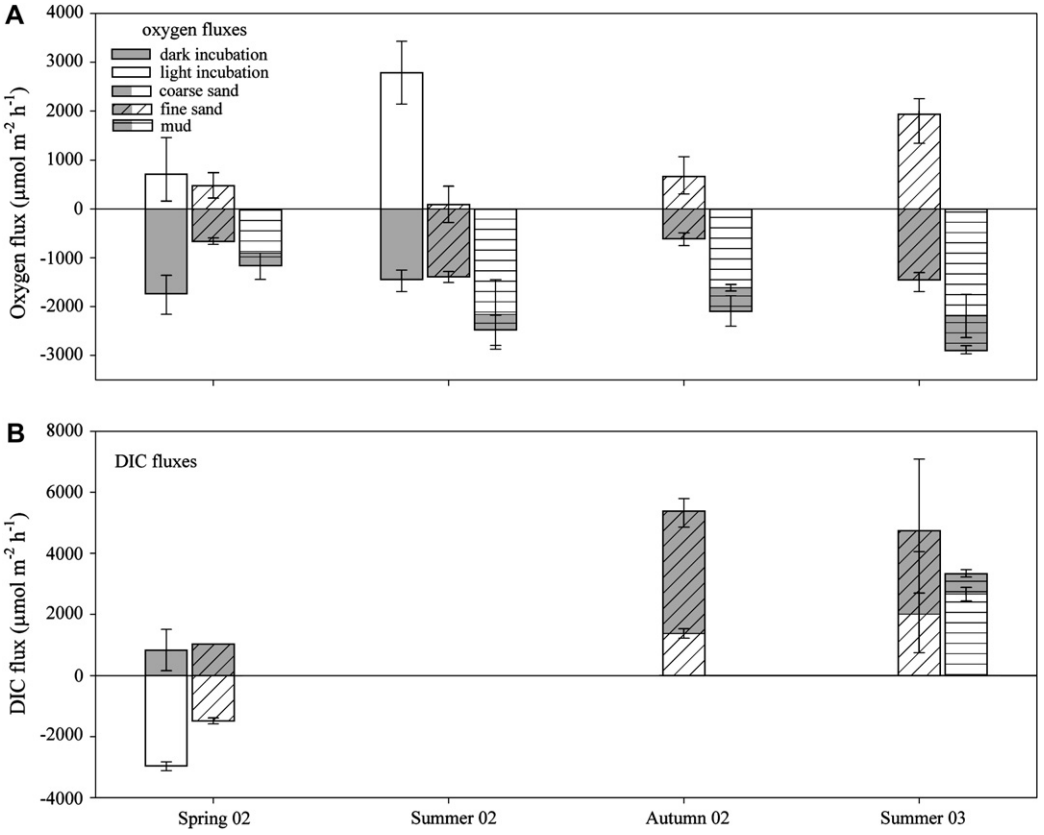

Fig. 4. Average benthic chamber fluxes of (A) oxygen and (B) DIC at the three study sites with range as error bars. Negative and positive values denote influx and efflux via the sediment surface, respectively.

Table 3
Net oxygen and DIC fluxes in μmol m^{-2} h^{-1} in dark and light incubations at the three study sites and calculated gross photosynthetic production of oxygen and consumption of DIC (GP). Negative and positive values denote influx and efflux via the sediment surface, respectively

	Coarse sand			Fine sand			Mud		
	Dark	Light	GP	Dark	Light	GP	Dark	Light	GP
Oxygen									
Spring 2002	−1737	718	2455	−676	482	1158	−1169	−903	266
Summer 2002	−1453	2788	4241	−1394	94	1488	−2483	−2159	325
Autumn 2002				−617	668	1284	−2098	−1613	485
Summer 2003				−1456	1942	3398	−2901	−2191	710
DIC									
Spring 2002	834	−2968	−3803	1035	−1486	−2521			
Summer 2002									
Autumn 2002				5499	1534	−3965			
Summer 2003				4751	2008	−2743	3350	2665	−684

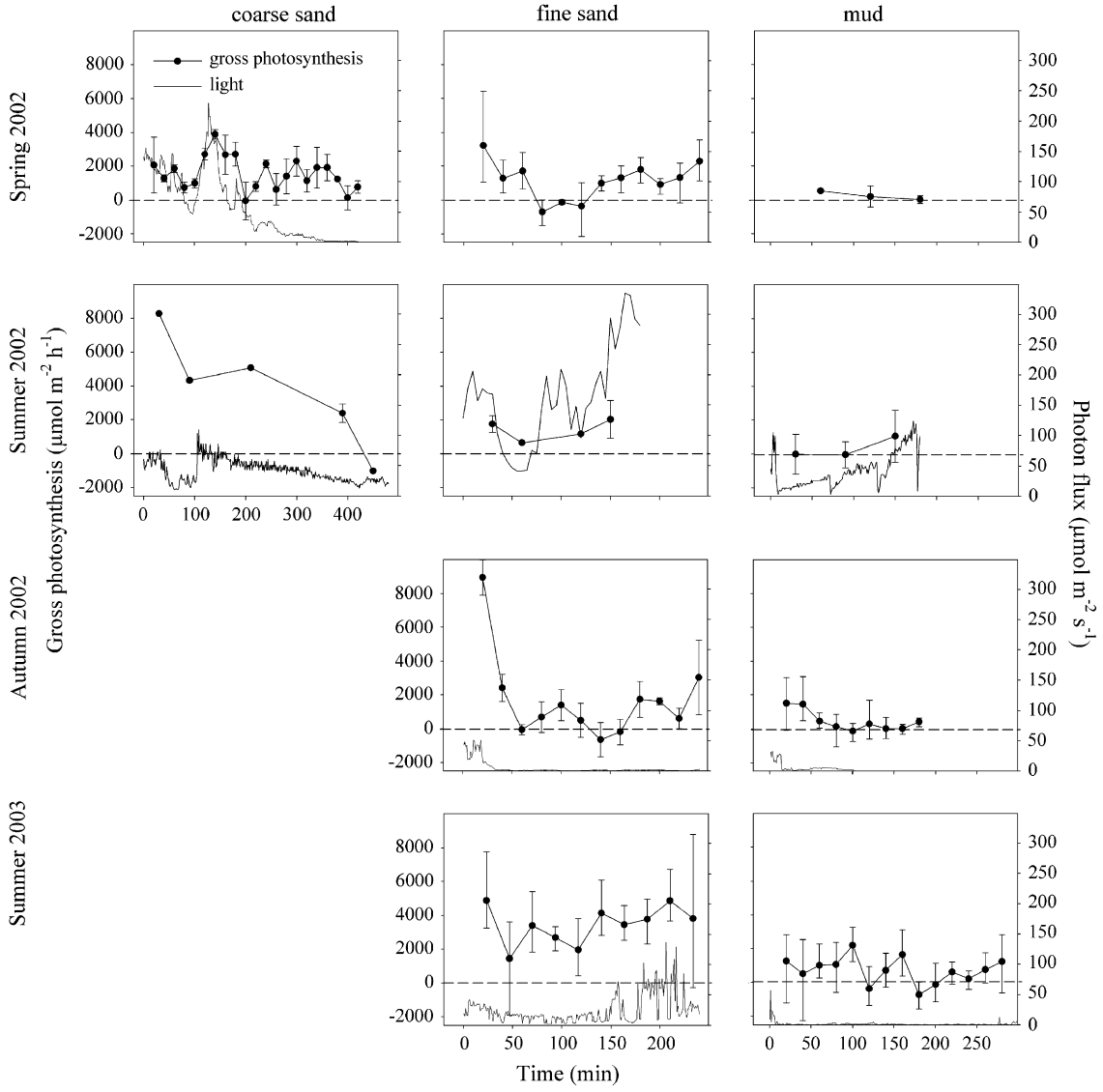

Fig. 5. Average gross photosynthesis (μmol m^{-2} h^{-1}) calculated from dark and light chamber incubations and in situ photon flux (μmol m^{-2} s^{-1}) at the three study sites. Error bars denote minimum and maximum estimates of gross photosynthesis. Dashed lines denote zero gross photosynthesis.

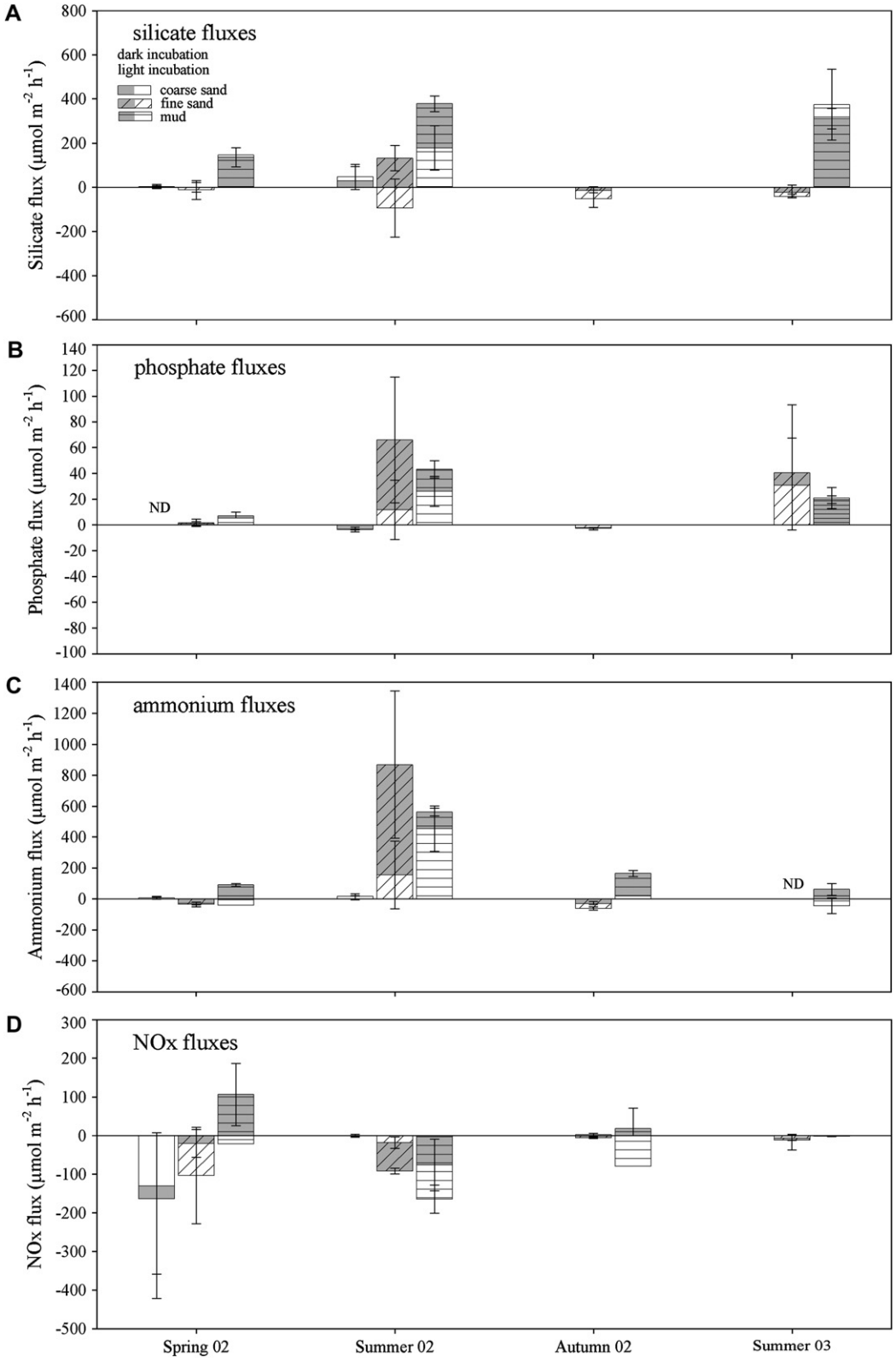

Fig. 6. Average benthic chamber fluxes of (A) silicate, (B) phosphate, (C) ammonium, (D) nitrate + nitrite (NO_x) at the three study sites with range as error bars. Negative and positive values denote influx and efflux via the sediment surface, respectively. ND denotes not detectable fluxes.

months at the two sandy sites (Fig. 6D). An efflux of NO_x was recorded in the dark incubations during Spring and Autumn at the mud site. There was no apparent causal connection between benthic photosynthesis and chamber NO_x fluxes (Fig. 6D). At the coarse sand site, very low nutrient fluxes resulted from the low organic content in this sediment (Table 2), and an effective nutrient cycling within the sediment by a very active microphytobenthic community, as reflected in the high

Table 4
Average nutrient concentrations (μmol L^{-1}) of the ambient seawater at the three study sites during the chamber incubations

Campaign	Coarse sand				Fine sand				Mud			
	Si	PO_4	NH_4	NO_x	Si	PO_4	NH_4	NO_x	Si	PO_4	NH_4	NO_x
Spring 2002	0.2	0.0	0.5	23.3	26.1	0.6	2.7	53.8	23.1	1.2	14.9	29.5
Summer 2002	2.5	0.4	2.7	0.8	8.5	0.6	5.9	2.6	15.1	1.5	10.6	2.6
Autumn 2002					8.2	1.1	5.9	1.9	31.5		7.0	3.7
Summer 2003					5.9	1.8	0.2	0.3	14.9	2.6	2.9	0.4

rates of gross photosynthesis at this site (Table 3). Relatively high release rates of phosphate and ammonium from the fine sand and mud during summer reflected higher mineralization and ensuing remobilization of bound phosphate due to a lowering of the oxygen penetration depths. The nutrient concentrations of the ambient seawater were generally highest at the mud site, intermediate at the fine sand and lowest at the coarse sand site (Table 4).

4. Discussion

Our study demonstrates that during inundation rates of benthic photosynthesis in sandy intertidal zones can be similar to those in mud flats, despite higher total chlorophyll content in the top cm of the mud sediment. Relatively high gross photosynthesis rates in the investigated tidal flats were associated with coarse grain size and high permeability of the sediment and resulted in a net-autotrophy for the two sandy study sites (Fig. 3). The mud site had lower photosynthesis rates and higher mineralization rates, which led to a net heterotrophy of the benthic community during inundation. The higher gross photosynthesis at the two sandy sites was surprising, as the total chlorophyll content of the top cm of the sediment was highest at the mud site. Thus, photosynthetic yield per unit chlorophyll was much higher in the sand than in the mud. Possible mechanisms causing the higher yield per chlorophyll in the sandy sediments that will be discussed here are (1) differences in metabolic state and life strategies of sand and mud microphytobenthos, (2) differences in light availability to the microphytobenthos, and (3) site specific nutrient limitation.

4.1. Metabolic state and sediment-dependent life strategies of the microphytobenthos

The higher gross photosynthesis at the sandy study sites may have been produced by a more active microphytobenthic community and different life strategies of the microphytobenthos in sands compared to muds. The measurement of phaeophytin content at the three study sites indicated an accumulation of chlorophyll degradation products in the muddy sediment, whereas no chlorophyll degradation products were measured in the top 3 cm of the sediment at the sandy sites. This is in agreement to other studies of intertidal flats (Cadee and Hegeman, 1977; Barranguet et al., 1997; Lucas and Holligan, 1999; Middelburg et al., 2000). Sandy sediments are sites of high organic matter turnover (Forster et al., 1996; Huettel and Rusch, 2000; D'Andrea et al., 2002) and algal cells can be rapidly degraded within these sediments (Ehrenhauss et al., 2004). Additionally, dead algal cells can be removed by advective flushing and resuspension of the permeable sand during inundation (de Jonge and van Beusekom, 1995; Lucas et al., 2000; Rusch et al., 2001). This is in contrast to fine grained sediments that accumulate organic matter (Table 2). This possibly involves settling of phytoplankton cells (Lucas and Holligan, 1999) that may not meet favourable conditions upon sedimentation on the mud flat and, hence, are less active.

More frequent resuspension and mixing in sandy sediment may also relocate the phototrophic community into deeper, dark layers, while cells from the aphotic sediment zone may end up in the photic surface layer. Relative constant chlorophyll concentrations (Fig. 3) indicate that this mixing affects the upper 3 to 6 cm of the sands and only the uppermost 1 to 2 cm in the mud (see also MacIntyre et al., 1996; Lucas and Holligan, 1999). Because many diatoms can survive over long time periods in the dark (Steele and Baird, 1968; French and Hargraves, 1980) and benefit from the higher nutrient concentrations at depth (Saburova and Polikarpov, 2003), frequent mixing of the sediment can keep a phototrophic community alive and active down to the mixing depth. The mixing may also reduce the potentially benthic-photosynthesis-diminishing effect of grazing (Hargrave, 1970; Connor et al., 1982), which is most intense at the sediment surface. In sands, the mixing of the sediment may quickly compensate for the grazing effect, while the recovery may take longer in muds, where phototrophs have to move or grow into the grazed surface areas.

Aside from the physical mixing, many benthic diatoms migrate vertically in synchrony with the solar and tidal cycle (Janssen et al., 1999; Mitbavkar and Anil, 2004). These diatoms move to the sediment surface during daylight exposure and descent during inundation to avoid resuspension (Round and Palmer, 1966; Paterson, 1989). Typically, a higher fraction of these mobile diatoms are associated with muddy sediment, while relatively immobile diatoms living firmly attached to the sediment grains are more common in sandy sediments (Barranguet et al., 1997). The migration of diatoms into deeper sediment layers during inundation may result in decreased photosynthesis in muddy sediment, which is characterized by strong light adsorption. In sandy sediments, the deeper light penetration and physical mixing of the microphytobenthos community during inundation can result in enhanced photosynthesis.

4.2. Light availability

The turbidity of the seawater increases from the relatively clear open North Sea towards the turbid near-shore areas (Postma, 1961). Light therefore limits primary production in the water column of the Wadden Sea (Colijn and Cadee, 2003) and likely also benthic primary production during inundation. Integral primary productivity of intact sediment has been previously shown to be saturated at a wide range of light intensities between 100 and 1260 μmol photons m^{-2} s^{-1} (MacIntyre et al., 1996 and references therein). Incident light intensities at the sea floor were generally below this level in our study, which caused a quick response of gross photosynthesis to incident light. Incident light intensities during inundation were generally lower at the mud site than at the fine sand site during all investigated study seasons (Fig. 5), which can partly explain the lower gross photosynthesis during inundation at the mud site as compared to the only 4 km distant fine sand site. The consequence of the more severe light limitation in the mud is a higher chlorophyll specific production at the sandy site during submersion.

In addition to differences in incident light, also the light distribution within the sediment varies between the mud site and the sands. Due to less adsorption in the sand, the benthic photic zone here was 2 to 3 times larger at same incident light intensities than in the mud (Fig. 2). The higher light absorption in the mud sediment cannot be explained by the higher total chlorophyll content, as chlorophyll was maximal 42 μg g^{-1} dry sediment in the mud. Note that the light availability in the mud is less than half of that in the sand, but that the chlorophyll content is doubled. Potentially, these effects cancel each other out with respect to total production, but again cause a higher chlorophyll specific production in the sand. The different optical properties of the sediments help explain why at the coarse sand site gross photosynthesis during inundation was 3 and 13 times higher during Summer 2002 than at the fine sand and mud site, respectively, despite relatively low incident light intensity at the sea floor (Fig. 5).

4.3. Potential nutrient limitation

Cook and Røy (2006) showed that advective flushing enhanced benthic primary production in a photosynthetically active permeable sand layer, because this flushing reduced CO_2 limitation of the microphytobenthos. Likewise, flushing may reduce limitation of nutrients due to high local photosynthetic rates. This effect may explain in situ observation of enhanced photosynthesis with increased sediment flushing (Wenzhöfer et al., in preparation). The flushing rates in our benthic chambers induced by the radial stirring (Huettel and Gust, 1992a,b; Janssen et al., 2005) reflected the different permeabilities of the three sediment types. The bromide tracer measurements documented the higher flushing rates in the coarse sand compared to the fine sand and mud sites. Enhanced transport of solutes with the advective pore water flows in the sands, thus, may have contributed to higher

Table 5
Comparison of annual rates of photosynthesis (g C m^{-2} a^{-1}) between sandy, mixed sand/mud and muddy sediments measured during inundation and exposure. Measurements in the laboratory study were conducted under conditions of light saturation, similar to the conditions during exposure

Study site	Sand	Sand/Mud	Mud	In situ/lab	Method	Authors
Exposure/laboratory						
Wadden Sea Ems Dollard estuary	99	108	314	In situ	Bell jars	van Es (1982)
Netarts Bay, Oregon, USA	129	153	72	In situ	Core incubation	Davis and McIntire (1983)
Bay of Fundy, Canada			20–84	In situ	^{14}C	Hargrave et al. (1983)
Wadden Sea Ems Dollard estuary	70–81	51–106	200–256	In situ	^{14}C	Colijn and de Jonge (1984)
Halifax Harbour, Nova Scotia, Canada	22			In situ	Core incubation	Grant (1986)
Savin Hill Cove, Boston, USA			250	In situ	^{14}C	Gould and Gallagher (1990)
Island of Fyn, Denmark	150–175			Laboratory	Core incubation	Kristensen (1993)
North Inlet Estuary, USA	93		191	Laboratory	Microsensors	Pinckney and Zingmark (1993)
Wadden Sea Westerschelde estuary			136	Laboratory	P/B estimate	de Jong and de Jonge (1995)
Wadden Sea Westerschelde estuary			2–28	Laboratory	Microsensors	Kromkamp et al. (1995)
Wadden Sea Sylt Königshafen	367	336	241	Laboratory	Core incubation	Kristensen et al. (1997)
Gironde Estuary, France			37–42	Laboratory	P/B estimate	Santos et al. (1997)
Wadden Sea Sylt Königshafen	329–362		355	Laboratory	Core incubation	Asmus et al. (1998)
Wadden Sea Westerschelde estuary	95[a]	111[a]		Laboratory	^{14}C	Barranguet et al. (1998)
Tagus Estuary, Portugal			156	Laboratory	Microsensors	Serodio and Catarino (2000)
Wadden Sea Büsum/Hedwigenkoog		42	35	Laboratory	Photosyn. light display	Wolfstein et al. (2000)
Douro River Estuary, Portugal	274–441		374	Laboratory	Core incubation	Magalhaes et al. (2002)
Colne Estuary, United Kingdom			53–191	Laboratory	Core incubation	Thornton et al. (2002)
Seto Inland Sea, Japan	434			Laboratory	Algae incubation	Montani et al. (2003)
Bay of Somme, France		110–147		In situ	Closed chamber CO_2 flux	Migne et al. (2004)
Inundation						
Wadden Sea Sylt Königshafen	68			In situ	Bell jars	Asmus (1982)
Wadden Sea Sylt Königshafen	39–67[a]			In situ	Bell jars	Asmus et al. (2000)
Ria Formosa, Portugal	64[a]		5	In situ	Bell jars	Asmus et al. (2000)
Sylt/Spiekeroog	24–65[a]	4[a]		In situ	Advection chambers	This study

[a] Calculated by multiplying the reported daily rates by 270 for temperate regions according to Cahoon (1999).

photosynthesis rates in these sands during inundation. Due to the relatively low stirring rates employed in our experiments, advective flushing and benthic photosynthesis may be even higher at in situ flow conditions than measured in the benthic chambers.

With the advection chambers we could measure only during inundation of the tidal flats and these measurements cannot be transferred to the exposure period. Table 5 compares potential annual productivity for different intertidal sediment types during inundation with rates during exposure or measured under saturating light conditions in the laboratory. Our calculated annual rates are in good range of values reported for the inundation period in other studies. Higher productivity in submerged intertidal sands than muds was also measured by (Asmus et al., 2000). During exposure and in laboratory studies, annual photosynthesis rates during exposure or measured in the laboratory generally exceed the rates during inundation as can be expected from the higher light availability during low tide. When comparing the different sediment types, some studies show muddy sediments to be more productive than sandy sediments during exposure. However, high photosynthesis in muddy sediments was in some studies associated with extraordinarily high nutrient concentrations produced e.g. by nearby wastewater outlets (van Es, 1982; Colijn and de Jonge, 1984; Thornton et al., 2002). Other studies reported little differences in productivity between sandy and muddy sediments or even higher productivity in sandy sediments during exposure (Table 5). Therefore, a budget over the entire tidal cycle is difficult to establish and subject to further studies.

5. Conclusions

For the period of inundation, our study demonstrated that benthic photosynthesis may be enhanced in intertidal sands compared to muds, mainly because of the higher availability of light and nutrients. Considering that sands can be equally productive as muds during the exposure period, sand flats thus can act as islands of net autotrophy in the heterogeneous Wadden Sea system that is generally considered net-heterotrophic (Gattuso et al., 1998; van Beusekom et al., 1999).

Acknowledgements

We thank M. Alisch, U. Werner, C. Hüerkamp and K. Vamvakopoulos for assistance during the cruises. We thank M. Alisch, G. Schüßler, S. Menger, D. Franzke and S. Pabel for their help with laboratory work and Cäcilia Wiegand for the preparation of the oxygen optodes. The technical assistance by J. Langreder, A. Nordhausen, G. Herz, A. Kutsche, P. Färber, V. Meyer and H. Osmers is gratefully acknowledged. Big thanks go to the crews of the Plattboden-ships and the Staff of the Wadden Sea station on Sylt (Alfred Wegener Institute) for their support and hospitality. We thank Dr. D.S. McLusky and two anonymous reviewers for their useful comments. This study was supported by the Deutsche Forschungsgemeinschaft (DFG) within the research group "Biogeochemistry of the Wadden Sea" (FG 432-5), coordinated by Prof. J. Rullkötter. We are grateful to Prof. B.B. Jørgensen and Dr. M.E. Böttcher for their support of this work and coordination of the sub-project "Biogeochemical processes at the sediment-water interface of intertidal sediments".

References

Admiraal, W., Peletier, H., Zomer, H., 1982. Observations and experiments on the population dynamics of epipelic diatoms from an estuarine mudflat. Estuarine, Coastal and Shelf Science 14, 471–487.

Asmus, R., 1982. Field measurements on seasonal variation of the activity of primary producers on a sandy tidal flat in the northern Wadden Sea. Netherlands Journal of Sea Research 16, 389–402.

Asmus, R., Jensen, M.H., Murphy, D., Doerffer, R., 1998. Primary production of microphytobenthos, phytoplankton and the annual yield of macrophytic biomass in the Sylt-Rømø Wadden Sea. In: Gätje, C., Reise, K. (Eds.), The Wadden Sea Ecosystem – Exchange, Transport and Transformation Processes. Springer, Berlin, Heidelberg, New York, pp. 367–391.

Asmus, R.M., Sprung, M., Asmus, H., 2000. Nutrient fluxes in intertidal communities of a southern European lagoon (Ria Formosa) – similarities and differences with a northern Wadden Sea Bay. Hydrobiologia 436, 217–235.

Barranguet, C., Herman, P.M.J., Sinke, J.J., 1997. Microphytobenthos biomass and community composition studied by pigment biomarkers: importance and fate in the carbon cycle of a tidal flat. Journal of Sea Research 38, 59–70.

Barranguet, C., Kromkamp, J., Peene, J., 1998. Factors controlling primary production and photosynthetic characteristics of intertidal microphytobenthos. Marine Ecology Progress Series 173, 117–126.

Bartoli, M., Nizzoli, D., Viaroli, P., 2003. Microphytobenthos activity and fluxes at the sediment-water interface: interactions and spatial variability. Aquatic Ecology 37, 341–349.

van Beusekom, J.E.E., Brockmann, U.H., Hesse, K.J., Hickel, W., Poremba, K., Tillmann, U., 1999. The importance of sediments in the transformation and turnover of nutrients and organic matter in the Wadden Sea and German Bight. Deutsche Hydrographische Zeitschrift 51, 245–266.

Blanchard, G.F., Guarini, J.M., Orvain, F., Sauriau, P.G., 2001. Dynamic behaviour of benthic microalgal biomass in intertidal mudflats. Journal of Experimental Marine Biology and Ecology 264, 85–100.

Cadee, G.C., Hegeman, J., 1974. Primary production of the benthic microflora living on tidal flats in the Dutch Wadden Sea. Netherlands Journal of Sea Research 8, 260–291.

Cadee, G.C., Hegeman, J., 1977. Distribution of primary production of the benthic microflora and accumulation of organic matter on a tidal flat area, Balgzand, Dutch Wadden Sea. Netherlands Journal of Sea Research 11, 24–41.

Cahoon, L.B., 1999. The role of benthic microalgae in neritic ecosystems. Oceanography and Marine Biology: An Annual Review 37, 47–86.

Colijn, F., Cadee, G.C., 2003. Is phytoplankton growth in the Wadden Sea light or nitrogen limited? Journal of Sea Research 49, 83–93.

Colijn, F., de Jonge, V.N., 1984. Primary production of microphytobenthos in the Ems-Dollard estuary. Marine Ecology Progress Series 14, 185–196.

Colijn, F., Dijkema, K.S., 1981. Species composition of benthic diatoms and distribution of Chl *a* on an intertidal flat in the Dutch Wadden Sea. Marine Ecology Progress Series 4, 9–21.

Connor, M.S., Teal, J.M., Valiela, I., 1982. The effect of feeding by mud snails, *Ilyanass obsoleta* (Say), on the structure and metabolism of a laboratory benthic algal community. Journal of Experimental Marine Biology and Ecology 65, 29–45.

Cook, P.L.M., Røy, H., 2006. Advective relief of CO_2 limitation in microphytobenthos in highly productive sandy sediments. Limnology and Oceanography 51, 1594–1601.

D'Andrea, A.F., Aller, R.C., Lopez, G.R., 2002. Organic matter flux and reactivity on a South Carolina sandflat: the impacts of porewater advection and macrobiological structures. Limnology and Oceanography 47, 1056–1070.

Davis, M.W., McIntire, C.D., 1983. Effects of physical gradients on the production dynamics of sediment-associated algae. Marine Ecology Progress Series 13, 103–114.

van Es, B., 1982. Community metabolism of intertidal flats in the Ems-Dollard estuary. Marine Biology 66, 95–108.

Ehrenhauss, S., Witte, U., Buhring, S.L., Huettel, M., 2004. Effect of advective pore water transport on distribution and degradation of diatoms in permeable North Sea sediments. Marine Ecology-Progress Series 271, 99–111.

Flemming, B.W., Ziegler, K., 1995. High-resolution grain size distribution patterns and textural trends in the backbarrier environment of Spiekeroog Island (southern North Sea). Senckenbergiana maritime. Frankfurt/Main 26 (1–2), 1–24.

Forster, S., Huettel, M., Ziebis, W., 1996. Impact of boundary layer flow velocity on oxygen utilisation in coastal sediments. Marine Ecology-Progress Series 143, 173–185.

Forster, S., Glud, R.N., Gundersen, J.K., Huettel, M., 1999. In situ study of bromide tracer and oxygen flux in coastal sediments. Estuarine, Coastal and Shelf Science 49, 813–827.

French, F.W., Hargraves, P.E., 1980. Physiological characteristics of plankton diatom resting spores. Marine Biology Letters 1, 185–195.

Gattuso, J.-P., Frankignoulle, M., Wollast, R., 1998. Carbon and carbonate metabolism in coastal aquatic ecosystems. Annual Review of Ecology and Systematics 29, 405–434.

Gould, D.M., Gallagher, E.D., 1990. Field measurement of specific growth rate, biomass and primary production of benthic diatoms Savin Hill Cove, Boston. Limnology and Oceanography 35, 1757–1770.

Grant, J., 1986. Sensitivity of benthic community respiration and primary production to changes in temperature and light. Marine Biology 90, 299–306.

Grasshoff, K., Kremling, K., Ehrhardt, M., 1999. Methods of Seawater Analysis. Wiley-VCH, Weinheim.

Guarini, J.M., Cloern, J.E., Edmunds, J., Gros, P., 2002. Microphytobenthic potential productivity estimated in three tidal embayments of the San Francisco Bay: a comparative study. Estuaries 25, 409–417.

Haardt, H., Nielsen, G.A.E., 1980. Attenuation measurements of monochromatic light in marine sediments. Oceanologica Acta 3, 333–338.

Hall, P.O.J., Aller, R.C., 1992. Rapid, small-volume, flow injection analysis for ΣCO_2 and NH_4^+ in marine and freshwaters. Limnology and Oceanography 37, 1113–1119.

Hargrave, B.T., 1970. The effect of deposit-feeding amphipod on the metabolism of benthic microflora. Limnology and Oceanography 15, 21–30.

Hargrave, B.T., Prouse, N.J., Phillips, G.A., Neame, P.A., 1983. Primary production and respiration in pelagic and benthic communities at two intertidal sites in the upper Bay of Fundy. Canadian Journal of Fisheries and Aquatic Sciences 40, 229–243.

Herman, P.M.J., Middelburg, J.J., Heip, C.H.R., 2001. Benthic community structure and sediment processes on an intertidal flat: results from the ECOFLAT project. Continental Shelf Research 21, 2055–2071.

Holst, G., Glud, R.N., Kühl, M., Klimant, I., 1997. A microoptode array for fine-scale measurement of oxygen distribution. Sensors and Actuators B – Chemical 38, 122–129.

Huettel, M., Gust, G., 1992a. Impact of bioroughness on interfacial solute exchange in permeable sediments. Marine Ecology Progress Series 89, 253–267.

Huettel, M., Gust, G., 1992b. Solute release mechanisms from confined sediment cores in stirred benthic chambers and flume flows. Marine Ecology Progress Series 82, 187–197.

Huettel, M., Rusch, A., 2000. Transport and degradation of phytoplankton in permeable sediment. Limnology and Oceanography 45, 534–549.

de Jong, D.J., de Jonge, V.N., 1995. Dynamics and distribution of microphytobenthic chlorophyll-*a* in the Western Scheldt estuary (SW Netherlands). Hydrobiologia 311, 21–30.

de Jonge, V.N., van Beusekom, J.E.E., 1995. Wind- and tide-induced resuspension of sediment and microphytobenthos from tidal flats in the Ems estuary. Limnology and Oceanography 40, 766–778.

Janssen, M., Hust, M., Rhiel, E., Krumbein, W.E., 1999. Vertical migration behaviour of diatom assemblages of Wadden Sea sediments (Dangast, Germany): a study using cryo-scanning electron microscopy. International Microbiology 2, 103–110.

Janssen, F., Faerber, P., Huettel, M., Meyer, V., Witte, U., 2005. Pore-water advection and solute fluxes in permeable marine sediments (I): Calibration and performance of the novel benthic chamber system *Sandy*. Limnology and Oceanography 50, 768–778.

Klimant, I., Meyer, V., Kühl, M., 1995. Fiberoptic oxygen microsensors, a new tool in aquatic biology. Limnology and Oceanography 40, 1159–1165.

Klute, A., Dirksen, C., 1986. Hydraulic conductivity and diffusivity: laboratory methods. In: Klute, A. (Ed.), Methods of Soil Analysis–Part 1 – Physical and Mineralogical Methods. American Society of Agronomy, pp. 687–700.

Kristensen, E., 1993. Seasonal variations in benthic community metabolism and nitrogen dynamics in a shallow, organic-poor Danish lagoon. Estuarine, Coastal and Shelf Science 36, 565–586.

Kristensen, E., Jensen, M.H., Jensen, K.M., 1997. Temporal variations in microbenthic metabolism and inorganic nitrogen fluxes in sandy and muddy sediments of a tidally dominated bay in the northern Wadden Sea. Helgoland Marine Research 51, 295–320.

Kromkamp, J., Peene, J., van Rijswijk, P., Sandee, A., Goosen, N., 1995. Nutrients, light and primary production by phytoplankton and microphytobenthos in the eutrophic, turbid Westerschelde estuary (The Netherlands). Hydrobiologia 311, 9–19.

Kühl, M., Jørgensen, B.B., 1992. Spectral light measurements in microbenthic phototrophic communities with a fiber-optic microprobe coupled to a sensitive diode array detector. Limnology and Oceanography 37, 1813–1823.

Kühl, M., Lassen, C., Jørgensen, B.B., 1994. Light penetration and light intensity in sandy sediments measured with irradiance and scalar irradiance fiber-optic microprobes. Marine Ecology Progress Series 105, 139–148.

Leach, J.H., 1970. Epibenthic algal production in an intertidal mudflat. Limnology and Oceanography 15, 514–521.

Lorenzen, C.J., 1967. Determination of chlorophyll and pheo-pigments: spectrophotometric equations. Limnology and Oceanography 12, 343–346.

Lucas, C.H., Holligan, P.M., 1999. Nature and ecological implications of algal pigment diversity on the Molenplaat tidal flat (Westerschelde estuary, SW Netherlands). Marine Ecology Progress Series 180, 51–64.

Lucas, C.H., Widdows, J., Brinsley, M.D., Salked, P.N., Herman, P.M.J., 2000. Benthic-pelagic exchange of microalgae at a tidal flat: 1. Pigment analysis. Marine Ecology Progress Series 196, 59–73.

MacIntyre, H.L., Geider, R.J., Miller, D.C., 1996. Microphytobenthos: the ecological role of the 'Secret Garden' of unvegetated, shallow-water marine habitats. I. Distribution, abundance and primary production. Estuaries 19, 186–201.

Magalhaes, C.M., Bordalo, A.A., Wiebe, W.J., 2002. Temporal and spatial patterns of intertidal sediment-water nutrient and oxygen fluxes in the Douro River estuary. Portugal. Marine Ecology Progress Series 233, 55–71.

Middelburg, J.J., Barranguet, C., Boschker, H.T.S., Herman, P.M.J., 2000. The fate of intertidal microphytobenthos carbon: an in situ ^{13}C-labeling study. Limnology and Oceanography 45, 1224–1234.

Migne, A., Spilmont, N., Davoult, D., 2004. In situ measurements of benthic primary production during emersion: seasonal variations and annual production in the Bay of Somme (eastern English Channel, France). Continental Shelf Research 24, 1437–1449.

Mitbavkar, S., Anil, A.C., 2004. Vertical migratory rhythms of benthic diatoms in a tropical intertidal sand flat: influence of irradiance and tides. Marine Biology 145, 9–20.

Montani, S., Magni, P., Abe, N., 2003. Seasonal and interannual patterns of intertidal microphytobenthos in combination with laboratory and areal production estimates. Marine Ecology Progress Series 249, 79–91.

Paterson, D.M., 1989. Short-term changes in the erodibility of intertidal cohesive sediments related to the migratory behavior of epipelic diatoms. Limnology and Oceanography 34, 223–234.

Pinckney, J., Zingmark, R.G., 1993. Modelling the annual production of intertidal benthic microalgae in estuarine ecosystems. Journal of Phycology 29, 396–407.

Pomeroy, L.R., 1959. Algal productivity in salt marshes of Georgia. Limnology and Oceanography 4, 386–397.

Postma, H., 1961. Transport and accumulation of suspended matter in the Dutch Wadden Sea. Netherlands Journal of Sea Research 1, 148–190.

Rasmussen, M.B., Henriksen, K., Jensen, A., 1983. Possible causes of temporal fluctuations in primary production of the microphytobenthos in the Danish Wadden Sea. Marine Biology 73, 109–114.

Revsbech, N.P., Jørgensen, B.B., 1986. Microelectrodes: their use in microbial ecology. In: Marshall, K.C. (Ed.), Advances in Microbial Ecology, vol. 9. Plenum Press, New York, London, pp. 293–352.

Round, F.E., Palmer, J.D., 1966. Persistent, vertical-migration rhythms in benthic microflora: II. Field and laboratory studies of diatoms from the banks of the River Avon. Journal of the Marine Biological Association of the United Kingdom 46, 191–214.

Rusch, A., Forster, S., Huettel, M., 2001. Bacteria, diatoms and detritus in an intertidal sandflat subject to advective transport across the water-sediment interface. Biogeochemistry 55, 1–27.

Saburova, M.A., Polikarpov, I.G., 2003. Diatom activity within soft sediments: behavioural and physiological processes. Marine Ecology Progress Series 251, 115–126.

Santos, P.J.P., Castel, J., Souza-Santos, L.P., 1997. Spatial distribution and dynamics of microphytobenthos biomass in the Gironde estuary (France). Oceanologica Acta 20, 549–556.

Serôdio, J., Catarino, F., 2000. Modelling the primary production of intertidal microphytobenthos: time scales of variability and effects of migratory rhythms. Marine Ecology Progress Series 192, 13–30.

Smith, D.J., Underwood, G.J.C., 1998. Exopolymer production by intertidal epipelic diatoms. Limnology and Oceanography 43, 1578–1591.

Steele, J.H., Baird, I.E., 1968. Production ecology of a sandy beach. Limnology and Oceanography 13, 14–25.

Thornton, D.C.O., Dong, L.F., Underwood, G.J.C., Nedwell, D.B., 2002. Factors affecting microphytobenthic biomass, species composition and production in the Colne estuary (UK). Aquatic Microbial Ecology 27, 285–300.

Tillmann, U., Hesse, K.J., Colijn, F., 2000. Planktonic primary production in the German Wadden Sea. Journal of Plankton Research 22, 1253–1276.

Tyler, A.C., McGlathery, K.J., Anderson, I.C., 2003. Benthic algae control sediment-water column fluxes of organic and inorganic nitrogen compounds in a temperate lagoon. Limnology and Oceanography 48, 2125–2137.

Underwood, G.J.C., Kromkamp, J., 1999. Primary production by phytoplankton and microphytobenthos in estuaries. In: Nedwell, D.B., Raffaelli, D.G. (Eds.), Advances in Ecological Research – Estuaries, vol. 29. Academic Press, New York, pp. 93–153.

Veldhuis, M.J.W., Colijn, F., Venekamp, L.A.H., Villerius, L., 1988. Phytoplankton primary production and biomass in the western Wadden Sea (The Netherlands); a comparison with an ecosystem model. Netherlands Journal of Sea Research 22, 37–49.

Wentworth, C.K., 1922. A scale of grade and class terms for clastic sediments. Journal of Geology 30, 377–392.

Wenzhöfer, F., Glud, R.N., Cook, P.L.M., Huettel, M. Benthic primary production of two sandy subtidal sediments, in preparation.

Widdows, J., Brinsley, M.D., Salked, P.N., Lucas, C.H., 2000. Influence of biota on spatial and temporal variation in sediment erodability and material flux on a tidal flat (Westerschelde, The Netherlands). Marine Ecology Progress Series 194, 23–37.

Wolfstein, K., Colijn, F., Doerffer, R., 2000. Seasonal dynamics of microphytobenthos biomass and photosynthetic characteristics in the northern German Wadden Sea, obtained by the photosynthetic light dispensation system. Estuarine, Coastal and Shelf Science 51, 651–662.

Yallop, M.L., Paterson, D.M., Wellsbury, P., 2000. Interrelationships between rates of microbial production, exopolymer production, microbial biomass, and sediment stability in biofilms of intertidal sediments. Microbial Ecology 39, 116–127.

Diversity and vertical distribution of magnetotactic bacteria along chemical gradients in freshwater microcosms

C.B. Flies, H.M. Jønkers, D. de Beer, K. Bosselmann, M.E. Böttcher, D. Schüler

This chapter is published in

FEMS MICROBIOLOGY ECOLOGY

52 (2): 185-195 APR 1 2005

ELSEVIER

FEMS Microbiology Ecology 52 (2005) 185–195

FEMS MICROBIOLOGY Ecology

www.fems-microbiology.org

Diversity and vertical distribution of magnetotactic bacteria along chemical gradients in freshwater microcosms

Christine B. Flies, Henk M. Jonkers, Dirk de Beer, Katja Bosselmann, Michael E. Böttcher, Dirk Schüler *

Max Planck Institute for Marine Microbiology, Celsiusstr. 1, D-28359, Bremen, Germany

Received 24 August 2004; received in revised form 1 November 2004; accepted 3 November 2004

First published online 26 November 2004

Abstract

The vertical distribution of magnetotactic bacteria along various physico-chemical gradients in freshwater microcosms was analyzed by a combined approach of viable cell counts, 16S rRNA gene analysis, microsensor profiling and biogeochemical methods. The occurrence of magnetotactic bacteria was restricted to a narrow sediment layer overlapping or closely below the maximum oxygen and nitrate penetration depth. Different species showed different preferences within vertical gradients, but the largest proportion (63–98%) of magnetotactic bacteria was detected within the suboxic zone. In one microcosm the community of magnetotactic bacteria was dominated by one species of a coccoid "*Alphaproteobacterium*", as detected by denaturing gradient gel electrophoresis in sediment horizons from 1 to 10 mm depth. Maximum numbers of magnetotactic bacteria were up to 1.5×10^7 cells/cm^3, which corresponded to 1% of the total cell number in the upper sediment layer. The occurrence of magnetotactic bacteria coincided with the availability of significant amounts (6–60 μM) of soluble Fe(II), and in one sample with hydrogen sulfide (up to 40 μM). Although various trends were clearly observed, a strict correlation between the distribution of magnetotactic bacteria and individual geochemical parameters was absent. This is discussed in terms of metabolic adaptation of various strains of magnetotactic bacteria to stratified sediments and diversity of the magnetotactic bacterial communities.

Keywords: Magnetotactic bacteria; Vertical distribution; Chemical gradient; Freshwater sediment; Microsensors

1. Introduction

Magnetotactic bacteria (MTB) are aquatic microorganisms whose swimming direction is influenced by magnetic fields [1]. The ability of magnetotaxis is based on magnetosomes, which are intracellular membrane-bound crystals of a magnetic iron mineral, such as magnetite or greigite [2,3]. The function of magnetotaxis is generally assumed to facilitate the bacteria finding and maintaining a favorable position in vertical chemical gradients in stratified environments [1,4], although it has not been fully explored how exactly this position is correlated to geochemical parameters. Despite the ubiquitous and abundant occurrence of diverse magnetotactic bacteria in many marine and freshwater habitats, only a small number of magnetotactic strains could be isolated in pure culture so far (for review see [2]). Although they provide valuable models for laboratory investigation, insights into their metabolism, magnetosome biomineralization, and ecophysiology may not necessarily be generalized for the vast natural diversity of magnetotactic bacteria, as the known cultivated species do not represent the dominant species in their natural environment [5,6]. Further investigations of

* Corresponding author. Tel.: +49 421 2028 746; fax: +49 421 2028 580.

E-mail address: dschuele@mpi-bremen.de (D. Schüler).

0168-6496/$22.00
doi:10.1016/j.femsec.2004.11.006

uncultivated magnetotactic bacteria are thus required. A variety of diverse MTB can be easily enriched without cultivation by taking advantage of their magnetically directed swimming behavior [7,8]. This has enabled us to explore the morphological and phylogenetic diversity of uncultivated magnetotactic bacteria in many studies (for review see [6,9]). However, much less is known about their ecology and distribution in sediments and stratified water columns.

In an early report, the distribution of magnetotactic bacteria in the permanently stratified water column of the Pettaquamscutt River Estuary (USA) was addressed [10]. Whereas magnetotactic cocci could be detected only in the oxic and microoxic zone, diverse morphotypes were abundant (up to 2×10^5 cells/cm^3) not only in the microoxic but also in the anoxic zone in the presence of up to 2 mM sulfide. It was therefore concluded that the distribution of different magnetotactic bacteria is determined by different optima in sulfide and oxygen gradients. Another study investigated the vertical distribution of magnetite- and greigite-producing MTB in the same habitat [11]. Generally, more magnetite producers were found at and above the oxic–anoxic transition zone (OATZ), whereas more greigite-producing magnetotactic bacteria were located in the anoxic sulfidic zone. Similar observations were reported for a stratified water column of a brackish water pond [12]. Magnetotactic bacteria were observed only in the upper 10 cm of South-Atlantic deep-sea sediments, while none were detected in the water column [13]. Because the majority of magnetotactic bacteria in this study were found in the anoxic zone, where nitrate was available, it was suggested that most MTB might reduce nitrate as the terminal electron acceptor.

The spatial distribution of an uncultivated giant MTB species (''Magnetobacterium bavaricum'') from a freshwater habitat (Lake Chiemsee) was analyzed by fluorescence in situ hybridization (FISH) [5]. In microcosm experiments the occurrence of ''M. bavaricum'' was restricted to the sediment. Most cells were present within the microoxic zone with a peak abundance of 7×10^5 cells/cm^3 equivalent to a relative abundance of $0.64 \pm 0.17\%$. Because of its unusual large size, ''M. bavaricum'' accounted for approximately 30% of the biovolume within a narrow layer of the sediment, which indicates that magnetotactic bacteria may play a dominant role in the microbial ecology of the sediment.

Although these studies have indicated that magnetotactic bacteria are major constituents of microbial communities in certain zones of aquatic habitats, the biogeochemical interactions controlling their occurrence in stratified sediments have remained poorly understood. In this study, we therefore investigated the vertical distribution of magnetotactic bacteria in several freshwater microcosms. Because of the inavailability of a group-specific probe for the universal detection of magnetotactic bacteria by FISH, we used viable counts and denaturing gradient gel electrophoresis (DGGE) analyses to identify magnetotactic bacteria in sediments. The purpose of our experiments was to correlate the occurrence of magnetotactic bacteria in different sediment layers to data obtained by simultaneous characterization of the chemical microenvironments using microsensor profiling, direct activity measurements of sulfate reduction and further biogeochemical methods.

2. Material and methods

2.1. Sampling and setup of microcosms

Sediment samples from the upper sediment layer and surface water were collected from several marine and freshwater habitats in Northern Germany. Microcosms were set up essentially as described earlier [14] in bottles (0.1–2 l) or aquaria (5 l) for larger sample volumes. Briefly, approximately two thirds of sediment was overlaid with one third of sample water. The loosely covered containers were incubated at room temperature in dim light without agitation. Microcosms were stored in complete dark to prevent photosynthesis for 5 days before analysis. Because of their high cell numbers of MTB, four microcosms from three different freshwater habitats were selected for comprehensive analysis, which had been previously incubated for 30 (A), 17 (B), 17 (C) or 6 (D) months, respectively, and originated from the following freshwater sampling sites: (A) drainage ditch in Bremen, (B, C) eutrophic pond in Staßfurt (Sachsen-Anhalt), (D) a lake in Bremen (''Waller See''). Staßfurt samples (B and C) were collected from the same site, but at different times (B: April 2001, C: October 2001). Microcosm A and D were collected in March 2000 and April 2003, respectively. Cores from microcosms A and B (9 mm in diameter) were incubated for 5 days before analysis to reestablish physico-chemical gradients. Wider cores (26 mm in diameter) were taken from microcosms C and D for more detailed analysis. To avoid compression of sediment cores that may lead to disturbation of chemical gradients, a moderate vacuum was applied to these cores during the sampling.

2.2. Viable counts and DAPI counts

One sediment core per microcosm was sliced into 1–13 mm increments. The sediment samples were immediately diluted with sterile habitat water (1:2) and homogenized. For enumeration, 3 μl of sediment slurry was placed as a hanging drop onto a microscopic slide [15]. Counting was performed using a Zeiss (Jena, Germany)

Axioplan phase contrast microscope at 400× magnification. Aliquots were diluted appropriately with sterilized habitat water, so that 50–300 MTB per drop could be counted. Cells with a characteristic motility and magnetic response, which accumulated at the edge facing the magnetic south pole of a bar magnet, were considered as magnetotactic. Counting was started when virtually all magnetotactic bacteria had reached the edge, which was typically after 10–12 min. Average MTB numbers were calculated from three different drops. To investigate the influence of atmospheric oxygen onto the migration of magnetotactic bacteria, a control sample was analyzed in parallel under oxygen-containing and oxygen-free atmospheres. Since both samples yielded nearly identical MTB numbers, the effect of oxygen was considered negligible and all counts were subsequently performed in the presence of air.

For DAPI counts, the samples were fixed with paraformaldehyde, washed, subjected to sonification and filtered onto polycarbonate filters (pore size 0.2 μm, Millipore) as described by Pernthaler et al. [16]. The cells were stained with 4′,6′-diamidino-2-phenylindole (DAPI, Sigma, Schellendorf, Germany) for 4 min and washed with H_2O and 70% ethanol. After the embedding in Citifluor (Citifluor Products, Canterbury, UK) total cell numbers were counted using a Zeiss Axioplan fluorescence microscope. Mean cell numbers were calculated from several randomly chosen fields on each filter, corresponding to a minimum of 1000 DAPI-stained cells.

2.3. Electron microscopy

MTB from different sediment horizons were collected by a magnet as described above and adsorbed onto 300-mesh formvar coated copper grids (Plano, Wetzlar, Germany), which were examinated without staining with an EM 301 transmission electron microscope (Philips; Eindhoven, Netherlands) at 80 kV.

3. Magnetic collection of cells for PCR

To strictly separate MTB from particles and contaminants, 50 μl of each horizon (either directly or after 1:2 dilution with sterile habitat water) was applied to a special separation chamber that was build from two cellulose stripes, which were separating the sediment slurry from a reservoir of sterile habitat water under a cover slip. By application of a magnetic field, magnetotactic bacteria were directed by swimming through the cellulose stripes from the slurry into the reservoir, from where the separated cells were collected after 45 min. After concentration by centrifugation cells were resuspended in 11 μl water. Alternatively, magnetotactic bacteria were collected from microcosms by attaching the south pole of a bar magnet outside the bottle 1 cm above the sediment surface.

3.1. PCR amplification

Bacterial 16S rRNA genes from the resuspended cells were amplified with the universal primer pair GM5F with a GC-clamp and 907R [17]. The PCR system from TaKaRa Bio Incorporation (Otsu, Shiga 520-2193, Japan) was used according to manufacturer's instructions. The touchdown PCR was initiated by one cycle at an annealing temperature of 65 °C, which was gradually decreased by 1 °C in every other cycle down to 55 °C. For cloning, nearly complete 16S rRNA genes were amplified using the same PCR system with the universal bacterial primer pair GM3F and GM4R [17]. PCR was performed by 33 cycles at an annealing temperature of 42 °C. The PCR product was cloned into the pCR®4-TOPO® vector and transformed into competent *Escherichia coli* cells (TOP10) from Invitrogen (Carlsbad, USA). The plasmid DNA from positive clones was isolated with a QIAprep Spin Miniprep Kit (Quiagen, Hilden, Germany) and sequenced with GM1 (5′-CCAGCAGCCGCGGTAAT-3′) and vector-specific primers.

3.2. Denaturing gradient gel electrophoresis (DGGE)

DGGE was performed using the D-Gene™ system (Bio-Rad Laboratories, Munich, Germany) as described previously [18]. DNA fragments were separated in a 1-mm thick polyacrylamide gel (6% wt/vol) with a 20–70% denaturant gradient and 1 × TAE electrophoresis buffer (40 mM Tris, 20 mM acetic acid, 1 mM EDTA, pH 8.3) at 60 °C. After 16 h electrophoresis at a constant voltage of 100 V, the gel was stained with ethidium bromide and documented by the Image Master from Amersham Pharmacia. DNA bands were excised and eluted in 100 μl water overnight at 4 °C. About 1–6 μl of the eluates were reamplified with GM5F and 907R and PCR products were purified using the gel extraction kit (Eppendorf, Hamburg, Germany) from agarose gels and subsequently sequenced.

3.3. Sequence analysis

Purified PCR products or plasmid DNA (100 ng) were used in the sequencing reaction. DNA sequences were determined by a capillary sequencer (Applied Biosystems/Hitachi 3100 Genetic Analyzer, Foster City, Canada) and compared against databases using the BLAST algorithm (http://www.ncbi.nlm.nih.gov/BLAST/). The nucleotide sequences of partial 16S rRNA genes of magnetotactic bacteria have been deposited in the GenBank, EMBL, and DDJB libraries with Accession No. AJ863135 (microcosm D), AJ863150 (microcosm B) and AJ863158 (microcosm A).

3.4. Microsensor measurements

Concentration profiles of oxygen, sulfide, nitrate and pH were measured using custom-build microsensors. Amperometric Clark type sensors were applied for oxygen and sulfide determinations, potentiometric glass sensors for pH, while biosensors were used for determination of nitrate profiles. The diameter of the sensors was 10 μm (oxygen, pH, and sulfide) or 30 μm (nitrate). See [19] for detailed description and working principle of used microsensors. To ensure temporary and lateral homogeneity, chemical profiles were measured repeatedly before sampling. If not indicated otherwise (e.g., Fig. 1), all measurements yielded nearly identical results.

3.5. Geochemical analysis

Sediment cores were sliced under a nitrogen atmosphere into 0.5–2 cm sections and pore water was immediately separated from the sediments by centrifugation through 0.45 μm membrane filters. The water content of sediment samples was determined gravimetrically after drying at 104 °C for 24 h. Dissolved iron was measured spectrophotometrically by adding reducing ferrozine immediately after filtration (Ferrozine reagent with 1% hydroxylamine-hydrochloride) to the pore water [20]. To discriminate between the Fe(II) and Fe(III) ions, the reducing agent was added to the ferrozine assay after a previous measurement in which hydroxylamine-hydrochloride was omitted [20]. In addition, high resolution measurements of dissolved iron and manganese in the pore water were performed using the technique of diffusive equilibration in thin films (DET; [21,22]). In this technique solutes equilibrate with the water of the hydrogels, which are removed from the sediment after 24 h and subsequently sliced and reequilibrated for 24 h with HNO_3 (2% s.p). Dissolved iron and manganese concentrations were analyzed by optical emission spectroscopy (ICP, Perkin–Elmer Optima 3000XL) using scandium as an internal standard.

Extractable iron includes fractions of iron (III) in sediments, which is available for chemical reduction and readily reacts with sulfide to form various iron sulfide minerals and eventually pyrite [23]. The proportion of extractable iron was quantified by the Ferrozine method (see above) after extraction for 1 h at room temperature with either buffered Na-dithionite solution [23] or 0.5 M HCl [24]. While the HCl-extraction reveals the amount of ferrihydrites and iron monosulfides, leachable iron extracted by dithionite represents both poorly and well-crystallized iron oxides, e.g., hematite, and minor iron bond to silicates [23,24]. Both extraction methods showed nearly similar results therefore only data from dithionite extraction are presented in the results.

Sulfate concentrations in the pore water were determined by ion chromatography (Waters). Microbial sulfate reduction rates were measured using the whole core incubation method. The sediment core (26 mm in diameter) was injected with a carrier-free $^{35}SO_4^{2-}$ tracer and incubated for 4 h at room temperature. Tracer recovery after microbial conversion was measured for both the fraction of acid-volatile sulfide (AVS, essentially FeS) and chromium-reducible sulfur (CRS, essentially elemental sulfur) by the two step distillation method [25,26]. Total gross sulfate reduction rate (SRR) is the sum of both fractions. The spatial distribution of bacterial sulfate-reducing activity was visualized by the application of the in situ 2D-photopaper monitoring technique, which is a modification of a method described in [27], and is based on the diffusion of hydro-

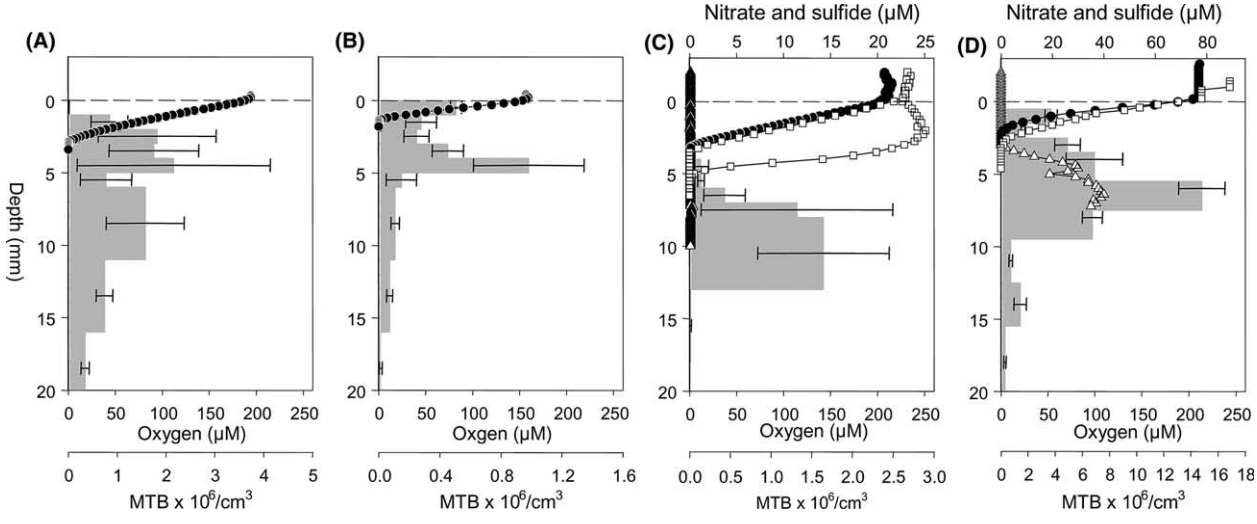

Fig. 1. Vertical distributions of magnetotactic bacteria in microcosms A, B, C and D in relation to downcore profiles of: oxygen (●), nitrate (□), and sulfide (△) concentrations. Numbers of magnetotactic bacteria (MTB) are shown as grey vertical bars with standard deviations indicated. Sediment surface is indicated as a dashed line. Two different nitrate curves were obtained from measurements at two different sites within the microcosm C.

gen sulfide into a photographic paper with subsequent Ag_2S formation. Photographic paper was incubated for 23–25 h followed by the fixation in a 2 M sodium thiosulfate solution.

To establish the nature of mineral phases of the solid phases that precipitated at the walls of the incubation vessels, FTIRspectroscopy (Mattson 3000 type FTIR spectrophotometer) and X-ray powder diffraction (Philips X-ray powder diffractometer) were used. Pore water profiles were additionally interpreted by the modeling program PROFILE [28] to calculate net rates of production or consumption as a function of depth.

4. Results

4.1. Development of microcosms

Typically, various characteristic morphotypes of magnetotactic bacteria including cocci, spirilla, rods and vibrios were present in most fresh samples. Both marine and freshwater microcosms underwent a characteristic succession within several weeks. Marine samples generally contained low numbers of MTB, which rapidly disappeared upon laboratory incubation. Generally, the total MTB numbers increased in most freshwater microcosms within several weeks. This was coincident with an apparent loss of diversity, and most microcosms were ultimately dominated by few morphotypes after prolonged incubation. In those samples, MTB populations remained apparently stable for periods of up to several years without obvious changes in cell numbers and morphologies. Therefore, four of these aged microcosms (A, B, C, D) from three different freshwater habitats were selected for further examination of distribution of magnetotactic bacteria.

4.2. Biogeochemical characteristics of microcosms

The succession in the MTB population coincided with a noticeable change in the appearance of microcosms. A characteristic stratification of the sediments became visible after several weeks of incubation, which reflected changes in the biogeochemical processes. The upper sediment layer of microcosm C had a silty appearance, while coarse-grained sediment prevailed below depth of about 18 mm. Surface sediments showed indications for bioturbation. The brownish sediment turned black below about 10 mm due to the reduction of Fe(III) minerals and the precipitation of iron monosulfides. The presence of FeS was proven by the smell of H_2S after liberation from the sediment upon attack with diluted hydrochloric acid. Below about 30 mm depth the sediment turned grey due to the formation of pyrite and it contained gas bubbles (presumably methane), besides plant residues. Water contents reached about 75% at the surface that decreased to below 30% in the coarse-grained bottom part. Microcosm D, containing more sandy sediment, displayed stratification marked by color change. The light-brownish-gray oxic surface extended over 3 mm and turned into a darker layer down to 30 mm depth. The following grey-colored section of the sediment was laminated with two distinct darker layers at about 40 and 50 mm depth.

During the time of sampling, maximum oxygen penetration depth varied between the four microcosms (A: 2.5 mm; B: 1.5 mm; C: 3.0 mm; D: 2.0 mm; Fig. 1), but displayed only slight variations (less than 0.5 mm) within a single setup. In microcosms C and D additional profiles of nitrate, sulfide and pH were obtained. In both microcosms nitrate was measurable and maximum penetration depth was generally 0.5 mm deeper than oxygen (Figs. 1C and D). However, at one particular spot in microcosm C, a deeper maximum penetration depth of nitrate was observed (5.0 mm), which was possibly due to locally enhanced nitrification rates (Fig. 1C). Although photopaper-monitoring techniques indicated the occurrence of dissolved sulfide in microcosm C (data not shown), no free sulfide (H_2S) was measurable by microsensors, probably due to the rapid reoxidation at the surface (Fig. 1C). In microcosm D hydrogen sulfide could be detected below the depth of 3.0 mm. Interestingly, dissolved sulfide did not overlap with either oxygen or nitrate (Fig. 1D). Values of pH decreased from 8.5 at the sediment surface to 7.0 in deeper sediment layers in microcosm C, but remained stable at 6.7 in the sediment of microcosm D (data not shown).

Maximum sulfate concentrations in the surface waters of microcosms C and D were 4 mM and 1.4 mM, respectively, and decreased downcore (Fig. 2). Modeling with PROFILE revealed a distinct zone of sulfate consumption in the upper 4 cm of microcosm C (data not shown). This result was further substantiated by the direct measurements of gross sulfate reduction rates (SRR). Gross SRR were found throughout the investigated sediment sections with maxima at about 4.5 cm depth (Fig. 2). The surface values of sulfate reduction rates of 10 nmol/cm^3/d increased up to maximum rates of 70 nmol/cm^3/d at 4.5 cm depth with a subsequent decline. Effected by reoxidation, sulfate reduction rates showed net production of AVS during short-time incubation just below 1.5 cm depth and reached maximum values at 4.5 cm depth. In microcosm D modeling with PROFILE did reveal sulfate depletion below the maximum of SRR at approximately 2.5 cm depth (data not shown). The rates were about 20 times higher compared to microcosm C. AVS started to accumulate just below 1.5 cm depth, indicating effective reoxidation in the top part of the sediment (Fig. 2).

In microcosm C an increase of Fe(II) was detected below 0.5 cm depth and reached up to 110 μM at 2

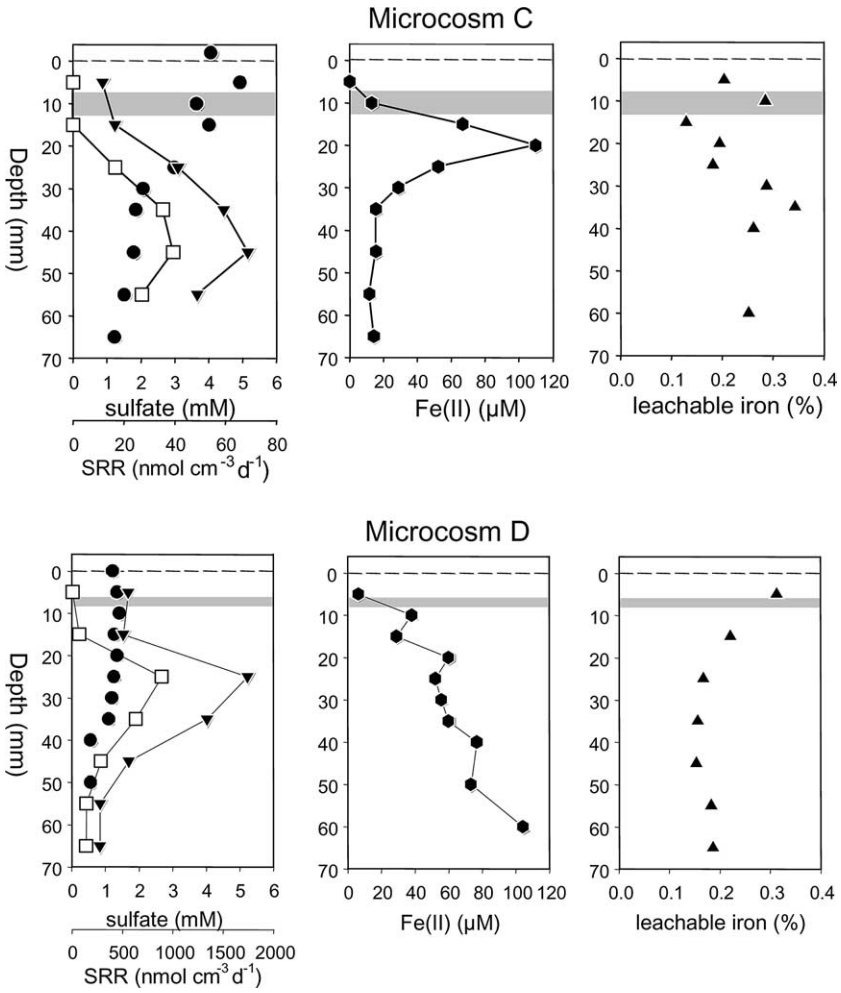

Fig. 2. Vertical distributions of magnetotactic bacteria in microcosms C and D in relation to downcore profiles of sulfate concentrations (●), gross (▼) and AVS (□) sulfate reduction rates, dissolved (⬟) and leachable (▲) iron. Horizons with maximum abundances of magnetotactic bacteria are indicated as grey vertical bars. Sediment surface is indicated as a dashed line.

cm depth (Fig. 2). In deeper sections, iron monosulfide was present contributing to the fraction extracted by Na-dithionite and leading also to a decrease in dissolved Fe(II) concentrations. For the upper sediment zone a net iron reduction rate of 17 nmol/cm^3/d was calculated (data not shown). Dissolved iron was released into the pore water below the oxygen penetration depth of about 5 mm up to 104 μM in microcosm D (Fig. 2). The depth profile of leachable iron indicates a depletion of Fe(III) below the first cm due to chemical reduction by sulfide in agreement with the accumulation of dissolved Fe(II) (Fig. 2). The combined results of SRR and Fe(III) reduction rates indicate that this is a zone where both chemical and microbial iron reduction takes place in both microcosms. The precipitation of ferrihydrites and manganese dioxides at the walls of microcosm D indicated that near surface metal reduction led at least temporary to the liberation of dissolved iron and manganese to the overlying water, where reoxidation took place.

4.3. Vertical distribution of magnetotactic bacteria

Analysis of viable cell numbers revealed a heterogeneous vertical distribution of magnetotactic bacteria in all microcosms. No magnetotactic bacteria were detectable in the oxic water columns and their occurrence was restricted to a narrow layer in the sediment, which was overlapping or closely below the OATZ. However, different microcosms displayed variations in the abundance and distributions of MTB.

In microcosm A highest numbers of MTB (2.3×10^6 cells/cm^3) were present between 4 and 5 mm depth (Fig. 1A). No other morphotypes than magnetotactic cocci were observed by microscopy. In contrast, two maxima of distribution were found in microcosm B (Fig. 1B). The first maximum of 5.1×10^5 MTB/cm^3 was found immediately below the surface in the microoxic sediment zone and consisted of different morphotypes including magnetotactic cocci and spirilla. A second peak (9.7×10^5 MTB/cm^3) occurred in the anoxic

zone between 4 and 5 mm depth and consisted exclusively of magnetotactic cocci.

Likewise, a heterogeneous distribution of different morphotypes was observed in microcosm C. Beside the presence of cocci, this microcosm was dominated by magnetotactic spirilla. Unlike magnetotactic cocci, spirilla performed a bidirectional swimming motility [4], but nevertheless displayed a north-seeking net polarity. Both cocci and spirilla were present in the oxic as well as in the anoxic zone of the sediment, but were most abundant between 8 and 13 mm depth (1.6×10^6 MTB/cm^3, Fig. 1C; proportion of cocci was 8.0%, data not shown). Interestingly, this peak did partially overlap the presence of soluble ferrous iron of 25–60 μM (Fig. 2). The number of magnetotactic bacteria steeply declined in deeper sediment layers.

In microcosm D, MTB could be detected in all horizons down to 45 mm. A single maximum of 14.8×10^6 MTB/cm^3 was detectable in the anoxic sediment between 6 and 8 mm depth where 6–40 μM Fe(II) is available (Figs. 1D and 2). Total cell numbers in this layer were determined by the DAPI method and were 10^9 cells per cm^3. Thus, magnetotactic bacteria accounted for approximately 1% of the total microbial population of this particular horizon. In contrast to magnetotactic cocci, which were most abundant at this depth (14.6×10^6 cells/cm^3), magnetotactic spirilla occurred in highest numbers (0.5×10^6 cells/cm^3) in the upper anoxic layer between 4 and 6 mm depth, but were absent from deeper sediment layers (Fig. 3A).

4.4. Morphological and phylogenetic diversity of magnetotactic bacteria from different horizons

Microscopic analysis indicated that the MTB distribution in our microcosms was heterogeneous not only with respect to cell numbers, but also to the composition of the magnetotactic population (Figs. 3C, D). Differences were observed between different sediment layers of a single microcosm as well as between microcosms from different sampling sites, as indicated by microscopy and 16S rRNA gene analysis of MTB, which were magnetically collected without depth fractionation. While for instance a sequence from microcosm A revealed high similarity to the uncultivated magnetotactic coccus maccs13 (CS103, Accession No. X61605), a sequence from microcosm B affiliated with a different uncultivated magnetotactic bacteria (Accession No. AJ223476).

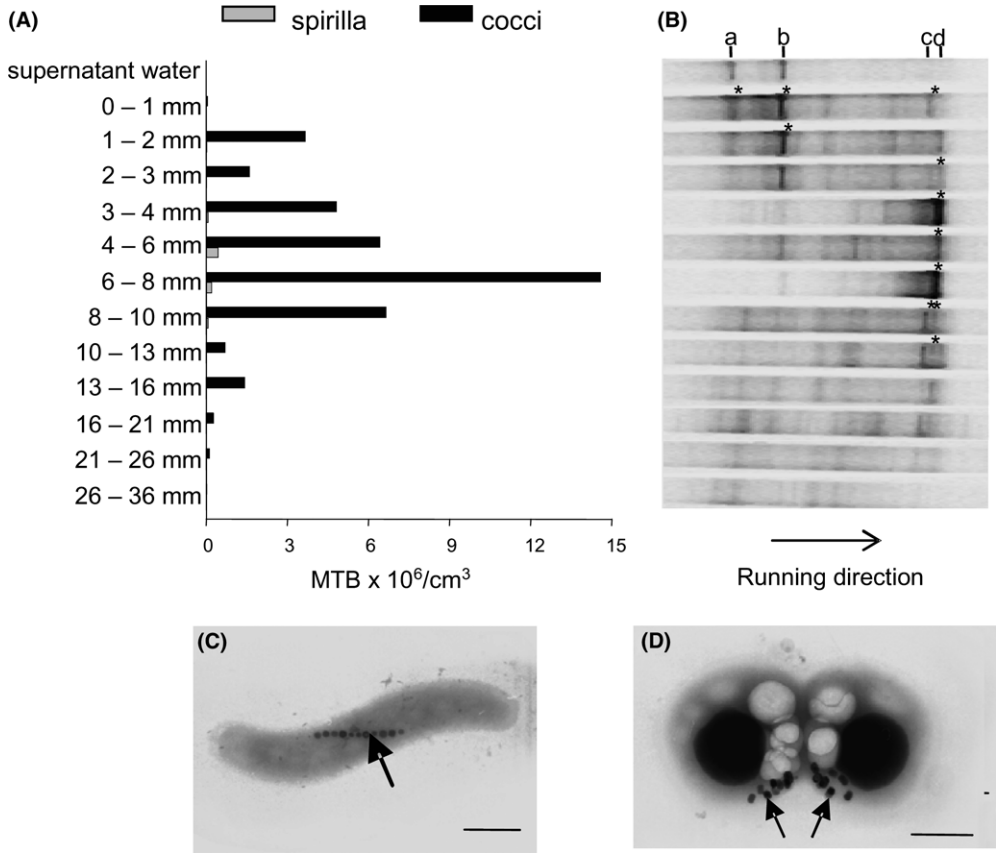

Fig. 3. (A) Vertical abundances of different morphotypes of magnetotactic bacteria in microcosm D. (B) DGGE band patterns obtained with primers GM5F + GC-clamp and 907R from cells that were magnetically purified from different horizons of microcosm D. The marked bands (*) were excised and sequenced. (C, D) Electron micrographs of different magnetotactic bacteria, which were characteristic for microcosm D. Arrows indicate magnetosome particles (bar = 0.5 μm).

To investigate the vertical distribution of different species, magnetotactic bacteria were collected from different sediment layers of microcosm D. Fig. 3B shows the results of the DGGE of PCR-amplified 16S rRNA gene fragments obtained from the water column and magnetically enriched cells from different sediment layers. Two major bands (a and b) were obtained from the water column. These bands were also present in the upper zone of the sediment, but their intensity decreased in deeper sediment layers. Sequences obtained from a and b displayed highest similarity to those from the *Cytophaga Flavobacterium Bacteroides* cluster, while a third band (c) from the upper and deeper sediment layers yielded a sequence closely related to *Pseudomonas spinosa*. A further distinct band (d) was abundant in DGGE patterns from 1 to 10 mm depth, which was coincident with the maximum abundance of magnetotactic bacteria. Sequencing of this band confirmed its identity in all horizons and revealed high sequence similarity to a sequence from an uncultivated magnetic coccus in the database (Accession No. X80996). To obtain extended sequence information, the nearly complete 16S rRNA gene was amplified from cells collected from 6 to 8 mm depth, the horizon that had revealed only one dominant band in DGGE. One sequence was obtained, which matched the partial sequences from b and d in the DGGE profile and displayed only four mismatches to the uncultivated magnetococcus [29]. Hence, the DGGE profiles from different sediment layers confirmed the heterogeneous vertical distribution of magnetotactic bacteria and were consistent with the distribution of total viable MTB numbers. However, molecular analysis did not fully reveal the diversity of magnetotactic bacteria observed by microscopy during cell counts and electron microscopy. Microscopy of the magnetotactic cells collected for PCR revealed that in contrast to direct counts in the hanging drop, only magnetotactic cocci were observed in significant numbers. This might be a consequence of the more stringent collection conditions employed for PCR amplification, which had resulted in the loss of other magnetotactic bacterial species (e.g., spirilla) below detection.

5. Discussion

Viable counts of magnetotactic bacteria possibly slightly underestimate the abundance of these bacteria, because the method is intrinsically biased for highly motile cells, while slow-moving bacteria or cells that were attached to sediment particles are possibly missed. Nevertheless, counts of magnetically separated cells have proven an effective and highly selective tool for the enumeration of magnetotactic bacteria in this study. All of our selected samples were characterized by the development of abundant populations of magnetotactic bacteria, however, these varied considerably in numbers and community compositions between different microcosms. The observed downcore profiles of microbial activity and dissolved constituents confirmed the presence of steep opposing gradients of reduced and oxidized compounds in the surface sediment of the investigated microcosms. In all samples this coincided with the occurrence of magnetotactic bacteria, which was restricted to a narrow layer in the upper sediment located closely to the OATZ. As most of the cultivated MTB strains are known to behave as typical microaerophiles, it was surprising that in all microcosms most magnetotactic bacteria were detected in the suboxic zone immediately below the OATZ (A: 63%, B: 92%, C: 98% and D: 91%). Maximum numbers were between 9.7×10^5 and 1.5×10^7/cm^3, thus accounting for at least 1% of the total cell numbers in this region. Interestingly, in microcosm B magnetic spirilla were more abundant in microoxic sediment layers, whereas magnetic cocci were predominantly found in the deeper suboxic zone, indicating that different species showed different preferences within the vertical gradients. The maximum MTB numbers in our study were considerably higher than MTB numbers estimated for environmental samples (10^3–10^4 MTB/cm^3, [14,30]), but were in the same range as reported previously for other laboratory enrichments [5,14,31,32].

Although all magnetotactic bacteria apparently displayed a very strict preference within the vertical chemical zonation, e.g., the restriction to a very narrow layer, the pathway of electron transfer and their putative mode of metabolism are not apparent from the distribution of potential electron donors and acceptors investigated. Cultivated magnetotactic bacteria are metabolically versatile and all investigated species are known to perform a strictly respiratory metabolism, which can be coupled to the oxidation of organic substrates, such as short-chained fatty acids. We did not measure organic compounds, but studies on other stratified environments, i.e., a microbial mat, showed that the occurrence of these typical fermentation products was restricted to the upper layers slightly below the oxic zone [33]. Analogous, the peak abundance of magnetotactic bacteria in our microcosms thus might reflect the availability of these organic carbon sources.

In addition, the availability of inorganic electron donors must be considered as an important factor controlling the distribution of magnetotactic bacteria. Several isolated MTB strains are able to grow by the oxidation of sulfide in opposing sulfide-oxygen gradients [34,35]. *Sox* genes, which encode enzymes essential for the oxidation of reduced sulfur compounds [36] are present in the genomes of various *Magnetospirillum* species (DOE Joint Genome Institute www.jgi.doe.gov/JGI_microbial/html; Flies and Schüler, unpublished), suggesting that the ability to oxidize reduced sulfur compounds is ubiquitous among MTB. In MV-1, evidence for a facultative autotrophic metabolism based on the oxidation of

sulfide or thiosulfate was found [35]. The majority of the magnetotactic bacteria found in our microcosms contained inclusions, which probably represented sulfur globules similar as reported in numerous uncultivated magnetotactic bacteria from freshwater and marine habitats [5,35,37–40]. Intracellular sulfur globules are commonly found in other bacteria as metabolic products of H_2S oxidation. Sulfide could be detected in microcosm D and sulfur intermediates (as S°) coincided with the occurrence of magnetotactic bacteria in this microcosm. In microcosm C monitoring by photopaper also demonstrated the presence of dissolved sulfide in sediment layers where magnetotactic bacteria were found. Thus, the assumption of a sulfide-oxidizing metabolism would be reasonable for the MTB populations in microcosm C and D.

Whereas sulphate-reducing bacteria (SRB) seem to be important in the shaping of gradients in the investigated sediments, no magnetotactic bacteria could be detected at the depth of maximum sulfate reduction. With the exception of *Desulfovibrio magneticus* from the "*Deltaproteobacteria*", all cultivated magnetotactic bacteria are unable of sulfate reduction. Indeed, the most abundant magnetotactic bacteria in microcosm D were identified as "*Alphaproteobacteria*", which are unlikely to respire sulfate. Thus, sulfate reduction is probably not a major metabolic pathway in most magnetotactic bacteria from freshwater.

Several previous reports have implicated magnetotactic bacteria in the reduction of iron and it has been suggested that they potentially derive energy from this process [41–43]. In our experiments, magnetotactic bacteria were found in a zone where abundant solid phase Fe(III) was present and thus, potentially might serve as an electron acceptor. However, there are no clear experimental indications that dissimilatory iron reduction is a metabolic pathway in cultivated magnetotactic bacteria, and its relevance for populations in our microcosm remains uncertain. However, besides its putative function in redox cycling, iron plays an eminent role in magnetotactic bacteria, since large amounts of iron are required for the synthesis of magnetosome crystals that account for 2–4% of the dry weight [14,44]. Intriguingly, the abundance of magnetotactic bacteria in our microcosms coincided with the availability of dissolved iron in the top surface sediments. Ferrous iron concentrations in the pore water of these sediment layers are in the range, which are saturating for both growth and magnetosome formation in cultures of *Magnetospirillum gryphiswaldense* and other magnetotactic bacteria [44–46]. Thus, the availability of iron for the synthesis of magnetosomes appears to be another factor affecting the distribution of magnetotactic bacteria.

With the exception of *D. magneticus*, all cultivated MTB strains can use molecular oxygen and nitrous compounds (i.e., nitrate or nitrous oxide) as terminal electron acceptors for respiration ([14,47–52]; Heyen and Schüler, unpublished). However, contrary to our expectations the occurrence of magnetotactic bacteria in our microcosms was not coincident with the presence of either nitrate or oxygen. The position of magnetotactic bacteria within multiple gradients of dissolved species might not be strictly determined by a single factor, but may rather represent a "trade-off" between the availability of electron donors and acceptors as well as iron. This potentially may involve temporary displacements between different zones, and energy taxis in combination with magnetic orientation may play an important role in the control of vertical distribution in MTB. One possible mode of metabolism would be that magnetotactic bacteria shuttle electrons by migration between zones of sulfide oxidation and oxygen or nitrate reduction. However, due to their small size the observed magnetotactic bacteria are unlikely to store significant amounts of an electron acceptor for the provision of energy during migration, such as for instance nitrate-storing sulfide-oxidizing *Thioploca* and *Beggiatoa* species do [53,54]. Thus, the predominant occurrence of magnetotactic bacteria in zones lacking an appropriate electron acceptor remains somewhat puzzling. Unless there is a so-far unknown capability of magnetotactic bacteria to derive energy by fermentation or respiration on different electron acceptors, for instance such as humic acids, their preferred occurrence closely to, but outside of oxic zones in our aged microcosms might alternatively reflect a resting or metabolically inactive state, which is occupied in the absence of higher concentrations of organic substrates. This would be consistent with the stunning observation that viable magnetotactic bacteria can be recovered in high numbers from sediment micro- and mesocosms even after many years of incubation in the dark without any addition of a carbon or energy source ([1]; Flies, unpublished observation). Thus, our aged microcosms may not generally reflect environmental conditions, as conditions in natural sediments are likely to be more dynamic due to the continuous influx of organic substance and the impact of photosynthesis. Further studies, such as in situ measurements of metabolic activity of magnetotactic bacteria in undisturbed sediments from marine and freshwater habitats are therefore urgently required.

Acknowledgements

We thank P.-L. Gehlken, Heiligenstadt, for carrying out the FTIR and XRD measurements, F. Mayer and M. Hoppert, Göttingen, for providing access to the electron microscope, and A. Schipper for help in the laboratory. This work was supported by the BMBF and the Max Planck Society.

References

[1] Blakemore, R.P. (1975) Magnetotactic bacteria. Science 190 (4212), 377–379.

[2] Bazylinski, D.A. and Frankel, R.B. (2004) Magnetosome formation in prokaryotes. Nat. Rev. 2, 217–230.

[3] Schüler, D. (2004) Molecular analysis of a subcellular compartment: the magnetosome membrane in *Magnetospirillum gryphiswaldense*. Arch. Microbiol. 181, 1–7.

[4] Frankel, R.B., Bazylinski, D.A., Johnson, M.S. and Taylor, B.L. (1997) Magneto-aerotaxis in marine coccoid bacteria. Biophys. J. 73 (2), 994–1000.

[5] Spring, S., Amann, R., Ludwig, W., Schleifer, K.-H., Van Gemerden, H. and Petersen, N. (1993) Dominating role of an unusual magnetotactic bacterium in the microaerobic zone of a freshwater sediment. Appl. Environ. Microbiol. 59 (8), 2397–2403.

[6] Spring, S. and Schleifer, K.-H. (1995) Diversity of magnetotactic bacteria. Syst. Appl. Microbiol. 18, 147–153.

[7] Wolfe, R.S., Thauer, R.K. and Pfennig, N. (1987) A capillary racetrack method for isolation of magnetotactic bacteria. FEMS Microbiol. Ecol. 45 (1), 31–36.

[8] Schüler, D., Spring, S. and Bazylinski, D.A. (1999) Improved technique for the isolation of magnetotactic spirilla from a freshwater sediment and their phylogenetic characterization. Syst. Appl. Microbiol. 22 (3), 466–471.

[9] Amann, R., Rossello-Mora, R., Flies, C.B. and Schüler, D. (2004) Phylogeny and in situ identification of magnetotactic bacteria In: Biomineralization (Baeuerlein, E., Ed.). Wiley-VCH, Weinheim.

[10] Stolz, J.F. (1992) Magnetotactic bacteria: Biomineralization, ecology, sediment magnetism, environmental indicator In: Biomineralization: Processes of Iron and Manganese; Modern and Ancient Environments (Skinner, H.C.W., Ed.), pp. 133–145. Catena-Verlag, Cremlingen-Destedt.

[11] Bazylinski, D.A., Frankel, R.B., Heywood, B.R., Mann, S., King, J.W., Donaghay, P.L. and Hanson, A.K. (1995) Controlled biomineralization of magnetite (Fe_3O_4) and greigite (Fe_3S_4) in a magnetotactic bacterium. Appl. Environ. Microbiol. 61, 3232–3239.

[12] Bazylinski, D.A. and Moskowitz, B.M. (1997) Microbial biomineralization of magnetic iron minerals: Microbiology, magnetism and environmental significance In: Geomicrobiology: Interactions Between Microbes and Minerals, pp. 181–223. Catena-Verlag, Cremlingen-Destedt.

[13] Petermann, H. and Bleil, U. (1993) Detection of live magnetotactic bacteria in South-Atlantic deep-sea sediments. Earth Planet. Sci. Lett. 117 (1–2), 223–228.

[14] Blakemore, R.P., Maratea, D. and Wolfe, R.S. (1979) Isolation and pure culture of a freshwater magnetic spirillum in chemically defined medium. J. Bacteriol. 140, 720–729.

[15] Schüler, D. (2002) The biomineralization of magnetosomes in *Magnetospirillum gryphiswaldense*. Int. Microbiol. 5 (4), 209–214.

[16] Pernthaler, J., Glöckner, F.-O., Schönhuber, W. and Amann, R. (2001) Fluorescence in situ hybridization (FISH) with rRNA-targeted oligonucleotide probes In: Methods in Microbiology (Paul, J.H., Ed.), pp. 207–226. Academic press, San Diego.

[17] Muyzer, G., Teske, A. and Wirsen, C.O. (1995) Phylogenetic relationships of *Thiomicrospira* species and their identification in deep-sea hydrothermal vent samples by denaturing gradient gel electrophoresis of 16S rDNA fragments. Arch. Microbiol. 164, 165–172.

[18] Muyzer, G., Brinkhoff, T., Nübel, U., Santegoeds, C., Schäfer, H. and Wawer, C. (1998) Denaturing gradient gel electrophoresis (DGGE) in microbial ecology (Akkermans, A.D.L., van Elsas, F.J. and de Bruijn, F.J., Eds.), Molecular Microbial Ecology Manual, vol. 3.4.4, pp. 1–27. Kluwer Academic Publishers, Dordrecht.

[19] Kühl, M. and Revsbech, N.P. (1999) Microsensors for the study of interfacial biogeochemical processes In: The Benthic Boundary Layer (Boudreau, B.P. and Jørgensen, B.B., Eds.), pp. 180–210. Oxford University Press, Oxford.

[20] Viollier, E., Inglett, P., Hunter, K., Roychoudhury, A. and Van Cappellen, P. (2000) The ferrozine method revisited: Fe(II)/Fe(III) determination in natural waters. Appl. Geochem. 15 (6), 785–790.

[21] Davison, W. and Zhang, H. (1994) In-situ speciation measurements of trace components in natural-waters using thin-film gels. Nature 367 (6463), 546–548.

[22] Zhang, H. and Davison, W. (1999) Diffusional characteristics of hydrogels used in DGT and DET techniques. Anal. Chim. Acta 398 (2–3), 329–340.

[23] Canfield, D.E. (1989) Reactive iron in marine sediments. Geochim. Cosmochim. Acta 53, 619–632.

[24] Kostka, J.E. and Luther, G.W. (1994) Partitioning and speciation of solid-phase iron in salt-marsh sediments. Geochim. Cosmochim. Acta 58 (7), 1701–1710.

[25] Fossing, H. and Jørgensen, B.B. (1989) Measurement of bacterial sulfate reduction in sediments - evaluation of a single-step chromium reduction method. Biogeochemistry 8 (3), 205–222.

[26] Kallmeyer, J., Ferdelman, T., Weber, A., Fossing, H. and Jørgensen, B.B. (2004) A cold chromium distillation procedure for radiolabeled sulfide applied to sulfate reduction measurements. Limnol. Oceanogr. Methods 2, 171–180.

[27] Lehmann, C. and Bachofen, R. (1999) Images of concentrations of dissolved sulphide in the sediment of a lake and implications for internal sulphur cycling. Sedimentology 46, 537–544.

[28] Berg, P., Risgaard-Petersen, N. and Rysgaard, S. (1998) Interpretation of measured concentration profiles in sediment pore water. Limnol. Oceanogr. 43 (7), 1500–1510.

[29] Spring, S., Amann, R., Ludwig, W., Schleifer, K.-H., Schüler, D., Poralla, K. and Petersen, N. (1994) Phylogenetic analysis of uncultured magnetotactic bacteria from the Alpha-Subclass of Proteobacteria. Syst. Appl. Microbiol. 17 (4), 501–508.

[30] Blakemore, R.P. (1982) Magnetotactic bacteria. Annu. Rev. Microbiol. 36, 217–238.

[31] Moench, T.T. and Konetzka, W.A. (1978) A novel method for the isolation and study of a magnetotactic bacterium. Arch. Microbiol. 119, 203–212.

[32] Petersen, N., Weiss, D.G. and Vali, H. (1989) Magnetic bacteria in lake sediments In: Geomagnetism and Paleomagnetism (Lowes, F.J., et al., Eds.), pp. 231–241. Kluwer Academic Publishers, Dordrecht.

[33] Jonkers, H.M., Ludwig, R., De Wit, R., Pringault, O., Muyzer, G., Niemann, H., Finke and de Beer, D. (2003) Structural and functional analysis of microbial mat ecosystem from a unique permanent hypersaline inland lake: ''La Salada de Chiprana'' (NE Spain). FEMS Microbiol. Ecol. 44, 175–189.

[34] Meldrum, F.C., Mann, S., Heywood, B.R., Frankel, R.B. and Bazylinski, D.A. (1993) Electron microscopy study of magnetosomes in two cultured vibrioid magnetotactic bacteria. Proc. R. Soc. Lond. Ser. B 251 (1332), 237–242.

[35] Bazylinski, D.A., Dean, A.J., Williams, T.J., Long, L.K., Middleton, S.L. and Dubbels, B.L. (2004) Chemolithoautotrophy in the marine, magnetotactic bacterial strains MV-1 and MV-2. Arch. Microbiol. 182 (5), 373–387.

[36] Friedrich, C.G. (1998) Physiology and genetics of sulfur-oxidizing bacteria. Adv. Microb. Physiol. 39, 235–289.

[37] Moench, T.T. (1988) *Bilophococcus magnetotacticus* gen. nov. sp. nov., a motile, magnetic coccus. Anton. Leeuw. 54, 483–496.

[38] Iida, A. and Akai, J. (1996) Crystalline sulfur inclusions in magnetotactic bacteria. Sci. Rep. Niigata Univ. Ser. E (Geology) 11, 35–42.

[39] Bazylinski, D.A. and Frankel, R.B. (2000) Biologically controlled mineralization of magnetic iron minerals by magnetotactic bacteria In: Environmental Microbe–Metal Interactions (Lovley, D.R., Ed.), pp. 109–143. ASM Press, Washington, DC.
[40] Cox, L., Popa, R., Bazylinsky, D.A., Lanoil, B., Douglas, S., Belz, A., Engler, D. and Nealson, K.H. (2002) Organization and elemental analysis of P-, S-, Fe-rich inclusions in a population of freshwater magnetococci. Geomicrobiol. J. 19, 387–406.
[41] Guerin, W.F. and Blakemore, R.P. (1992) Redox cycling of iron supports growth and magnetite synthesis by *Aquaspirillum magnetotacticum*. Appl. Environ. Microbiol. 58 (4), 1102–1109.
[42] Paoletti, L.C. and Blakemore, R.P. (1988) Iron reduction by *Aquaspirillum magnetotacticum*. Curr. Microbiol. 17, 339–342.
[43] Short, K.A. and Blakemore, R.P. (1986) Iron respiration-driven proton translocation in aerobic bacteria. J. Bacteriol. 167 (2), 729–731.
[44] Schüler, D. and Baeuerlein, E. (1998) Dynamics of iron uptake and Fe_3O_4 biomineralization during aerobic and microaerobic growth of *Magnetospirillum gryphiswaldense*. J. Bacteriol. 180 (1), 159–162.
[45] Schüler, D. and Baeuerlein, E. (1996) Iron-limited growth and kinetics of iron uptake in *Magnetospirillum gryphiswaldense*. Arch. Microbiol. 166, 301–307.
[46] Heyen, U. and Schüler, D. (2003) Growth and magnetosome formation by microaerophilic *Magnetospirillum* strains in an oxygen-controlled fermentor. Appl. Microbiol. Biotechnol. 61 (5–6), 536–544.
[47] Blakemore, R.P., Short, K.A., Bazylinski, D.A., Rosenblatt, C. and Frankel, R.B. (1985) Microaerobic conditions are required for magnetite formation within *Aquaspirillum magnetotacticum*. Geomicrobiol. J. 4 (1), 53–72.
[48] Bazylinski, D.A., Frankel, R.B. and Jannasch, H.W. (1988) Anaerobic magnetite production by a marine magnetotactic bacterium. Nature 334 (6182), 518–519.
[49] Matsunaga, T., Sakaguchi, T. and Tadokoro, F. (1991) Magnetite formation by a magnetic bacterium capable of growing aerobically. Appl. Microbiol. Biotechnol. 35, 651–655.
[50] Meldrum, F.C., Mann, S., Heywood, B.R., Frankel, R.B. and Bazylinski, D.A. (1993) Electron microscopy study of magnetosomes in a cultured coccoid magnetotactic bacterium. Proc. R. Soc. Lond. Ser. B 251 (1332), 231–236.
[51] Kimble, L.K. and Bazylinski, D.A. (1996) Chemolithoautotrophy in the marine magnetotactic bacterium, strain MV-1. In: Annual Meeting of American Society Microbiology.
[52] Dean, A.J. and Bazylinski, D.A. (1999) Genome analysis of several marine, magnetotactic bacterial strains by pulsed-field gel electrophoresis. Curr. Microbiol. 39 (4), 219–225.
[53] Zopfi, J., Kjaer, T., Nielsen, L.P. and Jørgensen, B.B. (2001) Ecology of *Thioploca* spp.: Nitrate and sulfur storage in relation to chemical microgradients and influence of *Thioploca* spp. on the sedimentary nitrogen cycle. Appl. Environ. Microbiol. 67 (12), 5530–5537.
[54] Mußmann, M., Schulz, H.N., Strotmann, B., Kjaer, T., Nielsen, L.P., Rossello-Mora, R.A., Amann, R.I. and Jørgensen, B.B. (2003) Phylogeny and distribution of nitrate-storing *Beggiatoa* spp. in coastal marine sediments. Environ. Microbiol. 5 (6), 523–533.

Conclusions & outlook

Conclusions and outlook

The aim of the present study was to verify the influence of temperature, organic matter load and sediment types on biogeochemical reactions in intertidal surface sediments on a seasonal scale. Rates of microbial sulfate reduction were related to the dynamics of reduced solid sulfur and reactive Fe and Mn phases under various sedimentary conditions. The comparison of depth integrated SRR on a seasonal basis underlined the relation between temperature and microbial activity. Remarkably high rates were observed in summer 2003, followed by the early summer month of June and the spring season, which mainly corresponds to the annual temperature trend. Microbial sulfate reduction was generally high at the mixed and muddy stations, ranging from values of 30-2800 nmol $cm^{-3}d^{-1}$ in the mud and from 50 nmol $cm^{-3}d^{-1}$ to 1650 nmol $cm^{-3}d^{-1}$ in mixed sediment. Sulfate reduction at the sand flat stations (S I+ S III) were orders of magnitude lower and varied seasonally from 20 nmol $cm^{-3}d^{-1}$ to 550 nmol $cm^{-3}d^{-1}$. These rates are in the range of previously determined SRR in other intertidal sediments (e.g. Kristensen et al., 2000; Böttcher et al., 2004; de Beer et al., 2005; Werner et al., 2006). Highest microbial activities were detected within the surface 10 cm of the sediment. This reflected the mutual effect of factors such as temperature and the availability of organic matter.

In intertidal sediments, steep vertical temperature gradients can develop under the influence of tides. Typical diurnal temperature fluctuations occur rapidly during the change between tidal inundation and exposure amplified by temperature variations between day and night. A new model was introduced that allows the correct prediction of the response of sulfate-reducer activity during daily temperature variations under the influence of the tidal dynamics. SRR predicted by the temperature model, reflected that rate calculations based on the average daily temperature may lead to overestimations of microbial activity which were found to range from 10 % up to 100 %. Therefore, the vertical distribution of temperature has to be taken into account for calculations of the microbial activity and the connected elementary carbon and S cycling in intertidal surface sediments on a daily base.

Compared to the organic-matter rich fine-grained stations, also permeable sediments showed considerably high mineralization rates on a seasonal base and point out the important role of marine sands for carbon and S cycling. The advective circulation of particulate and dissolved organic matter, electron acceptors and oxygen through the permeable sediments functions as an effective filtration mechanism for organic carbon supplied into sandy sediments and leads to an effective aerobic and anaerobic degradation (Shum & Sundby, 1996; D`Andrea et al., 2002; Huettel et al., 1996; de Beer et al., 2005). The highly dynamic conditions in the sandy intertidal systems enhanced the sediment mixing which stimulates microbial sulfate reduction and may compensate the effect of higher TOC content and generally elevated microbial density found in fine-grained sediments (Musat et al., 2006). Microbial activity decreased with depth, also at the organic rich stations (D and N) indicating that the input of fresh organic carbon is an important rate controlling factor for SRR in surface sediments.

The mixed and muddy stations represent highly productive sediments where intensive sulfate reduction leads to high accumulation of reduced inorganic S (TRIS). The lower TRIS content of the

sandy location compared to the station N and D was primarily due to enhanced chemical re-oxidation processes. Especially at the sandy station S III a short residence time of reduced S compounds indicated that intensive re-oxidation processes must have taken place at the sandy sediments.

Furthermore, the limited availability of reactive Fe phases or intermediate S species at the sandy sediments prevented a permanent fixation of sulfide into the thermodynamically more stable pyrite. The close coincidence of sulfate reduction and mobilization of Fe(III) and Mn(IV) as Fe^{2+} and Mn^{2+} into the pore water accompanied by the increase of Fe sulfides indicated that to a large extent the Fe reduction was coupled to sulfide oxidation (Pyzik & Sommer, 1981; Giblin & Howarth, 1984; Luther et al, 1992). This proves the assumption that even below the oxygen penetration depth abiotic sulfide oxidation can become a competing process to the biogenic sulfide production in the sediment. Tidal flushing resulted in deep oxygenation of permeable surface sediments which caused a stimulation of subsurface Fe and S-cycling. Thus, the measured SRR, especially at the surface (0-4 cm) of the sandy sediment, have been underestimated up to 90 % and reflects only gross but no net rates of sulfate reduction. Even at the mixed station, SRR were superimposed by re-oxidation processes and underestimated up to 10-40 %. These results demonstrated that intensive sulfate reduction was taking place in the oxygenated part of the sediment during incubation and that re-oxidation processes led to a rapid turnover and showed that improved knowledge of sulfide oxidation processes on a short time scale (4 hours) during incubation is important for accurate measurements of sulfate reduction.

The reactive part of the Mn and Fe phases provided an oxidizing reservoir to scavenge or oxidize H_2S. The solid Fe and Mn phases serve as important redox buffer in intertidal sediments (Morse, 1999). From the pore water profiles it becomes evident that the top 10-15 cm of the surface sediments are most important for Fe and Mn cycling and conditions at the sediment-water interface are controlling the metal flux into the water column. Gradients and concentrations established in the pore water responded to the seasonal variation of microbial sulphate reduction activity and the reservoir of reactive metal oxides. Therefore, Mn and Fe rich sediments such as station N and D are for a lesser extent controlled by the input of reactive Mn and Fe from the water column in contrast to the sandy locations (S I, S III). All investigated stations showed regular periods of loss and gain in the inventory of reactive Fe_{HCl} and Mn_{HCl}. The diffusion of dissolved Mn out of the sediment is only a small fraction of what is reduced within the sediment. The estimated Mn reduction rates pointed out that in fact 20-44 % of the reduced Mn^{2+} does not escape into the water column and thus indicated that an important part of the Mn cycle takes place within the sediment. Strongest seasonal amplitudes of loss and gain were found in the sandy sediments and culminate in a complete depletion of reactive Fe_{HCl} during summer. The prevalence of Mn release during spring and summer leads to a decrease of the sedimentary Mn_{HCl} inventory, which was higher than the external supply from the overlying water and not balanced by re-sedimentation as observed during the colder months. Nevertheless, calculated budgets showed that more than 90 % of released Mn^{2+} was recycled in the water column and re-precipitated to the sediment. The decline of the Mn_{HCl} inventory amounted to a pool size reduction of 56 % at station N I and up to 42 % at the sandy stations SI, S III until summer. On a seasonal basis, the relation of Fe/Mn reflects the different reaction kinetics and thermodynamics. Compared to the

Mn_{HCl} contents the $Fe_{HCl+AVS}$ pools showed only minor seasonal variations because the main Fe cycle was restricted to the sediment. No fluxes of dissolved Fe could be detected during the benthic chamber measurements because the oxidation of Fe^{2+} by Mn-oxides acts as a barrier to the upward diffusion of dissolved Fe on the way to the sediment-water interface. Furthermore, it is not possible to distinguish the bacterial Mn reduction from abiotic reduction processes by Fe^{2+} and H_2S in-situ. Experimental lab incubations showed that, theoretically, 90 % of carbon oxidation may be due to sulphate reduction at the mixed station N II and that dissimilatory Mn reduction potentially may become an important mineralization process but are hampered by other competing processes in-situ (Peters, 2004; Batel, 2003).

The composition of suspended particulate matter in the water column displayed a seasonal behaviour with increasing adsorbed Mn contents during summer and low Mn amounts during the colder months (Dellwig et al., 2007). The Mn cycle shifts seasonally from an external cycle in summer, when Mn^{2+} can diffuse out of the sediment, to an internal cycle, when decreasing reductive conditions lead to lower release rates and a major part of the Mn cycling was restricted to the sediment, during autumn and winter. The external input of Mn oxide enriched particles from of the water column generated during this month a regeneration of the sedimentary Mn_{HCl} pool. Dellwig et al. (2007) found that the particulate Mn concentration in the water column increased by a factor of nearly 2 from winter to summer. Therefore, it can be concluded that especially during temperate seasons the Mn inventory of tidal flat sediments forms a very important source for Mn and is replenished to a certain degree by the higher freshwater input during rainy fall and winter. Dellwig et al. (2007) estimated that freshwater discharge can explain more than 90 % of the total Mn inventory in the Wadden Sea water column during phases of high rain fall and reduced microbial activity during winter time.

Flux and pore water measurements below anoxic spots revealed locally high concentrations of Mn^{2+} probably due to the lateral draining of anoxic pore water downward the sand flat which was postulated by Billerbeck et al. (2006a). Furthermore, imbedded fine grained layers may function as sources for locally enhanced Mn^{2+} concentrations. This indicates that the continuing drop of the water level caused a pore water flow along the hydraulic gradient towards the low water line where pore water discharge zones emerged (Nielsen, 1990; Billerbeck et al., 2006a). Benthic chamber experiments also revealed that highest amounts of Mn (this study) and nutrients (Billerbeck et al., 2006a) were released from the tidal flat as soon as the regressing inundation exposed the top of the sand flat. A further hint for enhanced pore water seepage in these zones is the development of characteristic puddles filled with sulfidic pore water, so called `black spots`, which were visible during low tide. Mn fluxes, measured by benthic chambers showed distinct differences between stations and seasons. In July, highest Mn fluxes were 27 times higher at station N I whereas SRR were only 2-fold higher in relation to fluxes observed at station S III. This indicated that the enhanced oxygen penetration depths at the sandy station S III (Walpersdorf et al., in prep.) function as a barrier for Mn^{2+} outflux. Furthermore, measured Mn release rates showed a stronger response to biogenic sulfide production than to the oxygen consumption in the overlying water. Highest Mn^{2+} fluxes were measured at the mixed station N I which is due to the generally higher Fe and Mn contents and microbial activities. This was additionally

proved by the correlation of Mn fluxes to microbial sulphate reduction and temperature respectively and pointed out that the main seasonal factor (besides factors like e.g. Mn availability) was the rate of sulphate reduction which is in turn indirectly controlled by temperature.

The tidal area of the Lower Saxony Wadden Sea of 1411 km^2 consisted to 80 % of sands, 12 % mixed and 8 % muddy sediments (including 1,6 % mussel beds; Meyer & Ragutzki, 1999). Rough extrapolation of the measured Mn fluxes during all seasons (assumed that comparable environmental conditions prevail) would amount to 136-13011 mol d^{-1} which is equivalent to a yearly Mn release of 2,5-7 million mol a^{-1} into the water column of the Lower Saxony Wadden Sea.

The 2D Photopaper Technique provided a valuable in-situ monitoring technique to visualize the zonation of dissolved sulfide in a 2-dimensional manner. Therefore, the 2D Photopaper Technique provides information about the supply and the retention time of hydrogen sulfide (H_2S) at a high spatial resolution. Variances between calculated sulfide concentrations and pore water measurements point out that the S fixation on the photopaper is superimposed by rapid sulfide oxidation or precipitation processes. Therefore, the 2D Photopaper Technique is a monitoring tool for the mean retention time of free sulfide and allows a semi-quantitative estimation of sulfide production and consumption zones. Calibration experiments showed that the mean intensities of darkening were quantitatively related to the amount of Ag_2S. The sensitivity of this method covers concentration ranges (detection limits) from 50 µM for 24 hour incubation to more than 1000 µM with appropriate shorter deployment times. In addition to the expected 2 dimensional impression of sulfide distribution, the detailed resolution of the photo paper images permits information of textural changes visualizing details of internal sediment structures as grain sizes and particles such as mussels. The application of the photo paper technique in the field has been proved to show reliable results in various sediment types.

The interactions of aerobic and anaerobic processes in intertidal surface sediments were quantified to advance our understanding of their significance for element fluxes and the biogeochemical processes of the Wadden Sea. However the complexity and dynamic of this system requires the application of several methods in combination in order to obtain a comprehensive overview of the controlling factors and their interactions between geochemical and microbial processes.

The presented results showed that Mn and Fe are important for the electron transfer and are re-circulated through various redox processes. However, our understanding of the relationship between the distribution of microorganisms and the biogeochemical processes and the role of the hydrodynamic processes is still not satisfactory. What exactly are the microbial and abiotic processes and the corresponding microorganisms responsible for the re-oxidation of initially formed reduced species?

Of further interest is the quantitative importance of element fluxes and different respiration processes in sediments and their quantitative relation to processes in the water column. It has to be considered that benthic fluxes were mainly studied by the application of benthic chambers which only allow flux measurements during inundation of the tidal flats and exclude discharge rates during exposure. But

flux rates at the sand flat station S I during decreasing inundation pointed to the potential relevance of element discharge during low tide. Additionally, measurements of one-dimensional transport processes only lead to a considerable underestimation of pore water exchange and are not sufficient to assess the complete discharge of solutes. Seepage of pore water enriched in reduced species and nutrients draining of permeable sediments leads to the question how pore water flows or circulates trough the sand plate. The in-situ pore water transport in permeable sediments under dynamic intertidal conditions has not been fully understood. More detailed and continuous measurements of lateral transport processes are needed to comprise the importance of seepage zones for element budgets of the Wadden Sea.

Furthermore, the influences of temperature variations as controlling factor for biogeochemical process under at Intertidal surface sediments are still not sufficiently investigated.

Continuing investigations during the second phase already have, and during the third project phase of the research group `BioGeoChemistry of Tidal Flats`, will advance these investigations to provide the basis for the estimation of model calculations with the aim to establish a comprehensive budget for the Wadden Sea ecosystem.

Reference

Batel, S., 2003, Biogeochemische Umsatzprozesse in einem tidalen Oberflächensediment der südlichen Nordsee: Diploma Thesis, CvO Universität Oldenburg, 112.

Billerbeck, M., U. Werner, K. Bosselmann, E. Walpersdorf and M. Huettel, 2006a, Nutrient release from an exposed intertidal sand flat: Marine Ecology Progress Series, 316: 35-51.

Böttcher, M. E., B. Hespenheide, H. J. Brumsack and K. Bosselmann, 2004, Stable isotope biogeochemistry of the sulfur cycle in modern marine sediments: I. Seasonal dynamics in a temperate intertidal sandy surface sediment: Isotopes in Environmental and Health Studies, 40: 267-283.

D'Andrea, A. F., R. C. Aller and G. R. Lopez, 2002, Organic matter flux and reactivity on a South Carolina sandflat: The impacts of porewater advection and macrobiological structures: Limnology and Oceanography, 47: 1056-1070.

de Beer, D., F. Wenzhofer, T. G. Ferdelman, S. E. Boehme, M. Huettel, J. E. E. van Beusekom, M. E. Böttcher, N. Musat and N. Dubilier, 2005, Transport and mineralization rates in North Sea sandy intertidal sediments, Sylt-Rømø Basin, Wadden Sea: Limnology and Oceanography, 50: 113-127.

Dellwig, O., K. Bosselmann, S. Kölsch, M. Hentscher, J. Hinrichs, M. E. Böttcher, R. Reuter and H.-J. Brumsack, 2007, Sources and fate of manganese in a tidal basin of the German Wadden Sea: Journal of Sea Research, 57: 1-18.

Giblin , A. and R. W. Howarth, 1984, Pore water evidence for a dynamic sedimentary iron cycle in salt marshes: Limnology and Oceanography, 29:47-63.

Huettel, M., W. Ziebis and S. Forster, 1996, Flow-induced uptake of particulate matter in permeable sediments: Limnology and Oceanography, 41: 309-322.

Kristensen, E., J. Bodenbender, M. H. Jensen, H. Rennenberg and K. M. Jensen, 2000, Sulfur cycling of intertidal Wadden Sea sediments (Königshafen, Island of Sylt, Germany): Sulfate reduction and sulfur gas emission: Journal of Sea Research, 43: 93-104.

Luther, G. W., J. E. Kostka, T. M. Church, B. Sulzberger and W. Stumm, 1992, Seasonal Iron Cycling in the Salt-Marsh Sedimentary Environment - the Importance of Ligand Complexes with Fe(II) and Fe(III) in the Dissolution of Fe(III) Minerals and Pyrite, Respectively: Marine Chemistry, 40: 81-103.

Meyer, C. and G. Ragutzki, 1999, KFKI Forschungsvorhaben Sedimentverteilung als Indikator für morphodynamische Prozesse., Norderney, Niedersächsisches Landesamt für Ökologie, 43.

Morse, J. W., 1999, Sulfides in Sandy Sediments: New Insights on the Reactions Responsible for Sedimentary Pyrite Formation: Aquatic Geochemistry, 5: 75-85.

Musat, N., U. Werner, K. Knittel, S. Kolb, T. Dodenhof, J. E. E. van Beusekom, D. de Beer, N. Dubilier and R. Amann, 2006, Microbial community structure of sandy intertidal sediments in the North Sea, Sylt-Rømø Basin, Wadden Sea: Systematic and Applied Microbiology, 29: 333-348.

Peters, L., 2004, Zur Biogeochemie eines Sedimentkerns aus dem Mischwatt der südlichen Nordsee.: Diploma Thesis, CvO Universität Oldenburg, 113.

Pyzik, A. J. and S. E. Sommer, 1981, Sedimentary iron monosulfides: Kinetics and mechanism of formation: Geochimica et Cosmochimica Acta, 45: 687-698.

Werner, U., M. Billerbeck, L. Polerecky, U. Franke, M. Huettel, J. E. E. van Beusekom and D. de Beer, 2006, Spatial and temporal patterns of mineralization rates and oxygen distribution in a permeable intertidal sand flat (Sylt, Germany): Limnology and Oceanography, 51: 2549-2563.

Tab. A1: Sulfate reduction rates [nmol cm^{-3} d^{-1}], station NI

	SRR [nmol cm^{-3} d^{-1}]						
Depth	**05. 04.02**		**20.06.02**		**04.08.02**	**10.10.02**	
[cm]	4°C	16°C	16°C	27°C	28°C	10°C	16°C
0,5	49,2	68,2	58,4		1378,5	46,24	38,9
1,5	52,7	192,9	106,7	289,8	965,1	81,69	93,7
2,5	120,8	263,9		545,6	716,4	64,09	55,3
3,5	135,4	213,3		447,8	452,3	85,42	131,5
4,5	91,4	198,4	97,7	376,8	277,4	79,67	89,9
5,5	63,3	164,6	108,9	408,7	334,5	95,11	151,0
6,5	42,2	171,3	60,4	162,0	523,3	59,09	160,7
7,5	35,5	88,8	50,8	132,2	305,4	30,03	145,1
8,5	36,3	64,6		38,1	87,3	25,13	125,7
9,5	26,6	84,0	26,5	60,4	260,9	27,20	86,0
10,5	23,4	45,7	20,0	70,2	150,2	11,46	46,9
11,5	26,5	82,9	54,4	32,5	98,9	19,55	31,5
12,5	17,0	70,0	21,4	62,2	196,7	11,76	10,6
13,5	10,0		10,9	38,9	92,3	7,35	7,8
14,5	11,3			14,5	35,1	5,38	7,9

Tab. A2: Sulfate [mM], station NI

	SO_4 [mM]			
Depth				
[cm]	**05. 04.02**	**20.06.02**	**04.08.02**	**10.10.02**
0,5	25,9	25,9	29,8	24,4
1,5	25,2	25,2	23,6	24,3
2,5	25,0	25,0	22,1	23,6
3,5	24,3	24,3	23,1	23,3
4,5	24,4	24,4	23,1	22,7
5,5	23,7	23,7	23,5	22,0
6,5	24,1	24,1	24,4	21,9
7,5	23,7	23,7	22,4	22,4
8,5	23,4	23,4	22,3	22,3
9,5	23,4	23,4	21,8	22,3
10,5	23,4	23,4	21,5	22,2
11,5	23,4	23,4	21,2	22,2
14,5	23,4	23,4	20,9	22,1

Tab. A3: Dissolved [mM] and sedimentary [ppm] iron, station NI

	05. 04.02		20.06.02		10.10.02		10.12.02		04.08.03	
Depth	**Fe^{2+}**	**Fe III**	**Fe^{2+}**	**Fe III**	**Fe^{2+}**	**Fe III**	**Fe^{2+}**	**Fe III**	**Fe^{2+}**	**Fe III**
[cm]	**[µM]**	**[ppm]**	**[µM]**	**[ppm]**	**[µM]**	**[ppm]**	**[µM]**	**[ppm]**	**[µM]**	**[ppm]**
0,5	16,2	1981,6	183,6	1532,9	105,1	1258,5	56,6	1446,4	0,0	1458,5
1,5	14,2	2323,1	93,3	1091,6	9,7	1527,6	207,2	1556,5	10,7	1340,8
2,5	22,9	1500,4	102,9	1241,8	6,9	1497,8	211,4	1306,1	2,9	1309,2
3,5	21,9	1183,6	166,1	1635,8	6,0	1569,1	122,1	1082,9	1,8	1294,1
4,5	30,2	694,5	127,7	1499,3	21,5	1186,7	334,9	1247,3	4,1	1254,9
5,5	139,5	259,5	131,2	1239,2	20,6	1198,1	107,3	797,9	1,4	1102,5
6,5	177,3	845,8	73,8	1102,4	33,0	1079,4	52,9	797,9	2,9	883,8
7,5	149,2	1187,9	22,4	924,5	46,5	961,8	28,6	595,8	2,3	812,9
8,5	34,9	741,7	0,0	748,2	46,9	1273,2	24,3	585,2	2,5	1004,5
9,5	34,8	347,1	0,0	988,9	26,0	977,1	19,2	1092,0	2,7	1221,7

Tab. A4: Dissolved [mM] and sedimentary [ppm] manganese, station NI

	05. 04.02		20.06.02		10.10.02		10.12.02		04.08.03	
Depth	**Mn^{2+}**	**Mn IV III**	**Mn^{2+}**	**Mn IV III**	**Mn^{2+}**	**Mn IV III**	**Mn^{2+}**	**Mn IV III**	**Mn^{2+}**	**Mn IV III**
[cm]	**[µM]**	**[ppm]**	**[µM]**	**[ppm]**	**[µM]**	**[ppm]**	**[µM]**	**[ppm]**	**[µM]**	**[ppm]**
0,5	16,2	1981,6	183,6	1532,9	105,1	1258,5	56,6	1446,4	0,0	1458,5
1,5	14,2	2323,1	93,3	1091,6	9,7	1527,6	207,2	1556,5	10,7	1340,8
2,5	22,9	1500,4	102,9	1241,8	6,9	1497,8	211,4	1306,1	2,9	1309,2
3,5	21,9	1183,6	166,1	1635,8	6,0	1569,1	122,1	1082,9	1,8	1294,1
4,5	30,2	694,5	127,7	1499,3	21,5	1186,7	334,9	1247,3	4,1	1254,9
5,5	139,5	259,5	131,2	1239,2	20,6	1198,1	107,3	797,9	1,4	1102,5
6,5	177,3	845,8	73,8	1102,4	33,0	1079,4	52,9	797,9	2,9	883,8
7,5	149,2	1187,9	22,4	924,5	46,5	961,8	28,6	595,8	2,3	812,9
8,5	34,9	741,7	0,0	748,2	46,9	1273,2	24,3	585,2	2,5	1004,5
9,5	34,8	347,1	0,0	988,9	26,0	977,1	19,2	1092,0	2,7	1221,7

Tab. B1: Sulfate reduction rates [nmol cm^{-3} d^{-1}], station SI and station SIII

	SRR [nmol cm^{-3} d^{-1}]												
	Station S I							Station S III					
Depth	07.06.02		01.10.02		22.07.03	26.03.04		20.03.02	07.06.02		22.07.03	01.10.02	
[cm]	16°C	25°C	10°C	16°C	28°C	4°C	10°C	4°C	16°C	25°C	28°C	10°C	16°C
0,5		43,5	98,6	113,9	415,0	3,7	1,3	1,2		117,0	391,5	63,6	43,0
1,5	0,2	65,5	83,6	55,8	251,5	5,5	9,2	3,6	13,6	114,3	340,5	117,8	32,5
2,5	0,2	69,6	59,2	40,3	142,6	7,0	16,6	6,6	42,0	104,3	167,2	22,5	29,3
3,5	48,5	71,5	28,3	48,0	89,6	9,9	20,8	5,5	96,2	191,6	180,4	39,8	22,0
4,5	48,4	118,4	21,6	44,7	74,7	9,8	22,0	5,6	85,2	136,4	105,7	34,7	21,7
5,5	51,3	74,5	70,7	39,5	58,5	11,9	26,8	8,6	91,8	71,4	84,9	26,6	55,6
6,5	57,5	83,4	102,4	24,2	43,2	18,7	22,2	3,5	69,8	94,4	290,2	30,7	51,9
7,5	47,4	66,9	94,0	28,3	43,9	18,4	17,4	5,9	58,3	83,0	386,3	19,5	34,7
8,5	38,4	49,1	26,6	40,0	31,9	17,1	8,2	5,8	51,0	73,7	335,5	18,2	42,4
9,5	67,7	48,4	39,4	43,8	38,3	14,9	23,4	9,6	67,1		295,3	9,5	22,2
10,5	40,3	61,5	36,7	33,3	56,0	17,4	11,6	8,7	53,4		225,3	13,6	62,2
11,5	47,0	134,0	44,3	33,1	48,5	10,2	15,9	7,0	48,5	62,9	87,9	15,6	112,0
12,5	64,3	146,7	42,6	31,0	38,6	7,8	16,8	7,2	38,6	73,7	52,9	14,1	73,7
13,5	82,2	151,0	37,0	42,4	76,0	8,0	12,7	3,1	69,7	98,4	45,6	11,9	68,9
14,5	59,9	91,7	37,1	73,3	91,3	15,5	14,6	3,5	69,6		75,5	13,9	55,6

Tab. B2: Sulfate [mM], station SI and station SIII

	SO_4 [mM]							
	Station S I				Station S III			
Depth	07.06.02	01.10.02	22.07.03	26.03.04	20.03.02	07.06.02	01.10.02	22.07.03
[cm]								
0,5	25,0	25,8	24,7	24,9	22,91	25,8	24,47	25,7
1,5	24,3	26,8	21,4	23,2	24,0	26,9	30,3	27,7
2,5	25,3	26,5	19,0	23,5	24,3	24,9	28,1	28,6
3,5	23,3	25,9	18,4	23,6	25,0	25,7	25,6	26,3
4,5	23,5	26,1	17,0	21,5	24,9	25,9	29,6	26,9
5,5	23,9	25,7	15,3	22,7	27,1	25,7	24,7	26,9
6,5	25,6	26,1	13,7	22,4	29,5	26,0	25,3	26,3
7,5	23,8	26,0	13,5	23,3	26,4	26,2	24,4	26,5
8,5	23,4	26,1	12,9	22,4	24,7	25,7	24,0	27,7
9,5	23,4	25,9	12,5	22,0	25,3	25,6	28,3	27,2
10,5	25,2	25,7	12,0	21,2	25,3	25,6	21,5	26,7
11,5	25,2	25,3	13,0	20,6	25,3	25,6	24,6	26,3
14,5	25,2	25,9	12,1	19,9	25,3	25,6	24,6	26,3

Tab. B3: Dissolved [mM] and sedimentary [ppm] iron, station SI and station SIII

Station S I										
	07.06.02		01.10.02		10.12.02		22.07.03		26.03.04	
Depth	Fe^{2+}	Fe III	Fe^{2+}	Fe III	Fe^{2+}	Fe III	Fe^{2+}	Fe III	Fe^{2+}	Fe III
[cm]	[µM]	[ppm]	[µM]	[ppm]	[µM]	[ppm]	[µM]	[ppm]	[µM]	[ppm]
0,5	3,0	396,7	n.d.	288,8	5,4	712,6	48,5	0,0	1,7	308,6
1,5	28,4	425,3	n.d.	338,6	4,8	307,7	204,8	0,0	5,1	263,3
2,5	20,4	482,6	n.d.	306,2	8,3	794,1	109,4	0,0	20,4	258,0
3,5	59,3	337,8	n.d.	321,3	21,4	330,3	44,9	0,0	22,1	249,8
4,5	91,8	260,2	n.d.	245,8	23,1	514,3	39,2	0,0	38,3	266,5
5,5	67,1	248,1	n.d.	303,9	18,8	686,3	54,7	0,0	58,3	277,2
6,5	19,6	242,1	n.d.	240,6	18,5	457,0	67,8	0,0	59,6	294,0
7,5	3,5	290,3	n.d.		14,8	479,8	94,8	0,0		303,8
8,5	26,1	432,9	n.d.	381,6	10,3	520,3	71,3	0,0	59,8	263,9
9,5	167,0	389,1	n.d.	294,9	13,7	389,1	100,6	0,0	18,3	298,8

Station S III										
	20.03.02		07.06.02		01.10.02		10.12.02		22.07.03	
Depth	Fe^{2+}	Fe III	Fe^{2+}	Fe III	Fe^{2+}	Fe III	Fe^{2+}	Fe III	Fe^{2+}	Fe III
[cm]	[µM]	[ppm]	[µM]	[ppm]	[µM]	[ppm]	[µM]	[ppm]	[µM]	[ppm]
0,5	n.d.	230,8	n.d.	344,6	n.d.	264,7	3,1	255,4	35,8	0,0
1,5	n.d.	251,9	n.d.	294,1	n.d.	250,4	2,2	256,9	47,9	0,0
2,5	n.d.	248,1	n.d.	279,0	n.d.	231,5	0,4	243,2	68,1	0,0
3,5	n.d.	231,5	n.d.	233,8	n.d.	200,6	62,1	248,9	50,4	0,0
4,5	n.d.	235,3	n.d.	253,4	n.d.	138,0	69,3	223,2	46,7	0,0
5,5	n.d.	259,4	n.d.	240,6	n.d.	222,5	63,5	426,8	34,0	0,0
6,5	n.d.	285,8	n.d.	290,3	n.d.	193,1	141,5	205,9	18,8	0,0
7,5	n.d.	257,9	n.d.	227,0	n.d.	222,5	177,9	243,5	18,9	0,0
8,5	n.d.	325,8	n.d.	273,7	n.d.	254,1	179,2	234,0	25,1	0,0
9,5	n.d.	365,8	n.d.	257,2	n.d.	247,4	146,9	232,5	17,8	0,0

Tab. B4: Dissolved [mM] and sedimentary [ppm] manganese, station SI and station SIII

Station S I										
	07.06.02		01.10.02		10.12.02		22.07.03		26.03.04	
Depth	Mn^{2+}	Mn IV III	Mn^{2+}	Mn IV III	Mn^{2+}	Mn IV III	Mn^{2+}	Mn IV III	Mn^{2+}	Mn IV III
[cm]	[µM]	[ppm]	[µM]	[ppm]	[µM]	[ppm]	[µM]	[ppm]	[µM]	[ppm]
0,5	85,1	28,9	1,0	15,9	42,5	62,8	15,3	35,8	1,3	50,4
1,5	190,6	32,1	11,2	20,2	52,4	34,9	21,0	15,6	30,8	35,5
2,5	71,6	61,9	12,8	16,2	35,9	23,6	10,8	14,0	58,3	16,4
3,5	70,8	23,0	16,1	14,3	44,7	26,9	10,5	9,8	69,6	17,2
4,5	29,8	15,4	16,9	13,8	32,8	133,4	9,6	8,4	99,4	15,4
5,5	25,6	14,0	21,9	14,2	13,5	64,6	8,7	6,8	102,7	12,5
6,5	21,1	13,5	27,6	21,0	40,2	51,3	10,1	5,4	91,9	11,8
7,5	19,9	16,6	25,0	20,3	41,3	35,5	11,6	6,6		10,7
8,5	26,4	26,1	26,5	16,7	27,3	26,5	11,2	6,5	68,1	12,8
9,5	64,3	29,3	30,5	14,2	37,4	47,9	28,8	7,1	35,0	11,8

Station S III										
	20.03.02		07.06.02		01.10.02		10.12.02		22.07.03	
Depth	Mn^{2+}	Mn IV III	Mn^{2+}	Mn IV III	Mn^{2+}	Mn IV III	Mn^{2+}	Mn IV III	Mn^{2+}	Mn IV III
[cm]	[µM]	[ppm]	[µM]	[ppm]	[µM]	[ppm]	[µM]	[ppm]	[µM]	[ppm]
0,5	0,0	24,2	6,0	38,2	11,8	13,4	0,4	17,9	2,4	3,3
1,5	9,5	21,4	10,4	14,4	9,2	9,3	1,8	16,1	1,9	3,3
2,5	12,0	16,2	10,5	10,4	10,9	5,8	1,5	12,9	2,8	3,5
3,5	26,1	13,5	12,5	9,8	7,5	6,2	3,2	11,0	1,5	4,5
4,5	48,0	14,5	14,2	11,2	8,6	9,1	2,1		1,7	5,8
5,5	2,4	14,9	7,9	9,6	6,8	9,1	2,3	9,8	1,4	6,0
6,5	0,1	17,0	15,8	14,3	8,2	12,5	5,9	7,8	1,0	6,0
7,5	67,7	17,0	17,0	15,2	8,2	12,6	3,7	9,8	0,9	6,4
8,5	83,5	18,8	20,9	14,9	8,3	14,4	7,6	10,4	1,0	6,7
9,5	82,1	22,0	14,2	15,3	8,5	10,6	7,5	22,8	1,6	5,8

Acknowledgements - Danksagung

Mein besonderer Dank gilt Prof. Dr. Michael Böttcher für die Vergabe, Unterstützung und Betreuung dieser Arbeit.
Ganz herzlich möchte ich mich bei Prof. Dr. Hans-Jürgen Brumsack für die Begutachtung der Arbeit bedanken.
Prof. Dr. Gerd Liebezeit danke ich für seine Bereitschaft, als Prüfer zu fungieren.

Den Mitarbeitern des MPI danke ich für die Unterstützung mit Rat und Tat. Ein besonderer Dank geht an die Mitarbeiter der MPI Werkstatt, Alfred Kutsche und Georg Herz.
Free danke ich für ihre treue und zuverlässige Hilfe im Labor. Stephi und Lydia für ihren Beitrag zu meiner Arbeit und einer tollen Zeit am MPI.

Der Arbeitsgruppe Mikrobiogeochemie in Oldenburg danke ich für die Unterstützung bei analytischen Fragen und zahlreichen Messungen, ganz besonders Bernhard Schnetger.

Für die nette Arbeitsatmosphäre im Büro danke ich Sybille, Markus, Arne und Astrid für die aufmunternde Unterstützung.

Vielen Dank an die zähen Mitstreitern der Feldcrew: Eva Walpersdorf, Uschi Werner, Ingrid Dohrmann, Markus Billerbeck und Martina Alisch. Nicht zu vergessen, den Crews der Plattbodenschiffe für die Unterstützung im Watt bei Sturm und Eis.

Ganz herzlichen Dank an Eva Walpersdorf - geduldigste-und-ausdauernste-Korrekturleserin-von-Welt und Heiner Fabian, der mich vor den GAU beim Formatieren und Drucken bewahrt hat.

Den Kollegen des FTZ danke ich für die Versorgung mit Nervennahrung und viel Geduld. Ganz besonders danke ich Herrn Dr. Tischler für die gründliche Durchsicht meiner Arbeit.

Großer Dank geht an meine Freunde, die mir während dieser Zeit mit viel Geduld zur Seite standen und unermüdlich - zumindest mit meiner Kommunikationsbox redeten.

Mein größter Dank geht an meine Familie.
Meinen Eltern und meiner Schwester Heike danke ich, dass sie mich in jeder Situation begleitet, ermutigt und unterstützt haben. Nur mit Eurer Hilfe konnte ich das Ziel erreichen.

Diese Arbeit wurde von der Deutschen Forschungsgemeinschaft (DFG) im Rahmen der Forschergruppe FOR 432/2 „BioGeoChemie des Watts” gefördert.

Curriculum vitae

Name: Katja Bosselmann

Geburtsdatum: 31.07.1972

Geburtsort: Bremen

1979 -1983	Grundschule in Achim
1983 - 1985	Orientierungsstufe am Markt in Achim
1985 - 1989	Realschule Achim
1989 – 1992	Fachgymnasium Verden
1995 - 1997	Studium Diplom-Biologie und Erwerb des Vordiploms an der Universität Bremen
1997 - 2001	Hauptstudium an der Carl von Ossietzky Universität Oldenburg
Oktober 2001	Abschluss des Studiums: Diplomarbeit am Institut für Biologie und Chemie des Meeres (ICBM) in Zusammenarbeit mit dem Zentrum für Marine Tropenökologie (ZMT), `Geochemie quartärer Sedimentabfolgen eines Mangroven-Gebietes in Nordbrasilien`
2001 -2005	Promotion am Max-Planck-Institut für marine Mikrobiologie in Bremen
seit 2005	wissenschaftliche Angestellte am Forschungs- und Technologie-zentrum Westküste, Büsum. `Die Bedeutung des Stoffaustausches zwischen Sediment und Wassersäule für Umsatzprozesse im Pelagial.`

Erklärung

Hiermit versichere ich, dass ich die vorliegende Arbeit selbstständig angefertigt und keine anderen als die angegebenen Quellen und Hilfsmittel verwendet habe. Zusätzlich erkläre ich, dass diese Dissertation weder in ihrer Gesamtheit noch in Teilen einer anderen wissenschaftlichen Hochschule zur Begutachtung in einem Promotionsverfahren vorliegt oder vorgelegen hat.

Büsum, November 2007